CHARACTERISTICS OF SWIRLING FLAMES ISSUING FROM VANE SWIRLERS

by

G.G. Bafuwa, B.Sc.

Thesis submitted for the Degree of Ph.D.

to the Faculty of Engineering,

The University of Glasgow.

August, 1970.

ProQuest LLC.
789 East Eisenhower Parkway
P.O. Box 1346
Ann Arbor, MI 48106 – 1346

ACKNOWLEDGEMENTS

The author expresses his gratitude to Professor R. S. Silver, Dr. N. R. L. Maccallum and other members of the staff in the University for their advice and encouragement.

The author wishes to thank the Commonwealth Scholarship Commission in the United Kingdom.

CONTENTS

LIST OF TABLES

NOMENCLATURES

a	virtual origin of the jet
A	constant
B	constant
C	constant
C_v	specific heat at constant volume
C_p	specific heat at constant pressure
d	diameter
d_1	inner diameter
d_2	outer diameter
E	activation energy unless otherwise stated
g	acceleration due to gravity
G_x	axial flux of linear momentum
G_θ	axial flux of angular momentum
$\bar{G}$	defined in equation (2.27)
G'_r	ρrv = component of $\bar{G}'$ along r
G'_x	ρru = component of $\bar{G}'$ along x
$\bar{G}'$	mass velocity vector
h	mean convective heat transfer coefficient
H	enthalpy
k	thermal conductivity of fluid
K	reaction rate constant
L	flame length
m_j	mass fraction of component j
m_f	$m_{fu} - \frac{m_{ox}}{STC}$
$\dot{m}$	mass flow rate
M	molecular weight
p	static pressure

r	radial coordinate
r_1	inner radius
r_2	outer radius
$\bar{R}$	universal gas constant
S	swirl number
T	temperature
u,v,w	time mean velocity components in the x, r, θ directions
$U_{o,av}$	volumetric flow rate/flow area
$\bar{V}$	resultant velocity vector
V_s	$u^2 + v^2$
x	axial coordinate

Greek Alphabets

α, β, γ	are defined in relevant paragraphs
$\Gamma_{j,eff}$	effective turbulent exchange coefficient of component j
δ	angle subtended by the vane at the swirler axis
ϵ	total emissivity
η	variables defined in relevant paragraphs
θ	vane angle OR azimuthal coordinate
μ	absolute (dynamic) viscosity of the fluid
ν	kinematic viscosity of the fluid
ρ	density of the fluid
σ	Stephan-Boltzmann's constant
$\sigma_{i,j}$	shear stress on the i,j plane
ϕ	dependent variable
ψ	stream function
ω	vorticity

Subscripts

a	value on the jet axis
at	atmospheric value
eff	effective value of the parameter
f	flame
fu	fuel
m	maximum value
min	minimum value
mix	mixture
o	value at inlet
ox	oxidant
pr	product
r	in the radial direction
s	sphere
x	in the axial direction
θ	in the azimutal direction

ABSTRACT

The research work described in this thesis is a continuation of the previous studies carried out in the University of Glasgow on swirling jets issuing from vane swirlers.

A test-rig suitable for investigations of combustion systems was designed. The vane swirlers used for the investigations were to the same design as those used by Mathur (5) for investigating cold swirling jets. The measuring instruments were calibrated and the analysis for the temperature correction due to radiation from the thermocouple bead was carried out. For all the experiments, premixed stream of town gas and air was used.

Flame stabilisation tests were conducted mainly with hubless swirlers. With the hubless swirlers, stable flames are held at the junction of the swirler vane tips. With each of the annular swirlers, the chemical reaction started from inside the swirler tube. The results of the tests show that highly stable flames are obtainable with vane swirlers. The width of the stable flame region of the stability limits loop increases with swirl although for any given flow velocity, the fuel/air ratios at weak and rich blow-off limits increase with swirl. For flames issuing from swirlers with vane angles of 70 and 75 degrees with both geometries, wall flame jets were formed.

The aerodynamic measurements were made with hubless and annular swirlers. The analysis of the results show a strong dependence of the flow distributions in the flow field on the swirler exit conditions. As the rotational energy increases, a greater proportion of the nozzle fluid is forced into the outer part of the jet by the centrifugal forces. This concentration of stream lines causes increases in the flow velocities at those radial points in the swirler flow section as a result of which the static pressures at these points drop. The effect of this is that the maximum axial velocity components, temperatures and minimum static pressures are displaced from the jet axis near the swirler exit. The radial displacements of these aerodynamic variables increase with swirl. All the variables generally decay as the axial distance from the swirler exit increases and the rates of decay depend on the swirl number. The maximum values of the above parameters on cross-sectional planes (minimum for pressure) ultimately tend to the jet axis and the positions at which the values reach the axis depend on swirl. Throughout the lengths of the jets investigated, the static pressures remain subatmospheric.

The minimum swirler vane angle with which a recirculation vortex will be established in hubless swirler flames in 30 degrees. The corresponding angle with annular swirlers is 45 degrees. For the same swirler geometry, the characteristics and dimensions of the recirculation vortex increases with swirl.

The analyses made of the jet widths show that swirling jets expand rapidly immediately downstream of the exit and the rate of expansion increases with swirl. At sufficiently far axial distances from the swirler exit, the expansion rates become linear.

Computations of the axial fluxes of linear and angular momenta, and

and the mass flow rates at the cross-sectional planes of measurements show that the fluxes of momenta along the jet are conserved. The entrainment rates increase with swirl in both swirler geometries.

The comparison of the above results with cold swirling jets show differences in the jet developments. The minimum vane angle for the establishment of recirculation vortex in cold swirling jets increase to 45 degrees. For both swirler geometries and swirlers with corresponding vane angles, the maximum widths of the recirculation vortices increase in burning jets. The burning jets also have higher expansion and entrainment rates than the cold equivalents.

The prediction method formulated at Imperial College, London, (8),(9) was further developed for the computation of flow distributions in cold and burning swirling jets. The program was also modified for processing in a KDF9 or UNIVAC 1108 computer. The results predicted by the method are generally similar to those experimentally obtained. With specification of correct inlet profiles, the program will predict accurate results for cold jets. For burning jets, further improvements are still required in the inlet specification of the combustion parameters and also in the turbulence representation.

CHAPTER 1

GENERAL INTRODUCTION

1.1 The need for the investigation.

The effects of imposing a swirling motion on fluid flow fields have been of interest in many engineering disciplines such as aerodynamics, combustion, heat transfer and meteorology. In the design of internal combustion engines, papers have been published on this phenomenon from at least as early as 1934 but it was not until recently that interest was focussed on the effects of swirl on combustion in high output furnaces.

In order to obtain high intensity combustion, the reactants must be supplied at sufficiently high flow rates but when the component of the fluid velocity normal to the flame front exceeds the burning velocity of the combustibles, the flame will be swept away by the incoming high velocity stream. This therefore creates the problem of establishing a stable flame in a fast flowing stream. Various stabilising mechanisms have been in use in the past, the most important ones being

(a) can-type stabilisers,

(b) bluff-body stabilisers,

(c) opposed-jet stabilisers,

(d) swirling flows.

In each case, the flame is stabilised on the recirculation zone or the low velocity region within the flow field. Many reports and papers on the performance of the first three types of stabilisers and various modifications of them are available in the literature but very few (10),(11), (12) are available on flame stabilisation in flows with any form of rotation, none appears to be available on flame stabilisation in swirling flows issuing from vane swirlers. The need therefore arises for an investigation

of the effects of swirl on flame stabilisation for flows issuing from vane swirlers.

In addition to the knowledge of flame stabilisation in a combustion system, another design consideration among others, is the aerodynamic pattern of the flame. This is essential as the mixing rate of the reactants, the reaction rate, the heat release rate and the rate of wear of the combustion chamber wall depend on the aerodynamic characteristics of the flame. One approach to this aspect of the science of flames has been the use of cold models. Although the results of such tests show the general pattern of the aerodynamic variables, the high temperature gradients with the resultant high density gradients in flames cannot be taken into account whereas an observation of the Navier-Stokes equations of motion will indicate the over-riding influence of the density gradients on the aerodynamic variables.

1.2 Previous work at Glasgow University

The research programme on swirling jets in the Mechanical Engineering Department of Glasgow University was started by Kerr (1),(3),(4). He studied both cold jets and diffusion flame jets in the departmental boiler furnace using various combinations of primary and secondary swirlers. He was followed by Fraser (2),(3) who studied cold jets. Mathur (5),(6),(7) modified the design of the swirlers used by Kerr and Fraser to achieve a more effective deflection of the flow at exit. He mainly investigated free and enclosed swirling cold jets on a model test-rig.

1.3 Present work

After Mathur's experiments and considering the points discussed in Section 1.1, the logical follow-up is to carry out investigations on swirling flames. Thus the present research project was designed to further

the understanding of swirling flows by investigating the effects of swirl on combustion using the same design of vane swirlers as was used by Mathur.

For most oil burners, the properties of the flame depend, among other factors, on the transfer rates of heat, mass and momentum and also on the droplet size. In order to reduce the number of variables on which the chemical reaction will depend, a premixed stream of gaseous fuel and air was used. This eliminates the dependence of the combustion process on the mixing rate of the reactants in the flow field.

In confined flames, low frequency combustion oscillations are known to be associated with the combustion chamber dimensions (24). At this stage of the build-up of knowledge on swirling flows issuing from vane swirlers, it will be undesirable to further complicate an already complex flow field by the effects of this phenomenon, therefore, free swirling flames were studied.

The first task, which took a substantial part of the time available for the work, was the design of a combustion test-rig and the other necessary equipment for the experimental investigation.

The experimental part of the project was the investigation of flame stabilisation in swirling flows and of the aerodynamic features of free swirling flames of different swirl numbers and swirler exit geometries.

Until the recent work of Spalding et al (8) and a modification of it by Odlozinski (9), no method was available for solving the pertinent equations of motion in a reacting medium. Taking account of the economic advantages in being able to predict the distributions of the aerodynamic parameters in any flow field, the prediction method was modified for the analysis of free swirling flows with and without combustion.

CHAPTER 2

REVIEW OF LITERATURE

2.1 Introduction

Following the invention of the Bunsen burner, many papers on various aspects of flame characteristics have been published. The literature is so extensive that a comprehensive review cannot be accommodated in this thesis. Therefore, the review in this chapter is limited to some of those papers that are directly related to the present research project. Other relevant papers will be referred to at appropriate places.

2.2 On flame stabilisation

Although there is a fairly extensive literature on flame stabilisation in the first three types of stabilisers listed in Section 1.1, only very few references are available on investigations in which some form of rotation was imposed on either the nozzle stream or the flame environment.

Albright and Alexander (10) measured the stability limits, temperature and concentration profiles in free and confined cyclonic natural gas /air flames. The types of premixed and diffusion flames obtained were also observed. The cyclonic nozzle, shown in Figure 1, had inclined tangential ports drilled at 60 degrees apart on a ring. The ring was then pressed on a face-plate with a central convergent nozzle. Each of the experimental combustion chambers was 0.5 in. diameter. The lengths varied from 4 in. to 20 in. The whole nozzle mass flow was introduced through the ports except in diffusion flame studies when only air was so introduced whilst the fuel gas was injected through a central nozzle in the test apparatus. The different types of premixed free flames observed were the same as those observed in confined premixed or diffusion flames. Generally, stable flames were obtained within wider flow

conditions in the confined flames than in the free flames; the maximum blow-off velocity being 100 ft/s in free flames as compared with 700 ft/s in confined flames. The effect of increasing the length of the combustion chamber on the stability limits was found to be almost negligible, though the shorter ducts have wider range of stable flames at blow-off velocities less than 100 ft/s. In the confined diffusion flames, higher air/fuel ratios than in confined premixed flames were obtained for corresponding blow-off velocities. With a divergent section fitted to the cyclonic nozzle, maximum blow-off velocity obtained was about 900 ft/s. Compared with the results obtained for flames issuing from the convergent nozzle, smaller air/fuel ratios were recorded for corresponding blow-off velocities.

As a follow-up on previous studies on bluff-body stabilisers, Grover, Kesler and Scurlock (11) investigated the performance of a rotating bluff-body in a 1.5 in. diameter combustion chamber. The bluff-body, a 0.2 in. diameter cylindrical rod, was mounted on the lower part of the combustion chamber with its axis normal to the direction of flow. Visual observations of the premixed natural gas/air flames as well as the determination of the stability limits and combustion efficiency were the main objectives of the tests. With the stabiliser rotating at 7800 rpm, the stability limits loop obtained was smaller than that with a stationary stabiliser. This was shown mostly in the drop of the maximum blow-off velocity from about 425 ft/s for the stationary stabiliser flames to about 350 ft/s for the rotating stabiliser flames. As the speed of rotation was increased, the width of the stable flame zone of the stability limits decreased at any blow-off velocity. The reduction was more severe as the blow-off velocity decreased. Their results further showed that the volumetric heat release rate in the combustion chamber could be increased by rotating

the bluff-body stabiliser. Improvements in the combustion efficiency were obtained as the speed of rotation of the stabiliser increased.

Recently, Beer et al (12) published their findings on flames in a rotating environment. Premixed primary stream of methane/air or propane/air was introduced vertically upwards along the axis of a free rotating air environment. The rotating environment was generated by rotating a large cylindrical wire screen on its vertical axis. The effects of the rotating environment on stability limits, flame length and temperature distribution were studied in the laminar to turbulent flow range. Considerable increases in blow-off velocities at any value of fuel concentration (defined as ratio of fuel flow rate to the primary stream flow rate) were obtained with increase in the rotational speed of the screen. It was also observed that lifted flames could be re-established on the nozzle rim by increasing the speed of rotation of the environment.

2.3 On aerodynamics of swirling flows

Although swirling flows have been used for various purposes in the past, it was not until the early part of the last decade that detailed investigations started on the aerodynamic pattern of swirling flows. Since then, papers have been published on the flow patterns obtainable from different swirl generators.

2.3.1 Methods of generating swirl

Three main methods of generating swirl have been used in the past. These are

(a) by rotating the pipe

(b) by tangential entry

(c) by the use of vane swirlers.

The method of rotating a pipe was first used by Rose (15) in his experiments on axisymmetric air jets. Only weak swirl could be generated by this method even at a rotational speed of nearly 10,000 rpm and consequently this method has not been popular with investigators.

When swirl is generated by the method of tangential entry, as shown in Figure 2, part of or the whole of the nozzle mass flow is introduced into the swirl chamber through tangential ports. If part of the fluid is so admitted, the remainder will be introduced axially into the swirl chamber. Variations in the swirl intensity can therefore be obtained by varying the proportion introduced tangentially. This method has been used by many investigators (10), (13), (14) and for all investigations on swirling flows at the International Flame Research Foundation. It has therefore been established as an effective way of generating swirl. In addition to the energy lost at inlet to the swirler ports, a proportion of the rotary energy is also lost between the position of introduction and the nozzle exit as a result of viscous dissipation and pipe losses. The total energy loss was estimated as 30% in (13).

The third and probably the most common way of generating swirl particularly in combustion systems is the use of vane swirlers. Ullrich was reported in (13) to have used this method but obtained an asymmetric jet due to instability in the flow field. Kerr (1), (3),(4) and Fraser (2),(3) have used the same method. Stable axisymmetric swirling jets were obtained but no appreciable recirculation zone was reported. Mathur (5),(6),(7) modified the design of the swirlers and obtained stable axisymmetric jets with considerable recirculation zone. Many other investigators, e.g. (24) have also used vane swirlers for their investigations. The performance, therefore, of any vane swirler system will depend on the design. The deflection of the stream by the swirler vanes gives rise to a pressure drop

across the swirler. This pressure drop increases with swirl.

From the experiments of Chigier and Beer (13) and Mathur and Maccallum (6), both on annular swirling air jets, a comparison of the effectiveness of the method of tangential entry can be made with the use of vane swirlers. The result of this comparison (using the same definition of swirl) is shown in Table 1.

TABLE 1

Comparison of Methods of Generating Swirl

Method of generating swirl	Swirl number	Hub ratio	Length of recirculation zone / Outer dia. of nozzle	Max. width of recirculation zone / Outer dia. of nozzle
Tangential entry (11)	0.78	0.24	0.79	0.26
Vane swirlers (6)	0.72	0.32	3.70	0.47

A similar comparison of the dimensions of the recirculation zone in the wake of such flameholders as disc flameholders with and without divergent quarl, annular non-swirling jets, swirling jets generated by the tangential entry method and swirling jets issuing from vane swirlers had been made by Chigier and Gilbert (16) and they concluded that the size of the recirculation zone depends on

(a) swirl intensity,

(b) the blockage ratio,

(c) the geometry of the divergent wall,

and (d) the shape of the flameholder.

From the above table, it could be added that the size of the recirculation zone also depends on the method of generating the swirl.

It would also have been useful to compare the power required for generatinga finite swirl intensity using the two methods but sufficient information is not available from the literature. Fellows and Rivierre (in the discussion on reference (22)) carried out such an analysis and concluded that the mechanical devices, i.e. vane swirlers, required higher swirl generating power than the aerodynamic devices, i.e. tangential entry method. Noting the high pressure drop which can be expected from the screw-type of mechanical swirling device used by Fellows and Rivierre, it appears that the question is still open as to which of the two methods required the lesser power.

No attempt has yet been made to reduce the losses arising from the use of either the tangential entry method or the vane swirlers. When this is done, various designs of each device would be tested for performance. The criterion suggested by Ivanov (17) can be used for this assessment. The suggestion was to define the efficiency of a swirl burner as

$$E = \frac{E_o}{E_{in}} \qquad \ldots(2.1)$$

where E is the swirl burner efficiency,

E_o is the effective energy of the flow at swirler exit per unit volume of fluid

E_{in} is the energy of the flow at the swirler inlet per unit volume of fluid

$$E_o = \frac{\rho}{2g} (u_o^2 + v_o^2 + w_o^2) \qquad \ldots(2.2)$$

$$E_{in} = p + \frac{\rho \bar{v}^2}{2g} \qquad \ldots(2.3)$$

If such series of tests are properly planned the question of which of the two common methods of generating swirl required the lesser power can be quantitatively resolved.

However, from the qualitative results in Table I, the following conclusions can be made tentatively. Because of the greater volume of recirculated gases in swirling jets issuing from vane swirlers, stable flames will be obtained within a wider range of fluid flow conditions. A slightly higher rate of entrainment resulting from the possible increase in jet spread due to greater width of the recirculation vortex in jets issuing from vane swirlers can be expected. Thus some improvements in the volumetric heat release rate and the combustion efficiency may be obtained.

2.3.2 The definition of swirl

The main difference between a swirling flow and a non-swirling flow is the imposition of an angular momentum flux on the former. Any representation, therefore, of swirl must take account of this component of the momentum flux. Drake and Hubbard (18) suggested that swirl could be defined by a "median cone angle of air exit" having 50% of the air mass flow inside and the remaining 50% outside it whilst the use of the ratio of the axial flux of angular momentum to linear momentum has been suggested by Rose (13). One objection to the median cone concept is that it is not related to the axial flux of angular momentum. Also it will require experimental measurements.

The commonly used definition of swirl is the dimensionless expression

$$S = \frac{G_\theta}{G_x d_2} \qquad \ldots(2.4)$$

The nozzle geometry parameter is sometimes represented by r_2 instead of d_2. The use of an effective nozzle diameter has been suggested by Kerr and Fraser (3). This effective nozzle diameter was defined as that of an equivalent nozzle having the same flow area as that of the annular nozzle. In principle, it does not appear to matter which nozzle geometry parameter is used although the numerical values obtained will be different.

By multiplying the equations of axisymmetric, compressible, turbulent fluid motion in the axial and tangential directions by r and r^2 respectively, integrating the resultant equations from the jet axis to infinity, assuming that boundary layer approximations are applicable and neglecting the turbulent shear terms, the following equations can be derived for the axial fluxes of linear and angular momenta at any cross-sectional plane:

$$G_\theta = \int_0^\infty (p + \rho u^2)\, r\, dr \qquad \ldots(2.5)$$

$$G_x = \int_0^\infty \rho\, u\, w\, r^2\, dr \qquad \ldots(2.6)$$

At the exit plane of an annular nozzle, the integration limits will be from $(d_{1/2})$ to $(d_{2/2})$.

2.3.3 Experimental work

With a 6 in. outside diameter vertical combustion chamber, Hottel and Person (19) studied the characteristics of a vortex system with and without combustion. The air which has passed through vanes at the base of the combustion chamber was admitted tangentially into the combustor whilst the town gas was introduced through a central nozzle. A quenching

device for assessing the combustion efficiency was fitted to the top of the combustion chamber during some of the tests. In the cold tests, free and forced vortex cores were observed in the flow field. The forced vortex core occupied 80% of the chamber volume. Substmospheric static pressures were also recorded. The flow pattern was not affected by any variations of the flow rate or the vane setting. In the combustion tests, the combustion efficiency was independent of vane setting but varied with the length of the combustion chamber and the fuel/air ratio. The recirculation zone whose presence was assumed at the beginning of the experiment was found to be very insignificant.

As a continuation of their work on cyclonic flames, Albright and Alexander (20) used a modified form of their cyclonic nozzle (as in (10)) for measuring impact pressures, static pressures, temperatures and gas composition in confined cold jets and cyclonic flames. The vanes in the cyclonic nozzle were positioned with discs of various sizes. The impact pressures were measured with a calibrated pitot tube which could berotated from zero to 360 degrees. The impact pressure was taken as the maximum value at any measuring position and the static pressure taken as the value at 51 degrees from the position of the maximum pressure. Subatmospheric static pressures were recorded at all points in the flow field. Small recirculation zones were also observed. With premixed streams, flash-back occurred. This was eliminated by increasing the size of the positioning disc or by introducing the air and fuel in different streams. Differences between the profiles obtained in cold flows and those in the flames were reported.

Baluev and Troyankin (21) have investigated the flow distributions in an air model of a cyclone chamber. The fluid was let into the cyclonic

nozzle from a number of tangential ports. The effects of variations of the number of tangential parts, cyclone chamber height, diameter of exit, chamber wall condition and the relative cross-section of the tangential ports on the flow distribution were studied. The presentation of the results in the aforementioned paper was very brief and most of the results were not shown probably because of space limitation. However, the results shown in the paper did point out interesting features of the flow pattern in the cyclonic chamber. Five flow zones were identified in the chamber. Near the nozzle end of the chamber the central downstream flow zone was surrounded by an annular reverse flow zone. An annular downstream flow zone surrounding the first recirculation zone was also surrounded by another recirculation zone. Between this second recirculation zone and the chamber wall was the fifth flow zone which was a downstream flow zone. The pattern of the flow zones changed as the exit was approached. It can be surmised that the pattern of the flow will depend more on the diameter of the exit and combustion chamber diameter than any of the other relevant factors.

Ullrich was reported in (13) to have studied annular swirling jets issuing from vane swirlers but could not take measurements near the swirler exit because of the asymmetry in the jet. The first quantitative measurements on the aerodynamics of swirling flows was made by Rose (15) whose method of generating swirl was discussed in Section 2.3.1. The 17/32 in. bore and 100 diameters long pipe was rotated at 9500 rpm. Measurements of the mean velocities and turbulence intensities in air jets were made with a calibrated hot-wire anemometer. The results of the axial velocity profiles in the swirling jets were very similar to those of the non-swirling jets even at an axial distance of about 0.2 nozzle diameter from the

nozzle exit. This indicated that the swirl in the flow was very weak. Nonetheless, few characteristics of swirling flows were indicated by the results. At the same Reynold's number, the jet width, rate of decay of the axial velocity components along the jet axis and the rate of entrainment of ambient fluid along the length of the jet were slightly higher in the swirling jet than in the non-swirling jet.

Most of the recent papers have originated from the International Flame Research Foundation where various facets of the characteristics of confined swirling cold jets and diffusion flames have been studied. The combustion experiments were mainly on pressure-jet oil flames. The swirl in both cold and combustion investigations were generated by using tangential entry method. A detailed review of the various studies on annular swirling and non-swirling jets has been given by Chedaille, Leuckel and Chesters (22). In both cold and combustion studies, the boundaries of the recirculation zones were mapped and the effects of different swirl numbers and different divergent quarl geometries on the size of the recirculation vortices were reported. The critical swirl levels above which recirculation zones would be set up for different semi-divergent angles were determined. In the combustion tests, the atomised oil was sprayed into the recirculation vortex. The main conclusions were

(a) That the small recirculation wake just downstream of a bluff-body could be extended by using a divergent nozzle or swirl. Further increase of the size of the recirculation vortex could be obtained by increasing the swirl number but as the swirl number increased, the effect of the bluff-body on the recirculation vortex size decreased.

(b) That the combination of large divergent angles or narrow chambers with swirl would produce open-ended recirculation zones which would consequently result in the formation of wall jets.

(c) That shorter flame lengths and very high combustion intensity could be obtained by using swirl.

Using multi-concentric tubes for primary and secondary air streams with a rather complex vane system, Shagalova, Shnitser and Gromov (23) studied the aerodynamics of the flow in free bituminous coal flames. Large recirculation zones were detected. The distributions of the velocity components and static pressures were presented. It was observed that when ignition started near the nozzle exit, there was charring of the nozzles and slag formation on the burner.

Studies of the aerodynamics and combustion chamber performance of pressure-jet burner flames with vane-swirled oxidant stream have been carried out by Brown and Thring (24) in a marine-type boiler furnace and in a scaled-down model. In the aerodynamic investigations, measurements of the distributions of temperature, velocity components and combustion efficiency were made at various spray angles. The results showed that the spray angle had no effect on the relative velocity distribution but had dominant effect on the distribution of the fuel concentration. Central recirculation zone containing about one third of the nozzle mass flow and an outer recirculation zone containing about twice the nozzle mass flow were obtained in the flow field. The analysis of the combustion efficiency showed that as far as the heat release rate in the initial region of the flame was concerned, the outer recirculation zone had no significant effect. Based on the experimental results, the following suggestions for improving combustion in systems similar to that studied were given.

(a) The use of multi-atomiser per burner,

(b) The use of small refractory-lined combustion chamber.

(c) Altering the aerodynamic pattern of the air stream by either injecting air upstream from behind the flame or using flows with higher swirl.

Suggestions for the improved design of multi-burner combustion systems and for more effective heat transfer to water tubes in boilers were also given. From the flow patterns obtainable in a cyclone chamber, as shown by the work of Baluev and Troyankin (21) reviewed above, it appears that improved combustion efficiency and possibly higher heat releast rates could be achieved by using a cyclone chamber with the pressure jet burner. This will be so because of the heating effect of the outer recirculation zone which will extend nearly up to the nozzle inlet. Furthermore, the downstream flow of air at the wall of the combustion chamber will provide the required oxygen for combustion and this will eliminate the region of excessively rich mixture at the upstream corner of the combustion chamber. In fact, with the use of multi-atomisers per burner suggested by Brown and Thring, there appears to be a possibility of establishing about three annular flame fronts at the three low velocity regions between the reverse flow and forward flow zones.

Chigier and Chervinsky have carried out studies on the aerodynamics of free premixed swirling flames using butane/propane/air mixture. The tests were carried out for weak and moderate swirl. The flames obtained were stabilised at axial positions varying from 4.0 to 6.0 nozzle diameters from the exit. Detailed results of the distributions of the velocity components and temperature were presented. The axial and tangential velocity components were represented by similar profiles. This paragraph refers to (14).

In addition to the investigations on flow distributions in swirling flows, experiments have been conducted to assess the effects of swirl on flame length in diffusion flames. Assuming that the process of mixing could be described by the same phenomenon as entrainment, Cude (25) modified the entrainment equation derived by one of his contemporaries to obtain an expression for the flame length in swirling and non-swirling flames as

$$L = A \cdot \frac{\dot{m}_{fu}}{G_x} \qquad \ldots(2.7)$$

where A is a constant.

He conducted experiments to determine the numerical value of the constant A in swirling and non-swirling town gas or gas oil flames at various fuel/air ratios. The swirl was generated by tangential entry method. He found that the equation was applicable to non-swirling and swirling flames but not for flames resulting from the mixing of two streams or for flames in a combustion chamber whose diameter is less than one third of the free flame length. From his experimental measurements, shorter flames were observed with increase in swirl. Similar analytical and experimental investigations have recently been carried out by Maier (26) on swirling flames in a stagnant environment and by Beer et al (12) on non-swirling jet flames in a rotating environment. Maier recorded shorter flames with increasing swirl but Beer et al obtained longer flames with increase in the rotational speed of the environment. The explanation for this was the reduced entrainment resulting from the free vortical motion of the surroundings.

2.3.4 Previous work in Glasgow University

The research programme on swirling jets in Glasgow University was started independently but almost at the same time as at the International Flame Research Foundation by Kerr (1),(3),(4), Fraser (2),(3) and Mathur (5),(6),(7) have since worked on various aspects of the programme. The method of generating swirl has been the use of vane swirlers.

The first report was submitted by Fraser who mainly measured the nozzle reaction thrust and torque in cold jets. The measured values were compared with values obtained from velocity profiles and good agreement was obtained.

Kerr investigated air jets and confined diffusion flames in the Departmental boiler furnace using different combinations of angled slots for primary air and vane swirlers for secondary air. Measurements of velocity and temperature distributions were made. In the cold tests, the distribution of axial velocity components at any cross-sectional plane was represented by Gaussian error function. The axial fluxes of linear and angular momenta were found to be conserved along the length of the jet. In the combustion tests, optimum flame characteristics were obtained with swirl numbers varying between 0.1 and 0.3. The swirl number was calculated from the sums of the axial fluxes of linear and angular momenta in the primary and secondary streams and the effective diameter (discussed in Section 2.3.2) of the burner nozzle was used.

Whilst Kerr's and Fraser's investigations were still in progress, Mathur started his investigation on a cold model of the Departmental boiler furnace. This was necessitated by the limitations of the measurements taken in the furnace by Kerr. He modified the design of the vane swirlers to direct the stream more effectively. He carried out experimental

investigations of the pressure drop across the swirlers, velocity distributions across and along the air jets. Measurements of the static pressure along the jet axis were also made. In confined air jets, measurements of velocity and concentration profiles were made. Upstream of the position where the jets impinged on the duct wall, the velocity profiles were found to be the same as in free jets. Recirculation zones were found to be present in hubless swirler jets of vane angles of 45 degrees and above. Similar zones were detected in annular swirler jets with the same vane angles. In each swirler geometry, the size of the recirculation zone varied with swirl.

2.3.5 Theoretical work

A direct solution of the equations of motion in an axisymmetric compressible swirling flow is almost impossible with the present state of knowledge on the analysis of partial differential equations. Few methods are available for finding approximate solutions to the equations. These are:

(a) integral method,

(b) linearisation,

(c) method of undetermined coefficients,

(d) transformation of the equations of motion,

(e) finite-difference method.

Boundary layer approximations are usually invoked and the effects of turbulence are either neglected or the turbulence parameters substituted into solutions for laminar flow.

The integral method has been used by Lee (27) and by Chigier and Chervinsky (14),(28). In these analyses, the flow was assumed to be fully developed jet flow and thus self-preserving. The velocity distributions

were represented by

$$u = f_1(x) \cdot f_1(\eta) \qquad \ldots(2.8)$$

$$w = f_2(x) \cdot f_2(\eta) \qquad \ldots(2.9)$$

Lee assumed that

$$f_1(\eta) = \exp.\left[-\frac{r^2}{\phi(x)}\right] \qquad \ldots(2.10)$$

$$f_2(\eta) = f\left[\frac{r}{\phi(x)}\right] \qquad \ldots(2.11)$$

Chigier and Chervinsky assumed that

$$f_1(\eta) = f\left(\frac{r}{x+a}\right) \qquad \ldots(2.12)$$

$$f_2(\eta) = A\eta + B\eta^2 + C\eta^3 \qquad \ldots(2.13)$$

The solutions from the above are only applicable to flows with weak swirl and within this limitation, agreement with experimental results is good.

Linearised solutions have been published by Steiger and Bloom (29) and by Lewellen (30) for laminar incompressible flows.

The main set-back of the two methods discussed above is that some functional relationship in the final solution will have to be determined empirical or an assumption made about the distributions of the dependent variables. In the linearised solutions in particular, the solution procedures for the final equations are usually complex. The draw-back was eliminated in the analysis carried out by Loitsyanskii (31) in which he used the method of undetermined coefficients. He represented the stream function, swirl velocity and static pressure in a laminar incompressible swirling flow by series expressions whose terms have variable coefficients. These were substituted into the Navier-Stoke's equations of motion and also into the equations expressing the conservation of axial fluxes of linear and angular momenta. Equating the coefficients of like powers of the

axial coordinate, the following relations were obtained

$$u = \frac{2\alpha^2}{(1+\alpha^2\eta^2/4)^2} \cdot \frac{1}{x} - \tfrac{1}{2}\beta\alpha^2 \cdot \frac{1-3\alpha^2\eta^2/4}{(1+\alpha^2\eta^2/4)^3} \cdot \frac{1}{x^2} \qquad \ldots(2.14)$$

$$v = \nu^{\frac{1}{2}}\left[\frac{\alpha^2\eta^2(1-\alpha^2\eta^2/4)}{(1+\alpha^2\eta^2/4)^2} \cdot \frac{1}{x} - \tfrac{1}{2}\beta\alpha^2 \cdot \frac{\eta\,(1-3\alpha^2\eta^2/4)}{(1+\alpha^2\eta^2/4)^3} \cdot \frac{1}{x^2}\right] \qquad \ldots(2.15)$$

$$w = \gamma \frac{\alpha\,\eta}{(1+\alpha^2\eta^2/4)^2} \cdot \frac{1}{x^2} \qquad \ldots(2.16)$$

$$p = -\frac{2}{3}\gamma^2 \cdot \frac{1}{(1+\alpha^2\eta^2/4)^3} \cdot \frac{1}{x^4} \qquad \ldots(2.17)$$

where

$$\eta = \frac{r}{x} \cdot \nu^{-\frac{1}{2}} \qquad \ldots(2.18)$$

$$\alpha = \left(\frac{3\,G_x}{16\,\pi\mu}\right)^{\frac{1}{2}} \qquad \ldots(2.19)$$

$$\beta = \frac{u_o \cdot d_o^{\,2}}{8\,.\nu} \qquad \ldots(2.20)$$

$$\gamma = \frac{3\,G_\theta}{64\,\pi\,\mu^2} \cdot \left(\frac{3\,\rho\,G_x}{\pi}\right)^{\frac{1}{2}} \qquad \ldots(2.21)$$

By substituting the turbulent values of μ and ν into the above equations solutions for the turbulent case can be found. The above analysis has been carried a step further by Fal'kovich (32) who has calculated the third and fourth terms of the expressions. The application of the above solutions together with Fal'kovich's additional expressions is limited to flows without recirculation.

On the method of transforming the equations of motion, Ustimenko (33) rearranged the cylindrical polar coordinates such that the axial coordinate is represented by

$$\eta = f(x) \qquad \ldots(2.22)$$

keeping the radial coordinate unaltered. The equations of motion were written as follows:

x-momentum: $$\frac{\partial \bar{G}}{\partial \bar{\eta}_g} = \frac{\partial^2 \bar{G}}{\partial \bar{r}^2} + \frac{1}{\bar{r}} \frac{\partial \bar{G}}{\partial \bar{r}} \qquad \ldots(2.23)$$

θ-momentum: $$\frac{\partial \overline{(\rho w^2)}}{\partial \bar{\eta}_t} = \frac{\partial^2 \overline{(\rho w^2)}}{\partial \bar{r}^2} + \frac{1}{\bar{r}} \frac{\partial \overline{(\rho w^2)}}{\partial \bar{r}} \qquad \ldots(2.24)$$

r-momentum: $$\frac{\overline{(\rho w^2)}}{\bar{r}} = \frac{\partial \bar{p}}{\partial \bar{r}} \qquad \ldots(2.25)$$

Continuity: $$\frac{\partial \overline{(r \rho u)}}{\partial \bar{x}} + \frac{\partial \overline{(r \rho u)}}{\partial \bar{r}} = 0 \qquad \ldots(2.26)$$

where

$$\bar{G} = \frac{p + \rho u^2}{(p + \rho u^2)_o} \qquad \ldots(2.27)$$

$$\overline{(\rho w^2)} = \frac{\rho w^2}{(\rho w^2)_o} \qquad \ldots(2.28)$$

$$\bar{p} = \frac{p}{(\rho w^2)_o} \qquad \ldots(2.29)$$

$$\overline{(\rho u)} = \frac{\rho u}{(\rho u)_o} \qquad \ldots(2.30)$$

$$\overline{(\rho v)} = \frac{\rho v}{(\rho u)_o} \qquad \ldots(2.31)$$

$$\bar{x} = \frac{x}{r_o}, \quad \bar{r} = \frac{r}{r_o} \qquad \ldots(2.32)$$

$$\bar{\eta}_i = \frac{\eta_i}{r_o^2} \qquad \ldots(2.33)$$

(Suffix o refers to value at nozzle exit)

Using the appropriate boundary conditions and assuming an initial distribution of $f_o(r)$ at nozzle exit, the final solution was given as (for $\bar{G}$)

$$\bar{G}(\eta_g, \bar{r}) = \frac{\exp\left(-\frac{\bar{r}^2}{4\bar{\eta}_g}\right)}{2\bar{\eta}_g} \int_0^{r_o} f_o(r) \exp\left(-\frac{r^2}{4\bar{\eta}_g}\right) I_o\left(\frac{\bar{r}r}{2\bar{\eta}_g}\right) r\, dr \qquad \ldots(2.34)$$

where I_o is the Bessel function of zeroth order. It will be observed that the original equation (2.23) and its solution is the same as that of heat conduction in an infinite circular cylinder with initial temperature distribution of $f_o(r)$ (34). Equation (2.34) can be analysed using P-functions as tabulated by Masters (35) or by the use of what Ustimenko called "hydrodynamic integrands". The only empirical requirement is the dependence of η on x and this can be obtained by comparing the values obtained analytically with those experimentally determined on the jet axis. It is however not clear how this method will do for the analysis of the dependence of η_t on x as the value of (ρw^2) on the axis will be zero and its boundary conditions different from those of $\bar{G}$. However, very good agreement was obtained with experimental results (Figure 3) using the "hydrodynamic integrands" even when there was a recirculation vortex.

Recently Spalding et al (9) published a convenient finite difference method of solving the equations of motion in a general stream with recirculation. This method is the basis of the theoretical work to be discussed in Chapter 7 of this thesis and further details will therefore be given therein.

CHAPTER 3

EXPERIMENTAL DETAILS

3.1 Introduction

To execute the experimental programme, a test rig was designed to supply the required premixed combustible streams for the swirling flames issuing from hubless and annular swirlers. Allowance was also made for easy modification of the test rig for the study of diffusion flames with swirled or unswirled secondary and/or primary flow. The flow rates of the reactants were regulated by gate valves or by the speed controls installed on the drives of the superchargers and the flow rates were metered with square-edged orifice plates. As a precaution against any possible hazard, safety devices were incorporated on the test rig. A flue ducting was connected to a large chimney to carry the combustion products into the atmosphere.

The various swirlers to be used for the investigation were designed. Water-cooled probes for the aerodynamic measurements were also designed. The three-dimensional probe for velocity measurements was calibrated and an analysis of the temperature correction for radiation loss in the flame was carried out. For the accurate positioning of the probes and the determination of the axial and radial positions of measurement, a traversing mechanism was designed.

3.2 Description of the experimental test rig.

The general lay-out of the various parts of the test rig and further details of it are shown in Figures 4 (a) to (c).

3.2.1 The air flow-line.

Oil-free compressed air was delivered from a 14-piston Wellworthy-Ricardo supercharger into a 3 in. nominal bore steel pipe. The supercharger was driven by a 10 h.p. electric motor. A gate valve, square-edged orifice plate, pressure tappings located upstream and downstream of the orifice plate position and a thermometer pocket were incorporated in the air flow-line whose downstream end was connected to the mixing box. A bleed line with a separate gate valve was connected to the air flow-line near the supercharger.

3.2.2 The gas flow-line

A 3 in. nominal bore steel pipe conveyed the gas from the meter outlet to the modified inlet of a 14 cylinder Wellworthy-Ricardo supercharger driven via a speed reduction system by a 10 h.p. electric motor. Between the gas meter and the supercharger inlet, a non-return valve and a gate valve were fitted to the flow-line. A low pressure switch was also positioned near the supercharger end of the pipe line. The supercharger outlet led to a 1.5 in. nominal bore steel pipe on which a gate valve, square-edged orifice plate, pressure tappings and a thermometer pocket were provided. An electrically operated quick closing valve was also fitted to the gas flow line whose downstream end was connected to the mixing box.

3.2.3 The mixture flow lines

The mixture from the mixing box is discharged into the distributing box and between both boxes, a wire mesh and a convergent-divergent section having a 6 in. long throat and 1 in. inside diameter were fitted. The purpose of the convergent-divergent section was to provide a flow section of higher velocity gradients and thus increased turbulence intensity to

promote more homogeneous mixing of the reactants. The mixture from the distributing box can be allowed into either the primary flow line for investigations with hubless swirlers or into the secondary flow line for experiments with the annular swirlers. The burner ends of the flow lines are shown in Figure 5.

3.2.3.1 The secondary flow line

A horizontal 3 in. nominal bore and about 9 ft long steel pipe fitted with a gate valve was connected to the distributing box. A 90 degrees elbow of the same section linked the downstream end of the pipe to a short vertical pipe length of the same section from the upstream flange of the flame trap housing. The other end of the flame trap housing was connected via a short 3 in. nominal bore steel pipe to a small horizontal cylindrical tank. A gently tapered section welded to a 4 in. nominal bore and about 3.5 ft. long steel pipe was welded to the downstream end of the cylindrical tank. The downstream end of this section was gently tapered and a 6 in. long steel pipe of the same internal diameter as the outermost diameter of the annular swirler having the same outside diameter as the 4 in. pipe was welded to it. Allowance was also made for fitting the annular swirlers at the end of the flow line as shown in Figure 5. To ensure that each swirler would be fitted in the same position as in previous runs, a mark was made at the end of the secondary flow line. The outer pipe of the flow line was supported by a screw rod of adjustable length on a framework fixed to the laboratory floor.

3.2.3.2 The primary flow line

This was made of a vertical 1.5 in. nominal bore steel pipe with a gate valve near the distributing box. A 90 degrees elbow linked this pipe to a horizontal pipe of the same size and material and the downstream end

of the horizontal pipe was fitted to the flame trap housing flange. The downstream flange of the flame trap housing was connected to a 46 diameters long and 1 in. nominal bore steel pipe. A 6 in. long pipe with a gentle taper at its upstream end was welded to the 1 in. pipe. The taper on the 6 in. long pipe reduced the pipe bore to that of the hubless swirlers. A short stud was welded to the stepped end of this section to enable the hubless swirlers to be fitted in the same position as in previous runs. The primary flow line was passed coaxially through the secondary flow line beginning at the upstream end of the small cylindrical tank and it was welded to both ends of the cylindrical tank. Near the exit, the primary flow line was supported by three screw rods at 120° apart. The axis of the combination was 4.5 ft. from the floor level.

3.2.4 Control of motor speed.

Each of the electric motors had a variable speed device fitted to the drive shaft. On to this device, in each case, was fitted a 6 in. diameter aluminium pulley. This pulley was connected via a 3 in. diameter steel pulley to a turning handle located at a convenient place. The metal surface in the recess of each pulley was covered with rubber strip to prevent the connecting cable from slipping.

For the electric motor on the gas flow line, it was necessary to use a speed reduction system because it was not desirable to provide a bleed line. It is, of course, possible to connect a bleed line from near the supercharger outlet to the inlet pipe but this would lead to pressure build-up in the inlet pipe which will not be desirable. The speed reduction system was made up of two small pulleys, two bigger pulleys, two connecting belts, a central shaft and two blocks. For the hubless swirler experiments,

the system was designed for a speed ratio of 9:1 whilst the ratio was 3:1 for the annular swirler experiments.

3.2.5 The flue ducting

This included a water-cooled canopy, 3 ft. x 3 ft. at inlet connected to a 1.5 ft. diameter pipe which delivered the combustion products into the chimney at 16 ft above the floor level. The canopy inlet was positioned at about 5 ft. from the nozzle exit of the swirlers. The drawing of the flue ducting, whose photograph is shown in Figure 6, was prepared by the departmental draughtsman.

3.2.6 Safety devices

As a precautionary measure, various safety devices were designed. These devices can be classified as mechanical, electrical and electro-mechanical devices.

The mechanical devices were commercial flame traps and polythene bursting discs. One flame trap of appropriate size was fitted in each of the mixture flow lines and one bursting disc, 0.025 in. thick and 5 in. effective diameter, was fitted at the bottom of each of the mixing and distributing boxes. The flame trap was provided to extinguish the flame if there was any flashback whilst the bursting discs were installed to prevent the test rig from being blown into pieces if there was any explosion.

A photo-electric flame detector whose circuit diagram is shown in Figure 7 and a low pressure switch actuated by the static pressure in the gas flow line at inlet to the supercharger were connected independently to the gas line electric motor starter. The photo-electric flame detector was designed and made with the assistance of one of the technicians in the Electrical Engineering Department. The purpose of the flame detector was to stop the gas supply motor instantly if flame should flashback. The low

pressure switch was fitted into the test rig to stop the gas supply motor immediately the pressure in the inlet pipe was 0.1 in. mercury below atmospheric. This was to prevent the supercharger from drawing air from pipe joints into the gas supply lines in the neighbourhood if there should be a supply failure.

The electro-mechanical device, a coil-operated quick closing valve actuated by the gas supply electric motor starter, was fitted into the gas flow line. The valve is fully opened when the electric motor is switched on but is almost closed when the motor is switched off. The reason for fitting this unit in the test rig now follows. When the electric motor driving the supercharger is stopped, the pumping of the gas does not stop immediately because of the inertia which has been acquired by the pumping unit. The pumping continues at reducing rates as the inertia of the pumping unit is being reduced by frictional forces until such a time that the inertia can no longer overcome the frictional forces. Although this time is of the order of about 10 to 30 seconds, (depending on the initial running speed) it can be fatal in case there is a flashback to have the gas still being supplied as this will result in the flame travelling further back through the combustible mixture despite the fact that the electric motor has been stopped by the flame detector circuit. Therefore the unit was installed to reduce the gas flow rate to a negligible trickle immediately after the gas motor is switched off so that with the air flow rate still at its initial level, the mixture will be too weak to cause any danger.

3.2.7 Flow metering

The flow rates of the reactants were measured with square-edged orifice plates with four D and 0.5 D pressure tappings (D = pipe inner diameter). For experiments with the hubless swirlers, orifice plate diameter of $^{1}/_{3}$D was used for the plates in each of the fuel and air supply lines. To cope with the increased flow rates required for the annular flame experiments, orifice plate diameters of $\frac{1}{2}$D and $^{3}/_{5}$D were used in fuel and air supply lines respectively. All the orifice plates and adjacent pipe lengths upstream and downstream of the orifice plate location were designed according to British Standard (36) specifications.

As a result of the distrubance which a thermometer pocket would cause if installed in the same plane as the upstream pressure tappings, the thermometer pocket was recommended to be installed downstream of the orifice plate location. The corrections necessary for the accurate determination of the fluid temperatures at the plane of the upstream tappings were determined for each orifice plate and the results are shown in Figure 8(a) to (d).

The pressure differential across the orifice plate for each flow line was measured with water manometers. In the aerodynamic investigations with hubless swirlers, the manometers were inclined at 5 degrees to the horizontal. The upstream static pressure for each flow line was measured with a U-tube mercury manometer.

3.2.8 The traversing mechanism

Photograph of the mechanism during its alignment to the jet axis is shown in Figure 9.

3.2.8.1 Description

The main units of the traversing mechanism are the upper and lower aluminium blocks, screw rods, plain steel rods, turning handles, measuring scales, a vernier scale and a steel framework.

The upper aluminium block is carried by a screw rod and slides vertically on a plain steel rod. A central 1 in. diameter hole was drilled $\frac{3}{4}$ in. from the top of the block for inserting the probe carrying sleeves. The steel rod is screwed into a brass piece which was pressed into the lower aluminium block and the screw rod sits on a similarly fitted brass piece in the lower block. The lower block is carried by a screw rod supported by two steel rods on either side of the screw rod. The ends of the rods carrying the lower block were positioned in aluminium blocks mounted on the framework. One turning handle was fixed to the end of each screw rod and two scales were positioned for measuring the horizontal and vertical distances. A probe supporting unit was also fitted at the back of the upper block to keep the axis of the probe horizontal.

3.2.8.2 Alignment of the traversing mechanism with the jet axis

A 1.5 x 1.5 in section aluminium bar, 24 in long was machined to fit into a dummy "secondary swirler" positioned in the secondary flow-line. Using a spirit level, the screw rod supporting the end-pipe of the secondary flow line was adjusted until the pipe axis was horizontal. With another aluminium bar fitted into the hole of the upper block of the traversing mechanism and carrying a dial gauge at its other end, the position of the framework was adjusted until the change in the reading on the dial gauge, when moved along the surface of the rectangular bar to the downstream end was negligible. The alignment error in the 18 in. working length of the rectangular bar was 0.002 in.

With a spirit level, the framework was also adjusted into a horizontal position before it was fixed to the laboratory floor.

3.3 The reactants

Premixed stream of town gas and air was used for all the experiments. A sample of the gas from the laboratory was analysed and found to agree in composition with analysis at the Gas Works. The composition of the gas varied slightly from time to time. A typical composition of the gas is shown in Table 2(a) and the results of the calculation of some of its properties are shown in Table 2(b).

TABLE 2(a) Composition of Fuel

Constituent	% Composition by volume
H_2	55.6
CO	04.0
CH_4	15.0
C_2H_4	00.8
C_2H_6	01.1
C_3H_8	01.4
C_4H_{10}	02.8
C_nH_m	00.0
CO_2	16.3
N_2	02.3
O_2	00.7

C_nH_m represents the unsaturated hydrocarbon content.

TABLE 2(b) Some Properties of the Fuel

Stoichiometric fuel/air ratio by volume	0.232
Net calorific value (Btu/ft^3) at S.T.P.	474
Molecular weight	15.5
Density (lb_m/ft^3)	0.04

3.4 The vane swirlers

Annular and hubless swirlers of vane angles 15°, 30°, 45°, 60°, 70° and 75° were prepared according to the modified design of Mathur (5) and the design parameters are shown in Table 3. The vane angle is defined as the

TABLE 3

Design Parameters for Annular Swirlers (see Figure 10(b))

Parameter	Value
Z1	$\frac{d_1 \sin \frac{\delta}{2}}{\tan \theta}$
Z2	$\frac{d_2 \sin \frac{\delta}{2}}{\tan \theta}$
Z3	$\frac{d_1 \sin \frac{\delta}{2}}{\sin \theta}$
Z4	$\frac{d_2 \sin \frac{\delta}{2}}{\sin \theta}$
Z5	$0.5 \left(d_2 - d_1 \cos \frac{\delta}{2}\right)$
Z6	$0.5 (d_2 - d_1) \cos \frac{\delta}{2}$
Z7	$0.5 (d_2 - d_1)$

where θ = swirler vane angle

δ = angle at the vane tip (= 75°)

angle of inclination of each swirler vane to the swirler tube axis. Both types of swirler geometries are shown in Figure 10(a) to (e).

Except for annular swirlers with vane angles of 15° and 30°, each annular swirler has an overlap of 30° between adjacent vanes. For the 15° and 30°, annular swirlers, the overlaps are -13° and 27° respectively. The overlaps for the hubless swirlers can be taken as corresponding to that of the equivalent annular swirlers because the design principles are the same.

Each hubless swirler was made of an 8 in. long brass tube, 0.934 in inner diameter and 1.114 in. outer diameter at the exit end. Eight brass vanes, each 0.020 in. thick, were positioned in slots cut through the swirler tube wall and silver-soldered internally and externally. Theoretically, all the vane-tips should meet on the swirler axis but this is not practicable because of the thickness of each vane.

The outer tube of each annular swirler was made of 3.86 in. internal diameter, 4.110 in. outer diameter and 6 in. long brass tube. The brass inner tube has an outer diameter of 1.25 in., an internal diameter of 1.114 in. and a length of 7 in. Initially, eight brass vanes, each 0.020 in. thick, were silver-soldered in slots on the inner tube. They were then machined to fit perfectly into the outer tube before being silver-soldered to it. When these swirlers were used in the test run, the vanes were destroyed by the flames. New swirlers were therefore made using 0.032 in. thick mild steel vanes. Three studs were also silver-soldered between the outer surface of the inner tube and the inner surface of the outer tube. These studs, positioned near the upstream end of the swirler, were used to reduce the strain on the vanes.

3.4.1 Swirler positioning

Three $\frac{1}{4}$ in. diameter holes were provided 5 in. from the annular swirler exit and three corresponding tapped holes were provided at the swirler end of the secondary flow line. By means of this arrangement, the annular swirlers could be fitted rigidly in position. In order to fix the swirler in the same position for each run, a mark corresponding to that on the downstream end of the secondary flow pipe was made on each swirler. For each annular swirler, a dummy "primary swirler" with blanked off flow area was provided. The downstream surface of this tube was made flush with the downstream end of the swirler's inner tube. The upstream end of each tube was made to fit into the primary flow line.

To position the hubless swirlers, a dummy "secondary swirler" with blanked off flow area, of the same dimensions and features as the experimental annular swirlers was made. As will be observed in Figure 10 (a), the hubless swirler dimensions are such that it would fit into this tube up to the last 1 in. at the upstream and where its outer diameter is the same as that of the inner tube of the annular swirler. A notch was provided at the upstream end of each hubless swirler to fit into the stud at the downstream end of the primary flow line. This, together with the dummy swirler fixed to the outer pipe of the secondary flow line, prevented any movement of the swirler in any direction and also allowed the swirler to be fitted in the same position for each run.

3.4.2 Swirl numbers

Consider an annular swirler with vane angle θ. Let the resultant velocity vector parallel to the plane of the vane surface be $\bar{V}$. The axial and tangential velocity components at exit are

$$u_o = \bar{V} \cos \theta \qquad \ldots(3.1)$$

$$w_o = \bar{V} \sin \theta = u_o \tan \theta \qquad \ldots(3.2)$$

(radial velocity component negligible).

Assuming further that the pressure term in the equation for axial flux of linear momentum is negligible, the following expressions are obtained

$$G_x = 2\pi \int_{\frac{d_1}{2}}^{\frac{d_2}{2}} \rho u_o^2 r \, dr \qquad \ldots(3.3)$$

$$G_\theta = 2\pi \int_{\frac{d_1}{2}}^{\frac{d_2}{2}} \rho u_o w_o r^2 dr = 2\pi \int_{\frac{d_1}{2}}^{\frac{d_2}{2}} \rho u_o^2 \tan \theta \, r^2 dr \qquad \ldots(3.4)$$

From the definition of swirl

$$S = \frac{G_\theta}{G_x d_2} = \frac{\tan \theta}{d_2} \left\{ \frac{\int_{\frac{d_1}{2}}^{\frac{d_2}{2}} \rho u_o^2 r^2 \, dr}{\int_{\frac{d_1}{2}}^{\frac{d_2}{2}} \rho u_o^2 r \, dr} \right\} \qquad \ldots(3.5)$$

For constant density and uniform profile of u_o,

$$S = \frac{\tan \theta}{3 d_2} \left[\frac{d_2^3 - d_1^3}{d_2^2 - d_1^2} \right] \qquad \ldots(3.6)$$

$$= \frac{\tan \theta}{3} \left[\frac{1 - Z^3}{1 - Z^2} \right] \qquad \ldots(3.7)$$

where $Z = \frac{d_1}{d_2}$ the hub ratio

For a hubless swirler, $Z = 0$ and

$$S = \frac{\tan \theta}{3} \qquad \ldots(3.8)$$

The swirl numbers of the experimental swirlers are shown in Table 4, hub ratio for the annular swirlers being 0.3238.

TABLE 4 Swirl Numbers of Experimental Swirlers

Vane Angle (degrees)	Swirl Numbers	
	Hubless swirlers	Annular swirlers
15	0.0893	0.0965
30	0.1925	0.2078
45	0.3333	0.3599
60	0.5774	0.6236
70	0.9158	0.9891
75	1.2440	1.344

3.5 Ignition of the flames

The flames were ignited by means of a premixed flame of butane and air. Stabilisation of the pilot flame was ensured by using a rod stabiliser fixed in a short duct which was pressed into the copper pipe at exit. As soon as the main flame was ignited, the pilot flame was removed from the flow region.

3.6 Measuring instruments

Instruments were designed for measuring the flow velocities, static pressures and temperatures. All the measuring probes were water-cooled and the water-cooling jacket constituted the probe stem. Each of the measuring probes was aligned to the jet axis. This was carried out by inserting a conical block in the dummy "primary swirler" fixed in the flow line and adjusting the probe position until its working section touched the tip of the conical block. The probe stem was then marked. By this means, the zero of the vertical scale was simultaneously determined.

3.6.1 For velocity measurements

The velocity distributions in a three-dimensional flow field, such as in a swirling jet, are usually measured with three-dimensional probes (hereafter referred to as 3-D probes). Various designs of 3-D probes are available in the literature (37) among them the five-hole spherical probe by Lee and Ash (38) and a pitch and yaw meter by Merrington (39). An automatic balancing system for five-hole probes has been designed by Taylor and Davies (40).

3.6.1.1 The 3-D probe

Fechheimer (41) showed that for a $\frac{1}{4}$ in. diameter cylinder placed across a stream, the pressure on the surface of the cylinder at a point 40 degrees from the stagnation point would be equal to the static pressure of the fluid at that point. Thus by providing a second hole at equivalent position on the other side of the stagnation point, the tube can be used to measure the yaw angle of the flow at any point. The yaw angle is defined as the inclination of the plane containing the velocity vector to the horizontal plane of the jet axis.

The design of the tube used by Albright and Alexander (20) for measuring the impact and static pressures in the cyclonic flow field was based on this principle. Hiett and Powell (42) modified the Fechheimer tube to produce a three-hole 3-D probe. The cylindrical probe tip with a hemispherical end had a 120 degrees V-groove at some distance from the end. Two pressure tappings were located 72 degrees apart on one side of the groove's flank (hereafter referred to as holes 1 and 2) and a third hold (hole 3) was located on the other flank on the same axial plane as hole 1.

Because of the relative ease of manufacture and suitability for

combustion research, the 3-D probe design of Hiett and Powell was used. Figures 11(a) and (b) show the probe-tip and a photograph of the probe with its water-cooling jacket respectively. The 120 degree V-groove was located 0.5 in. from the hemispherical end of the 0.375 in. diameter probe. All the three pressure holes were located as described in the paragraph above and the diameter of each hole was 0.025 in. Each of the holes drilled along the length of the probe tip and linked with each of the pressure holes on the groove's flanks had a diameter of 0.047 in ($\frac{3}{64}$). The overall length of the probe tip was 1 in. and was made of Nimonic 80A.

For the investigations of the hubless swirler flames, a smaller probe tip of 0.25 in. diameter was used in order to reduce the aerodynamic disturbance of the probe's presence in the smaller jets from the swirlers. Beginning from 0.375 in. from the V-groove, the diameter of the probe tip was gradually increased to 0.375 in. to fit into the outer tube of the water-cooling jacket. The overall length of the probe tip was reduced to 0.875 in. and it was made of Nimonic 105 which being a tougher material required the use of high speed solid carbide drills to bore the pressure holes.

Two of each type of probe tips were made and 19 s.w.g. stainless steel hypodermic tubes were soldered to the outlet of the pressure holes. The tubes of the water-cooling jacket were then silver-soldered on to the probe tips.

An attempt was made to design an automatic balancing system for the 3-D probe but because of the very high magnification needed before the output voltage (in millivolts) from the electronic micromanometer could operate the balancing system, there was a rather high zero error in the voltage amplifier output. This error was attributed (by one of the staff members of the Electrical Engineering Department) to the high magnification

by the voltage amplifier of the noise level arising from the transmission at nearby radio and television stations. As a result of the difficulty in eliminating this interference, the attempt was abandoned.

3.6.1.2 Calibration of the 3-D probe

In order to determine the response of the probe at any pitch angle, it was necessary to calibrate the probe. The pitch angle is defined as the angle between the probe axis and the velocity vector.

The calibration was carried out in a vertical air stream whose velocity profile has been made uniform at the horizontal plane through the probe tip by inserting various combinations of wire meshes at about 2.5 ft from the exit of the vertical 2.5 in. diameter pipe.

For the calibration, the velocity head of the stream at the position of the probe tip was first measured with a pitot static tube. The probe, held in the probe carrier, was positioned at the centre of the flow field and its distance from the pipe exit was 4.5 in. The hypodermic tubes of the probe were connected via a manifold for selecting pressure differences to a pre-calibrated electronic micromanometer. Two protractors were fitted on the probe carrier to indicate the pitch angle and the angle of rotation of the probe.

The calibration was carried out for pitch angles varying in steps of 5 degrees from 30 to 150 degrees. In any position, the probe was rotated until the pressure difference between holes 1 and 2 was zero at which stage the plane of the velocity vector would bisect the angle between holes 1 and 2. The probe was then rotated backwards through 36 degrees so that holes 1 and 3 faced the flow. Pressure differences between holes 1 and 3, $(p_1 - p_3)$, and holes 1 and 2, $(p_1 - p_2)$ as well as the pitch angle were recorded. The ratios of $(p_1 - p_3)$ to $(p_1 - p_2)$ and of $(p_1 - p_2)$ to the velocity head were plotted against the pitch angles.

To find the effect of Reynolds number on the probe performance, the calibration was carried out at four flow velocities ranging from 20 ft/s to 100 ft/s. Typical calibration curves are shown in Figures 12(a) and (b). The condition for the suitability of the probe in three-dimensional flow measurements is that each of the calibration profiles must be single-valued at any given pitch angle. It can be seen from Figures 12(a) and (b) that this condition is fulfilled for pitch angles between 45 and 120 degrees and that the probe's response in this range is independent of Reynolds number. Almost all the experimental pitch angles were within this range. The fact that both positions (45 and 120 degrees) are not symmetrical about 90 degrees and that the profiles of the ratios of $(p_1 - p_3)$ to $(p_1 - p_2)$ against pitch angles do not pass through 90 degrees point at zero must be due to slight asymmetry at the tip of the tool used for machining the V-groove.

3.6.1.3 Method of use

A sleeve/protractor unit with a ring of chrome plated metal, serving as a reflector, was fitted into the hole on the upper aluminium block of the traversing mechanism and the sleeve/protractor unit was locked in position with its zero degree horizontal. A smaller sleeve, on which a pointer and a device for locking the probe in position on to the sleeve/protractor unit has been fitted, was positioned in the sleeve/protractor unit. With a split-sleeve fitted on it, the probe was inserted in the smaller sleeve and locked on it. A photograph of the probe positioning unit is shown in Figure 13. At the beginning of each run, a line scribed on the probe stem and passing through the axis of hole 1 would be lined up with the pointer at zero yaw angle. For the lining up, lines were scribed on each of the sleeves.

With the probe in position, the null point was determined as

discussed in Section 3.6.1.2. The yaw angle, $p_1 - p_3$ and $p_1 - p_2$ were then recorded. From the calibration charts, the pitch angle and the absolute velocity head were determined.

3.6.1.4 Velocity components

As shown in Figure 14, the axial, radial and tangential components of velocity can be obtained from the measurements of the resultant velocity vector, the pitch angle and the yaw angle. The pitch angle can vary from zero to 180° whereas the yaw angle can vary from zero to 360°.

Taking the positive directions of the axial, radial and tangential velocities along the direction of the stream, vertically upwards and in the anti-clockwise direction respectively, the following expressions can be derived.

For vertical traverse

$$u = \bar{V}_{AN} \cos\beta = \bar{V} \sin\alpha \cos\beta \qquad \ldots(3.8)$$

$$v = \bar{V}_{AN} \sin\beta = \bar{V} \sin\alpha \sin\beta \qquad \ldots(3.9)$$

$$w = \bar{V}_{AD} = \bar{V} \cos\alpha \qquad \ldots(3.10)$$

where α and β are the pitch angle and yaw angle respectively.

3.6.2 For static pressure measurements

A disc type static pressure probe to the design of Miller and Coming (43) and shown in the photograph of Figure 15 was used for this purpose. The probe, of 0.25 in. disc diameter, was initially made of Nimonic 80A but was flaking very badly in the flame. Because the accuracy of the static pressure measurements is dependent on the smoothness of the disc's surface another set of the same diameter were made of Nimonic 105. These maintained fairly smooth surfaces despite repeated use. A hypodermic tube was soldered to the pressure hole of each probe tip before soldering the tubes of the water-cooling jacket to the probe tip.

In use, the probe was mounted in the same fixture as the 3-D probe and was rotated until the plane of the disc was in line with the plane of the resultant velocity vector. This therefore meant that the velocity traverses had to be carried out before the static pressure measurements.

3.6.3 Measurements of pressure differences.

The hypodermic tubes from the probes were connected by plastic tubes via a manifold for selecting pressure differences to a pre-calibrated electronic micromanometer which for accurate and steady response had to be kept at constant temperature. The output of the electronic micromanometer (in millivolts) was measured on a multi-range recorder. The recorder response was initially tested and found to be accurate to within 0.001 mV. The micromanometer is accurate to within $\pm$ 0.0005 in. water.

3.6.4 For temperature measurements

3.6.4.1 The Thermocouple

Temperature measurements were made with 0.010 in. diameter Platinum-5% Rhodium: Platinum - 20% Rhodium thermocouple wires passed through 0.098 in. diameter twin-bore ceramic insulators. The insulators were inserted in a 0.125 in. diameter, 0.010 in. wall stainless steel tube which formed part of the water-cooling jacket of the probe.

The hot junction of the thermocouple was formed into a spherical bead whilst the cold junction (during the experiment) was immersed in ice at 0°C. The complete circuit was connected to a recorder for the measurement of the thermocouple response.

It is usual in the fabrication of thermocouples to coat the surface of the hot junction with a thin layer of silica so as to prevent catalytic reactions taking place at the hot junction. This will necessitate the

recalibration of the thermocouple and determining its emissivity. No standard thermocouple was available in the Department or from anywhere in the neighbourhood, therefore the hot junction was not coated. It is however highly unlikely that this would have affected the results in any sense because the combustion was very far advanced at all planes where measurements were taken as could be verified from the temperature profiles obtained. Also the temperature measurements were usually repeatable to within $\pm$ 5°C in the high temperature zones.

3.6.4.2 Temperature correction

The temperature measured by a thermocouple can be expected to differ from the true gas temperature because of two major factors, viz.

(a) conduction along the wires and their neighbouring support

and (b) radiation from the hot junction.

The conduction error can be reduced or eliminated by ensuring that the hot junction and its neighbouring parts are adequately immersed in the stream. In the design of the thermocouple used, this was achieved by increasing the depth of immersion of the hot junction and the ceramic tube until any further increment showed no change in the temperature reading. For example, the readings obtained with depths of immersion of 0.125 in., 0.5 in., 0.75 in., 1.0 in., 1.25 in. were 1032°C, 1249°C, 1262°C, 1265°C, 1265°C respectively. The radiation error was taken into account as discussed below.

3.6.4.3 Radiation correction

For Reynold's number in the range of 17 to 70,000, the convective heat transfer to a spherical hot junction in a flow field is (44)

$$\left(\frac{h\, d_s}{k}\right) = 0.37 \left(\frac{\rho\, \bar{V}\, d_s}{\mu}\right)^{0.6} \qquad \ldots(3.11)$$

and the heat balance equation representing the equality of heat loss by radiation and that resulting in the temperature difference ΔT is

$$h\, \Delta T = \epsilon\, \sigma\, T^4 \qquad \ldots(3.12)$$

Substituting for h from equation 3.11,

$$\Delta T = \frac{\epsilon\, \sigma\, d_s^{0.4}\, T^4}{0.37\, k} \left(\frac{\mu}{\rho\, \bar{V}}\right)^{0.6} \qquad \ldots(3.13)$$

Kaskan (45) has determined the radiation correction for a thermocouple junction with a cylindrical shape.

Owing to the difficulty of calculating the transport properties of complex mixtures such as in flames, μ and k for air are usually used. Thus μ was calculated from the equation (46)

$$\mu_{(\text{poises})} = \frac{145.8\, T^{1.5}}{T + 110.4} \times 10^{-7} \qquad \ldots(3.14)$$

(T in ^{o}K)

and k is calculated from the equation (47)

$$k = k_i \left(\frac{\mu}{\mu_i} \cdot \frac{C_v}{C_{vi}}\right) \qquad \ldots(3.15)$$

with k in cal/cm.s.^{o}C

μ in poises

C_v in cal/g ^{o}C

Suffix i represents values at $0^{o}C$.

Values of C_v were calculated from the values of C_p. To find the value of C_p at any temperature, tabulated values in (47) were plotted and the result is shown in Figure 16. The straight line graph can be represented by the expression

$$C_p = 0.240 + 4.039 \cdot 10^{-5} \cdot T\ (^{\circ}C) \qquad \ldots(3.16)$$

This equation is valid up to 1400°C with a maximum error of $\pm$ 1.25% within the range.

For the emissivity, the platinum and rhodium materials were taken as contributing the percentage of their composition to the emissivity of the hot junction at any temperature. On this basis, the total emissivity of the hot junction was calculated at various temperatures with the data obtained from (48) and a plot of the calculated values is shown in Figure 17. The variation of the emissivities with temperature can be represented by

$$\epsilon = 0.031 + 5.619 \cdot 10^{-5} \cdot T\ (^{\circ}F) \qquad \ldots(3.17)$$

This equation is valid up to the maximum temperature at which the data was available (3000°F) with a negligible maximum error (less than 1%).

CHAPTER 4

STABILISATION OF FREE SWIRLING FLAMES

4.1 Introduction

As mentioned in Section 1.1 various flame holding devices are in use. Depending on a number of factors some of which will be discussed in this chapter, the range of flow conditions within which stable flames can be obtained differs from one device to the other. (The term flow condition refers to the average nozzle velocity of the mixture and the fuel/air ratio). Therefore, experiments were conducted to map the range of flow conditions within which a particular type of flame (if any) could be obtained.

The experiments were carried out using all the hubless and annular swirlers. Extensive measurements could not be made with the annular swirlers because of the limitations of the gas supply and the maximum operating pressures of the superchargers. The tests, with the annular swirlers, were consequently carried out only in the range of flow conditions to be used in the aerodynamic investigations of the flames.

For each of the hubless swirler flames, the limits of the weak blow-off, lift, drop back and rich blow-off were determined. Visual observations of the changes in the flame structure from one flow regime to the other were also made.

4.2 Procedure

The flow rates of the reactants were initially adjusted to obtain a stable flame after which the test rig was allowed about thirty minutes to warm up.

At the first run with each swirler, salt powder was injected into

the flame at a short axial distance from the swirler exit. This was done in order to ascertain whether any recirculation vortex was present in the flame or not.

In determining the weak blow-off limits, the fuel flow rate was set to a level and the air flow rate was slowly increased until the limit was reached. For the rich blow-off limit, the air flow was maintained at a level whilst the fuel flow rate was increased. The procedure for determining the lifting position was the same as for the determination of the rich blow-off limit but for drop back, the fuel flow rate for the lifted flame was reduced until the flame was re-established in its initial anchoring position. In all these cases, some time was allowed for the attainment of steady flow conditions before any further adjustment was made to the flow rates. After obtaining the desired limit, the readings of the orifice pressure differences for the air and fuel flow rates were noted. The flow adjustment was then reversed to obtain a flame just prior to the determined limit. The limit was re-determined, this time the flow rate was more carefully adjusted to obtain the desired limit. The weak blow-off limit was taken as the condition when a stable flame could be obtained for not more than about 20 sec., lifted flame taken as when a stable flame would establish itself in its anchoring position for not more than about 20 sec., drop back taken as when a lifted flame could maintain its position for not more than about 20 sec., and the rich blow-off was taken as the instant when a lifted flame could not maintain itself after about 20 sec.

Having determined the limit sought for, the orifice pressure difference, orifice upstream pressure and the corrected orifice upstream temperature near the exit were also recorded. From these data, the air, fuel and

consequently the mixture flow rates and fuel/air ratios by volume were determined. The average nozzle velocity was calculated from the mixture flow rate and the swirler flow area. In calculating the swirler flow area, the blockage effect of the swirler vanes was taken into account.

4.3 Structure of swirling flames

Depending on the average nozzle velocity, fuel/air ratio, swirl number and swirler exit, several types of flames were observed. Each type of flame was obtainable within a defined flow regime (or condition).

4.3.1 With hubless swirlers

Figures 18(a) to (f) show the photographs of stable flames from all the hubless swirlers. For any swirler with vane angle of 60 degrees or less, the stable flames were anchored at the junction of the vane tips on the jet axis. From this point, the flame spread out into the incoming stream, thus the flame was conical in shape near the swirler exit. For any swirler of vane angle greater than 60°, a wall flame jet was formed and the effects of the swirler vanes were very pronounced, thus eight individual wall jets were formed.

When the fuel flow rate of a stable flame was reduced, the blue flame became less visible as the weak blow-off limit was approached. At very low velocities, below about 75 ft/s, the flame could sometimes spread round the perimeter of the nozzle. This was very frequent with the 15° swirler flame.

If the fuel flow rate was increased, the flame became deeper in colour. If the increase continued, two things could happen. The flame might lift from its anchoring position or it might blow-off. The rest of the discussions in this paragraph refer to the observed characteristics of those flames that lifted. Photographs of lifted flames are shown in

Figure 19. Rough combustion was observed close to the lifting position. As a result of this, the jet boundary became very irregular. The flame noise also increased and the pitch of the noise decreased as the lifting position was approached. Two types of lifted flames were observed. These can be discussed more precisely by referring to them as partially and fully lifted flames. In the partially lifted flame, a small tail of flame was still anchored on the jet axis whilst the main body of the flame has lifted to a downstream position. Initially the flame tail was at the junction of the vane tips but as the fuel/air ratio increased, it moved some distance downstream. The shape of this tail was observed to be different for each swirler. After moving to a downstream position, the flame tail was very unstable although this did not seem to affect the overall stability of the flame. As the fuel flow rate was increased, a stage would be reached when the flame tail would be forced to the same position as the main body of the flame. At this stage, the flame could be described as fully lifted. The partial and full lift concept could not be applied to the 15° swirler flame as no flame tail was observed. Instead the flame lifted from the junction of the vane tips and stabilised itself on the nozzle exit plane. The shape of the flame remained unchanged. In this position, the flame was very unstable and could be easily blown off.

With further increase in the fuel flow rate of a lifted flame, two things could happen. The flame might blow-off or the flame might become increasingly long. Some flames from swirlers of vane angle of 30° and above extended from the nozzle exit into the canopy of the flue ducting. At low velocities and with very rich mixtures, the flame could sometimes drop back from the lifted position to establish itself on the perimeter of the nozzle. In the very long flames, the turbulence characteristics of the flame appeared to change. The change observed was such that the scale of turbulence was greater in these long flames.

In the flames from swirlers of vane angles of 45 degrees and above, a strong odour of partially burnt gases was prevalent in the laboratory. The intensity of the odour increased with swirl number. As would be expected, the intensity of the odour also increased with fuel/air ratio.

4.3.2 With annular swirlers

Photographs of the annular flames are shown in Figure 20(a) to (f). The combustion in annular swirling flames started from inside the swirler nozzle almost on the swirler vanes. This was the reason why all the first set of annular swirlers made with brass vanes were destroyed. As in the hubless swirlers, annular swirlers with vane angle greater than 60 degrees produced individual wall jets. The odour of partially burnt gases was detected and the intensity increased with the swirl number and fuel/air ratio. Because of the higher flow rates and the larger size of the annular flames, the intensity of the odour from any annular swirler was greater than that from a corresponding hubless swirler.

4.4 Stability limits of swirling flames

From the preliminary salt injection tests, recirculation vortices were observed in flames from hubless swirlers of vane angle of 30 degrees and above. Similar zones were observed in flames from annular swirlers of vane angle of 45 degrees and above.

The results of the stabilisation tests for hubless swirlers of vane angles varying from 15 to 60 degrees are shown in Figures 21 to 24. Because of the structure of the flames from swirlers of 70 and 75 degrees vane angles, these flames are not likely to be of industrial importance and thus the stability limits were not determined. For the swirlers investigated, only the peak velocity for the 15 degrees swirler flames could be determined. This was because of the limitation of the gas supply and the maximum

operating pressures of the superchargers. Also at very high flow velocities, the ignition of the flame by the pilot flame was becoming increasingly difficult. As will be observed in the results, the effects of the limitations were becoming increasingly severe as the swirl number increased. However, sufficient data was obtained with the 30 degree swirler to show the main stabilisation characteristics of swirling flames. The remaining part of this section will be concerned with the results of the hubless swirler flames.

In order to ascertain the consistency of the results a few data points at each limit were determined several days after the main test. The weak limits, as will be observed in the results, were very consistent but the limits on the rich side of stoichiometric ratio were much less so. The inconsistency increased with the swirl number. The discrepancy could probably be due to slight changes in the atmospheric conditions and the resultant effect of this on entrainment rates.

The profiles of the weak blow-off limits showed that the flow velocities at blow off increased rather slowly at first with increasing fuel/air ratios. This rate of change increased as the velocities increase, and from the trend of the 30 and 45 degrees profiles, the profiles appeared to be tending to an asymptotic distribution as the peak velocity was approached. At any flow velocity, the required fuel/air ratio at the weak limit increased with swirl. This applied only to flow fields with recirculation vortices. For example, at an average nozzle velocity of 200 ft/s, the fuel/air ratios at weak blow-off limits were 0.14, 0.19, 0.24 in the 30, 45 and 60 degrees swirler flames respectively.

At the rich limits, similar increases in mixture strength with swirl number were shown at corresponding flow velocities. Also the required decrease in the mixture strength before a lifted flame dropped back at any

flow velocity increased with swirl. For each swirler, this region was almost constant throughout the flow conditions investigated.

From the results of the 30 degree swirler, (and possibly of swirlers of higher vane angles), it can be seen that at any flow velocity above 420 ft/s, the flame did not lift from its anchoring position before blowing off.

4.5 Discussion of results

The investigation of the flame stabilisation in swirling flows issuing from vane swirlers shows that, as in non-swirling flames, different types of flames are obtainable. The type of flame is determined by the average nozzle velocity, mixture strength, swirl number and the swirler geometry.

The formation of wall jets can be explained as follows. At any flow velocity, the tangential velocity at the inlet plane increases with swirl. At this plane, the radial velocity component is zero. If it is then assumed that the turbulent shear terms of the Navier-Stoke's equation of motion in the radial direction are negligible, the equation of motion can be written as

$$\frac{\rho w^2}{r} = \frac{\partial p}{\partial r} \qquad \ldots(4.1)$$

This implies that the centrifugal forces resulting from the rotational motion imposed on the flow is balanced by the radial gradients of pressure. If, therefore, the rotational energy of the flow was such that the pressure gradients can not balance the centrifugal forces, the tendency will be for the flow's streamlines to be forced away from the axis of the flow by the centrifugal forces. Within the swirler nozzle, this tendency will be restricted by the nozzle wall but just outside the nozzle exit, the particles of the fluid will be flung away from the jet axis by the centrifugal forces to form wall jets.

It is interesting to note the difference in the location of the flame bases of the hubless swirler flames and those of the annular swirler flames. This clearly shows one of the effects of swirler geometry on flame stabilisation in the type of swirlers used. It also shows the importance of carrying out tests with both swirler geometries. The initiation of the combustion from within the annular swirler nozzle may be due to the effects of possible boundary layer thickness on the swirler vanes. Within the boundary layer, the flow velocity will be sufficiently low to support the establishment of a flame. This possibility is strengthened by the observation that the flame does not extend from the surface of one swirler vane to its adjacent neighbour but there is a region in between them where there is no flame. In this region the fluid velocities must be higher than the weak blow-off velocity of the mixture at the particular fuel/air ratio. It can be expected however that at very high flow velocities, the region of no flame between adjacent swirler vanes will increase to such an extent that the flame will be swept away from the surface of the vanes. Under these circumstances, the flame is unlikely to be held on the small recirculation vortex downstream of the central bluff-body because of the high flow velocity. The flames will therefore be stabilised on the recirculation zone in the flow field if there is any. The establishment of the flame base, in hubless swirlers, at the junction of the swirler vane tips can be considered as the bluff-body effect of the tips of the vanes. The flame stabilisation potential of this bluff-body effect is very small and thus the small stability limits loop obtained with the 15 degree swirler flames. From this, it can be said that the stability limits loop obtainable with annular swirlers of 15 and 30 degrees will depend on the characteristics of the boundary layer on their vanes.

The establishment of flames on the swirler rim at the low velocities is to be expected. These low velocity flames are of the common "Bunsen" burner type. The observed flame behaviour of partial and full lift in hubless swirler flames as discussed in Section 4.3.1 is not likely to be characteristic of swirling flames in general but is most likely to be due to the aerodynamic effect of the 3.86 in. outer diameter dummy secondary swirler in which all the hubless swirlers were fitted and also to the effect of the outer pipe of the secondary flow line. These two factors will have the effect of altering the axial entrainment characteristics within their radial distance of influence. There is also the effect of the reverse velocities of the gases in the recirculation zone. This point raises the question of what happens to the recirculation zone when a flame is lifted. Attempts were made to investigate this phenomenon using the salt injection method but the fluid temperature was too low to make the method applicable. Although this phenomenon does not seem to be of much industrial importance, it will be a stimulating academic exercise to ascertain the fate of the recirculation zone when the flame is lifted.

The importance of the recirculation vortex in flame stabilisation is clearly shown by the comparing the stability limits loop of the 15 degrees swirler flame which has no recirculation zone with that of the 30 degrees swirler flame which has a recirculation vortex. In any flame without a recirculation zone, the flame will be established in the low velocity region resulting from the combined effects of the factors discussed in the third paragraph of this Section. In any flame with a recirculation zone, the hot combustion products fed back towards the nozzle will, by process of turbulent exchange, conduction and to a lesser extent radiation, supply the required energy for ignition. This means, therefore, that the size of the stability limits loop will depend on the size of recirculation vortex as confirmed by the results presented.

The lateral shifting of the stability limits loop towards rich mixture ratios with increasing swirl can be attributed to the combined effect of three factors. These are entrainment of ambient fluid, the temperature of the recirculated gases and gradients of the absolute velocity. It has been verified experimentally in cold jets that the rate of entrainment increases with the swirl number. The entrained air which will have the effect of lowering the temperature of the gases in the flow field will thus have increasing influence on the temperature of the gases as the swirl increases. The recirculated gases contain mainly combustion products with a high CO_2 content. As a result of the exchange by turbulence and molecular diffusion of the recirculated gases with the incoming stream, the effective fuel/air ratio of the stream will be reduced. Furthermore, the length of the recirculation zone increases with swirl and thus the temperatures of the recirculated gases originating from near the downstream end of the vortex will be lower for higher swirl numbers. Hence, at any flow velocity, a higher mixture strength will be required in order to obtain sufficiently higher temperatures in the recirculation zone for igniting the incoming stream. Concerning the third phenomenon, it is known (49) that flame extinction may occur if the velocity gradients at any part of the flame front exceed a maximum value at the fuel/air ratio. In Figure 3 of reference (13) by Chigier and Beer, the distributions of the axial and tangential velocity components are shown at the nozzle exit. It can be deduced from this figure that at any particular flow velocity, the velocity gradients increase with swirl. It therefore follows that for any particular fuel/air ratio, flames issuing from swirlers of higher vane angles will blow-off at lower velocities.

4.6 Conclusions

This investigation has demonstrated that highly stable flames can be obtained within a wide range of flow conditions. The position at which the combustion is initiated depends on the geometry of the swirler. The influence of the recirculation vortex in flame stabilisation is clearly shown.

At any flow velocity, the fuel/air ratio at weak blow-off increases with swirl. This is also true at the rich limits for lift and drop back. The size of the stability limits loop increases with swirl. The flow regime between lift and drop back remains constant in each swirler flame but the width of this zone increases with swirl.

CHAPTER 5

THE AERODYNAMIC INVESTIGATION OF FREE SWIRLING FLAME JETS.

5.1 Introduction

In order to study the distributions of the aerodynamic variables in swirling flames, tests were conducted with flames issuing from hubless and annular swirlers of various vane angles. Flames from swirlers whose vane angles are greater than 60 degrees were not studied because of the reasons given in Section 4.3. The variables measured were the velocities, static pressures and temperatures at various points along and across the flames. The velocity distributions were measured first so as to have the required data for the static pressure measurements. The velocity components, mass flow rates, and the axial fluxes of linear and angular momenta were calculated from the results.

5.2 Details of the experiments.

The flow rates of the reactants were measured as discussed in Section 3.2.7 of Chapter 3. The necessary data for calculating the flow rates at the desired average nozzle velocities were obtained from preliminary tests. For each run, the experimental test-rig was allowed thirty minutes to warm up before starting to take readings.

Preliminary tests were carried out on the measurements of the velocity distributions. These tests showed that a clearer understanding of the changes in the directions of the flow velocities would be obtained if measurements started from the outer boundary of the jet. The tests also showed that it would be necessary during the main experiments to blow compressed air through the pressure tappings of the probes because they could sometimes be blocked by any small particle. After some experience with

the measuring instruments, it was quickly evident whenever any of the pressure holes was probably blocked as this caused the probe response to be inconsistent with previous readings.

Due to the differences in the geometrical features of the hubless and annular swirlers, the tests could not be carried out with the same input conditions. Further details of the tests with each swirler geometry are therefore given below.

5.2.1 With hubless swirlers

The aerodynamic tests were carried out using an average nozzle velocity of 80 ft/sec. The blockage effect of the thickness of the vanes was taken into account in calculating the flow area for each swirler. The details of each swirler are given in Table 5.

TABLE 5. Details of hubless swirlers

Vane Angle (degrees)	Swirl Number	Flow Area (in^2)	Position of junction of vane tips from exit (nozzle diameter)	Experimental Fuel/Air ratio (by volume)
15	0.0893	0.608	1.104	0.20
30	0.1925	0.599	0.535	0.20
45	0.3333	0.579	0.301	0.20
60	0.5774	0.536	0.167	0.25

As shown in Table 5, a volumetric fuel/air ratio of 0.2 was used for the flames issuing from all the hubless swirlers except that with 60 degrees vane angle. In the 60 degrees swirler, the flow condition of 0.20 fuel/air ratio and 80 ft/sec was very close to the weak limit as can be seen in Figure 24 and thus the flame was almost invisible in daylight.

Furthermore, the flame was blowing off occasionally. This is understandable when the method of determining the stability limits (as discussed in Section 4.2) is considered. As a result of the above, a volumetric fuel/air ratio of 0.25 was used. The average nozzle velocity was kept the same as for the other swirlers. This fuel/air ratio might have been used for all the hubless swirler flames but for the limitation that it was very close to the rich stability limits of the 15 degree swirler flames at the desired flow velocity. This too can be observed in Figure 21.

The measurements were made in cross-sectional planes at axial positions of 1.0, 2.0, 3.0, 4.0, 6.0, 8.0 and 10.0 nozzle diameters (henceforth, "diameters" associated with hubless swirlers refers to the nozzle diameter) from the exit. Radial distances were usually taken at intervals of 0.125 in. but sometimes at 0.25 in. when the trend of the rate of change of the measured variable permitted this. The measurements of the static pressure and temperature distributions were made at the same points as for the velocity measurements.

Because of the effect of buoyancy on each flame jet, the physical axis of the jet did not correspond with the geometrical axis of the jet tubes. This deviation started at some axial distance downstream of the swirler exit and the difference increased as the axial distance increased. However, it was possible to estimate the positions of the jet axis to within a maximum error of $\pm$ 0.625 in. from measurements of the velocities (hence others) made at radial intervals of 0.125 in. As explained below, this was made possible by the changes in the measured yaw angles and in the pitch angle parameter $(p_1 - p_3)/(p_1 - p_2)$. The segments containing the yaw angles when measuring above the axis differed from those for points below the jet axis. As would be observed in the 3-D probe calibration

chart in Figure 12(a), the pitch angle parameters at points above the axis would vary from positive values to - 0.015 (i.e. for pitch angles varying from zero to 90 degrees) whilst the values would be lower than - 0.015 only if the measuring position was below the axis. The position of the axis was more accurately determined by taking readings at the midpoint of the estimated 0.125 in. range. This, therefore, made it possible to determine the jet axis at any cross-sectional plane to an accuracy of about $\pm$ 0.031 in. maximum error.

In all swirler flames, readings were not taken throughout the jet radius below the axis but were limited to a radial distance of 0.5 in. from the determined axis. This was because of the small gradient on the small probe-tip used. The details of this gradient were given earlier.

5.2.2 With annular swirlers

In these flames, measurements were made in cross-sectional planes at axial distances of 0, 0.5, 1.0, 1.5, 2.0, 2.5, 3.0, 5.0 and 7.0 diameters (henceforth "diameter" associated with annular swirlers refers to the outer diameter of the flow area unless otherwise stated). The radial distances were taken at intervals of 0.125 in. at the swirler exit and near the estimated location of the jet axis. At other measuring positions, a radial interval of 0.25 in. was used. A few readings were taken using an interval of 0.5 in. when the trend of the rate of change permitted this.

Due to the strong odour of partially burnt gases discussed in Section 4.3, an extension was fitted to the canopy of the flue ducting. At positions upstream of the extension, measurements were taken when it was in place but it was removed when the measuring position was approaching it. The effect of the extension was checked at the last axial plane of measurement by taking measurements on this plane with the extension removed.

These readings were compared with the results obtained when it was in position and no appreciable change was observed. The downstream end of the outer pipe of the secondary flow line was kept at a temperature between 30°C and 40°C. This was achieved by water-cooling the swirler end of the pipe. The reason for this was to prevent the swirler vanes from being damaged by the flame. After completing the tests, the water-cooling system was removed and the test-rig was run for about two hours. This was done in order to see if the swirler vanes would be destroyed by the flame. Although the swirler end of the outer pipe of the secondary flow line was fairly hot, the swirler vanes were not destroyed.

The procedure for determining the jet axis was the same as for the hubless swirler flames. The measurements were taken above and below the determined jet axis down to the lower edge of the jets. Due, probably, to slight inaccuracies in the fabrication of the swirlers, the jets showed slight asymmetry although the results presented later have been plotted symmetrically. The results were plotted from the average of the values at corresponding radial distances from the determined jet axis.

The volumetric fuel/air ratio used for all the flames was 0.15 and the average nozzle velocity was 50 ft/sec. The effect of the vane thickness was also considered in the calculation of the flow areas.

Details of the annular swirlers are shown in Table 6.

TABLE 6. Details of annular swirlers

Vane Angle (degrees)	Swirl Number	Flow Area (in^2)	Position of the bluff-body surface from exit (diameter)	Experimental Fuel/Air ratio (by volume)
15	0.0965	10.124	0.242	0.15
30	0.2078	10.084	0.194	0.15
45	0.3599	9.998	0.130	0.15
60	0.6236	9.802	0.113	0.15

5.3 Velocity distributions in swirling flame jets

From the measurements of yaw angle and the pressure differences $(p_1 - p_2)$ and $(p_1 - p_3)$ of the 3-D probe, the pitch angle and the absolute velocity head parameter were determined from the calibration charts. A computer program was written for calculating the absolute velocity head, the gas density, absolute velocity and the velocity components at each measuring point. The input in the program included the calibration constant of the electronic micromanometer, static pressure readings and the temperature readings. In calculating the gas density at each point, the measured static pressure and the corrected temperature together with the calculated value of the molecular weight of the combustion products were used in the equation of state

$$\rho = \frac{p M_{pr}}{\bar{R} T} \qquad \ldots(5.1)$$

The absolute velocity was calculated from

$$\bar{V} = 18.29 \left[\frac{\text{Velocity head (in. water)}}{\rho} \right]^{\frac{1}{2}} \qquad \ldots(5.2)$$

The calculation of the molecular weight was based on the calculated composition of the combustion products at complete combustion assuming that for a mixture with N components

$$M_{pr} = \sum_{i}^{n} (\% \text{ composition of N by volume}) \times \text{molecular weight of N} \quad \ldots(5.3)$$

The components of absolute velocity were calculated using equations (3.8) to (3.10).

5.3.1 Velocity distribution in hubless swirling flames.

In this section, the results of the distributions of the velocity components are presented. The axial velocity components along the jet axis, the maximum axial velocity component at each cross-sectional plane and the maximum tangential velocity at each plane were made dimensionless by the corresponding values at 1.0 diameter from the swirler exit.

5.3.1.1 Axial velocity profiles

The distribution of the axial velocity components are shown in Figures 25 to 28 for the 15, 30, 45 and 60 degrees swirler flames respectively. The shape of the profiles at corresponding radial planes differed from one swirler to another, thus indicating the effect of swirl on the flow distributions. In the 15 degree swirler flame, the maximum value of the axial velocity occurred on the jet axis at the first axial measuring position of 1.0 diameter and remained so throughout the length of the jet. Close to the swirler exit, the rate of drop of the axial velocity components from the maximum value on the axis to zero on the jet boundary was very rapid but as the jet opened out, the gradients became smaller.

On a cross-sectional plane close to the swirler exit, the profile along the radius of the 30 degree swirler flame showed an off-centre maximum axial velocity with a reduced value on the axis. Near the swirler exit, the reduced values were negative but further downstream, positive values were obtained. The negative axial velocities indicated the region of reverse flow. Beginning from an axial distance of 6.0 diameters from the swirler exit, the maximum axial velocity component at any cross-sectional plane was obtained on the jet axis. A maximum radial width of the feed back region of 0.44 in. was obtained at 1.0 diameter from the exit and the maximum reverse flow velocity which was also on this plane was 18 ft/sec. The shapes of the profiles in the initial region of the 45 degree swirler flame were similar to those in the 30 degree swirler flame in the same region. The double-crest/central trough profile, i.e. off-centre maximum with reduced value on axis, was obtained on each plane down to 6.0 diameters. Beyond this, the profiles steadily flattened out to almost uniform distributions near the jet axis. The radial width of the recirculation zone reached a maximum value of 0.5 in. at a downstream axial distance of 2.0 diameters on which plane the maximum reverse velocity was 20 ft/sec. In the 60 degree swirler flame, the double-crest/trough profiles were obtained at all planes throughout the length of the jet investigated. The positions of maximum feed back conditions, the maximum reverse velocity and the maximum radial width of the recirculation vortex in the jet were 2.0 diameters, 46.0 ft/sec. and 1.0 in. respectively. In all the swirler flames with recirculation vortices, high axial velocity gradients along the jet radius were also obtained in the initial regions of the jets.

The rates of decay of the axial velocity components along the jet

axis and the rates of decay of the maximum axial velocity components along the length of all the hubless swirler flames are shown in Figures 29 and 30 respectively.

In the 15 degree swirler flame, the axial velocity components on the jet axis decreased throughout the length of the jet investigated but in the flame from each of the other swirlers, the results showed that starting from the upstream stagnation point of the reverse flow zone, the reverse velocities on the jet axis increased to a maximum value before decreasing to zero at the downstream stagnation point, further downstream of the downstream stagnation point, the positive values of the axial velocities on the jet axis increased to a maximum value before dropping. It was difficult to specify the axial position of this maximum but it could be estimated as lying between 7.0 and 8.0 diameters in the 30 degree and 45 degree swirler flames and beyond 10.0 diameters in the 60 degree swirler flame. From the trend of the rates of decay, it could be said that downstream of the positions of maximum values, the rates of decay of the axial velocity components on the axis of each jet would increase with swirl. The axial positions of the downstream stagnation points of the reverse vortices could be determined more precisely from Figure 29. In the 30, 45 and 60 degrees swirler flames the positions were 2.3, 3.2, and 4.5 diameters respectively.

In flames from swirlers with vane angles of 45 degrees and less, the maximum axial velocity components along the length of the jets decreased with increasing axial distance from the nozzle exit. This characteristic was maintained in each of the jets throughout the length investigated. In the 60 degree swirler flame, the rate of decrease of the maximum axial velocity components was fairly slow near the swirler exit. This was

followed by a relatively rapid rate of decay between 3.0 and 4.0 diameters. Although the rate of decay in the 60 degree swirler flame was slower than in the 45 degree swirler flame within the investigated length of the jets, it could be deduced from the trends of the rates of decay curves that the rate of decay in the 60 degree swirler flame would ultimately be higher than in the 45 degree swirler flame. It was not unexpected that the rate of decay in the 60 degree swirler flame would be slower than in the 45 degree swirler flame. The reasons for this will be discussed later.

5.3.1.2 Tangential velocity distributions

Figures 31 to 34 show the profiles of the tangential velocity components in the 15, 30, 45 and 60 degrees swirler flames respectively. In each flame, the tangential velocity components on each cross-sectional plane increased from zero on the jet axis to a maximum value before dropping to zero on the jet boundary. Between the swirler exit and an axial distance of 2.0 diameters downstream, the profiles obtained in the 45 and 60 degrees swirler flames showed some distortion near the axis. The extent of this distortion increased with swirl. As the axial distance increased, the distortion phased out.

The rates of decay of the maximum tangential velocity components along each of the jets are shown in Figure 35. The values for each jet decreased as the axial distance increased and the flames from swirlers of higher vane angles showed higher rates of decay.

5.3.1.3 Discussion of Results

The results presented in the last two subsections are likely to have been influenced by two main factors arising from the design of the vane swirlers. The first is the position of the junction of the vane tips from the swirler exit. As the vane angle increases, the position from the swirler exit at which the vane tips meet gets closer to the swirler exit. Thus the position of the junction of the vane tips in the 60 degree swirler is the nearest to the exit. The second is the effect of the small wakes behind the swirler vanes. The influence of these factors on the profiles will be discussed in the relevant paragraphs below.

In the axial velocity distributions of the 15 degree swirler flame, the maximum axial velocity components cannot be expected on the jet axis near the junction of the vane tips. This is so because of the bluff-body effect of the junction. The central trough in the profile must, however, have been very small and thus the maximum axial velocity was measured on the jet axis at 1.0 diameter from the exit. The same phenomenon, i.e. the effect of the junction of the vane tips, can be expected to aid the establishment of a recirculation zone in each of the flames issuing from the other swirlers. Its effectiveness will decrease as the nozzle velocity increases. In the tests herein reported, it was not possible to assess the influence of the junction since measurements were made at one value of Reynolds number. Furthermore, it was established from the salt injection tests that the upstream stagnation point of each recirculation vortex coincided with the position of the junction of the vane tips on the tube axis. This, therefore, means that the effective length of the reverse flow vortex is greater than that determined from the distance between the downstream stagnation point and the swirler exit. The effective

lengths of the recirculation zones for the 30, 45 and 60 degrees swirler flames are 2.84, 3.50, 4.67 diameters respectively. For easy access, features of the recirculation vortices are shown in Table 7.

TABLE 7

Dimensions of the Recirculation Zones in the Hubless Swirler Flames.

	Swirler vane angle (degrees)			
	15	30	45	60
Effective length	-	2.835	3.501	4.667
Max. width (in) (radially)	-	0.44	0.50	1.00
Axial position of maximum width (diameters)	-	1.0	2.0	2.0
Max. reverse velocity (ft/sec)	-	18.0	24.0	46.0
Axial position of maximum reverse velocity (diameters)	-	1.0	2.0	2.0

Generally it was found from the yaw angle measurements that the recirculation zone was surrounded at about the downstream half by an annular zone where the flow was towards the axis. This indicated that the radial velocities were negative in this region. The zone increased in width as the axial distance increased. The zone could not be mapped because of the difficulty in determining its outer boundary but its width appeared to increase with swirl. The observation of this zone confirms similar zones found by Leuckel and Chesters (50) in their experiments on cold swirling flow.

In the 45 and 60 degrees swirler flames, the maximum values of the axial velocity components will be fully established on the jet axis somewhere further downstream than the maximum axial position at which

measurements were taken. The position at which this is attained will depend on the swirl number. As the jet moves further downstream, the effect of the initial rotation imposed on the flow will be steadily reduced by fluid friction and entrainment. Thus the profiles of the axial velocity components will gradually tend to those obtainable in a non-swirling flow field although the axial position at which the jet attains this stage will also depend on the swirl number. After this development, it will be possible to represent the profiles by Gaussian error functions whose parameters will depend on the swirl number.

The rates of decay of the axial velocity components on the axis and the maximum value along the jet of the 60 degree swirler flame require some comments. From a comparison of the rate of decay of the axial velocity components on the axis of the 30 and 45 degree swirler flames, it appears that the swirler flames with smaller vane angles attained their maximum values faster than those with higher vane angles. But the 60 degree swirler flame had still not attained its maximum value at 10.0 diameters. Furthermore, the 60 degree swirler flame showed a slower rate of decay of the maximum axial velocity components along the length of the jet than the 45 degree swirler flame whereas the flames from swirlers with lower vane angles showed that the rate of decay increased with swirl. These two features are attributable to the higher volumetric fuel/air ratio used for the 60 degree swirler flame. The higher ratio will give higher density gradients than would have been obtained with a ratio of 0.2 and this will slow down the rates of decay. One feature, however, which is peculiar to the jet is the slow rate of decay of the maximum axial velocity component near the swirler exit. This can be explained as follows.

As can be observed in Figure 28, the annular forward flow area at 1.0 diameter is about the same as that at 2.0 diameters. This means that although the jet width at 2.0 diameters is greater than that at 1.0 diameter, the increase in the width of the recirculation zone has prevented any appreciable increase in the forward flow area and thus the decay of the maximum axial velocity component is bound to be slowed down. It can, in fact, be expected from the principles of continuity that if the forward flow area at 2.0 diameters, had been less than that at 1.0 diameter, the fluid would accelerate at the expense of pressure in order to flow past the smaller flow area at 2.0 diameters.

The distortion in the tangential velocity profiles of the 45 and 60 degree swirler flames can be attributed to either the shape of the velocity profiles of the stream at the swirler exit or to the design of the swirlers. It may also be due to the combined effect of both. That the first is a possible explanation is suggested by the extent to which increases in swirl numbers can alter the profiles of the velocity components at the swirler exit. This is shown in Figure 3 of reference (13) by Chigier and Beer. The second is also a possibility because Figure 15 in reference (6) by Mathur and Maccallum showed such distortions. Although the distortions in (6) were shown in annular swirlers, it can be expected that in hubless swirler flames with sufficiently wide recirculation vortices, distorted profiles can be obtained, and, of course, the bluff-body effect of the junction of the vane tips makes the geometry of a hubless swirler almost similar to that of an annular swirler.

The rate of decay of the maximum tangential velocity components in the 60 degree swirler flame showed the same trend as in other swirler flames despite the higher fuel/air ratio. One might probably have expected

the rate of decay to show similar differences as observed in the rates of decay of the axial velocity parameters. No reason could be given for the result obtained because it is possible that the rate of decay might have, indeed, been slower than would be obtained with a fuel/air ratio of 0.2 but this cannot be confirmed on the basis of the present experiments.

In general terms, the profiles of the tangential velocity components indicate a central forced vortex core where the tangential velocities increase from zero on the axis to a maximum somewhere along the radius of the jet. This central core is surrounded by an annular free vortex region where the tangential velocities decrease from the said maximum to zero on the jet edge.

5.3.2 Velocity distribution in annular swirling flames.

The profiles of the velocity components at the exit of each of the swirlers are not included among the results presented. This is because of the irregularities at some of the measuring points resulting from the effect of the wakes behind the vanes of the swirlers. The axial velocity components on the axis, the maximum axial velocity components along the jet and the maximum tangential velocity along the jet were non-dimensionalised by the axial and tangential velocity components at the nozzle exit of each swirler flame. The maximum axial velocity components were 144, 137, 149 and 129 ft/sec at the exit planes of the 15, 30, 45 and 60 degrees swirler flames respectively. These results are no doubt affected by the swirler vanes.

5.3.2.1 Axial velocity distributions

Within the initial region of each of the flame jets, the profile at each plane, as shown in Figures 36 to 39 for the 15, 30, 45 and 60 degrees swirlers respectively, showed two off-centre crests representing

the maximum value and a central trough representing the reduced value. In the flames from swirlers with vane angle of 45 degrees and above, the reduced velocities were negative, thus indicating the recirculation vortices.

In the 15 degree swirler flame, the double-crest/trough profile was obtained down to an axial distance of 0.5 diameter. Beyond this and down to an axial distance of 2.0 diameters, the profiles were almost uniform near the jet axis. From 2.5 diameters and for the remaining length of the jet, the maximum axial velocity component was fully established on the jet axis from where the values decrease to zero on the jet boundary. In this downstream region, the profiles were similar in shape to Gaussian error functions. In each of the other swirler flames, the central trough in the profiles existed throughout the 7.0 diameters length of the jets investigated. The profiles were, however, gradually flattening out near the jet axis as the distance downstream increased.

The maximum reverse velocity of 25 ft/sec in the 45 degree swirler flame was obtained at 0.5 diameters. In the 60 degree swirler flame, the corresponding velocity of 35 ft/sec was obtained at 1.5 diameters. The maximum radial widths of the recirculation vortices were 1.625 in. and 3.5 in. in the 45 degree and 60 degree swirler flames respectively. This maximum width was obtained at 1.0 diameter in the 45 degree swirler flame and for the 60 degree swirler flame, the position was the same as the position of maximum reverse velocity.

The rate of decay of the axial velocity components along the axis of each of the 15, 30, 45 and 60 degrees swirler flames are shown in Figure 40. Within the 15 degree swirler flame, the axial velocity component on the axis increased to a maximum value at 0.5 diameter after which the values decreased. The rate of decrease of the values was

rather slow. In the other flames, the axial velocity components on the axis of each of them decreased initially to a reduced value which could be positive or negative depending on the absence or presence of a recirculation vortex. From this value, the parameter increased. In the 30 degree swirler flame, the rate of increase was almost constant for the remaining length of the jet investigated whereas an initial rapid increase in each of the 45 degree and 60 degree swirler flames was followed by a slow rate of change. The minimum axial velocity component on the axis of the 30 degree swirler flame was obtained at 2.5 diameters. The positions of the downstream stagnation points were 1.9 and 3.1 diameters.in the 45 and 60 degree swirler flames respectively.

Figure 41 shows the rate of decay of the maximum axial velocity components along the length of each of the 15, 30, 45 and 60 degree swirler flames. From the swirler exit down to an axial distance of about 3.5 diameters in each of the flames, no generalisation of the results could be made but further downstream, the rate of decay increased with swirl.

5.3.2.2 Tangential velocity profiles

The profiles obtained in all the annular swirler flames were generally similar in form to those obtained in the hubless swirler flames. The results are shown in Figures 42 to 45 for the 15, 30, 45 and 60 degree swirler flames respectively. The pattern of the distribution within the recirculation vortex was more clearly shown in these profiles. In this zone, the tangential velocities were small but within a short radial distance from the boundary of the zone, the values increased fairly rapidly to attain the maximum value on the cross-sectional plane. The distortion of the profiles in the flames from swirlers with vane angle equal to and less than 45 degrees was limited to 1.0 diameter from the exit but in

the 60 degree flame, this extended to about 2.5 diameters. The "forced vortex core" occupied the greater part of the flow section at each plane in the initial region of each of the jets but downstream of the jets, the free vortex region occupied the greater part.

Figure 46 shows the rate of decay of the maximum tangential velocity components along the length of each of the jets. The results did not show any generalised trend near the swirler exit in each of the flames but further downstream, the rates of decay were higher for swirlers with higher vane angles.

5.3.2.3 Discussion of results

The design of the swirlers is such that the distance of the bluff-body surface from the exit of the swirler reduces as the vane angle increases. This will, therefore, have similar effects as the position of the tips of the vanes had on the profiles obtained in the hubless swirler flames. Thus the effective lengths of the recirculation vortices are 2.03, 3.21 diameters in the 45 and 60 degree swirler flames respectively. Details of the recirculation vortices are shown in Table 8.

TABLE 8

Dimensions of the Recirculation Zones in the Annular Swirler Flames.

	Swirler vane angle (degrees)			
	15	30	45	60
Effective length	-	-	2.030	3.213
Max. width (in) (radially)	-	-	1.625	3.500
Axial position of max. width (diameters)	-	-	1.0	1.5
Max. reverse velocity (ft/sec)	-	-	25.0	35.0
Axial position of max. reverse velocity (diameters)	-	-	0.5	1.5

Judging from the development of the 15 degree swirler flame jet, each of the other jets will, at some axial distance (greater than the investigated length), have the maximum axial velocity component at that plane on jet axis and the profiles will ultimately assume the Gaussian error profiles. The position at which this development is attained will depend on the swirl number.

An annular zone of inward flow surrounding the recirculation zone was again observed in the annular flames. The thickness of this zone appears to increase with the size of the recirculation zone.

The effect of the restraint on increases of the forward flow annular area in jets with large recirculation zones on the rate of decay of the maximum axial velocity components is again clearly shown in the results for the 60 degree swirler flame. In this flame, the forward flow area at 1.0 diameter is almost equal to that at 0.5 diameter and as discussed in Section 5.3.1.2, the effect of this restriction in the expansion of the forward flow area is the phenomenon responsible for the

increase in the maximum axial velocity component at 1.0 diameter as ompared with the value at 0.5 diameter.

Possible reasons have earlier been given for the distortion in the profiles of the tangential velocity components. It is interesting to note the trend in the rates of decay of the maximum tangential velocity components along the jets. At a sufficient distance downstream, the rates of decay will be equal in all the jets despite the differences in swirl numbers. This claim is strengthened by the results in Figure 8 of reference (13) by Chigier and Beer and in Figure 6(b) of reference (14) by Chigier and Chervinsky. The above statement also applies to the hubless swirler flames.

5.3.3 Variation of jet width along the length of the jet.

When designing the flame for a combustion chamber, it will be vital to know the width of the jet to be expected because this is one of the factors which will determine the rate of wear of the combustion chamber wall. Theoretically, the width of the jet at any cross-sectional plane should be the radial distance between the jet axis and the position on the outer edge of the jet where the flow velocity is zero. The parameter can, of course, be defined from one jet edge to the other on the same cross-sectional plane. As the position of measurement approaches the jet boundary, the effect of the aerodynamic disturbance of the measuring instrument becomes severe. Apart from this, the jet boundary, particularly flame jets, will be subject to fluctuations arising from the turbulent momentum exchange between the jet and the surrounding fluid. Any specification, therefore, of the jet width represents an average. The method adopted in this work is to take the jet boundary at any cross-sectional plane as the position at the outer part of the jet where the axial velocity component is one-tenth of the maximum value at that plane.

5.3.3.1 Hubless swirler flames.

The changes in the jet width along the length of each of the 15, 30, 45 and 60 degree hubless swirler flames are shown in Figure 47. The results showed that the jets expand rapidly immediately after exit from the swirlers. This initial expansion increased with swirl. For example, the jet widths of the 15, 30, 45 and 60 degree swirler flames at 2.0 diameters were 1.35, 1.45, 1.9 and 2.07 in. respectively. Further downstream, starting from about 6.0 diameters, the rate of expansion of each jet was almost linear.

5.3.3.2 Annular swirler flames

The results for each of the 15, 30, 45 and 60 degree swirler flames were similar to those of the hubless swirler flames with corresponding vane angles. Figure 48 shows the results. The widths of the 15, 30, 45 and 60 degree swirler flames at 1.0 diameter were 3.65, 3.90, 4.60 and 5.65 in. respectively. Beginning from about 3.0 diameters, the rates of expansion in the 30, 45 and 60 degree jets were linear and almost independent of swirl.

5.3.3.3 Discussion of results

The marked difference in the expansion of the hubless 30 and 45 degree swirler flames is similarly shown in the annular swirler flames with the same vane angles. Similar difference was shown in the expansion of hubless and annular 15 and 30 degree cold jets (6). This phenomenon can be attributed to the non-linear dependence of the jet expansion on swirl and the added complexity of combustion.

The rapid expansion of each jet immediately after the nozzle exit can be explained by the same principles as for the formation of a wall jet. This was discussed in Section 4.5. In the case of the flames studied, the

radial pressure gradients are sufficient to cope with the centrifugal forces. As the rotational energy increases, the centrifugal forces increase and thus the increase in the expansion of the jet as the swirl number increases.

5.4 Static pressure distributions in swirling flames

The procedure and instrumentation for measuring the static pressures in the flow fields have been given in Section 3.6.2. The measured values were the differences between the atmospheric pressure and the pressure at the point of measurement.

5.4.1 Hubless swirler flames.

The results of this investigation are shown in Figures 49 to 52 for the 15 to 60 degree swirler flames respectively. Within all the flames and at all measuring positions, the static pressures were below atmospheric. The 15 degree swirler flame results showed that the minimum static pressure was on the jet axis at 1.0 diameters from the swirler exit. From the axis, the static pressure increased along the radius of the jet to the atmospheric value at the edge of the jet. This characteristic remained so throughout the length of the jet investigated. In the other swirler flames, the profiles near each swirler exit had the shape of two off-centre crests and a central trough like some of the profiles of the axial velocity components. This profile meant that, at the cross-sectional planes concerned, the static pressure decreased along the jet radius to a minimum value after which the values increased to atmospheric value on the jet boundary. The central trough gradually closed up and within the 10.0 diameters investigated, the minimum static pressure was obtained on the axis of each of the jets. Within the 30 degree swirler flame, the minimum value was first obtained on the axis at about 6.0 diameters but

in the flames from the swirlers with higher vane angles, the profiles on the same plane showed almost uniform distribution near the axis of each of the jets. Further downstream, the minimum pressures were measured on the axis of each of these flames.

The variations of the static pressures along the axis of the 15 to 60 degree hubless swirler flames are shown in Figure 53. The readings obtained at the planes of measurement showed that the static pressures increased along the axis of each of the jets. The rate of change of the pressures was fairly rapid between the swirler exit and about 4.0 diameters in each of the 15 to 45 degree swirler flames. Further downstream, the rate of change was relatively small. In the 60 degree swirler flame, the rate of change was almost constant between 1.0 and 3.0 diameters from the exit. Between 3.0 and 4.0 diameters, the rate of increase was very rapid.

The variations of the minimum static pressures along the lengths of each of the flames are shown in Figure 54. The results obtained at the planes where measurements were taken showed that the pressures in each flame increased rapidly near the swirler exit. This was followed by a relatively small rate of change.

5.4.2 Annular swirler flames

Figures 55 to 58 show the results obtained in the 15, 30, 45 and 60 degree swirler flames respectively. The static pressures throughout the jets were also subatmospheric. Generally, the shape of the profiles were similar to those obtained in the hubless swirler flames and the minimum static pressures were also obtained on the jet axis within the length investigated in each flame. In the 15 degree swirler flame, the minimum was first measured on the axis at 0.5 diameters from the swirler

exit. The corresponding positions in the 30, 45 and 60 degree swirler flames were 1.5, 2.0 and 2.0 diameters respectively.

The variations of the static pressures along the axis of each of the flame jets are shown in Figure 59. Between the exit of each swirler and a downstream axial distance of about 4.0 diameters, no generalisation could be made on the behaviour of the jets but further downstream, the rate of decay increased with swirl. The 60 degree swirler flame results showed that the static pressure on the jet axis decreased to a minimum value at 1.5 diameters before increasing rapidly at first and at a relatively reduced rate further downstream.

Similar characteristics to those presented in the above paragraph for hubless swirler flames were shown by the results of the variations of the minimum static pressure at different planes along the length of each of the jets. These results are shown in Figure 60. The initial drop in the static pressures of the 60 degree swirler flame attained the minimum in the flow field at 1.0 diameters from the exit.

5.4.3 Discussion of results

The effect of the increase of the fuel/air ratio on the rate of decay of static pressures with the flow field is again clearly shown by comparing the results in the 60 degree swirler flame with those obtained in the 45 degree swirler flame. The comparatively higher density gradients resulting from the comparatively higher mixture strength slowed down the rates of decay.

In the initial region of the hubless and annular swirler flames, the results did not indicate any clear-cut dependence of the changes in static pressure on swirl numbers. Similar results were shown in Figures 7(a) and 9(a) of reference (6) and also in Figure 2 of reference (51).

The assertion can therefore be made that the static pressure changes in swirling flows, cold or burning, depend on the swirl number in a rather complex way.

The measurements in the 60 degree annular flame point out two important characteristics. The first is the pressure drop between the swirler exit (apparently) and an axial distance of 1.0 diameters where the least static pressure in the flow field was obtained. The importance of this pressure drop will be discussed in Section 5.8. The second factor is the position of the minimum static pressure in the flow field in relation to the position of the minimum static pressure on the jet axis. The least value in the flow field was obtained at 1.0 diameter whereas the least value on the jet axis was obtained at 1.5 diameters. This is understandable because in a region of high axial static pressure gradients, the rate of change of the static pressure on the axis cannot be expected to follow the same pattern on the same plane as the pressure in the dominant annular forward flow zone. The statement that the annular forward flow region is dominant will be explained in Section 5.8. The minimum pressure on the jet axis will be downstream of the position of the minimum in the flow field. If the axial pressure gradients are low, the convection pattern of the fluid particles may be such that the minimum pressure on the axis and the minimum pressure in the flow field will be on the same plane.

5.5 Temperature distributions in swirling flames

The method and instrumentation for the measurement of this variable were discussed in Section 3.6.4. For each swirler flame, the variations of the temperature rise along the jet axis and the variations of the maximum temperature rise at each measuring cross-sectional plane

were plotted as ratios of the maximum temperature rise measured in the flame.

5.5.1 Hubless swirler flames

As shown in Figures 61 to 64 for the 15, 30, 45 and 60 degree swirler flames respectively, the temperature profiles varied from one swirler to another. In the 15 degree swirler flame, the maximum temperature on the cross-sectional plane was on the jet axis at 1.0 diameter from the exit. On the planes close to the swirler exit, the temperatures dropped very rapidly along the jet radius to the atmospheric value. As the jet expanded, the rate of decrease reduced and the shape of the profiles became similar to Gaussian error curves. In each of the 30 to 60 degree swirler flames, the maximum temperatures on planes near the swirler exit were obtained at the same radial distance from the jet axis. The radial displacement of the position of maximum temperature on each cross-sectional plane increased with swirl and the axial position at which the maximum temperature was first measured on the axis varied with swirl. In the 30 degree swirler flame, the maximum temperature was first measured on the axis at 2.0 diameters from the exit. The corresponding positions within the 45 degree and 60 degree swirler flames were about 6.0 and 4.0 diameters respectively. In those flames with recirculation vortices, the temperatures therein showed almost uniform distribution from the jet axis out to a radial position. This radial position varied with swirl and the axial position. For instance, in the 45 degree swirler flame, the temperature profile at 1.0 diameter was nearly uniform for a radial distance of 0.375 in. and the equivalent distance in the 60 degree swirler flame was also 0.375 in. At 1.5 diameters, the corresponding distances were almost zero and 0.625 in. in the 45 and 60 degree swirler flames respectively.

The variations of the temperatures on the axis of each of the jets are shown in Figure 65. The result of the 15 degree swirler flame showed a slight increase initially after which an almost constant ratio was maintained before starting to drop at about 3.5 diameters from the exit. Within each of the other flames, the temperature on the axis decreased as the axial distance increased. In general, the rate of decay increased with swirl within those flames with the same fuel/air ratio.

The variations of the maximum temperatures along the length of each jet showed similar results to those described in the above paragraph. The results are shown in Figure 66. The location of the maximum flame temperature in the 15 degree swirler jet was spread between 2.0 and 4.3 diameters from the exit. In the 30 degree swirler flame, the maximum flame temperature was measured at 2.0 diameters from the exit. In the other swirlers, the maximum temperatures were measured at 1.0 diameters.

5.5.2 Annular swirler flames

The results obtained in these flames are shown in Figures 67 to 70 for the 15 to 60 degree swirler flames respectively. The shapes of the profiles were similar to those described in the previous section for hubless swirler flames. Within the 15 degree swirler flame, an almost uniform profile was obtained near the jet axis at cross-sectional planes lying between the swirler exit and 3.0 diameters downstream. The maximum temperatures were obtained on the axis at 5.0 diameters in each of the 30 and 45 degree swirler flames. There was still a slight crest in the 60 degree swirler flame profile at the last axial station at which measurements were taken.

The variations of the temperatures on the jet axis and of the

maximum temperatures along the length of each of the jets are shown in Figures 71 and 72 respectively. In Figure 71, each of the 15 and 30 degree swirler flames showed slight increases near the swirler exits, with the increase in the 15 degree swirler flame being more pronounced. After this initial increase, the temperatures on the axis of each of the jets dropped. Each of the other swirler flames results showed continuous drop from the nozzle exit.

In Figure 72, the maximum temperatures in each of the 15 to 45 degree swirler flames increased in the initial regions of the jets. The 60 degree swirler flame showed continuous decrease as did the other swirler flames after the initial increases. The position of the maximum flame temperatures extended from 1.0 to 1.5 diameters and 1.0 to 2.0 diameters in the 15 and 30 degree swirler flames respectively. The maximum temperatures were measured at the swirler exit and 0.5 diameters in the 60 degree and 45 degree swirler flames respectively.

5.5.3 Discussion of results

Despite the refinements made in the analysis of the temperature correction for radiation losses from the thermocouple bead, the computed corrections were low. They were usually less than $5^{\circ}F$. The reason for this is that the velocities are usually high in the high temperature regions. This will thus make the term $\left(\frac{\mu}{\rho v}\right)$ very small.

In the hubless swirler flames with fuel/air ratio of 0.2, the calculated adiabatic flame temperature was $1760^{\circ}C$ and with the fuel/air ratio of 0.15 in the annular swirler flames, the corresponding temperature was $1460^{\circ}C$. In the calculation of these values, dissociation has been taken into account using the I.T. Diagram method in (47). The maximum flame temperatures obtained from the measurements were 1451, 1392 and $1258^{\circ}C$

in the 15, 30 and 45 degree hubless swirler flames. The corresponding values were 1289, 1311, 1333 and 1280°C in the 15, 30, 45 and 60 degree annular swirler flames. These temperatures are lower than the calculated adiabatic flame temperatures. The various factors contributing to the above are as follows. In the first instance, the calculation of the adiabatic flame temperature assumes complete combustion whereas this is not the case in the flames. This is indicated by the odour of partially burnt gases reported earlier. The main factor which will contribute to the lower temperatures obtained is flame radiation. The entrainment of ambient fluid particularly in flames within which the maximum temperatures were measured at some axial distance downstream of the exit and the dilution of the nozzle fluid by recirculated gases are other factors which will contribute in some degree to the lower temperatures observed.

For both swirler geometries, the distance from the swirler exit at which the maximum temperature in the flow field is measured reduces as swirl increases. This indicates that the distance from the swirler exit at which "complete" combustion is achieved reduces as swirl increases. Effectively, the flame length reduces and for the same flow rate and mixture fuel/air ratio, the required length of combustion chamber will decrease as swirl increases

5.6 Mass flow rates

In a combustion system, the oxidant required for the chemical process can be provided by

(a) supplying the oxidant from a concentric annular stream,

(b) mixing the oxidant with the fuel before exit from the nozzle,

(c) allowing the jet to draw in air from the surrounding,

or (d) mixing a proportion of the combustion air with the fuel before exit from the nozzle and using the air drawn into the jet from the surrounding to make up for the deficiency.

With the last two methods, the rate of combustion will depend on the rate at which the jet draws in fluid from the environment. In the other methods, the entrained air influences the temperature distributions and the rate of decay of the jet parameters.

The first significant analysis of entrainment phenomenon in gas burners was carried out by Silver (52). The analysis was carried out for a "Bunsen" type of burner. In the analysis, the kinetic energy at inlet was equated to the summation of the energy requirements of the various related factors. The final equation obtained show good agreement with experimental data. For a jet flow in a stagnant environment, Ricou and Spalding (53) obtained the expression

$$\frac{\dot{m}}{\dot{m}_o} = 0.32 \frac{x}{d_o} \left(\frac{\rho_1}{\rho_o} \right)^{\frac{1}{2}} \qquad \ldots(5.1)$$

where ρ_1 is the density of the surrounding fluid. For a swirling air jet in a medium of the same density, Kerr and Fraser (3) obtained

$$\frac{\dot{m}}{\dot{m}_o} = (0.35 + 1.40S) \frac{x}{d_e} \qquad \ldots(5.2)$$

where d_e is the equivalent diameter of a nozzle whose flow area equals that of the annular flow section.

5.6.1 Determination of mass flow rates

The mass flow rates at different planes along the length of the jets were calculated from the equation

$$\dot{m} = \int_0^\infty \rho\, u\, r\, dr \qquad \ldots(5.3)$$

by numerical integration using a Lagrange type of integration formula (54)

$$\int_{x_o}^{x_n} f(x)dx = \delta x\left[-\frac{1}{24} f_{-1} + \tfrac{1}{2} f_o + \frac{25}{24} f_1 + f_2 + \ldots\ldots + f_{n-2} + \frac{25}{24} f_{n-1} + \tfrac{1}{2} f_n - \frac{1}{24} f_{n+1}\right] \qquad \ldots(5.4)$$

where δx is the equal interval between two consecutive data points and

$$f_n = (\rho\, ur)$$

represents the numerical value at the nth data point.

Because some of the required data points did not correspond with points at which measurements were taken, some of the data were obtained from the experimental profiles. A computer program was written for this analysis.

5.6.2 Entrainment in hubless swirler flames

The results of the analysis are shown in Figure 73 for all the swirler flames. The mass flow rates obtained from the computation had been non-dimensionalised by the nozzle mass flow rate. The results showed that the entrainment rates in the initial regions of each of the jets were very high. Beyond about 4.0 diameters, the entrainment rates were relatively slower and almost linear. Also the entrainment rates increased with swirl.

5.6.3 Entrainment in annular swirler flames

As shown in Figure 74 for all the annular swirler flames, the results showed the same characteristics and dependence on swirl as in hubless swirler flames.

5.6.4 Discussion of results

There is some scatter in the results of the computation. This is probably inevitable because of errors inherent in all numerical integration formulae and the slight errors arising from the data obtained from the graphs.

The entrainment rates in the hubless swirler flames are higher than those in the annular swirler flames with corrcsponding vane angles. This is probably due to the higher fuel/air ratio used in the experimental investigation of the hubless swirler flames.

In the initial regions of the jets, the rate of entrainment in each of the jets did not show a linear dependence on swirl number or the distance of the axial station from the exit. Thus, the results could not be described by any of the linear equations stated in this chapter.

As pointed out in Section 5.3.3, the jet boundary is a turbulent region. Entrainment can therefore be explained on the basis of the momentum imparted by turbulent exchange to the surrounding fluid in the neighbourhood of the jet boundary. In the results of the variation of jet width presented earlier, it was shown that the jet width increases with swirl, thus the surface area of the jets at corresponding cross-sectional planes will increase with swirl. Furthermore, the velocity gradients at the outer part of any cross-sectional plane near the swirler exit appear to be higher in swirlers with higher vane angles and thus the intensity of turbulence at the jet boundary in the initial region will increase with swirl. This factor together with the greater surface area explains the increase in the entrainment rate as swirl increases. As the distance from the nozzle exit increases, however, the effect of the turbulence intensity will decrease because of the higher rates of decay of the jet parameters in jets with higher swirl numbers. It can even be speculated

that as the axial distance increases, the effect of turbulence will be in favour of jets with smaller swirl number because of the slower rates of decay of the jet parameters. This view point, although not very clearly vindicated by the above results, is more so in Figure 9 of reference (13) by Chigier and Beer where the rates of change of the mass flow rate parameter in the region of the last two measuring planes are higher in jets with smaller swirl.

5.7 Axial fluxes of linear and angular moments

These parameters were calculated as in equations (2.5) and (2.6). The measured static pressures were used in calculating the axial flux of linear momentum. The computations of both parameters were included in the program written for calculating the mass flow rates. Equation (5.4) was used with f_n representing the relevant term for the calculations. From the computation of the two parameters above, the swirl number on each plane and in each jet was computed.

Although there was some scatter in the results due to possible sources of error mentioned in the preceeding subsection and also to inaccuracies arising from the aerodynamic disturbance of the measuring probes, the axial fluxes of linear and angular momenta appear to be conserved along the length of each of the jets.

The average swirl number calculated from the values obtained at each cross-sectional plane in the flow field of each jet was higher than the values calculated from equation (3.7) by almost a factor of 2. This is not surprising because in addition to the sources of error mentioned above, equation (3.7) was derived on the assumption that the static pressure was negligible.

The results of the axial flux of linear momentum did indicate the strong influence of the static pressure. The ratios of the modulus of the static pressure term to the axial velocity term of the linear momentum flux varied from about 3% in swirlers with low swirl numbers to about 80% in swirlers with high swirl numbers. As will be expected, the effect of the static pressure diminished as the distance downstream increased.

5.8 General discussion

It has been stated earlier that because of the rotational energy on the flow at exit from the swirler, the fluid particles will be drawn away from the jet axis and the stream lines will therefore be concentrated near the outer part of the jet. As a result of this, the axial velocities at points in the outer part of the jet will have to increase sufficiently before the flow can be maintained. This explains why the profiles in the initial regions of the jets have the double-crest/central trough shapes. Furthermore, because of the conservation of the axial momentum flux, the increases in the axial velocities can be achieved only at the expense of further pressure drop at the points concerned. This also explains why the static pressure profiles were as obtained. It is therefore clear that the radial positions of the maximum axial velocity will correspond to the radial positions of the minimum static pressure on the same cross-sectional plane. A comparison of the profiles of the axial velocity profiles and the static pressure profiles confirm the above.

From previous discussions and that in the preceeding paragraph, it is now possible to examine the mechanism responsible for the establishment of a recirculation zone. Consider the condition when a swirling flow is near the exit of the swirler. As a result of the centrifugal forces due to the rotational energy, the fluid stream lines will be concentrated near the outer wall of the swirler. As the swirl number increases, the fluid

particles will be forced further away from the jet axis on to the swirler wall. As the fluid particles are forced further into this congested zone, the axial velocities at these points will increase correspondingly in order to maintain the flow. The increase in the axial velocity will give rise to a pressure drop. (This is confirmed by the result that the radial position of the maximum axial velocity component increases with swirl in the initial region of the jet. Further confirmation is shown in Figure 3 of reference (13)). Consider now the instant when the fluid from the swirler with the high swirl number is injected into the atmosphere. At that instant, the fluid particles in the congested outer section will fly out radially leaving a central core with little or no flow. The jet will therefore expand rapidly (as shown in the initial regions of the jets) until the radial pressure gradients can counter balance the effects of the centrifugal forces. As the jet flows downstream, the static pressure will increase and the jet's stream lines will converge towards the axis to form a homogeneous jet. Because of the axial pressure gradients, fluid particles will be drawn into the central core towards the swirler exit where the static pressures are lower. Thus a recirculation vortex will be established.

With the setting up of the recirculation zone, there is now another factor to be reckoned with. This factor is the width of the zone. The effect of the recirculation vortex width will be to displace any forward flowing fluid which might have been in the central core into the annular forward flow zone and thus causing some congestion of the stream lines there. Because the radial pressure gradients at all planes are sufficient to cope with the centrifugal forces, the jet will not expand further. For the jet to maintain the flow, the static pressure will drop. This pressure drop will take place upstream of the position of the maximum recirculation zone width. (This is confirmed by the results in the 60 degree annular

swirler flame). The effect of the width of the recirculation vortex and consequently the quantity of pressure drop required will depend on the swirl. The theory discussed in the preceeding paragraph and the present one therefore suggests that the development of the flow in the annular forward-flow zone is the dominant factor that moulds the pattern of the flow field.

From the above discussion, the formation of wall jets can now be examined in a new light. The effect of the pressure drop resulting from the width of the recirculation zone will be to reduce the radial pressure gradients on the plane. If the swirl number is sufficiently high, the radial pressure gradients can be so reduced that an unstable condition will tend to set in because the radial pressure gradients will not be sufficiently high to balance the centrifugal forces and thus a wall jet will be formed.

5.9 Conclusions

The results and discussions in the preceeding sections of this chapter have shown that

1. The profiles of the aerodynamic variables in a swirling flame depend, among other factors, on the swirler exit geometry and the swirl number. The profiles, in the initial region of each of the jets, usually have the shape of two off-centre crests and a central trough. Downstream of the exit, the dip in profile gradually phases out as a result of the decay of the variable along the jet.
2. A swirling flow consists of a central forced vortex core surrounded by an annular free vortex region which extends to the jet boundary.

3. With the hubless swirlers of vane angle of 30 degrees and above, recirculation vortices are present in the flames. With the annular swirlers, recirculation zones are present in the 45 and 60 degree swirler flames. The dimensions of the recirculation zone depend on the swirler geometry and the swirl number. The recirculation zone is surrounded by an annular forward flow layer where the flow is directed inwards. The thickness of this layer increases with the size of the reverse vortex.

4. The expansion rate of a swirling flame is very high in the initial region of the jet because of the effects of the centrifugal forces on the fluid particles. The expansion of the jet increases with swirl.

5. The rate of entrainment in a swirling flame does not depend linearly on the swirl number or the axial distance from exit and therefore cannot be represented by any of the available expressions in the initial region.

6. The integrated values of the axial fluxes of linear and angular momenta are conserved along each of the jets.

7. The characteristics observed in a swirling flow field are determined by the changes which take place in the forward flow section near the swirler exit. With sufficiently high swirl number, a recirculation zone of such size as can trigger the formation of a wall jet can be obtained. The formation of wall jets or the establishment of a recirculation within a flow field depend on the changes in the static pressures in the jet. It is therefore totally unrealistic to neglect pressure forces in an analysis of swirling jets.

CHAPTER 6

COMPARISON WITH COLD SWIRLING JETS

6.1 Introduction

The results of the distributions of the aerodynamic variables in swirling flames presented in the previous chapter can now be compared with the corresponding variables in cold swirling jets. The comparison will be made with the work reported in (6). The work therein reported was carried out with swirlers of the same geometries and dimensions as those used in the work reported in this thesis.

6.2 Velocity distributions

The cold experiments in (6) were carried out using average nozzle velocities of 100 ft/sec. and 40 ft/sec. with the hubless and annular swirlers respectively.

6.2.1 Axial velocity components

With the 15 degree hubless swirler, the profile obtained in the flame at the first cross-sectional plane of measurement (1 diameter) shows a maximum value on the axis. In the corresponding cold jet, a double-crest/central trough profile was obtained in cross-sectional planes between the exit and a downstream axial distance of about 4 diameters. With all the other hubless swirlers, the shape of the profiles in the initial region of either the cold or the burning jet show the double-crest/central trough form. The distances from the nozzle exit at which the maximum axial velocity components are obtained on the axis are smaller in burning jets.

The main differences are shown in the characteristics and the dimensions of the recirculation vortices. The minimum vane angle (considering the hubless swirlers used) required for the establishment of a reverse

flow vortex is higher in cold jets than in burning jets. The minimum angles are 45 degrees and 30 degrees in cold and burning jets respectively. The positions of the upstream stagnation points in the cold 45 and 60 degree hubless swirler jets are 0.3 and 0.1 diameters respectively from the swirler exit plane. In the flame jets issuing from corresponding swirlers, the upstream stagnation points are at the junction of the swirler vane tips. The effective lengths of the recirculation vortices in burning jets are greater than the values in corresponding cold jets. In both cases, the effective length increases with swirl. The maximum widths of the vortices in burning jets are greater than those in cold jets and the difference increases with swirl. The increase in the maximum width with increasing swirl shown in the cold results are similarly obtained in the burning jets. The maximum reverse velocities, calculated as ratios of the average nozzle velocities, do not show any clear dependence on the thermodynamic state of the jet. The distance from the swirler exit of the radial plane on which the maximum reverse velocities are obtained are constant in burning jets as in cold ones. These features and others are shown in Table 9.

TABLE 9

Recirculation Vortices in Cold and Burning Hubless Swirler Jets

Swirler Vane Angle (degrees)	Type of Jet	Effective Length (diameter)	Max. Width (in)	Max. reverse vel. / Nozzle vel.	Position of max. reverse velocity (diameters)
15	Cold	-	-	-	-
	Burning	-	-	-	-
30	Cold	-	-	-	-
	Burning	2.835	0.44	0.225	1.0
45	Cold	2.900	0.20	0.330	1.0
	Burning	3.501	0.50	0.300	2.0
60	Cold	3.900	0.20	0.400	1.0
	Burning	4.667	1.00	0.575	2.0

The rate of decay of the maximum axial velocity components in both cold and burning jets increases with swirl but the slow rate of decay of the maximum axial velocity components in the burning 60 degree hubless swirler jet is not shown in the corresponding cold results.

With the annular swirlers, the differences and similarities of the profiles are the same as those with the hubless swirlers. The features of the recirculation vortices are shown in Table 10.

TABLE 10

Recirculation Vortices in Cold and Burning Annular Swirler Jets

Swirler Vane Angle (degrees)	Type of Jet	Effective Length (diameter)	Max. Width (in)	Max. reverse vel. / Nozzle vel.	Position of max. reverse velocity (diameters)
15	Cold	-	-	-	-
	Burning	-	-	-	-
30	Cold	-	-	-	-
	Burning	-	-	-	-
45	Cold	3.700	0.858	0.350	1.06
	Burning	2.030	1.625	0.500	0.50
60	Cold	5.000	1.430	0.700	1.17
	Burning	3.213	3.500	0.700	1.50

In the jets from these swirlers, the recirculation vortices are shorter in flame jets than in cold ones. The distances of the cross-sectional planes on which the maximum reverse velocities are obtained remain almost constant in the cold annular swirler jets as in the cold hubless jets. This is not so in the burning jets. The maximum widths of the recirculation zones are greater in burning jets than in corresponding cold jets. The critical vane angle at which recirculation is established in cold jets is the same as in burning jets.

The axial velocity component on the axis of each of the cold jets decreases immediately after exit from the swirler. The minimum values are observed at about 1.0 diameter from the exit. The same applies for the hubless swirler cold jets. In the burning jets, the reductions are observed only in hubless swirler flames with recirculation vortices. In the annular

swirler flames, the 15 degree swirler flame results show an increase whilst the other swirler flames show reductions although the positions of the minimum values are not almost constant as in cold jets.

The rates of decay of the maximum axial velocity components appear to be higher than those of the cold jets in the initial regions of the jets. Further downstream, the rates of decay in the burning jets are slightly lower.

6.2.2 Tangential velocity components

The results obtained with the cold and burning hubless swirler jets show the central forced vortex core surrounded by the annular free vortex region. In each of the cold jets, about half the mass flow is contained within the forced vortex core near the swirler exit but as the axial distance increases, the proportion in the free vortex region increases. In the burning jets, similar behaviour is observed though it appears that the increase with axial distance of the proportion contained within the free vortex region is much more rapid than in cold jets. The slight distortion in the profiles of the 45 and 60 degree hubless swirler flames at axial distances of 1.0 and 2.0 diameters are not shown in the corresponding cold jets.

With the annular swirlers, the profiles are similar to those described for the hubless swirler jets. The proportion of fluid within the forced vortex core remained almost half of the total in the initial region of the cold jets but in the burning jets a greater proportion is contained within the zone. The situation is reversed very rapidly, particularly in flames with low swirl, as the distance downstream increases. The distortion which is shown in all the profiles of the swirler flames is obtained in cold jets with any swirler whose vane angle is equal to or greater than 45 degrees.

6.3 Jet width

The variations of the widths of some of the cold and burning jets are shown in Figures 75 (a) and (b). The cold jets expand rapidly immediately after the nozzle exit but within a short distance downstream. the variations become almost linear and independent of swirl. In the burning jets, the expansion rate near the swirler exit is much higher than in the corresponding cold jet. Although the expansion rate tends to be a constant as the axial distance increases, the axial position where this trend begins to show is greater in burning jets than in cold jets. As the distance from the exit increases, the expansion rate of the cold jets become greater than those of burning jets with corresponding vane angles. Between 7.0 and 9.0 diameters from the exit, the width of cold and burning jets of corresponding vane angle and swirler geometry will become equal. Further downstream the width of the cold jets will be greater than those of the burning jets.

6.4 Static pressure

The static pressure measurements in the cold experiments were made only on the axis of each of the hubless and annular swirler jets. It is therefore not possible to compare the static pressure profiles reported earlier with any cold results. In fact, no detailed static pressure measurements in swirling jets appear to have been made previously.

The static pressures measured on the axis of each of the hubless and annular jets are subatmospheric as in the burning jets. In the hubless swirler jets higher values are recorded in cold jets than in the burning jets with corresponding vane angles. For example, in the cold jets, the static pressures at about 1.0 diameter are 0.45, 0.90 and 2.26 in water with the 15, 30 and 60 degree swirlers. In the burning jets, the corresponding values are 0.105, 0.075 and 0.1100 in. water respectively.

All the results in the cold jets show continuous increase of static pressure and the rates of decay of the static pressure are much faster than in burning jets.

With the annular swirlers, the non-linear variation of static pressure with swirl is evident in the cold results. Similar results were reported earlier for the burning jets. The magnitudes of the pressures at corresponding axial positions are much closer than those of the hubless swirler jets. The rates of decay of the values with cold jets are higher at planes close to the exit but further downstream, they are almost equal.

6.5 Axial fluxes of linear and angular momenta

From the results of the velocity profiles in (6), the required data for calculating these parameters were obtained. The method of calculation was the same as those discussed previously. The pressure terms were not included in the analysis because these data were not available.

The results of the axial fluxes of the above parameters appear to indicate that they are conserved along the length of the jets. There are some deviations in the results as in those of the burning jets. The calculated values of the fluxes are higher than the values obtained in the burning jets. The calculated swirl numbers, although still slightly higher, are closer to the values calculated from equation (3.7) than the values obtained for the burning jets.

6.6 Mass flow rates

The mass flow rates for all the hubless and annular swirlers were calculated from the results in (6). Some of the results obtained are shown in Figures 76 (a) and (b). As in the burning jets, the entrainment

rates increase with the axial distance. The increases in the cold jets are almost linear with axial distance but there is a slight non-linearity near the exit in the results with the burning jets. The entrainment rates in the burning jets are higher than those in the cold jets.

6.7 Discussions

The differences outlined in the preceeding sections of this chapter confirm that the aerodynamic field of a swirling flame is quite different from that of a cold jet. The outstanding differences are shown, mostly, by the characteristics and dimensions of the recirculation vortices.

As previously discussed, the characteristics of the recirculation vortex in a swirling flow field depend to a great extent on the balance between the centrifugal forces generated by the swirl at the nozzle exit and the static pressure gradients. Even without a recirculation zone, this factor is still of great importance. The centrifugal forces depend on the values of the tangential velocities which in turn depend on the distribution of the absolute velocities at the exit, The crux of the whole phenomenon is, therefore, the effects of the density gradients on the inlet conditions.

The results of the flame stabilisation tests show that the position where combustion is initiated in a hubless swirler flame is different from that in an annular swirler flame. Therefore the positions of the flame fronts will be different in both geometries and as a consequence of this, the position where the transformation of the density gradients take place will differ. This explains the differences in the compared results of jets from hubless and annular swirlers. The changes in the density gradients will necessarily be accompanied by changes in the distribution of the absolute velocity profile at the inlet plane.

This, therefore, highlights the importance of taking measurements at the exit plane of the swirler. In doing this, any results taken on a vertical or horizontal plane will be affected by the wakes behind the swirler vanes. It will, hence, be required to design a traversing mechanism to enable measurements to be made along a radius which is at the midpoint of two adjacent vanes. This can be combined with results obtained along a horizontal or vertical radius to obtain a general average.

In addition to the observations on the recirculation vortices, it is similarly interesting to note the results for the variations of jet width. This result is no doubt connected with the combustion pattern in the flames but how it is so appears to be rather obscure. One possible explanation is deducible from observations of the results obtained during the aerodynamic investigations at the exit plane of the annular swirlers. When the measuring position is around the midpoint of two adjacent vanes and close to the outer wall of the swirler, the measured velocity heads are usually high but the temperatures are low. The calculated velocity components are then low. The possible effect of this will be to reduce the effective jet width in the initial region of the jet. The reduction will result from the inability of the jet to avail itself of the added expansion which would have been due to the combustion of the mixture that excaped the reaction zone.

The increased entrainment rates of the burning jets can be attributed to two factors. The first one is the increased surface area of the burning jets upstream of about 7.0 diameters from the swirler exit. The second factor is the lesser density of the gases in the burning jets. This is shown by the inverse proportion of the entrainment rate to nozzle fluid density as given in equation (5.1). The equation (5.2) suggested by Kerr and Fraser does not fit the data points.

6.8 Conclusions

The combustion at the exit plane of a swirling jet alters the distribution of the aerodynamic variables on this plane. As a result of this, the characteristics of the distributions of the variables in flames are different from those in cold jets although the general pattern remains almost the same.

The critical vane angle at which a recirculation vortex is established in a hubless swirler flame is less than that in a cold jet. With the annular swirlers, the critical angles are the same.

The maximum width of the recirculation zone is greater in burning jets than in cold jets with both swirler geometries. The lengths of the recirculation zones in burning jets are less than the values in cold jets with annular swirlers. With the hubless swirlers, the lengths are almost equal.

The integrated values of the axial fluzes of linear and angular momenta indicate that these parameters are conserved in cold and burning jets from both swirler geometries.

The burning jets are wider than the cold equivalents in the initial region of the jets. Between 7.0 and 9.0 diameters, the width of a burning jet becomes equal to that of a cold jet. Further downstream, the cold jets become wider than the burning jets. As a result of the greater jet width and the lesser density in the burning jet, the entrainment rates are higher in burning jets than in cold ones.

CHAPTER 7

PREDICTION METHOD

7.1 Introduction

The direct analysis of the equations of fluid motion in a three-dimensional flow field is almost a formidable problem. Fortunately, most flow fields of interest in engineering are axisymmetric. As a result of this, the number of relevant terms in the equations are reduced. Non-theless, the dependent variables are still interconnected and the closed-form solutions available are usually applicable to cold flows. Consequently, the design of combustion systems have to be based on empirical data from tests on either cold models or on prototypes. The data from cold tests are, no doubt, very inadequate and investigations with prototypes are expensive. The provision, therefore, of a prediction method for the analysis of the flow distributions in a general stream, cold or burning, will be of tremendous practical value.

Recently, Spalding et al (8) formulated a computational procedure for the analysis of the equations of motion in a general two-dimensional flow field by finite-difference method. A computer program was written for solving the finite-difference equations. From this general foundation, Odlozinski (9) developed a prediction method for flow distributions in a confined premixed flame stabilised on a bluff-body. In Odlozinski's analysis, the geometry of the flow field was as shown in Figure 77 and a uniform inlet velocity was specified.

A swirling jet issuing from any of the common swirl generators is axisymmetric and effectively, it is a two-dimensional flow. The computational procedure discussed above is, hence, applicable. The prediction method discussed in this thesis was developed from the work of Odlozinski. The computer program was developed for the analysis of the flow distributions

in cold and burning swirling jets and also for processing in either a KDF9 or UNIVAC 1108 computer. The geometry of the flow field used is shown in Figure 78.

7.2 Theory of the prediction method.

7.2.1 The transformed equations

By using the concepts of stream function and vorticity, the equations expressing the conservations of mass, momentum along each of the coordinate directions and chemical species together with the mathematical statement of the First Law of Thermodynamics can be transformed into elliptic equations for the analysis of the flow distributions in a flow field with reaction-rate-controlled combustion. The general form of the elliptic equation is

$$\alpha_1 \bar{G}' . \text{ grad } \varphi = \text{div } \alpha_2 \text{ grad } (\alpha_3 \varphi) + \alpha_4 \qquad \ldots(7.1)$$

where the coefficients α_1, α_2, α_3 and α_4 for each of the dependent variables are shown in Table 11 in cylindrical coordinates.

The details of the derivation and simplification of the equations are given in Appendix A1. The left hand side of equation (7.1) can be referred to as the convection term. The first term of the right hand side of the equation can be called the diffusion term whilst α_4 can be called the source term. The equations of the dependent variables as shown in the Table can be used for the analysis of laminar and turbulent flows. In the case of turbulent flows, the transport properties are represented by the "effective" turbulent values.

TABLE 11

Relations for α_1, α_2, α_3 and α_4 as in Equation (7.1)

φ	α_1	α_2	α_3	α_4
$\frac{\omega}{r}$	1	1	μ_{eff}	$\frac{1}{r}\left[\frac{\partial \rho}{\partial r} \cdot \frac{\partial}{\partial x}\left(\frac{V_s^2}{2}\right) - \frac{\partial \rho}{\partial x} \cdot \frac{\partial}{\partial r}\left(\frac{V_s^2}{2}\right) + \frac{\partial}{\partial x}\left(\frac{\rho w^2}{r}\right) + 2\mu_{eff}\frac{\partial}{\partial r}\left(\frac{\omega}{r}\right)\right]$
ψ	0	$\frac{1}{r^2}$	1	$\rho\left(\frac{\omega}{r}\right) - \frac{1}{\rho r^2}\left[\frac{\partial \psi}{\partial x} \cdot \frac{\partial \rho}{\partial x} + \frac{\partial \psi}{\partial r} \cdot \frac{\partial \rho}{\partial r}\right]$
w	1	μ_{eff}	1	$-\frac{w}{r}\left[\frac{\mu_{eff}}{r} + G'_r + \frac{\partial \mu_{eff}}{\partial r}\right]$
m_{fu}	1	$\Gamma_{fu,eff}$	1	$-K\, m_{fu}\, m_{ox}\, \rho^2\, T \cdot e^{-\frac{E}{RT}}$
H	1	Γ_{eff}	1	0
mf	1	Γ_{eff}	1	0

7.2.2 Finite-Difference form

It will be observed in Table 11 that the transformed equations are still as complex as the original equations because of the interdependence of the variables. Because of this, the equations will have to be solved simultaneously. At present, there is no possibility of obtaining closed-form solutions and thus the solutions have to be obtained by the finite-difference method.

In using this method, the flow field is divided into grid points and the finite-difference form is obtained by integrating the partial differential equations for a dependent variable over the control volume.

The partial derivatives of the variables at any grid point in the flow field is represented by the differences in the values of the variables at the point and its neighbouring grid points. The general form of the final finite-difference equation is

$$\phi_p = \alpha_e\varphi_e + \alpha_w\varphi_w + \alpha_n\varphi_n + \alpha_s\varphi_s + \beta \qquad \ldots(7.2)$$

7.2.3 Details of the computations

7.2.3.1 Grid Spacing

The flow field is divided into a number of grid points. Along the length of the flow field a non-uniform grid distribution varying in geometrical progression is used. Along the radius of the jet, the grid spacing varies uniformly within the inlet plane of the swirler, and at the outer grid points, the variation is according to geometrical progression. Specifications for the 16 x 14 grid system is given in the program for hubless and annular jets.

7.2.3.2 Dependent variables

The dependent variables are specified in order of solution inthe program. For cold jets the dependent variables of interest are the vorticity, stream function and tangential velocity. For burning jets additional variables have to be solved for and these are the fuel mass fraction and the enthalpy.

7.2.3.3 Enclosing boundary

In the solution of elliptic partial differential equations, the values of the dependent variables on the enclosing boundary must be specified. The boundary conditions used will be discussed in the next section.

7.2.3.4 Computational procedure

Together with the boundary values, initial guesses are made for the distribution of each dependent variable at points not on the boundary. The initial values can be zero or as specified in the program. From experience, it does not appear to matter what these initial guesses are but when a burning jet is being considered, solutions are usually obtained faster with non-zero initial values. Starting from a grid point one mesh away from the inlet plane, new values are calculated for the variable and the new value immediately replaces the previous value. This makes it possible to use the updated value in updating the values at its neighbouring grid points. This procedure is carried out for all non-boundary grid points in the flow field after which the boundary values are recalculated (if need be). The cycle is then repeated until the fractional difference between two successive iterations is either equal to or less than a specified minimum. This minimum value is referred to as the convergence criterion. During the processing of the solutions, the values of the axial and radial components of velocity are calculated after each iteration. This is to obtain the values of these parameters for use in evaluating the source terms of some of the variables. Furthermore, the maximum differences and fractional differences in the flow field for each dependent variable are printed after each iteration and after a specified number of iterations, the dependent variables are printed.

Although it is generally known that there are intermediate stages in a combustion process, a simple chemical reaction whereby the reactants combine in a fixed (stoichiometric) proportion is considered. As a result of the combustion, the temperature, and thus density and viscosity, are no longer constant. The temperature is calculated from

the updated values of the fuel mass fractions and the enthalpy by the equation

$$T = \frac{(H - m_{fu} \cdot HC)}{C_p} \qquad \ldots(7.3)$$

where HC is the net calorific value of the fuel.

The density is calculated from the equation

$$\rho = \frac{pM_{mix}}{\bar{R}T} \qquad \ldots(7.4)$$

where p is the static pressure and is assumed to be atmospheric, and M_{mix} is the mixture molecular weight and is calculated from

$$M_{mix} = \frac{1}{\frac{m_{fu}}{M_{fu}} + \frac{m_{ox}}{M_{ox}} + \frac{m_{pr}}{M_{pr}}} \qquad \ldots(7.5)$$

The value of m_{ox} at each grid point is calculated from the values of the fuel mass fraction and the mixture fraction (mf). If the mixture fraction is not computed for, its values are deduced from those of the enthalpy since both are represented by equivalent equations as shown in equations (A.29) and (A.31) of Appendix A1. The mass fraction of the combustion products is evaluated from

$$m_{fu} + m_{ox} + m_{pr} = 1 \qquad \ldots(7.6)$$

Because of the strong influence of the density gradients, under-relaxation was used in the analysis. An under-relaxation parameter (ROWF) is specified such that from the density calculated at the end of each cycle, the value of the density used in the next cycle is calculated from

$$\rho_2 = ROWF. \rho_2' + (1 - ROWF). \rho_1 \qquad \ldots(7.7)$$

where ρ_2 is the value used in next iteration,

ρ_2' is the value obtained from the calculated temperature in next iteration,

ρ_1 is the value of density in previous iteration,

and ROWF is the under-relaxation parameter.

In the analysis of the flow distributions in a combustion system, the computation is first carried out for a cold flow and the values obtained for each of the variables are used as the initial values in the combustion system. In the present analysis, the computation is not necessarily carried out until converged solutions are obtained and it does not appear to be absolutely necessary for convergence to be obtained before proceeding with the computation of the cmmbustion system. For the solutions obtained, under-relaxation is used in the computation of the variables when combustion is taking place.

7.2.3.5 Specification of physical parameters

The numerical values of some of the physical input parameters are constant. These are specified in the main program and will not be discussed here.

In the derivation of the equations, the laminar viscosity is replaced by the "effective" turbulent equivalent. The representation of μ_{eff} used in the analysis is the dimensionally derivable expression

$$\mu_{eff} = A\, D^{\frac{2}{3}}\, L^{-\frac{1}{3}}\, \rho^{\frac{2}{3}}\, (\dot{m}\, \bar{V}^{-2})_o^{\frac{1}{3}} \qquad \ldots(7.8)$$

where A is a constant,

D is the diameter of the enclosing boundary,

L is the axial length of the enclosure,

ρ is the density at a grid point,

and $(\dot{m}\, \bar{V}^{-2})_o$ is the kinetic energy at inlet.

The effective turbulent exchange coefficients of the fuel mass fraction, enthalpy and mixture fraction are assumed to be equal and representable by a mean value Γ whose ratio to the effective viscosity is assumed to be 1. The ratio μ_{eff}/Γ_{eff} is referred to as the turbulent Prandtl or Schmidt number.

The derivation of the equation for enthalpy assumes that the specific heats of the various components of the fluid are equal and that this value is independent of temperature. This, of course, is not the physical situation in the stream. In the present analysis, however, the specific heat is represented by a provisional value of 0.24.

The rate of comsumption of the fuel by chemical reaction per unit volume is given by the reaction rate equation

$$R_{fu} = - K m_{fu} m_{ox} \rho^2 \quad T \quad e^{-\frac{E}{\bar{R}T}} \qquad \ldots(7.9)$$

When combustion is occurring within a small volume or when the chemical reaction is taking place in a well-stirred combustor, e.g. in a well-stirred reactor, the chemical reaction rate will be almost uniform within the reaction volume. The reaction rate constant (K) for this type of combustion system is usually calculated from data on stability limits and combustion efficiency. With the data obtained from the work of Longwell and Weiss (56), Odlozinski made this calculation for various mixture ratios. The value of the reaction rate constant used in the program was obtained from this calculation. For the activation energy (E), Longwell and Weiss suggested a value of above 45,000 calories per mole. Further experiments conducted by them (56) confirm that the above value could be used for most hydrocarbon flames.

7.3 Boundary conditions

The boundary conditions specified in the program are those for free swirling jets. A fictitious outer boundary is assumed, the criterion of its location being to have it as far away as possible from the jet axis so that free jet conditions will effectively prevail. The modification of the program for the analysis of confined swirling jets is a relatively simple matter and for the sake of future users, the details of the boundary conditions for confined jets will be included. Some of the boundary conditions will be discussed with reference to Figure 79.

7.3.1 Gradient-type

At some of the boundaries, it is not possible to deduce the values of some of the dependent variables from physical factors. Assuming then a parabolic distribution of the variable between the boundary grid point (point 1 in Figure 80) and the adjacent two grid points (points 2 and 3) on the grid line normal to the boundary point and that the partial differential $(\partial\varphi/\partial n)$ on the wall is zero, the value of the variable on the boundary can be calculated from

$$\varphi_1 = \varphi_2 \left[\frac{1}{1 - \left(\frac{n_1}{n_2}\right)^2} \right] - \varphi_3 \left[\frac{1}{1 - \left(\frac{n_1}{n_2}\right)^2} - 1 \right] \qquad \ldots(7.10)$$

where n_1 is the distance of point (2) from the boundary

n_2 is the distance of point (3) from the boundary

and $\varphi_{1,2,3}$ are the corresponding values of the variable at these points.

The use of this boundary condition at various positions of the boundary is shown in Figure 80.

7.3.2 Vorticity

The solution for the vorticity is the nucleus of the prediction method for two reasons. Firstly it represents the x-momentum and r-momentum and secondly it has a strong influence on the source term (α_4) of the stream function whose solution influences all the dependent variables. Special consideration was therefore given in (8) to the vorticity boundary conditions especially at wall points.

7.3.2.1 Wall points

At these points, the vorticity is calculated from two parameters g_1 and g_2 and the vorticity at one grid point away from the wall. The expression is

$$\left(\frac{\omega}{r}\right)_P = g_1 + g_2 \left(\frac{\omega}{r}\right)_{NP} \qquad \ldots(7.11)$$

where P is the wall point and NP is the grid point away from the wall. The geometrical details are shown in Figure 81. The values of g_1 and g_2 for various conditions are shown in Table 12.

7.3.2.2 On the inlet plane

The definition of vorticity is

$$\omega = \frac{\partial v}{\partial x} - \frac{\partial u}{\partial r} \qquad \ldots(7.12)$$

From the specified distribution of the axial velocity components at inlet, the vorticity can be calculated at points which are not on the pipe walls.

7.3.2.3 Along the axis of symmetry

The value of v on the axis of symmetry is zero and so is the differential of u with respect to the radial coordinate. Thus ω is zero. The parameter used in the analysis is not ω but ω/r. This therefore creates the problem of the exact value of vorticity on the axis because

$$\frac{\omega}{r} = \frac{0}{0} \qquad \ldots(7.13)$$

and this is mathematically indeterminable. However, the vorticity parameter was represented as zero in this analysis.

TABLE 12

Expressions for g_1 and g_2 in Equation 7.11

Axisymmetric flows	Horizontal Walls	$g_1 = \dfrac{(\psi_P - \psi_{NP}) / n^2_{NP}}{R\left[\rho_P\left(\frac{R}{3} + \frac{5}{24} kn_{NP} + \Delta\rho\left(\frac{5}{24}R + \frac{3}{20} kn_{NP}\right)\right]\right.}$ $g_2 = -\dfrac{(R + kn_{NP})\left[\rho_P\left(\frac{R}{6} + \frac{kn_{NP}}{8} + \Delta\rho\left(\frac{R}{8} + \frac{kn_{NP}}{10}\right)\right]\right.}{R\left[\rho_P\left(\frac{R}{3} + \frac{5}{24} kn_{NP}\right) + \Delta\rho\left(\frac{5}{24}R + \frac{3}{10} kn_{NP}\right)\right]}$
	Vertical Walls	$g_1 = \dfrac{\psi_P - \psi_{NP}}{(r^2 n^2_{NP})\left(\frac{1}{3}\rho_P + \frac{5}{24}\Delta\rho\right)}$ $g_2 = -\dfrac{\frac{1}{6}\rho_P + \frac{1}{8}\Delta\rho}{\frac{1}{3}\rho_P + \frac{5}{24}\Delta\rho}$
Plane flows	Horizontal and Vertical Walls	$g_1 = \dfrac{\psi_P - \psi_{NP}}{n^2_{NP}\left(\frac{1}{3}\rho_P + \frac{5}{24}\Delta\rho\right)}$ $g_2 = -\dfrac{\frac{1}{6}\rho_P + \frac{1}{8}\Delta\rho}{\frac{1}{3}\rho_P + \frac{5}{24}\Delta\rho}$

(See Figure 81 for geometrical details)

R = distance of the wall from axis of symmetry

$\Delta\rho = \rho_{NP} - \rho_P$

k = 1, when n and radial distance (r) are measured in the same direction

= - 1, when n and r are measured in opposite directions

7.3.2.4 Along B1 - B2, B2 - B3 and B8 - B7. (See Figure 79)

The boundary values along these walls are calculated from the relevant expressions in Table 12. The calculations along B2 - B3 do not include the points B2 and B3 because these lie effectively on B1 - B2 and the axis respectively.

7.3.2.5 Along B7 - B6 and B4 - B5

The gradient type of boundary condition is used. For B7 - B6 and B4 - B5, it is possible to calculate the boundary values from the values of the axial and radial velocity components. Care is, however, needed in doing this on the B7 - B6 plane as it can cause the solution to oscillate particularly when there is combustion. Also this procedure slows down the rate of convergence.

7.3.2.6 Along B6 - B5

In the results presented later, the vorticities are put equal to zero. It is possible to use the gradient type of boundary condition.

7.3.2.7 Confined jets

The modifications needed for analysis of confined jets are for the conditions along B7 - B6 and B6 - B5. At these planes, the values must be calculated from relevant expressions in Table 12.

7.3.3 Stream functions

7.3.3.1 On the inlet plane

The inlet distribution of the stream function at any radial position r is obtained from

$$\psi_r = \int_0^r \rho u \, r \, dr \qquad \ldots(7.14)$$

7.3.3.2 Along B1 - B2, B2 - B3 and B8 - B7

For points on the plane B1 - B2, the values are equal to that at the point B1. Similarly values along B8 - B7 are equal to that at B8. For B2 - B3, the values are equal to that at B2. The above is applicable because there is no additional flow across these surfaces into the stream.

7.3.3.3 Along the axis

Values at points along the axis are equal to that at E2. This is so because of the reason given in the above paragraph.

7.3.3.4 Along B7 - B6

In the consideration of free jets, allowance must be made for entrainment. Along the above plane, v is zero but the values of u are not known and there does not appear to be any analytical method of obtaining them. The values are therefore obtained from the computed values at the two adjacent normal grid points using equation (7.10). The stream function is then obtained by integration using the trapezoidal integration method.

7.3.3.5 Along B6 - B5

The gradient type of boundary condition is used at all the points on this plane. It is also possible to calculate the values using the same method as in the previous subsection.

7.3.3.6 Along B4 - B5

Gradient type of boundary condition is used. It is possible to calculate the values from the axial velocity components in which case, the values of the axial velocity components will have to be calculated as stated in subsection 7.3.3.4.

7.3.3.7 Confined jets

For the analysis of such jets, the values along B7 - B6 and B6 - B5 must be put equal to the value at the point B7.

7.3.4 Tangential velocity

7.3.4.1 On the inlet plane

The tangential velocities are calculated from the equation

$$w_o = u_o \tan \theta$$

where θ is the vane angle of the swirler.

7.3.4.2 Along B1 - B2, B2 - B3, B3 - B4, B8 - B7, B7 - B6 and B6 - B5

The tangential velocities at points on these planes are equal to zero.

7.3.4.3 Along B4 - B5

The values are calculated from the expression for gradient type of boundary conditions.

7.3.4.4 Confined jets

The above conditions are applicable in confined jets.

7.3.5 Fuel mass fraction

7.3.5.1 On the inlet plane

The values specified in the program on this plane are rather arbitrary. In order to initiate the combustion, the specified values must be sufficiently low.

7.3.5.2 Along B1 - B2, B2 - B3, B3 - B4, B8 - B7 and B4 - B5

The values along these planes are calculated using the gradient type of boundary conditions.

7.3.5.3 Along B7 - B6

The fuel mass fraction at each point is specified as zero.

7.3.5.4 Along B6 - B5

For the first six grid points along these planes, the values are specified as zero and gradient type of boundary condition used at other points.

7.3.5.5 Confined jets

For these jets gradient type of boundary conditions must be used along B7 - B6 and B6 - B5.

7.3.6 Enthalpy

7.3.6.1 On the inlet plane

The variable computed in the program is the dimensionless enthalpy. The inlet distribution must therefore be specified accordingly. For each point on the plane, the dimensionless enthalpy must be calculated from the equation

$$\frac{(c_p T + m_{fu} \cdot HC)}{HP} \qquad \ldots(7.15$$

where HC is the net calorific value of the fuel and HP is the reference enthalpy at inlet.

7.3.6.2 Along B1 - B2, B2 - B3, B3 - B4, B4 - B5 and B8 - B7

The method of calculation is the same as for the fuel mass fraction.

7.3.6.3 Along B7 - B6

The values here are calculated from equation (7.15) using HC = 0 and the atmospheric temperature.

7.3.6.4 Along B6 - B5

The method of calculation is the same as for the fuel mass fraction except that the values at the first six grid points are calculated as in the preceeding subsection.

7.3.6.5 Confined jets

Similar modifications mentioned in subsection 7.3.5.5 will be required.

7.4 Computed results

The program has been used for the computation of the flow distributions in both cold and burning swirling jets. The results obtained with cold jets were for 15 and 45 degree vane swirlers. With the burning jets the results for the 15 degree swirler was obtained. The effect of the variation of some of the input parameters were also analysed. The results presented here are for annular jets issuing from swirlers of the same geometry and dimensions as those used in the experimental investigations.

7.4.1 Cold swirling jets

A triangular axial velocity profile is specified at the inlet of the annular flow section. In the program, the velocity head (in. water) is specified at each point on the inlet plane and the velocity is calculated from it. The maximum axial velocity of 80 ft/sec was at the midpoint of the flow section.

The results obtained with the 15 degree swirler are shown in Figure 82. The shape of each of the profiles near the exit showed the double-crest/central trough form which is characteristic of swirling jets. The tangential velocity profiles showed the forced-vortex/free-vortex profiles of swirling jets. A comparison is made between the computed results and the experimental data in (6) and as will be observed, the result showed good agreement.

The results with the 45 degrees swirler is shown inFigure 83. The features of the axial and tangential velocity profiles are very similar to those obtained from experimental investigations. A recirculation zone is

established in the flow field and the maximum width (radially) is about 0.64 in. The maximum axial velocity component has not yet reached the axis within the 10.2 diameters axial length for which solutions were obtained.

The rates of decay of the axial velocity components along the axis and that of the maximum axial velocity components along each of the 15 and 45 degrees swirler jets are shown in Figure 84. The position of the maximum reverse velocity in the 45 degree swirler is about 1.0 diameter which corresponds with the cold experimental results in (6). The length of the recirculation zone is about 16.0 in. The maximum axial velocity components decayed continuously along the length of each of the jets.

The entrainment rates obtained from the values of stream function are shown in Figure 85 for both jets. The entrainment rates increase with axial distance and the increase in the entrainment rate with swirl is also shown.

7.4.2 Burning swirling jets

In each of the computations, the same specification of velocity heads as those for the cold jets are used. This was purely for convenience. As a result of the combustion, the maximum axial velocity component was higher than that with cold flow. For each of the computations, the specified inlet distribution of the fuel mass fraction is shown on the corresponding diagram. The dimensionless enthalpy was not calculated from equation (7.15) but was assumed to be uniform across the inlet plane.

For uniform distribution of the fuel mass fraction at inlet, the results are shown in Figures 86 (a) and (b). The results for a different specification of the fuel mass fraction distribution as shown in Figures 87 (a) and (b). The results show the general characteristics obtainable in swirling flames. All the above results were computed with

the value of 45,000 calories per mole for the activation energy. With the conditions in the computation whose results are presented in Figures 87 (a) and (b), other computations were made with values of 30,000 and 60,000 calories per mole for the activation energy. The results of these computations showed that the effect of the variation of the value of activation energy is almost negligible.

7.5 Discussion of results

For the sake of future users, it will be desirable to give further comments on the computations reported above.

The computations of the flow distributions with the 15 and 45 degrees swirlers were carried out together. The solutions for the 15 degree jet was used as the initial values for the 45 degrees jet. This appears to be a necessary procedure because the first computation for the 45 degrees swirler in which this procedure was not used diverged. The reason for this is the strong dependence of the source term for vorticity on the centrifugal force parameter

With burning jets, the computation was first carried out for the cold model and the results are used as initial values for the computations with the burning jet. It does not appear to be necessary that a converged solution of the cold model should be obtained but the computation should be carried sufficiently far to give reasonable initial values. Furthermore, it was necessary to under-relax the dependent variables. This was in addition to the density relaxation parameter. The relaxation factor for density was 0.10. This is probably too low and higher values may be possible. The relaxation parameter for the dependent variables was 0.25.

The value of the specific heat used in the computation is low and this will give higher temperatures than should have been obtained. More accurate values can be obtained from equation (3.16) for the variation of specific heat of air with temperature or from similar expressions. This will enable the variation of specific heat with temperature to be taken into account in the computation and this in turn will lead to greater accuracy.

Although the initial aim of the mathematical analysis was to obtain results particularly for burning jets which could be compared with the experimental results presented earlier, the success in this direction is limited. This is due to shortage of time. However, the program at its present stage gives good results judging from the comparison of the predicted 15 degrees swirler results and those experimentally determined in (6).

7.6 Conclusions

The prediction method at its present stage of development gives quantitatively and qualitatively good results for cold swirling jets. The predicted distributions, however, depend strongly on the specified inlet profiles and the boundary conditions. In using the program for the analysis of practical cold swirling flows, it will be necessary to measure the inlet profiles of the axial and tangential velocity components.

The results of the burning jets are quantitatively good in as much as the patterns of the predicted flow distributions are similar to those experimentally determined. It is believed that with accurate specification of the inlet profiles for the axial and tangential velocity components, temperature and fuel mass fraction and specification of temperature dependent specific heat, the program will give qualitatively good results.

CHAPTER 8

GENERAL CONCLUSIONS AND FURTHER DEVELOPMENTS

8.1 Conclusions

From the results of the experimental and theoretical investigations, the following conclusions are arrived at.

8.1.1 Flame stabilisation

Swirling flames issuing from vane swirlers are highly stable and the position of anchorage of the flame base depends on the swirler geometry. As the fuel/air ratio and average nozzle velocity of the mixture change, the structure of the resultant flame changes.

Attendant to the changes in the flame structure are variations in the stability limits of the flames. For the same flow velocity, the fuel/air ratios at weak and rich blow-off limits increase with swirl. The increases at the rich blow-off limits are greater than the increases at the weak blow-off limits, thus the range of flow conditions at which stable flames are obtained increase with swirl.

8.1.2 Aerodynamic characteristics of swirling flames

The profiles of axial velocity components show off-centre maximum values but as the axial distance from the nozzle exit increases, the maximum values tend to the jet axis. Near the swirler exit, the radial displacements of the maximum axial velocity components increase with swirl. The position along the jet where the maximum reaches the axis depends on the swirl.

A central forced vortex core exists in a swirling jet. This core is surrounded by an annular free vortex region which extends to the edge of the jet. The proportion of the nozzle fluid contained within each type of vortex varies with swirl and as the tangential

velocity components decay with increasing distance from the swirler exit, the proportion in the forced vortex core decreases.

The rotation of the nozzle fluid gives rise to a centrifugal action which forces increasing proportions of the fluid away from the axis as the swirl increases. The concentration of the fluid near the outer edge of the jet gives rise to velocity increases which in turn gives rise to pressure drop. Consequently, the static pressure in a swirling flow field is subatmospheric and remains so beyond about 10.0 diameters from the exit although the values increase as the axial distance increases. The static pressure drop at a point caused by the rise in fluid velocity increases with the required velocity increment and thus the static pressure decreases from the jet axis to a minimum at the radial position of maximum velocity. This gives the static pressure profile a double-crest/central trough shape in flows with sufficiently high swirl.

As a result of the fluid displacement, off-centre maximum temperatures are obtained in swirling flames. The degree of the displacement from the axis depends on swirl. The position at which the maximum flame temperature is measured decreases with swirl and thus the flame length effectively decreases.

The expansion of the gases due to combustion coupled with the centrifugal effect of swirl causes a rapid increase in the jet width immediately downstream of the nozzle exit. The expansion rate increases with swirl and consequent on this, the entrainment rate of the jet increases with swirl.

With increasingly high swirl, the centrifugal effect causes sufficient jet expansion and pressure drop that a recirculation zone

is established. The characteristics of the recirculation vortex depend on the swirler exit flow distributions which in turn depend on the swirl number and swirler geometry. For hubless swirlers, the minimum swirler vane angle with which a recirculation vortex will be established is 30 degrees. For annular swirlers, the corresponding angle is 45 degrees.

The increase in the size of the recirculation zone causes a pressure drop which, if sufficiently high, will off-set the balance between the radial static pressure gradients and the centrifugal forces and lead to the formation of a wall jet.

8.1.3 Comparison with cold swirling jets

The pattern of the flow distribution in a cold jet is almost similar to that in a burning jet of the same swirl number although the rates of development of the jets differ.

The differences in the jet development result in variations in the characteristics and dimensions of the recirculation vortices (if present) and also in greater expansion and entrainment rates in burning jets.

8.1.4 Prediction of flow distributions

It is possible to obtain good predictions for cold swirling jets and quantitatively good results for burning jets with the prediction method at its present state. The accuracy of the predicted results for cold jets will be improved by the specification of exact inlet profiles in practical cases. For burning jets, improvements are required in the specifications of the combustion parameters and also in the representation of turbulence.

8.2 Suggestions for further research

The most important characteristic of a swirling jet, with reference to combustion, is the recirculation vortex in the flow field. It has been shown that the establishment of this zone depends on the flow pattern at the swirler exit. The development of the exit conditions start from inside the swirler tube and it will be very illuminating to study the flow distributions upstream of the swirler exit.

The fuel/air ratio and the flow rate of the reactants vary from one combustion system to another. It will therefore be of industrial interest to study the effect of the variations of fuel/air ratio and Reynolds number on the characteristics and dimensions of recirculation vortices.

The free jet results presented in this thesis are not applicable to confined flames unless the combustion chamber is sufficiently wide to make the assumption reasonable. Even then, slight differences will still arise from the entrainment of ambient fluid which will not apply with confined jets. Experiments can be conducted to study the differences between confined and open swirling flames. The effect of the combustion chamber diameter can be studied so that a critical ratio of chamber to nozzle diameter can be found at which free jet conditions effectively prevail.

The wall flame jets formed with swirlers of vane angles 70 and 75 degrees are of no practical use in the design of premixed flames. In diffusion flames, however, it is possible that the combination of a hubless swirler having a vane angle of 70 or 75 degrees with a high velocity secondary air flow with little or no swirl can give high intensity combustion.

APPENDIX A

DERIVATION OF THE EQUATIONS AND THE FINITE-DIFFERENCE FORMS

Introduction

In this section, details of the derivation of the equations and the formulation of the finite difference equivalents will be given.

A.1 Derivation of the equations

A.1.1 The equations of motion

Defining

$$G'_x = \rho u \qquad \ldots(A.1)$$

and $$G'_r = \rho v \qquad \ldots(A.2)$$

the equations of time-steady motion for an axisymmetric $\left[\frac{\partial}{\partial\theta}(\ ) = 0\right]$ compressible swirling fluid in cylindrical polar coordinates are:

Continuity:

$$\frac{\partial}{\partial x}(r\,G'_x) + \frac{\partial}{\partial r}(r\,G'_r) = 0 \qquad \ldots(A.3)$$

x-momentum:

$$G'_x\frac{\partial u}{\partial x} + G'_r\frac{\partial u}{\partial r} = -\frac{\partial p}{\partial x} + \frac{\partial \sigma_{xx}}{\partial x} + \frac{1}{r}\frac{\partial}{\partial r}(r\,\sigma_{rx}) \qquad \ldots(A.4)$$

r-momentum:

$$G'_x\frac{\partial v}{\partial x} + G'_r\frac{\partial v}{\partial r} - \frac{\rho w^2}{r} = -\frac{\partial p}{\partial r} + \frac{\partial \sigma_{rx}}{\partial x} + \frac{1}{r}\frac{\partial}{\partial r}(r\,\sigma_{rr}) - \frac{\sigma_{\theta\theta}}{r} \qquad \ldots(A.5)$$

θ-momentum:

$$G'_x\frac{\partial w}{\partial x} + G'_r\frac{\partial w}{\partial r} + \frac{\rho v w}{r} = \frac{\partial \sigma_{\theta z}}{\partial x} + \frac{1}{r^2}\frac{\partial}{\partial r}(r^2\sigma_{r\theta}) \qquad \ldots(A.6)$$

The expressions relating the shear stress terms in the above equations to the velocity gradients are:

$$\sigma_{xx} = \mu_{eff}\left(2\frac{\partial u}{\partial x} - \frac{2}{3}\,\mathrm{div}\,\bar{V}\right) \qquad \ldots(A.7)$$

$$\sigma_{rr} = \mu_{eff}\left(2\frac{\partial v}{\partial r} - \frac{2}{3}\,\mathrm{div}\,\bar{V}\right) \qquad \ldots(A.8)$$

$$\sigma_{\theta\theta} = \mu_{eff}\left(\frac{2v}{r} - \frac{2}{3}\,\mathrm{div}\,\bar{V}\right) \qquad \ldots(A.9)$$

$$\sigma_{xr} = \sigma_{rx} = \mu_{eff} \left(\frac{\partial u}{\partial r} + \frac{\partial v}{\partial x} \right) \qquad \ldots(A.10)$$

$$\sigma_{x\theta} = \sigma_{\theta x} = \mu_{eff} \left(\frac{\partial w}{\partial x} \right) \qquad \ldots(A.11)$$

$$\sigma_{r\theta} = \sigma_{\theta r} = \mu_{eff} \cdot r \cdot \frac{\partial}{\partial r} \left(\frac{w}{r} \right) \qquad \ldots(A.12)$$

where μ_{eff} is the effective turbulent viscosity.

By continuity and axisymmetry

$$\text{Div } \bar{V} = \frac{1}{r} \left[\frac{\partial}{\partial x} (ru) + \frac{\partial}{\partial r} (rv) \right] = 0 \qquad \ldots(A.13)$$

A.1.1.1 Equation for vorticity

The pressure terms in equations (A.4) and (A.5) can be eliminated by

$$\frac{\partial}{\partial x} \left[A.5 \right] - \frac{\partial}{\partial r} \left[A.4 \right]$$

The result is

$$\frac{\partial}{\partial x} \left(G'_x \frac{\partial v}{\partial x} + G'_r \frac{\partial v}{\partial r} - \frac{\rho w^2}{r} \right) - \frac{\partial}{\partial r} \left(G'_x \frac{\partial u}{\partial x} + G'_r \frac{\partial u}{\partial r} \right)$$

$$= \frac{\partial}{\partial x} \left[\frac{\partial \sigma_{rx}}{\partial x} + \frac{1}{r} \frac{\partial}{\partial r} (r \sigma_{rr}) - \frac{\sigma_{\theta\theta}}{r} \right] - \frac{\partial}{\partial r} \left[\frac{\partial \sigma_{xx}}{\partial x} + \frac{1}{r} (r \sigma_{rx}) \right] = T \text{ (say)} \qquad ..(A.14)$$

By defining vorticity (ω) as

$$\omega = \frac{\partial v}{\partial x} - \frac{\partial u}{\partial r} \qquad \ldots(A.15)$$

equation (A.14) can be expanded to obtain

$$\frac{\partial}{\partial x} (\omega G'_x) + \frac{\partial}{\partial r} (\omega G'_r) + \frac{\partial \rho}{\partial x} \left[\frac{\partial}{\partial r} \left(\frac{V_s^2}{2} \right) \right] - \frac{\partial \rho}{\partial r} \left[\frac{\partial}{\partial x} \left(\frac{V_s^2}{2} \right) \right] - \frac{\partial}{\partial x} \left(\frac{\rho w^2}{r} \right) = T \qquad \ldots(A.16)$$

where $V_s^2 = u^2 + v^2$

Representing equation (A.10) by

$$\sigma_{xr} = \sigma_{rx} = \mu_{eff} \left(\omega + 2 \frac{\partial u}{\partial r} \right) \qquad \ldots(A.17)$$

and substituting for other shear stress terms from equations (A.7) to (A.13), the equation (A.16) can be expanded to obtain

$$\frac{\partial}{\partial x}(\omega G'_x) + \frac{\partial}{\partial r}(\omega G'_r) + \frac{\partial \rho}{\partial x}\left[\frac{\partial}{\partial r}\left(\frac{V_s^2}{2}\right)\right] - \frac{\partial \rho}{\partial r}\left[\frac{\partial}{\partial x}\left(\frac{V_s^2}{2}\right)\right] - \frac{\partial}{\partial x}\left(\frac{\rho w^2}{r}\right)$$

$$= \frac{\partial}{\partial x}\left[\frac{\partial}{\partial x}(\mu_{eff}\omega)\right] + \frac{\partial}{\partial r}\left[\frac{\partial}{\partial r}(\mu_{eff}\omega) - \mu_{eff}\frac{\omega}{r}\right] + 2\mu_{eff}\left[\frac{1}{r}\frac{\partial \omega}{\partial r} - \frac{\omega}{r^2}\right]$$

$$+ \frac{\partial \mu_{eff}}{\partial x}\left[2\frac{\partial^2 u}{\partial x \partial r} + 2\frac{\partial^2 v}{\partial r^2} + \frac{1}{r}\frac{\partial v}{\partial r} - \frac{2v}{r^2}\right] + \frac{\partial \mu_{eff}}{\partial r}\left[2\frac{\partial^2 u}{\partial x^2} + 2\frac{\partial^2 v}{\partial x \partial r} + \frac{2}{r}\frac{\partial u}{\partial r}\right]$$

$$+ \frac{\partial^2 \mu_{eff}}{\partial x^2}\left[2\frac{\partial u}{\partial r}\right] - \frac{\partial^2 \mu_{eff}}{\partial r^2}\left[2\frac{\partial v}{\partial x}\right] - \frac{\partial^2 \mu_{eff}}{\partial x \partial r}\left[2\frac{\partial u}{\partial x} - 2\frac{\partial v}{\partial r}\right] \qquad \ldots(A.18)$$

Neglecting the partial derivatives of μ_{eff} and defining stream function (ψ) in terms of parameters of the axial and radial velocity components as

$$\frac{\partial \psi}{\partial r} = \rho u r = r G'_x \qquad \ldots(A.19)$$

$$\frac{\partial \psi}{\partial x} = -\rho v r = -r G'_r \qquad \ldots(A.20)$$

equation (A.18) becomes

$$\frac{\partial}{\partial x}\left(\frac{\omega}{r}\frac{\partial \psi}{\partial r}\right) - \frac{\partial}{\partial r}\left(\frac{\omega}{r}\frac{\partial \psi}{\partial x}\right) + \frac{\partial \rho}{\partial x}\left[\frac{\partial}{\partial r}\left(\frac{V_s^2}{2}\right)\right] - \frac{\partial \rho}{\partial r}\left[\frac{\partial}{\partial x}\left(\frac{V_s^2}{2}\right)\right] - \frac{\partial}{\partial x}\left(\frac{\rho w^2}{r}\right)$$

$$= \frac{\partial}{\partial x}\left[r\frac{\partial}{\partial x}\left(\mu_{eff}\frac{\omega}{r}\right)\right] + \frac{\partial}{\partial r}\left\{r\left[\frac{1}{r}\frac{\partial}{\partial r}(\mu_{eff}\omega) - \mu_{eff}\frac{\omega}{r^2}\right]\right\} + 2\mu_{eff}\frac{\partial}{\partial r}\left(\frac{\omega}{r}\right) \qquad \ldots(A.21)$$

Multiplying both sides by $\frac{1}{r}$ and rearranging the final equation for vorticity is

$$\frac{1}{r}\left[\frac{\partial}{\partial x}\left(\frac{\omega}{r}\frac{\partial \psi}{\partial r}\right) - \frac{\partial}{\partial r}\left(\frac{\omega}{r}\frac{\partial \psi}{\partial x}\right)\right] = \frac{1}{r}\left\{\frac{\partial}{\partial x}\left[r\frac{\partial}{\partial x}\left(\mu_{eff}\frac{\omega}{r}\right)\right] + \frac{\partial}{\partial r}\left[r\frac{\partial}{\partial r}\left(\mu_{eff}\frac{\omega}{r}\right)\right]\right\}$$

$$+ \frac{1}{r}\frac{\partial \rho}{\partial r}\frac{\partial}{\partial x}\left(\frac{V_s^2}{2}\right) - \frac{\partial \rho}{\partial x}\left[\frac{\partial}{\partial r}\left(\frac{V_s^2}{2}\right)\right] + \frac{\partial}{\partial x}\left(\frac{\rho w^2}{r}\right) + 2\mu_{eff}\frac{\partial}{\partial r}\left(\frac{\omega}{r}\right)\Bigg\} \qquad \ldots(A.22)$$

The final equation can also be written in the general precise form (7.1) as

$$\bar{G}'.\ \text{grad}\left(\frac{\omega}{r}\right) = \text{div}\left[\text{grad}\left(\mu_{eff}\frac{\omega}{r}\right)\right] + \frac{1}{r}\left\{\frac{\partial\rho}{\partial r}\left[\frac{\partial}{\partial x}\left(\frac{V_s^2}{2}\right)\right] - \frac{\partial\rho}{\partial x}\left[\frac{\partial}{\partial r}\left(\frac{V_s^2}{2}\right)\right] + 2\mu_{eff}\frac{\partial}{\partial r}\left(\frac{\omega}{r}\right) + \frac{\partial}{\partial x}\left(\frac{\rho w^2}{r}\right)\right\} \quad \ldots(A.23)$$

A.1.1.2 Equation for stream function

From the definition of vorticity in equation (A.15) and the stream function expressions (A.19) and (A.20)

$$\omega = \frac{\partial v}{\partial x} - \frac{\partial u}{\partial r} = \frac{\partial}{\partial x}\left(-\frac{1}{\rho r}\frac{\partial\psi}{\partial x}\right) - \frac{\partial}{\partial r}\left(\frac{1}{\rho r}\frac{\partial\psi}{\partial r}\right) \quad \ldots(A.24)$$

Multiplying both sides by $\frac{1}{r}$, the equation for stream function is

$$0 = \text{div}\left[\frac{1}{\rho r^2}\ \text{grad}\ \psi\right] + \frac{\omega}{r} \quad \ldots(A.25a)$$

By multiplying equation (A.24) by $\frac{\rho}{r}$, the stream function can also be written as

$$0 = \text{div}\left[\frac{1}{r^2}\ \text{grad}\ \psi\right] + \frac{\rho\omega}{r} - \frac{1}{r^2\rho}\left(\frac{\partial\psi}{\partial x}\frac{\partial\rho}{\partial x} + \frac{\partial\psi}{\partial r}\frac{\partial\rho}{\partial r}\right) \quad \ldots(A.25b)$$

A.1.1.3 Equation for tangential velocity component

Substituting for the shear stress terms in equation (A.6) using the stream function expressions (A.19) and (A.20), the equation for the tangential velocity will be obtained as

$$\bar{G}'.\ \text{grad}\ w = \text{div}\left[\mu_{eff}\ \text{grad}\ w\right] - \frac{w}{r}\left(\frac{\mu_{eff}}{r} + \frac{\partial\mu_{eff}}{\partial r} + G_r'\right) \quad \ldots(A.26)$$

A.1.2 Equations for the combustion parameters

A.1.2.1 Equation for fuel mass fraction

For a component i of the mixture in a reacting medium, the net flow rate by convection, molecular and turbulent diffusion together with its consumption or formation by the chemical reaction is independent of time. The equation representing this can be written as

$$\bar{G}' . \text{ grad } m_i = \text{div}\left[\Gamma_i \text{ grad } m_i\right] + R_i \qquad \ldots(A.27)$$

For the fuel mass fraction i becomes fu. The same equation will apply for the mass fractions of the oxidant, combustion product and inert gases in the stream or for the combined variable defined as

$$(m_{fu} - \frac{m_{ox}}{STC})$$

which is called "mixture fraction". For the rate of consumption of the fuel, the reaction rate equation used is

$$R_{fu} = - K\, m_{fu}\, m_{ox}\, \rho^2 \quad T \quad e^{-\frac{E}{RT}} \qquad \ldots(A.28)$$

The final form of the equation for the fuel mass fraction is

$$\bar{G}' . \text{ grad } m_{fu} = \text{div}\left[\Gamma \text{grad } m_{fu}\right] - K\, m_{fu}\, m_{ox}\, \rho^2 \quad T \quad e^{-\frac{E}{RT}} \qquad \ldots(A.29)$$

A.1.2.2 Equation for the stagnation enthalpy

In a combustion system, the kinetic energy is usually small relative to the enthalpy of the combustible stream, thus the stagnation enthalpy is represented by

$$H = C_p\, T + m_{fu} . HC \qquad \ldots(A.30)$$

The representation also implies that the specific heats of the mixture components are represented by a mean value. Assuming further that the turbulent exchange coefficients of fuel and heat are equal, the equation for the enthalpy is

$$\bar{G}' . \text{ grad } H = \text{div}\left[\Gamma \text{grad } H\right] \qquad \ldots(A.31)$$

A.1.3 Summary

The equations for the dependent variables of interest can now be summarised.

For Vorticity

$$\bar{G}' \cdot \text{grad}\left(\frac{\omega}{r}\right) = \text{div}\left[\text{grad}\left(\mu_{eff}\ \frac{\omega}{r}\right)\right] + \frac{1}{r}\left\{\frac{\partial\rho}{\partial r}\left[\frac{\partial}{\partial x}\left(\frac{V_s^2}{2}\right)\right] - \frac{\partial\rho}{\partial x}\left[\frac{\partial}{\partial r}\left(\frac{V_s^2}{2}\right)\right] + 2\,\mu_{eff}\,\frac{\partial}{\partial r}\left(\frac{\omega}{r}\right) + \frac{\partial}{\partial x}\left(\frac{\rho w^2}{r}\right)\right\} \quad \ldots(A.23)$$

For Stream Function

$$\dot{\rho} = \text{div}\left[\frac{1}{r^2}\,\text{grad}\,\psi\right] + \frac{\rho\omega}{r} - \frac{1}{r^2\rho}\left(\frac{\partial\psi}{\partial x}\frac{\partial\rho}{\partial x} + \frac{\partial\psi}{\partial r}\frac{\partial\rho}{\partial r}\right) \quad \ldots(A.25b)$$

For Tangential Velocity

$$\bar{G}' \cdot \text{grad}\, w = \text{div}\left[\mu_{eff}\,\text{grad}\, w\right] - \frac{w}{r}\left(\frac{\mu_{eff}}{r} + \frac{\partial\mu_{eff}}{\partial r} + G_r'\right) \quad \ldots(A.26)$$

For Fuel Mass Fraction

$$\bar{G}' \cdot \text{grad}\, m_{fu} = \text{div}\left[\Gamma\,\text{grad}\, m_{fu}\right] - K\, m_{fu}\, m_{ox}\, \rho^2\, T\, e^{-\frac{E}{RT}} \quad \ldots(A.29)$$

For Enthalpy

$$\bar{G}' \cdot \text{grad}\, H = \text{div}\left[\Gamma\,\text{grad}\, H\right] \quad \ldots(A.31)$$

For Mixture Fraction

$$\bar{G}' \cdot \text{grad}\, mf = \text{div}\left[\Gamma\,\text{grad}\, mf\right] \quad \ldots(A.32)$$

A.2 Analysis of the finite-difference equations

The general form of the partial differential equations of each of the dependent variables is

$$\alpha_1 \bar{G}' . \text{ grad } \varphi = \text{div}\left[\alpha_2 \text{ grad } (\alpha_3 \varphi)\right] + \varphi_4 \qquad \ldots(7.1)$$

The finite-difference form of this equation is obtained by integrating it over the control volume such as is shown in Figure 78.

Taking the convection term for example,

$$\alpha_1 \bar{G}' . \text{ grad } \varphi = \frac{\alpha_1}{r}\left[\frac{\partial}{\partial x}\left(\varphi \frac{\partial \psi}{\partial r}\right) - \frac{\partial}{\partial r}\left(\varphi \frac{\partial \psi}{\partial x}\right)\right] \qquad \ldots(A.33)$$

Considering the first term of the expanded form and assuming uniform value of the dependent variable along the sides of the control volume

$$\int_{r=SP}^{NP}\int_{x=WP}^{EP} \frac{\alpha_1}{r}\left[\frac{\partial}{\partial x}\left(\varphi \frac{\partial \psi}{\partial r}\right)\right] dx\, dr \approx \left(\frac{\alpha_1}{r}\right)_P \int_{r=SP}^{NP}\left[\left(\varphi \frac{\partial \psi}{\partial r}\right)_{EP} - \left(\varphi \frac{\partial \psi}{\partial r}\right)_{WP}\right] dr$$

$$\approx \left(\frac{\alpha_1}{r}\right)_P \left[\varphi_{EP} \int_{r=SP}^{NP}\left(\frac{\partial \psi}{\partial r}\right)_{EP} dr - \varphi_{WP} \int_{r=SP}^{NP}\left(\frac{\partial \psi}{\partial r}\right)_{WP} dr\right]$$

$$\approx \left(\frac{\alpha_1}{r}\right)_P \left[\varphi_{EP}\left(\psi_{ne} - \psi_{se}\right) - \varphi_{WP}\left(\psi_{nw} - \psi_{sw}\right)\right] \qquad \ldots (A.34)$$

Carrying out the same operation on the second term

$$\int_{x=WP}^{EP}\int_{r=SP}^{NP} (\alpha_1 \bar{G}' . \text{ grad } \varphi)\, dx dr = \left(\frac{\alpha_1}{r}\right)_P \left[\varphi_{EP}(\psi_{ne}-\psi_{se}) - \varphi_{WP}(\psi_{nw}-\psi_{sw})\right.$$

$$\left. + \varnothing_{SP}\,(\psi_{se}-\psi_{sw}) - \varphi_{NP}(\psi_{ne}-\psi_{nw})\right] \qquad \ldots(A.35)$$

In the analysis, $\varnothing$ takes the value upstream of each of the faces nw-sw, sw-se, se-ne, ne-nw of the control volume. For example if the flow through the face sw-se is in the positive radial direction, φ_{SP} becomes φ_s. If on the other hand the flow is in the negative radial direction φ_{SP} becomes φ_P. The value of the stream function at any corner of the control volume

is represented by the average of the values at the four neighbouring grid points for example $\psi_{ne} = \frac{1}{4}(\psi_P + \psi_E + \psi_{NE} + \psi_N)$. In the program, the expressions in equation (A.35) are represented by

$$\iint (\alpha_1 \bar{G}' . \text{ grad } \varphi)\, dx\, dr = Z\, U\, \varphi_P - AU \qquad \ldots(A.36)$$

The diffusion term in equation (7.1) can be expanded to

$$\text{div}\left[\alpha_2 \text{ grad } (\alpha_3\varphi)\right] = \frac{1}{r}\left\{\frac{\partial}{\partial x}\left[r\alpha_2 \frac{\partial}{\partial x}(\alpha_3\varphi)\right] + \frac{\partial}{\partial r}\left[r\alpha_2 \frac{\partial}{\partial r}(\alpha_3\varphi)\right]\right\} \qquad \ldots(A.37)$$

The first term can be integrated to obtain

$$\int_{r=SP}^{NP} \int_{r=WP}^{EP} \frac{1}{r} \frac{\partial}{\partial x}\left[r\alpha_2 \frac{\partial}{\partial x}(\alpha_3\varphi)\right] dx dr$$

$$\approx \left(\frac{1}{r}\right)_P \left[(\alpha_2 r)_{EP} \cdot \frac{(\alpha_3\varphi)_E - (\alpha_3\varphi)_P}{x_E - x_P} \cdot (r_{NP} - r_{SP}) - (\alpha_2 r)_{WP} \cdot \frac{(\alpha_3\varphi)_P - (\alpha_3\varphi)_W}{x_P - x_W} \cdot (r_{NP} - r_{SP})\right] \qquad \ldots A.38$$

Similar integrations can be performed on the second term to obtain the final expression

$$\iint \text{div}\left[\alpha_2 \text{ grad}(\alpha_3\varphi)\right] dx dr = \left(\frac{1}{r}\right)_P \left[(\alpha_2 r)_{EP} \Delta r \cdot \frac{(\alpha_3\varphi)_E - (\alpha_3\varphi)_P}{x_E - x_P} + (\alpha_2 r)_{WP} \Delta r \cdot \frac{(\alpha_3\varphi)_W - (\alpha_3\varphi)_P}{x_P - x_W} + (\alpha_2 r)_{NP} \Delta z \cdot \frac{(\alpha_3\varphi)_N - (\alpha_3\varphi)_P}{r_N - r_P} + (\alpha_2 r)_{SP} \Delta z \cdot \frac{(\alpha_3\varphi)_S - (\alpha_3\varphi)_P}{r_P - r_S}\right] \qquad \ldots(A.39)$$

The equation can be written as

$$\iint \text{div}\left[\alpha_2 \text{ grad } (\alpha_3\varphi)\right] dx dr = CE\,(\alpha_3\varphi)_E + CW\,(\alpha_3\varphi)_W + CN(\alpha_3\varphi)_N + CS(\alpha_3\varphi)_S - (\alpha_3\varphi)_P\,(CE + CW + CN + CS) \qquad \ldots(A.40)$$

The source term is represented by

$$\iint (d)\, dx\, dr = \text{SOURCE} - ZQ\, (\varphi)_P \qquad \ldots(A.41)$$

From equations (A.36), (A.40) and (A.41)

$$\varphi_P = \frac{CE(\alpha_3\varphi)_E + CW\,(\alpha_3\varphi)_W + CN\,(\alpha_3\varphi)_N + CS\,(\alpha_3\varphi)_S + \text{SOURCE} + AU}{ZU + ZQ + (CE + CW + CN + CS)} \qquad \ldots(A.42)$$

APPENDIX B

BRIEF DESCRIPTION OF PROGRAM SUBROUTINES

B.1 Introduction

The program is divided into various subroutines and functions each of which carry out a particular part of the computation.

B.2 The MAIN Program

This is the principal section of the program. All the required input data are specified here and it also reads the alphanumeric data. The geometrical distribution of the grid points, the inlet distribution of axial velocity components and the initial values for the dependent variables are specified here.

B.3 Subroutine ONINA

This subroutine is called by the "MAIN" program and it evaluates the inlet distributions of the fuel mass fraction and dimensionless enthalpy.

B.4 Subroutine DPROF

The density profile on the inlet plane is calculated in this subroutine which is called by the "MAIN" program.

B.5 Subroutine HEADCT

The heading and information of the physical input parameters are caused to be printed out by this subroutine. It is called by the "MAIN" program.

B.6 Subroutine SOLVCT

The iteration process is started in this subroutine which is called by the "MAIN" program. It also prints the fractional and maximum differences between successive iterations for each of the dependent variables. Terminating statements are included in this subroutine which causes remarks on the state of the program at termination to be printed out.

B.7 Subroutine PROFIL

This subroutine which is called by SOLVCT, computes the inlet distributions of vorticity, stream function and the tangential velocity components.

B.8 Subroutine MVBCCT

The mass velocities in the axial and radial directions on each of the boundary planes are calculated here.

B.9 Subroutine MVELCT

Similar variables to those in Section 6.8 are computed at points not on any of the boundary planes. The values are calculated from the computed stream functions.

B.10 Subroutine FDEQCT

This is the subroutine in which the "finite-difference" analysis is carried out. It is called by the subroutine SOLVCT. The values of each of the dependent variables are updated as soon as new values are computed. The fractional and maximum differences between two successive iterations for each of the dependent variables are calculated here.

Specifications for the calculation of vorticities at wall points are also given in the subroutine.

B.11 Subroutine SORCCT

The source terms for each of the dependent variables are evaluated in the subroutine which is called by FDEQCT.

B.12 Subroutine COEFCT

The coefficients CW, CS, CE and CN of the diffusion terms for each dependent variable are computed in the subroutine which is called by

B.13 Subroutine CONVEC

The ZU and AU of the convection terms (as in equation A.33) are determined in this subroutine. The subroutine is called by FDEQCT. For points adjacent to solid walls, the evaluation is carried out implicitly as is done with the calculations of vorticity on solid walls.

B.14 Subroutine BCONDT

The boundary conditions for all the dependent variables are specified in this subroutine. The expressions for wall vorticity calculations are included here.

B.15 Subroutine PRINCT

This subroutine prints the values of the dependent variables at interval of NPRIN iterations and also at the end of the computations.

B.16. Subroutine TABUCT

The calculated values of the dependent variables, axial and radial velocity components, density, viscosity and temperature (if applicable) are tabulated after the end of the computations.

B.17 Subroutine DENSCT

The density of the fluid is computed in this subroutine.

B.18 Subroutine VISCCT

Values of the effective viscosity of the fluid at the grid points in the flow field are evaluated here.

B.19 Function T

In the function subprogram, temperature values are computed.

B.20 Function VS2

The value of $u^2 + v^2$ at each grid point is determined in this function subprogram.

B.21 Subroutine PLOTT

Approximate contour plots of the dependent variables can be obtained by calling this subroutine. In the computation reported in this thesis, this subroutine was not used.

B.22 Function ADF

This function subprogram computes the partial derivatives of any variable of interest at any point in the flow field.

B.23 Subroutine PRESCT

The static pressure distribution in the flow field can be obtained by using this subroutine. The values are obtained by integrating the x-momentum and r-momentum equations. A reference value at a point in the inlet plane must be specified.

B.24 Subroutine ENCHK

The total enthalpy, heat energy, fuel flow rates at inlet and outlet and the combustion efficiency between inlet and outlet are evaluated in this subroutine.

APPENDIX C

MEANINGS OF FORTRAN SYMBOLS

Symbol	Meaning
A (I,J, 1 to 7)	dependent variables
ACTE	activation energy
AGEOM	alphanumeric array for swirler geometry
ANAME	full names of the dependent variables for use in print out
ASYMBL	symbol array for the dependent variables
ATITLE	array containing title of problem
AU	finite-difference approximation for convection term
BB	coefficient in the gradient type of boundary condition
CC	convergence criterion
CPREF	reference specific heat
FMX	non-dimensionalising factor for mixture fraction
G1 (I,J)	mass velocity in x-direction
G2 (I,J)	mass velocity in r-direction
GC	gravitational constant
GCPM	universal gas constant
GLOB	reaction rate constant
HC	net calorific value of fuel
HP	non-dimensionalising factor for enthalpy
IA,IN	see Figure 78.
IE	number of equations to be solved
IEND	print-out indicator, if equal to 222, all variables of interest are printed, otherwise only the dependent variable being solved for and temperature will be printed.
IENTA	control index for inlet profile.

IGEOM	control index for analysis of hubless or annular jets
ILIN,ILEX	indicators for enthalpy calculation in ENCHK for values of 1, 1; 2,2; and 1,2 respectively, the enthalpy will be calculated at inlet plane, exit plane and both planes respectively.
IMIN(J)	value of I on Jth grid-line at left-hand boundary
INDE(K)	when equal to 1, the dependent variable with sequence K will be solved for.
INDG	control index for type of flow: 1,2 for cylindrical, cartesian coordinates respectively
INDZMU	control index for viscosity; 1 for variable viscosity
JA, JB, JN	see Figure 78
LNI, LNJ	number of columns and rows respectively on output listing used by PLOTT

Ordering and indentifying index of the dependent variables

NW	vorticity
NF	stream function
NVT	tangential velocity
NZMM	fuel mass fraction
NZML	dimensionless enthalpy
NZMH	dimensionless mixture fraction
NP	static pressure

MMAX	maximum number of iterations
NPRIN	intervals of iterations at which results are printed out
NVJ	number of values to be plotted for any dependent variable
PR(1 to 7)	turbulent Prandtl or Schmidt numbers
PREF	reference static pressure
REFVL	non-dimensionalised enthalpy of the surrounding
RO(I,J)	mixture density
ROREF	reference density
ROWF	under-relaxation factor for density

RP (1 to 7)	relaxation factors for dependent variables
STC	stoichiometric air/fuel ratio by weight
SOURCE	source term
T (I,J)	absolute temperature
TMPR (IN,JN)	storage location for temperatures
TREF	reference temperature
VANGLE	vane angle of swirler
VINP(J)	axial velocity at inlet plane
VJ (1 to NVJ)	values of the dependent variables being plotted
WC1H, WC2H ; WC1V, WC2V	equivalents for g_1 and g_2 respectively for horizontal and vertical walls (Table 12)
X1(I)	x for grid-line I
X2(J)	r for grid-line J
ZJC	Joule's constant
ZMU (I,J)	effective viscosity μ_{eff}
ZMUK	constant A in the effective viscosity expression in equation (7.8)
ZMUREF	reference viscosity
ZMW (1 to 3)	molecular weights for fuel, oxidant and products respectively

LIST OF FIGURES

BIBLIOGRAPHY

1. KERR, N.M. — An aerodynamic study of swirling jets and flames. Ph.D. thesis, Glasgow University, May 1965.

2. FRASER, D. — Investigation into swirl in air jets with application to an oil-fired furnace. M.Sc. thesis, Glasgow University, June 1964

3. KERR, N.M. and FRASER, D. — Swirl. Part 1: Effect on axisymmetrical turbulent jets. Journal of the Institute of Fuel, December 1965, p.519-526

4. KERR, N.M. — Swirl. Part 2: Effect on flame performance and the modelling of swirling flames. Journal of the Institute of Fuel, December 1965, p.527-538

5. MATHUR, M.L. — An aerodynamic study of swirling jets with application to burners. Ph.D. thesis, Glasgow University, May 1966

6. MATHUR, M.L. and MACCALLUM, N.R.L. — Swirling air jets issuing from vane swirlers. Part 1: Free jets. Journal of the Institute of Fuel, May 1967, p.214;225

7. MATHUR, M.L. and MACCALLUM, N.R.L. — Swirling air jets issuing from vane swirlers. Part 2: Enclosed jets. Journal of the Institute of Fuel, June 1967, p.238-245

8. GOSMAN, A.D. PUN, W.M. RUNCHAL, A.K. SPALDING, D.B. and WOLFSHTEIN, M.W. — Heat and mass transfer in recirculating flows. Imperial College of Science and Technology, Department of Mechanical Engineering, DOC. No. SF/R/3, October 1968.

9. ODLOZINSKI, G.A. — A procedure for predicting the distributions of velocity and temperature in a flame stabilised behind a bluff-body. Imperial College of Science and Technology, Department of Mechanical Engineering, DOC No. EF/R/G/2, October 1968

10. ALBRIGHT, L.F. and ALEXANDER, L.G. — Stable cyclonic flames of natural gas and air. Jet Propulsion, October 1956, p.867-873

11. GROVER, J.H. KESLER, M.G., and SCURLOCK, A.C. — Preliminary evaluation of a rotating flame stabiliser. Jet Propulsion, April, 1957, p.386-391.

12. CHIGIER, N.A., BEER, J.M., GRECOV, D. and BASSINDALE, K. — Jet flames in rotating flow fields. Department of Fuel Technology and Chemical Engineering, University of Sheffield, Report No. FTCE/33/NAC, January, 1969.

13. CHIGIER N.A. and BEER, J.M. — Velocity and static pressure distributions in swirling air jets issuing from annular and divergent nozzles. Journal of Basic Engineering, December 1964, p.788-796

14. CHIGIER, N.A. and CHERVINSKY, A. — Aerodynamic study of turbulent burning free jet with swirl. 11th Symposium (International) on Combustion, p.489-499, The Combustion Institute, 1967.

15. ROSE, W.G. — A swirling round turbulent jet. 1- Mean flow measurements. Journal of Applied Mechanics, December, 1962, p.615-625.

16 CHIGIER, N.A. and GILBERT, J.L. — Paper 2. Recirculation eddies in the wake of flameholders. Symposium on Combustion in Marine Boilers, The Institute of Marine Engineers and the Institute of Fuel, January, 1968.

17. IVANOV, A.G. — A method of estimating the flow section of vortex burners. Thermal Engineering, vol. 15, No. 5, p.44-49, 1968.

18. DRAKE, P.F. and HUBBARD, E.H. — Effect of air swirl on the completeness of combustion. Journal of the Institute of Fuel, September, 1963, p.389-390.

19. HOTTEL, H.C. and PERSON, R.A. — Heterogeneous combustion of gases in a vortex system. 4th Symposium (International) on Combustion, p.781-788, The Williams and Wilkins Co. 1953.

20. ALBRIGHT, L.F. and ALEXANDER, L.G. — Flame stabilisation in gases flowing cyclonically: flow characteristics, temperatures and gas analyses. 6th Symposium (International) on Combustion, p.464-472, Reinhold Publishing Corp. 1956.

21. BALUEV, E.D. and TROYANKIN, Yu,V. — Study of the aerodynamic structure of gas flow in a cyclone chamber, Thermal Engineering, Vol. 14, No. 1, p.84-87, 1967.

22. CHEDAILLE, J., LEUCKEL, W. and CHESTERS, A.K. — Aerodynamic studies carried out on turbulent jets by the International Flame Research Foundation. Proceedings of the 3rd Symposium on Flame and Industry, "The Use of Models" p.c1-c27, The Institute of Fuel, 1966.

23. SHAGALOVA, S.L. SHNITSER, I.N. and GROMOV, G.V. — Aerodynamic characteristics of flow produced by a burner with guide vanes. Thermal Engineering, Vol. 12, No. 6, p.31-37, 1965.

24. BROWN, A.M. and THRING, M.W. — The application of pressure jet burners to marine boilers. 10th Symposium (International) on Combustion, p.1203 - 1218, The Combustion Institute, 1965.

25. CUDE, A.L. — The length of oil and gas flames. Journal of the Iron and Steel Institute, November, 1953, p.304-312.

26. MAIER, P. — The length of turbulent swirling flames burning in free surroundings. Journal of the Institute of Fuel, November 1968, p.419-422.

27 LEE S. — Axisymmetrical turbulent swirling jet. Journal of Applied Mechanics, June, 1965, p.258-262.

28. CHIGIER, N.A. and CHERVINSKY, A. — Experimental investigation of swirling vortex motion in jets. Journal of Applied Mechanics, June, 1967, p.443-451.

29. STEIGER, M.H. and BLOOM, M.B. — Linearised swirling wakes. The Physics of Fluids, vol. 5, No. 9, p.1027-1032, September 1962.

30. LEWELLEN, W.S. — Linearised vortex flows. A.I.A.A. Journal, vol. 3, No. 1. p.91-98, January, 1965.

31. LOITSYANSKII, L.G. — Mechanics of Liquids and Gases. Pergamon Press, 1966, p.593.

32. FAL'KOVICH, S.V. — Spreading of a twisted stream in an infinite space flooded by the same fluid. P.M.M., (Journal of Applied Mathematics and Mechanics), Vol. 31, No. 2, p.282-288, 1967.

33. USTIMENKO, B.P. — Calculation of free turbulent very twisted jets. Teplofiz. i Prakt. Szhiganiya Gaza, Leningrad, Nedra, No. 3, p.20-26, 1967.

34. CARSLAW, H.S. and JAEGER, J.C. — Conduction of heat in solids. 2nd Edition, p.260, Clarendon Press.

35. MASTERS, J.I. — Some applications in physics of the P-Function. Journal of Chemical Physics, Vol. 23, No. 10, p.1865-1874, October 1955.

36 — Methods for the measurement of fluid flow in pipes. British Standard 1042: Part 1, 1964.

37 WINTERNITZ, F.A.L. — Probe measurements in three-dimensional flow. Aircraft Engineering, Vol. 28, p.273-278, August, 1956.

38. LEE, J.C. and ASH, J.E. — A three-dimensional spherical pitot probe. Trans. A.S.M.E., April, 1956, p.603-608.

39. MERRINGTON, G.L. — A pitch and yaw meter. Journal of Basic Engineering, June, 1968, p.314-316.

40. TAYLOR, D.S. and DAVIES, T.W. — Self-balancing servo-drive system for a five-hole pitot probe. Control, April, 1968, p.312-315.

41 FECHHEIMER, C.J. — Measurements of static pressure. Trans. A.S.M.E., vol. 48, p.965-977, 1926.

42. HIETT, G.F. and POWELL, G.E. — Three-dimensional probe for investigation of flow patterns. The Engineer, January, 1962, p.165-170.

43. MILLER D.R. and COMINGS, E.W. — Static pressure distribution in the free turbulent jet. Journal of Fluid Mechanics, Vol. 3, 1957-58, p.1-16.

44. McADAMS W.H. — Heat transmission. 3rd Edition, p.265, McGraw-Hill, 1954.

45. KASKAN, W.E. — The dependence of flame temperature on mass burning velocity. 6th Symposium (International) on Combustion, p.134-143, Reinhold Publishing Corp. 1956.

46. HILSENRATH, L. BECKETT, C.W., BENEDICT, W.S. FANO, L., HOGE, H.J. MASI, J.F., NUTTALL, R.L., TOULOUSKIAN, Y.S. and WOOLLEY, H.W. — Tables of Thermodynamic and Transport Properties of Air, Argon, Carbon Dioxide, Carbon Monoxide, Hydrogen, Nitrogen, Oxygen and Steam. Pergamon Press, 1960.

47. SPIERS, H.M. — Technical data on fuels. 6th Edition, The British National Committee, World Power Conference.

48. WIEBELT, J.A. — Engineering Radiation Heat Transfer. Hott, Rinehart and Winston, p.223, 1966.

49. REED, S.B. — Flame stretch - A connecting principle for blow-off data. Combustion and Flame. vol. 11, No. 3, June 1967, p.177-189.

50. LEUCKEL, W. and CHESTERS, A.K. — First experiments on isothermal swirling flow from divergent nozzles. International Flame Research Foundation, Doc. No. G 02/a/92, Ijmuiden, April, 1966.

51. BEER, J.M. and CHIGIER, N.A — Swirling jet flames issuing from an annular burner. International Flame Research Foundation, Doc. No. K 20/a/9, Ijmuiden, August, 1963.

52. SILVER, R.S. — The calculation of air entrainment in gas burners. Publication GRB 39/23, The Gas Research Board, December, 1948.

53. RICOU, F.P. and SPALDING, D.B. — Measurements of entrainment by axisymmetrical turbulent jets. Journal of Fluid Mechanics, vol. 11, p.21-32, 1961.

54 HARTREE, D.R. — Numerical analysis 2nd Edition, p.114, Clarendon Press.

55. LONGWELL, J.P. and WEISS, M.A. — High temperature reaction rates in hydrocarbon combustion. Industrial and Engineering Chemistry, vol. 47, No. 8, p.1634-1643, August, 1955.

56. WEISS, M.A., LANG, R.J. and LONGWELL, J.P. — Combustion rates in spherical reactors: Effects of inlet temperature and fuel type. Industrial and Engineering Chemistry, vol. 50, No. 2, p.257-246, February, 1958.

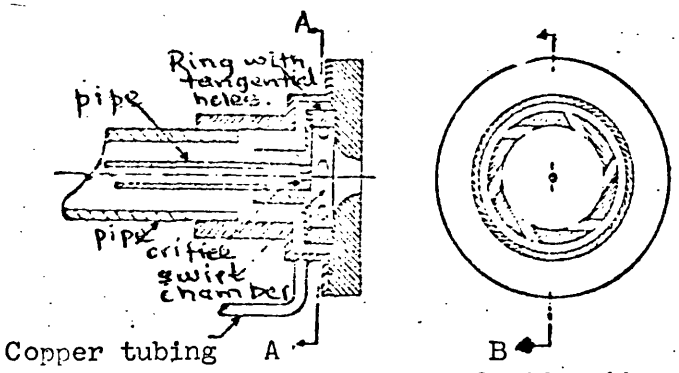

Figure 1 Cyclonic nozzle (Albright and Alexander (10))

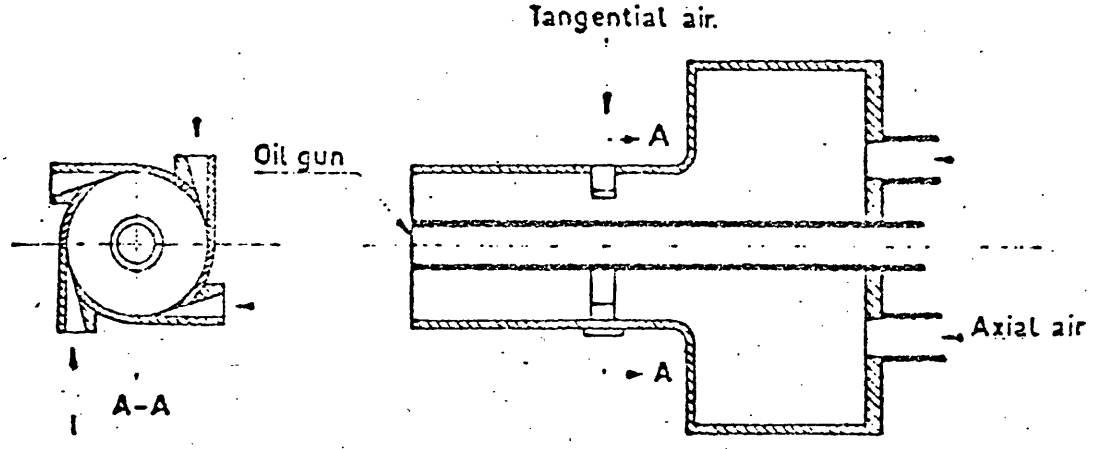

Figure 2. Swirl generator with tangential entry.
(International Flame Research Foundation)

_____ by hydrodynamic integrand .

--- from equation (2.34)

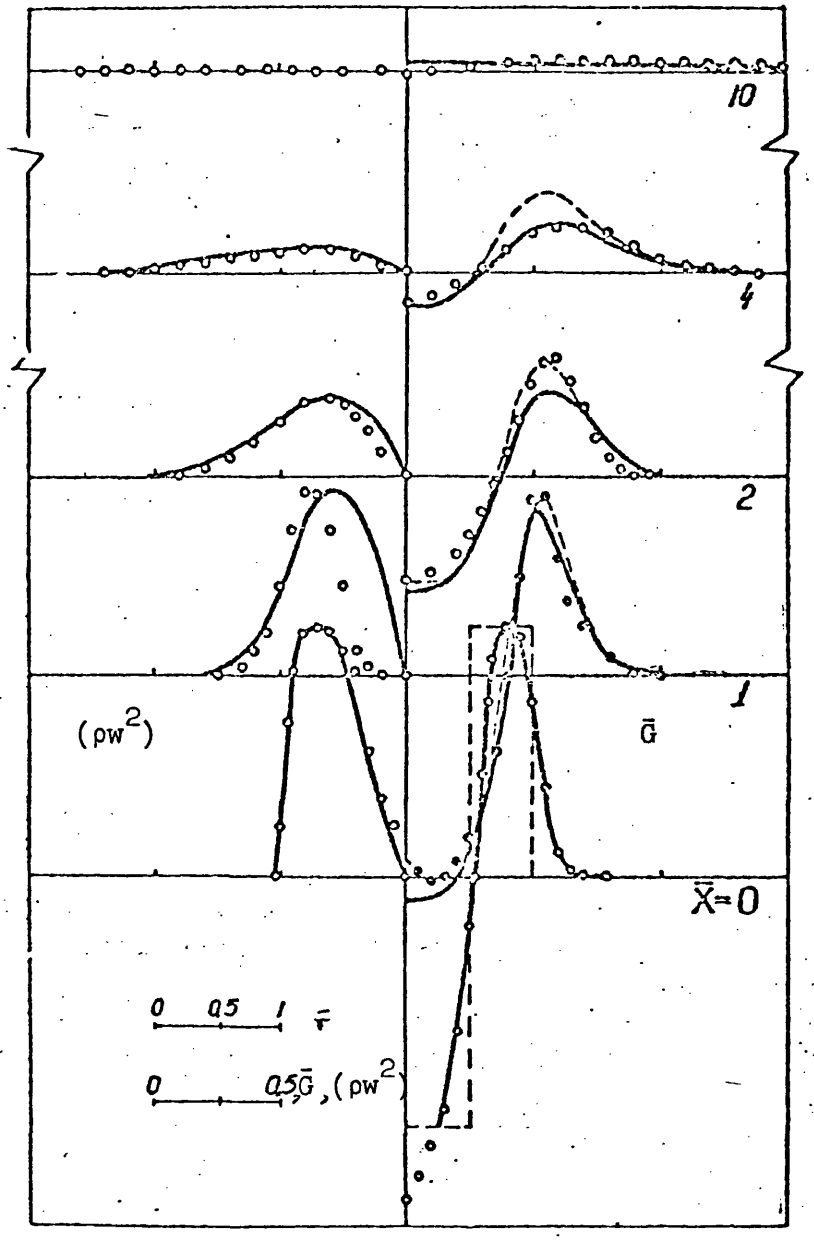

Figure 3. Results from Ustimenko's analysis (33)

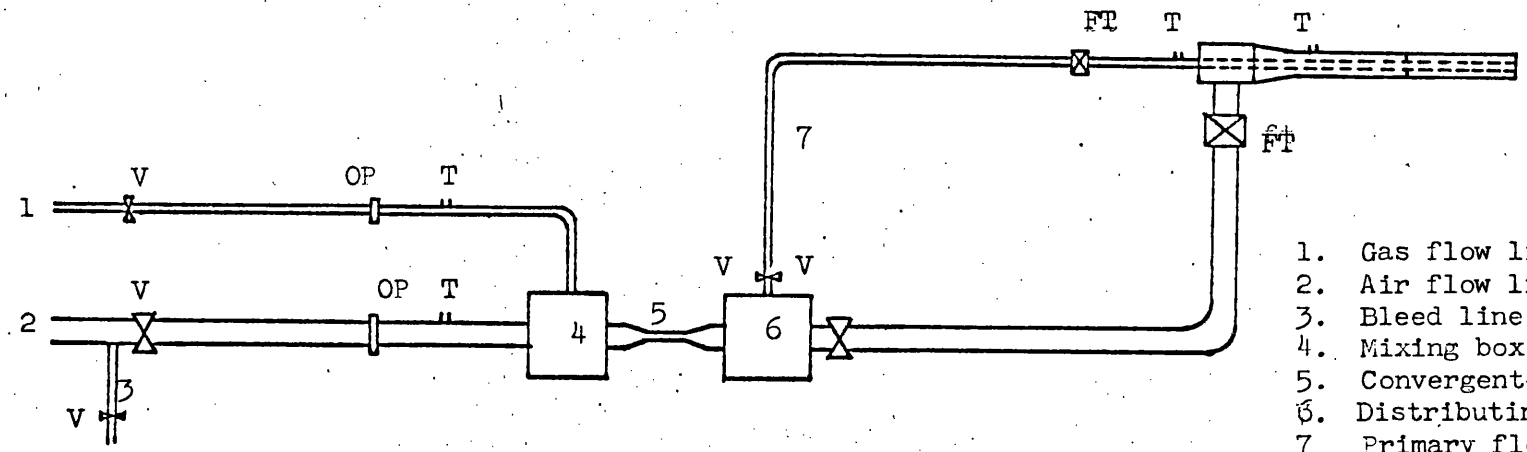

1. Gas flow line
2. Air flow line
3. Bleed line
4. Mixing box
5. Convergent-divergent section
6. Distributing box
7. Primary flow line
8. Secondary flow line

FT Flame trap
OP Orifice plate
T Thermometer Pocket
V Gate valve

Figure 4(a) Flow diagram for test rig.

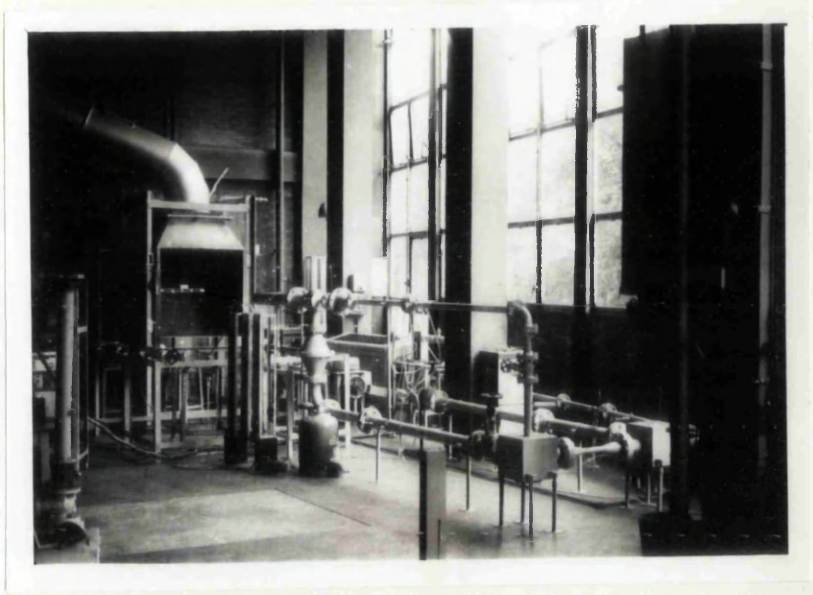

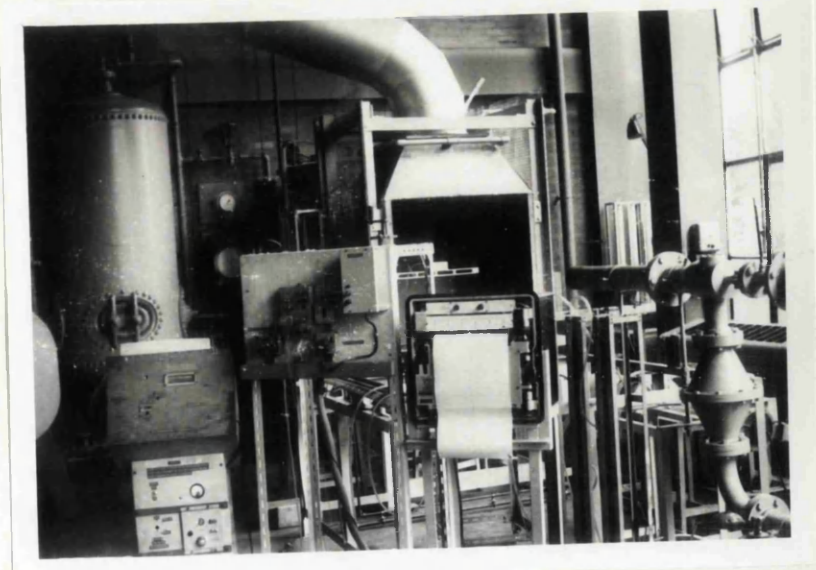

FIGURES 4(b) - (c) Photographs of sections of test-rig

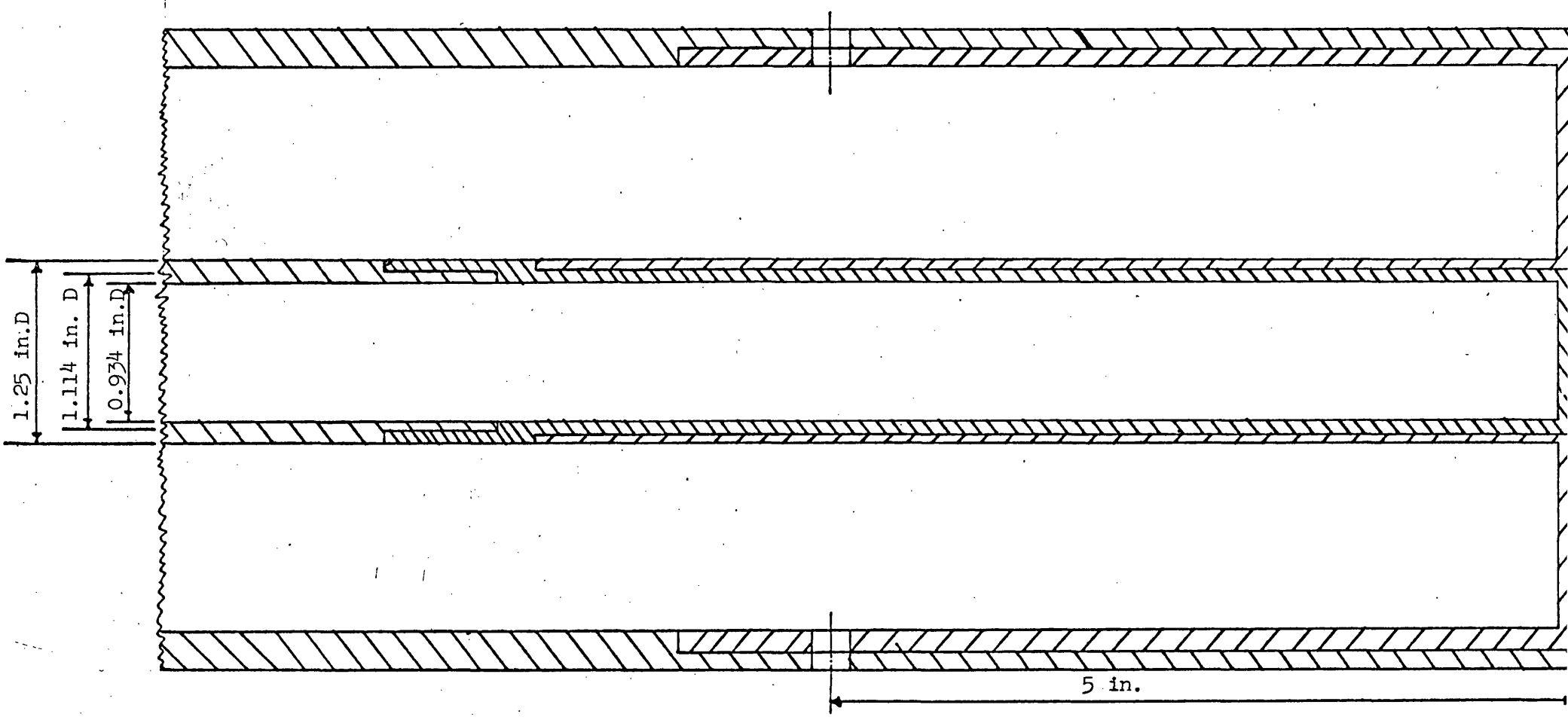

Figure 5. Burner ends of primary and secondary flow lines.

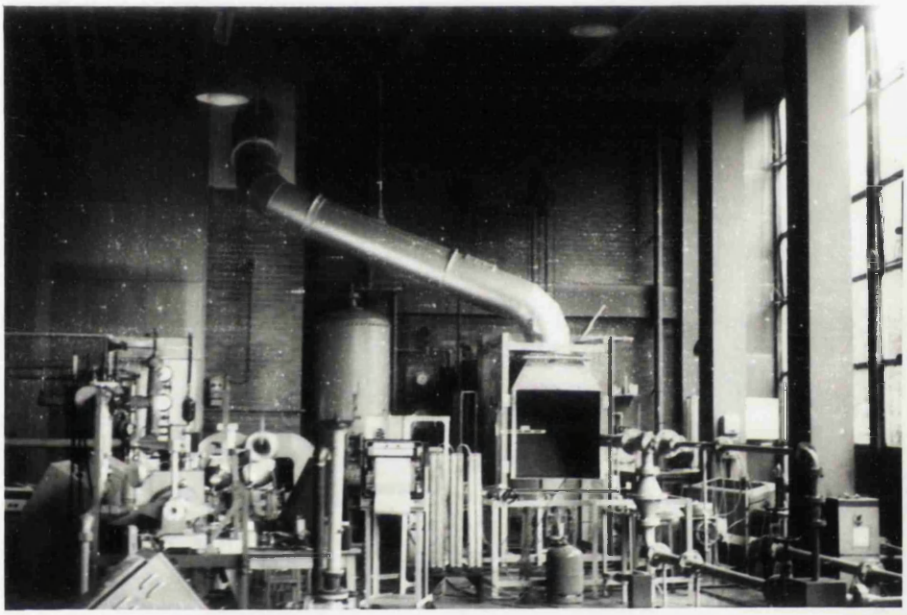

FIGURE 6 Photograph of flue ducting

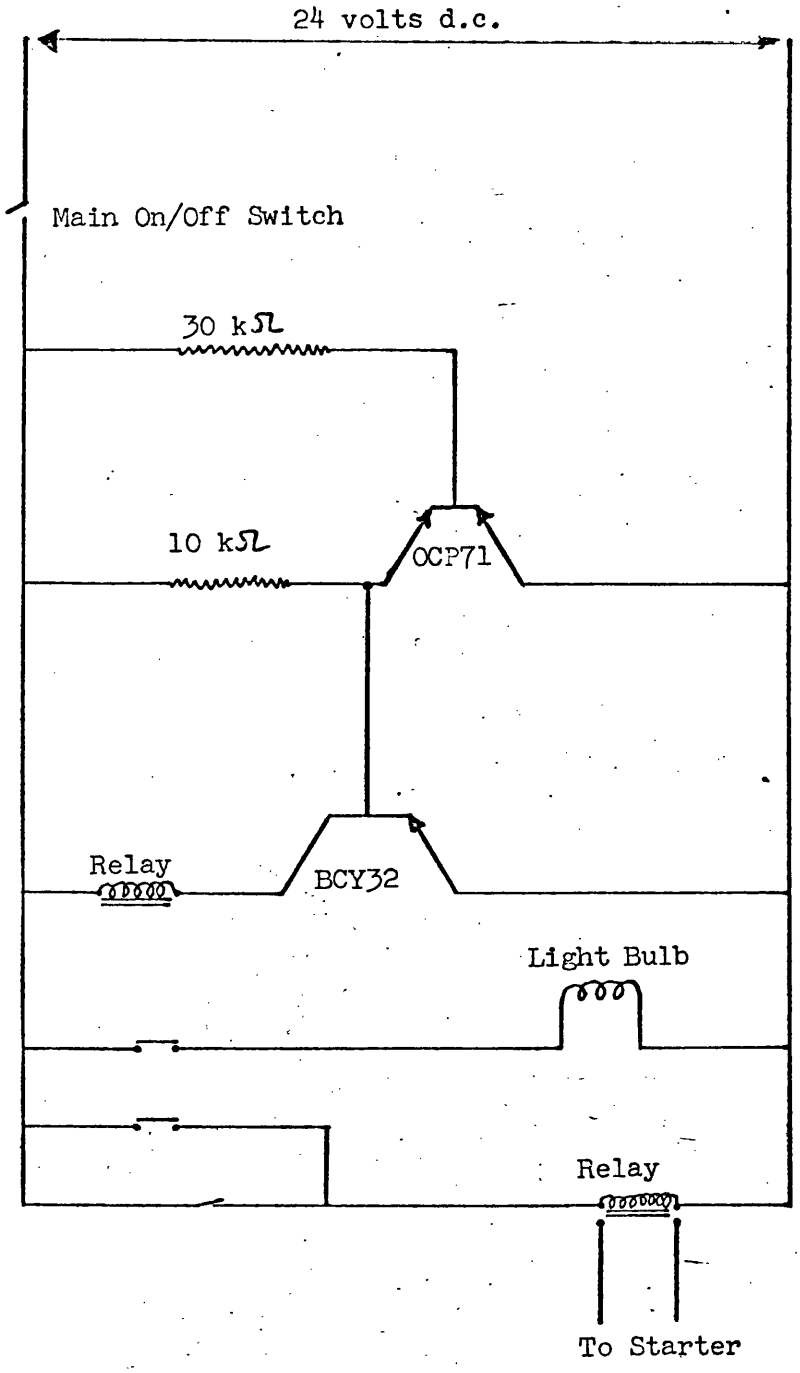

Figure 7. Circuit diagram of photo-electric flame detector.

Figure 8(a) Air flow with hubless swirlers

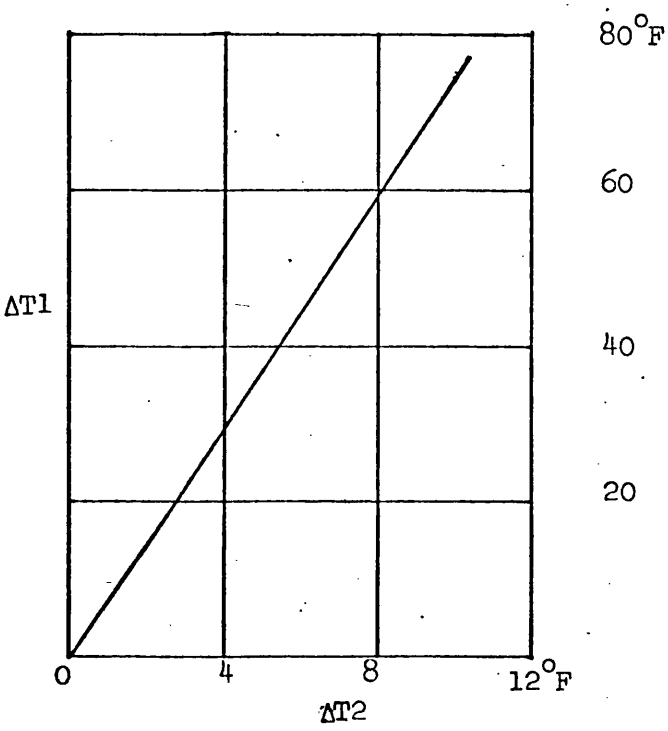

Figure 8(b) Fuel flow with hubless swirlers

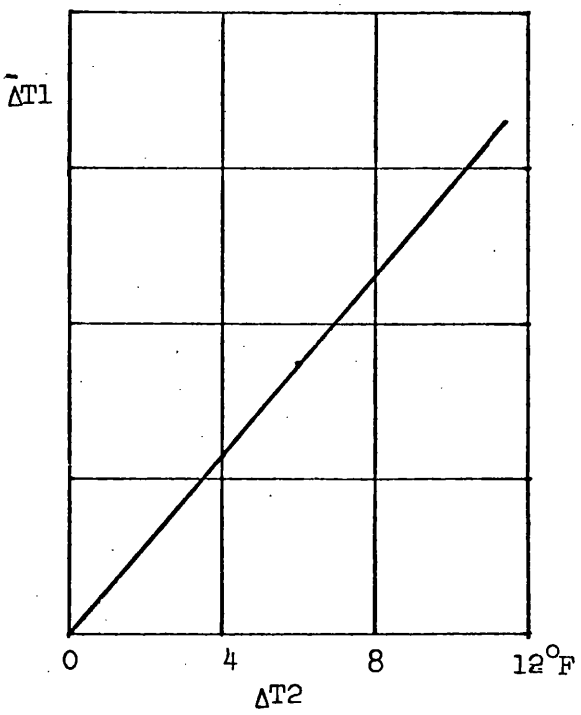

Figure 8(c) Air flow with Annular swirlers

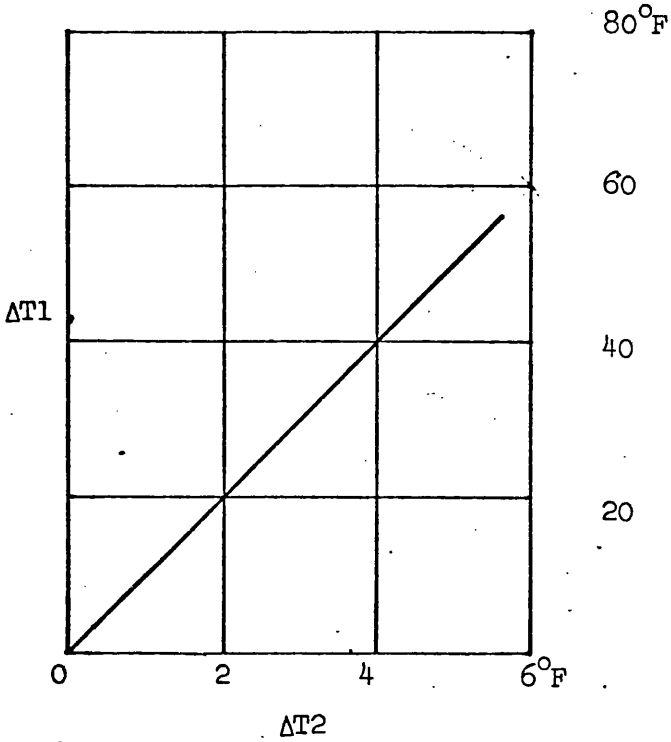

Figure 8(d) Fuel flow with annular swirlers

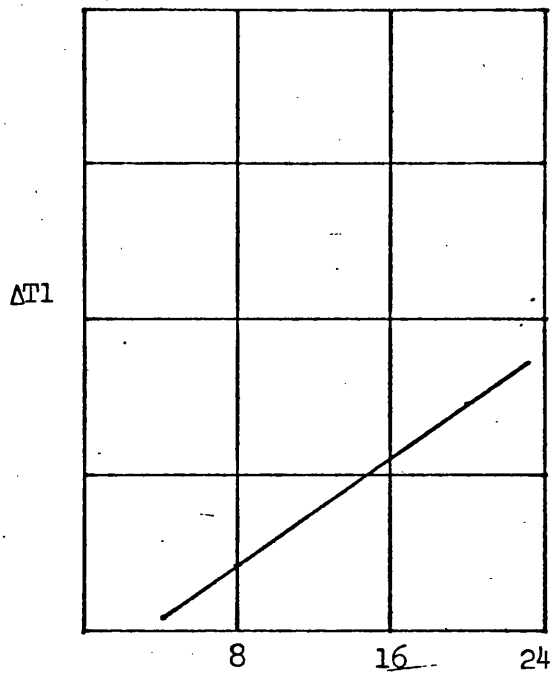

(ΔT1 = Measured temperature - ambient temperature)
(ΔT2 = Orifice temperature - measured temperature)

Figure 8(a) - (d) Fluid temperature correction at orifice plate locations.

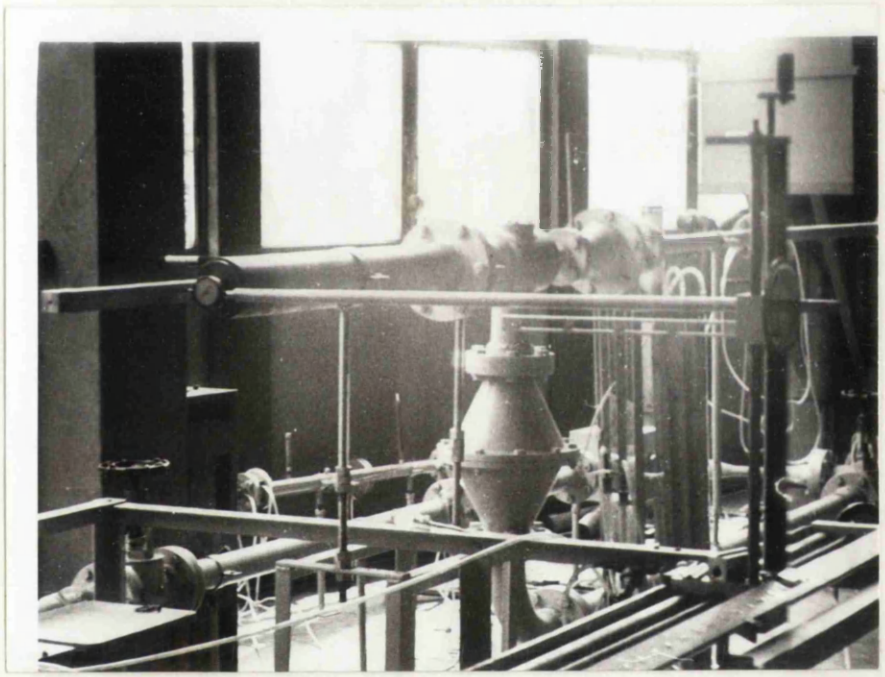

FIGURE 9. Photograph of traversing mechanism during alignment

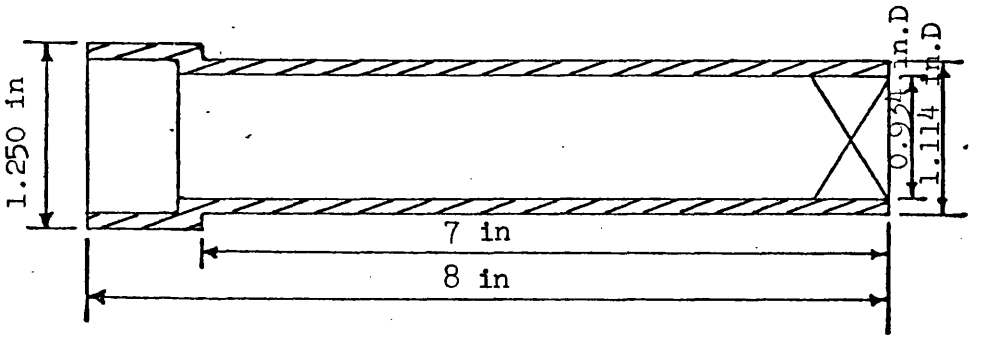

Figure 10(a) The hubless swirler

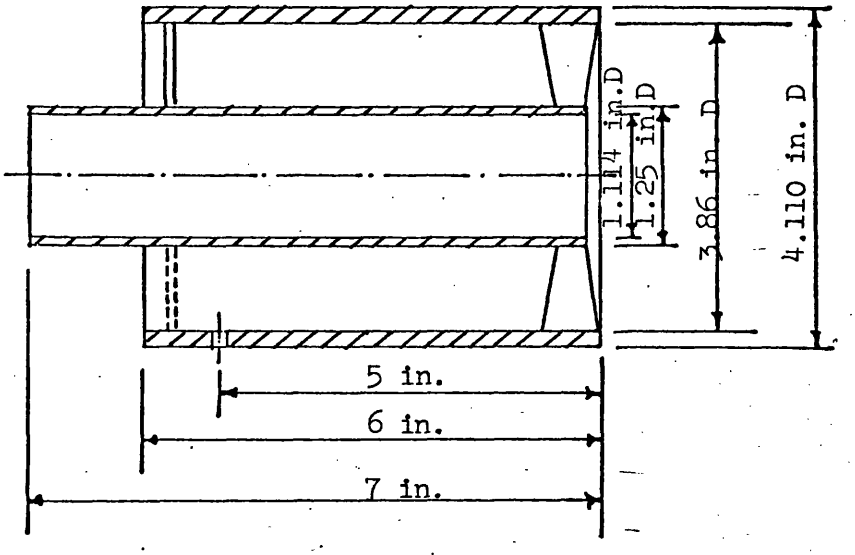

Figure 10(b) The annular swirler

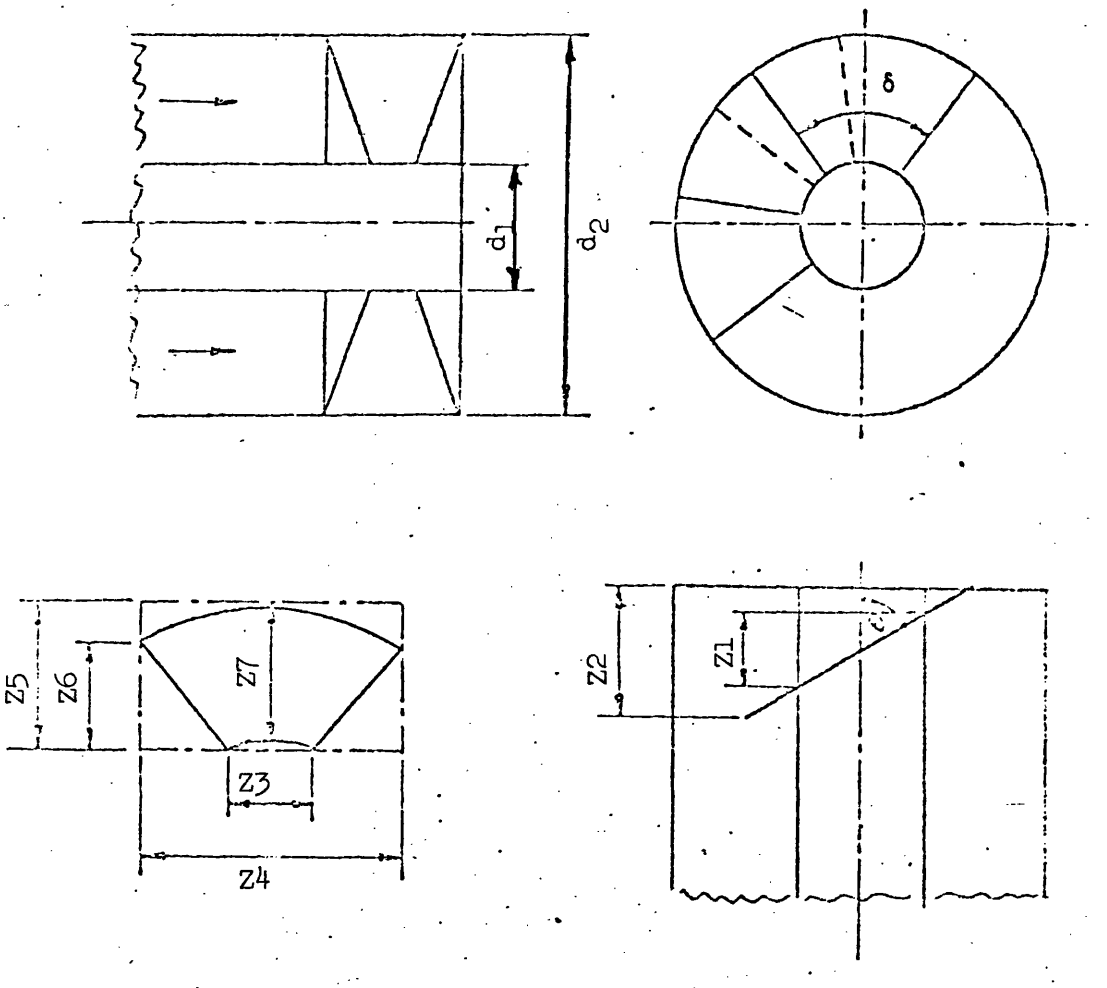

Figure 10 (c) Details of terms in Table 3.

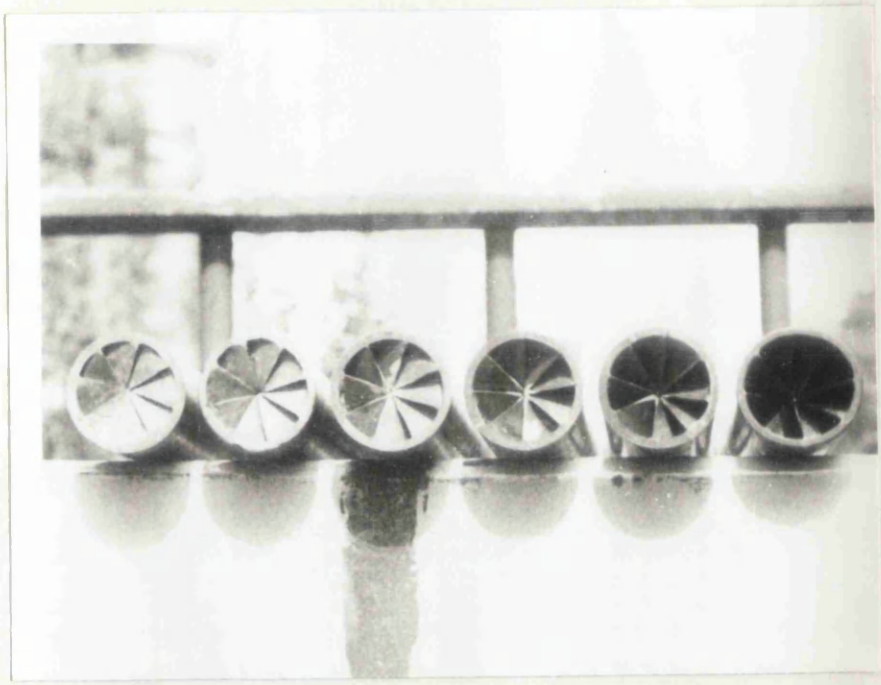

FIGURE 10(d) Photograph of hubless swirlers

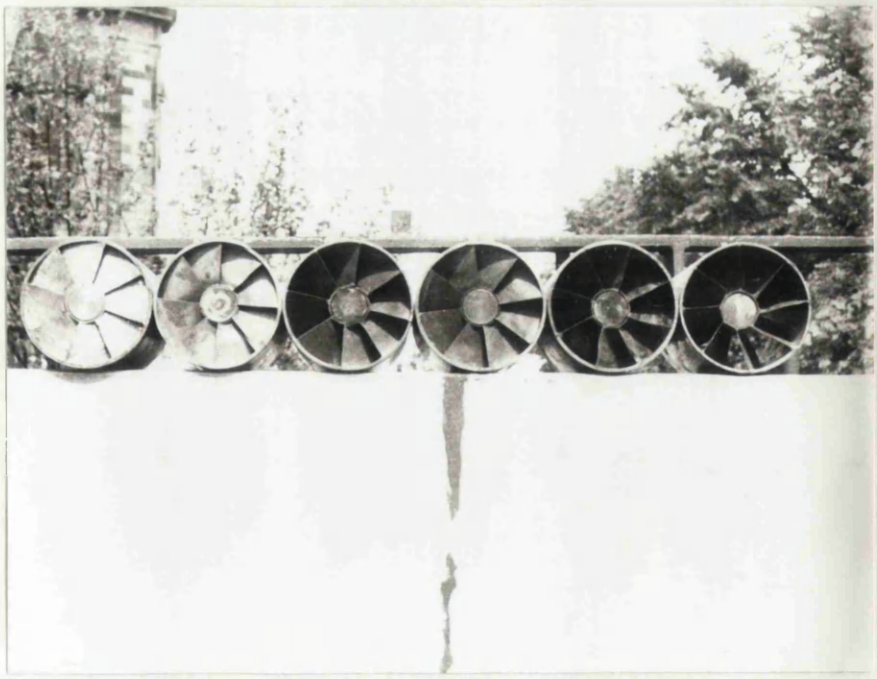

FIGURE 10(e) Photograph of annular swirlers

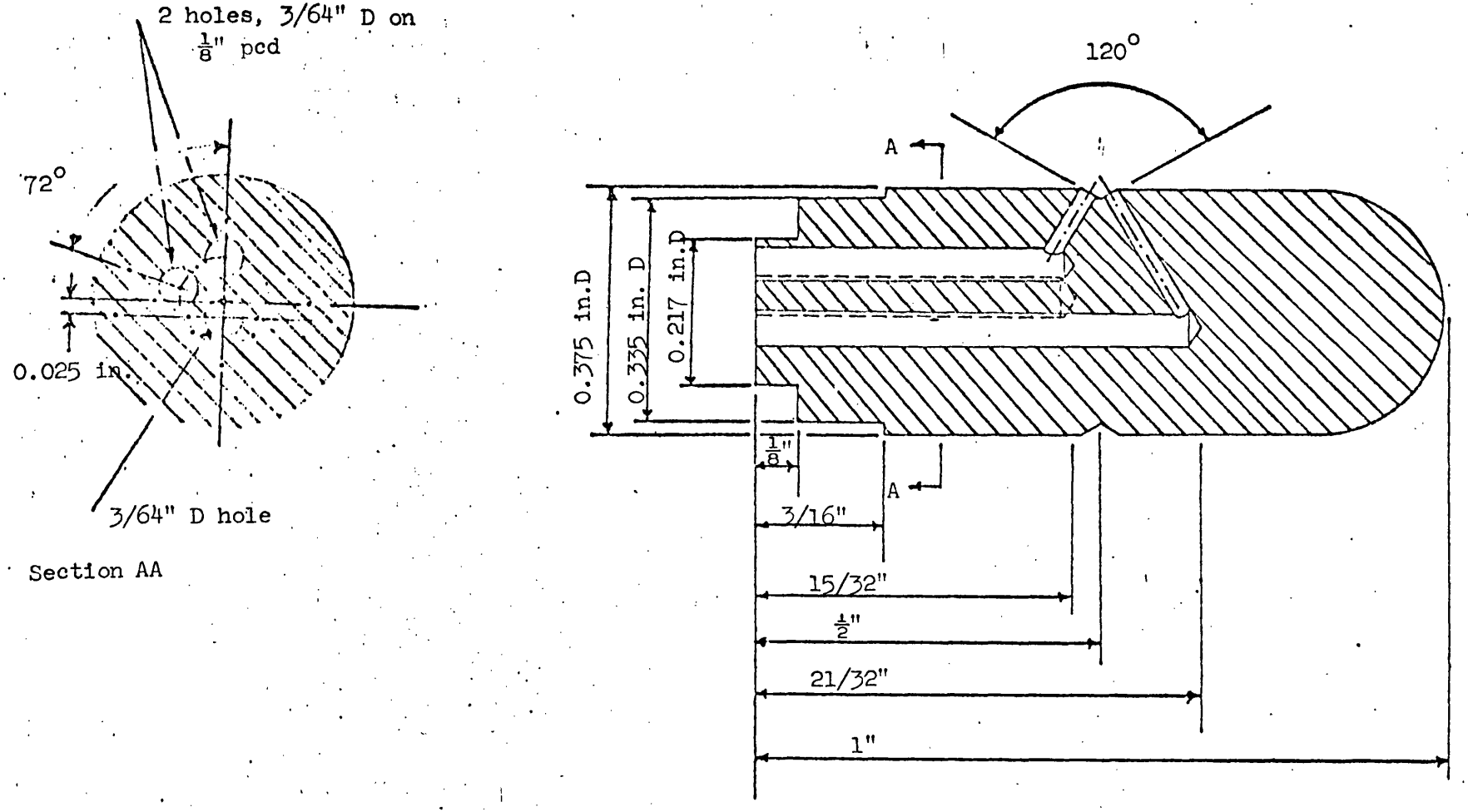

Figure 11(a) The 3-D probe tip.

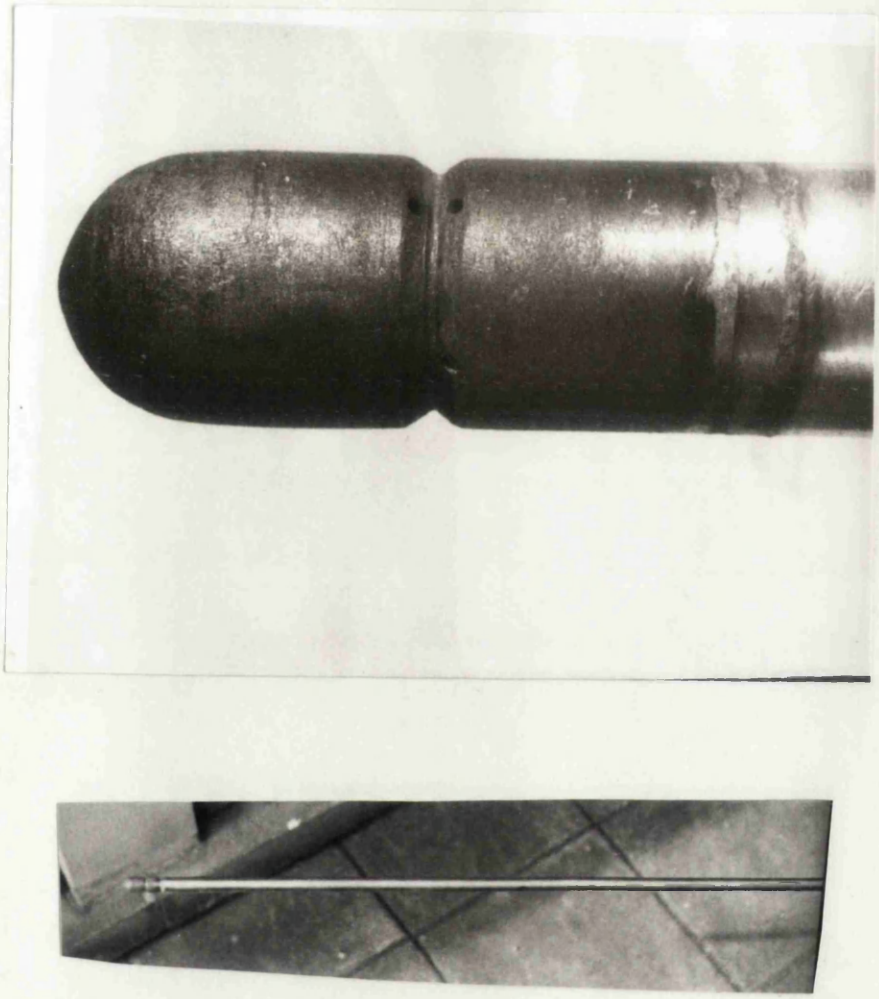

FIGURE 11(b) Photograph of the probe tip and water-cooling jacket

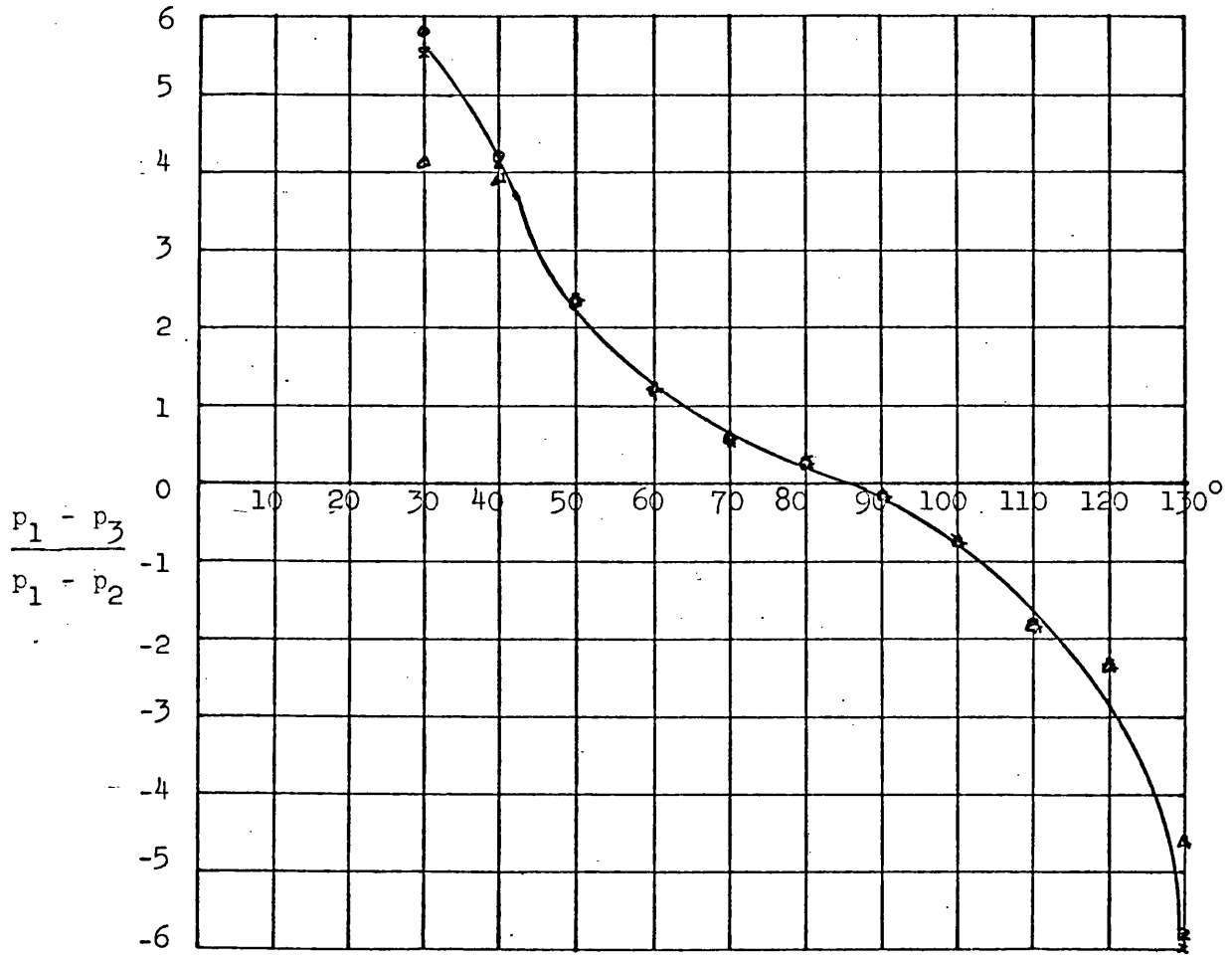

Figure 12(a) Pitch angle parameter ($\frac{p_1-p_3}{p_1-p_2}$) vs. Pitch angle.

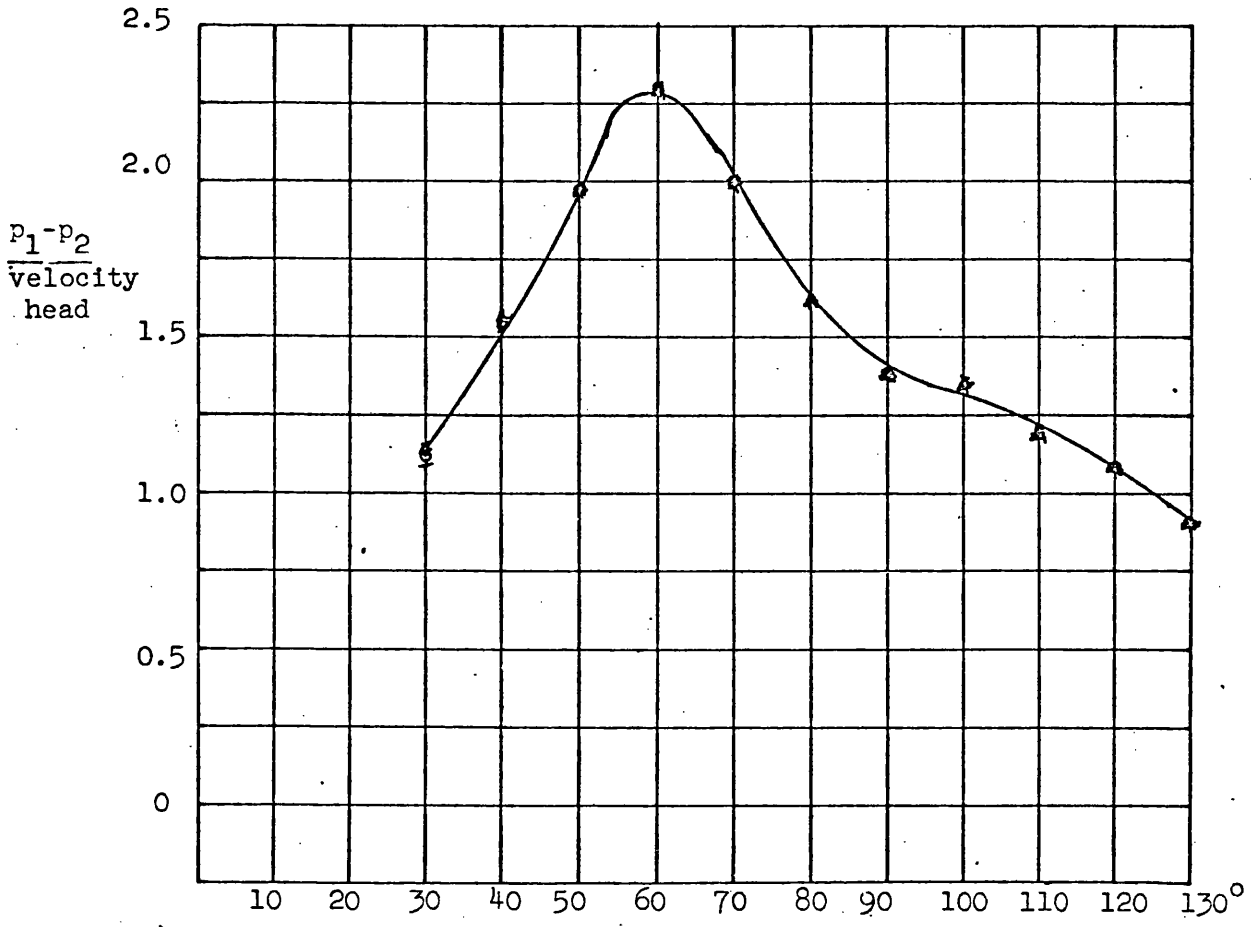

Figure 12(b) Velocity head parameter vs. Pitch angle.

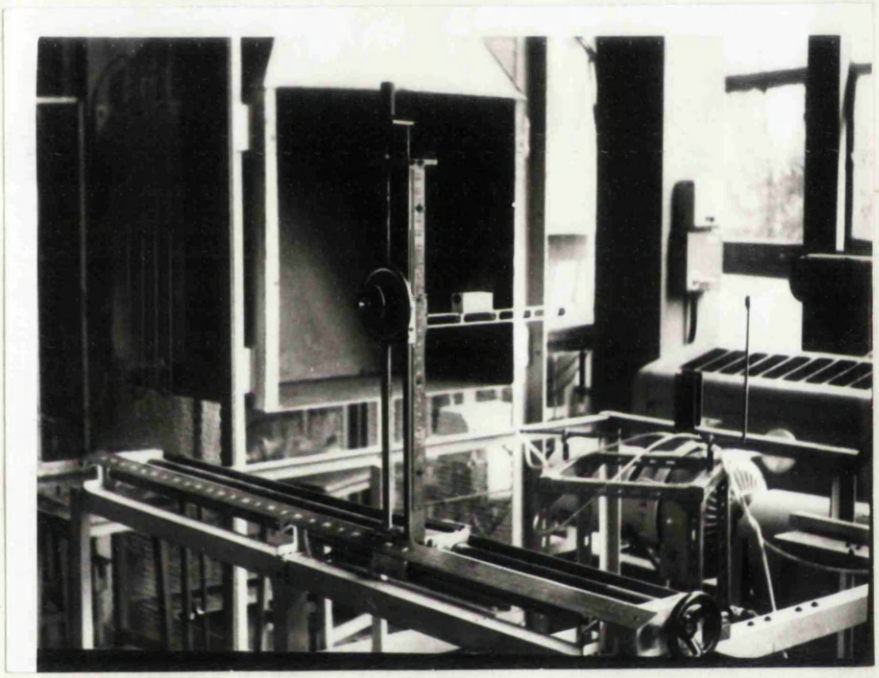

FIGURE 13 Photograph of the probe positioning unit

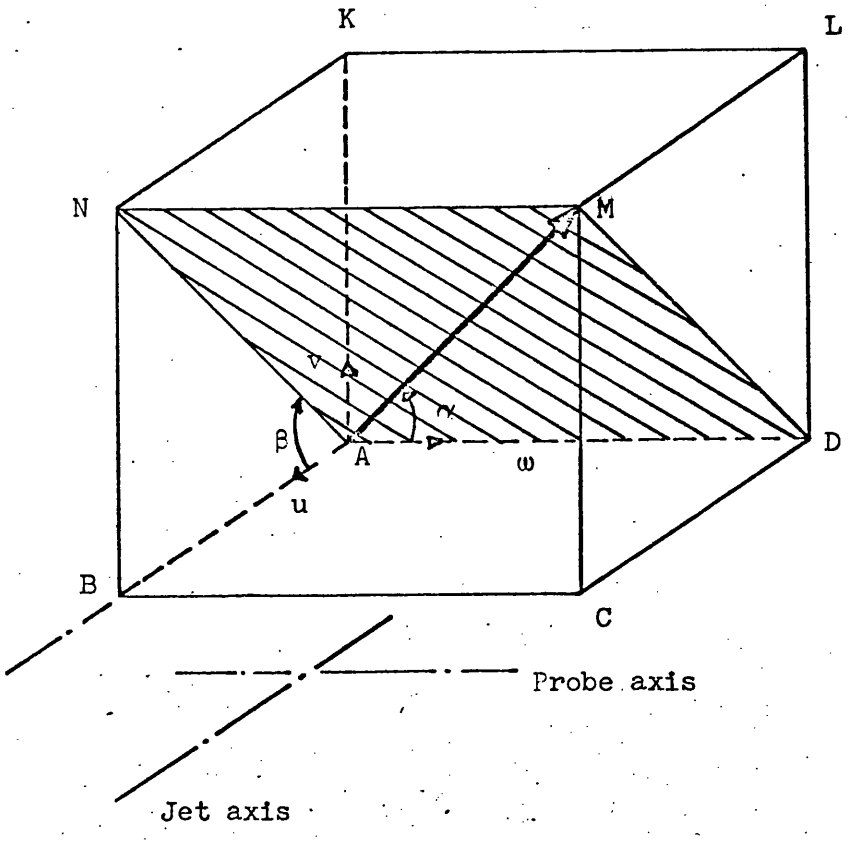

Figure 14. Resolution of resultant velocity

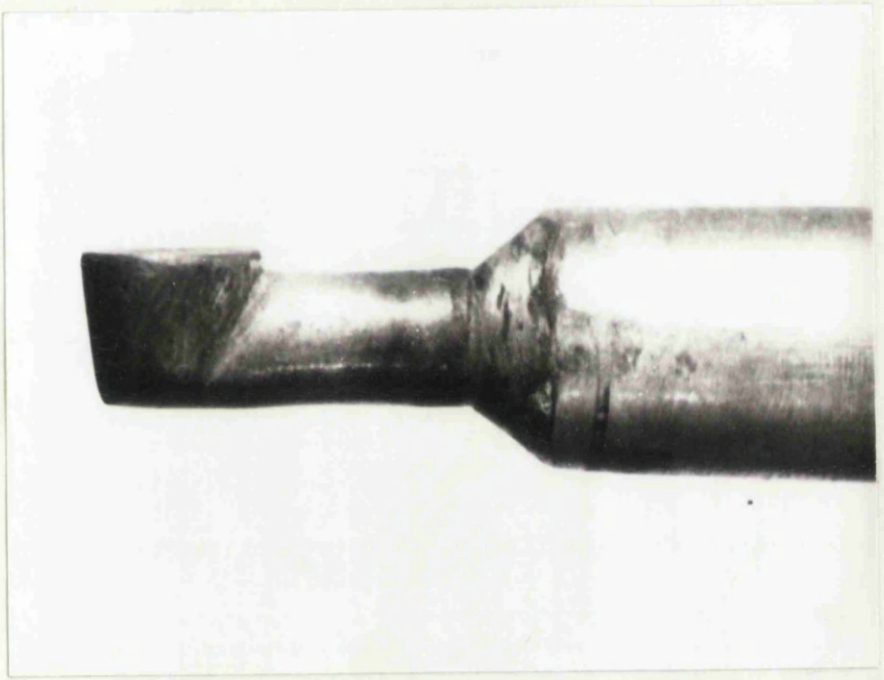

FIGURE 15. Photograph of static pressure probe

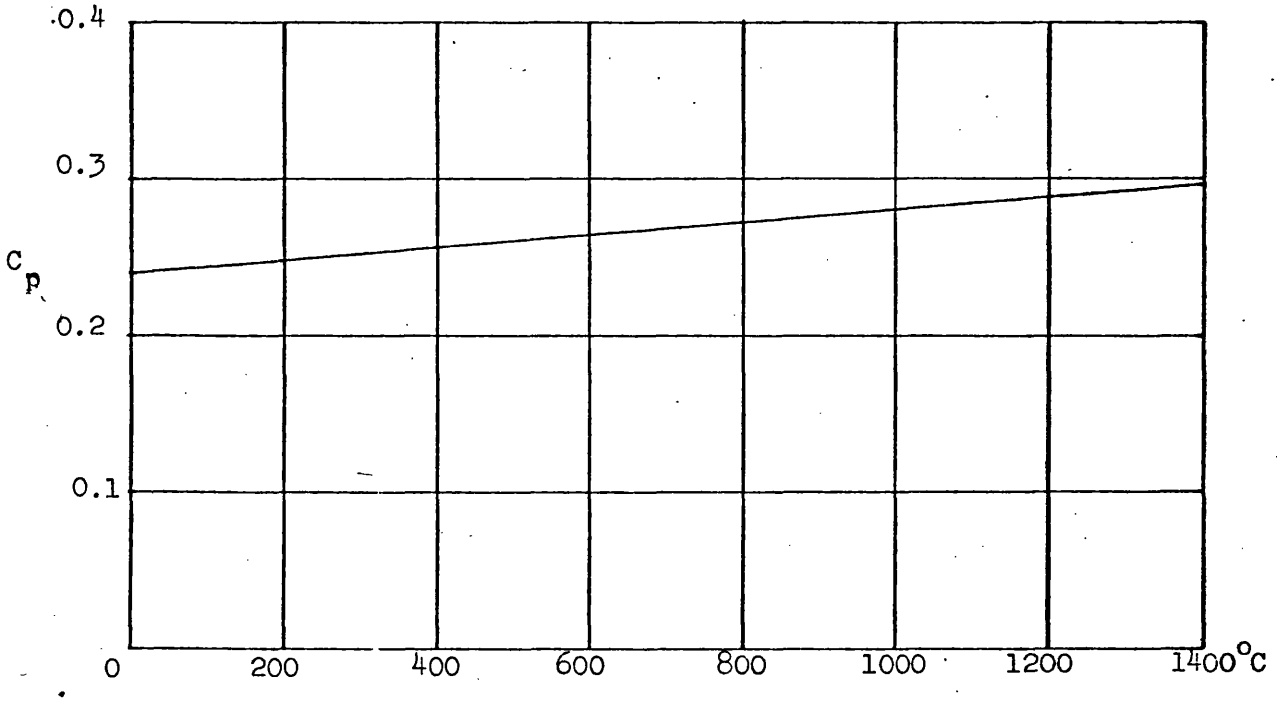

Figure 16. Variation with temperature of the specific heat at constant pressure (C_p) for air.

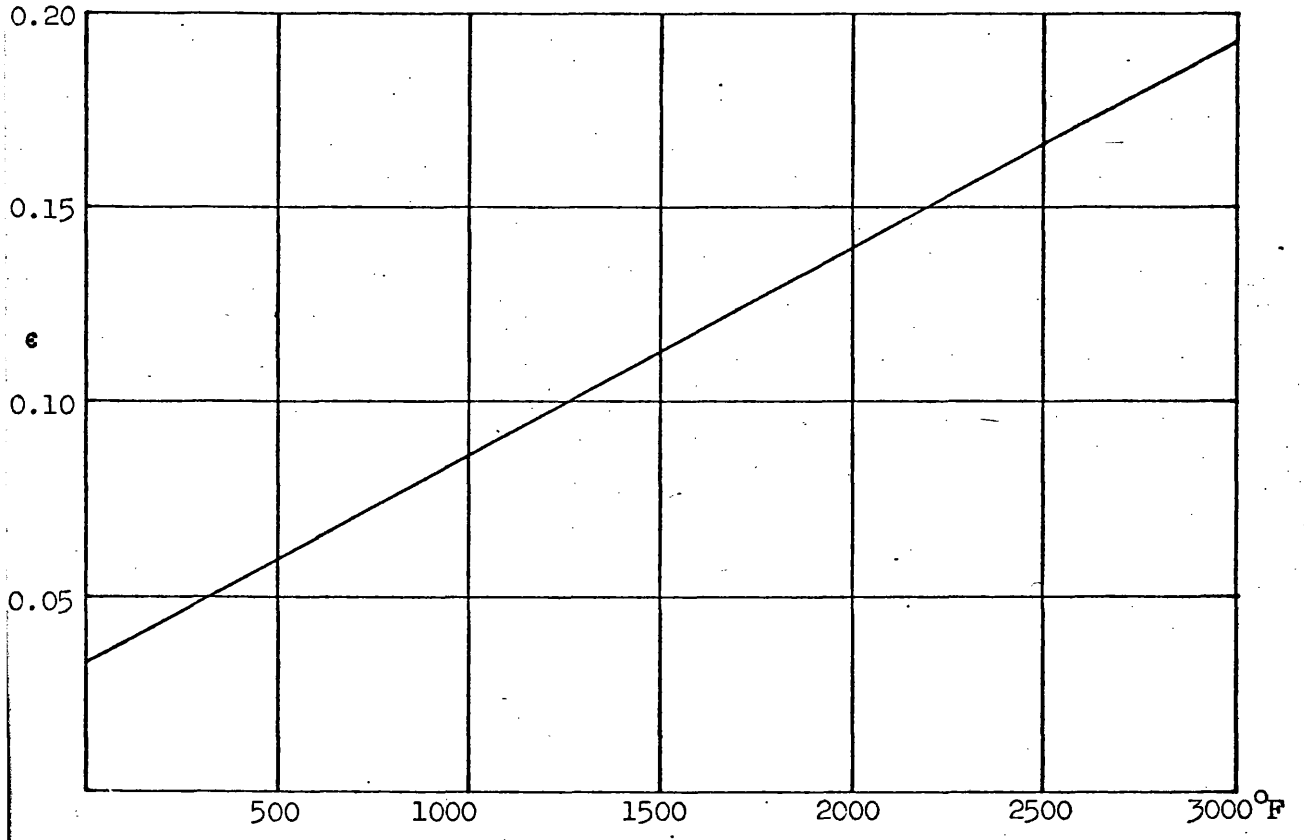

Figure 17. Variation with temperature of the emissivity of the thermocouple hot junction

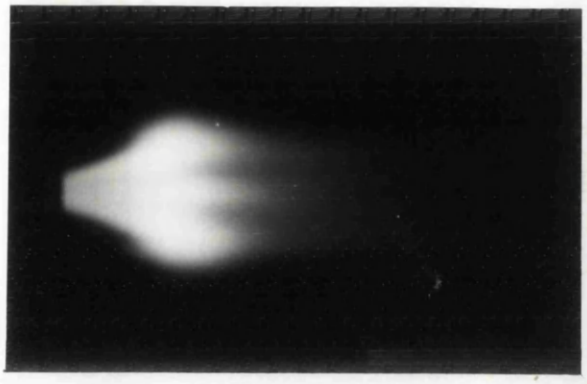

18(a)

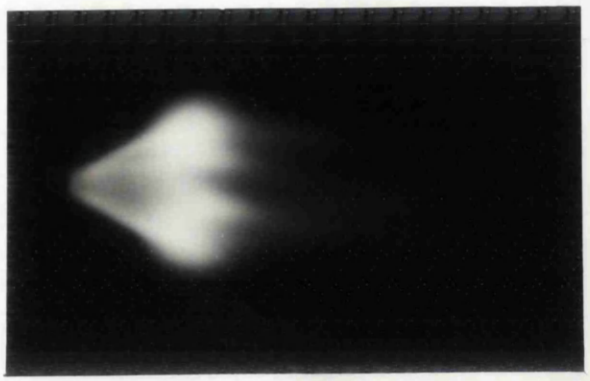

18(b)

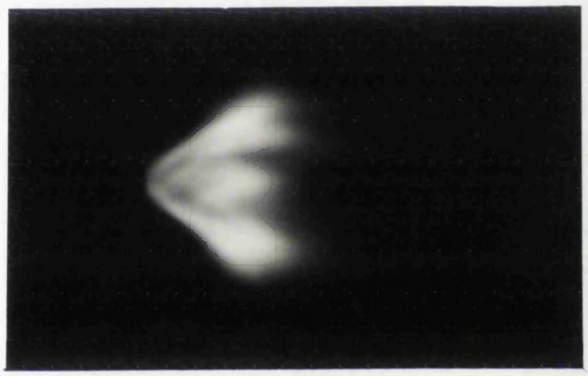

18(c)

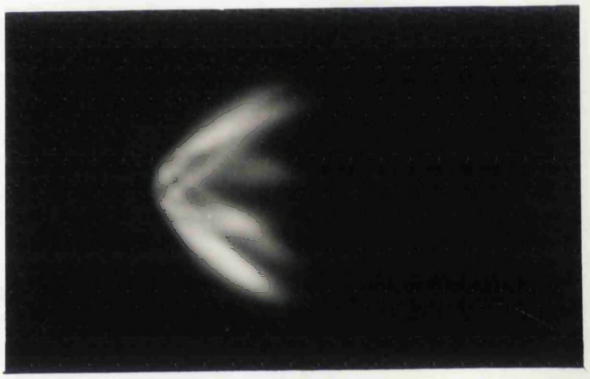

18(d)

18(e)

18(f)

FIGURES 18(a) - (f) Photographs of 15, 30, 45, 60, 70, 75° hubless swirler flames respectively

30° : partially lifted flame

30° : fully lifted flame

60° : fully lifted flame

FIGURES 19(a) - (c) Photographs of lifted hubless swirler flames

20(a)

20(b)

20(c)

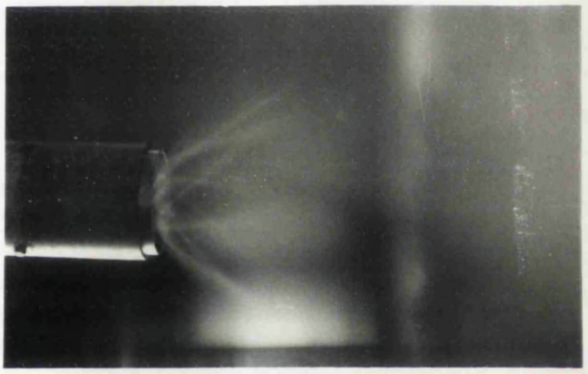

20(d)

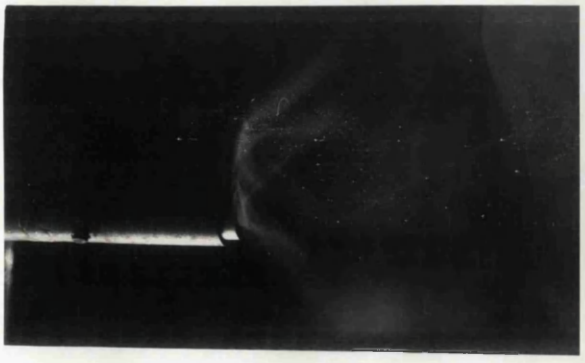

20(e)

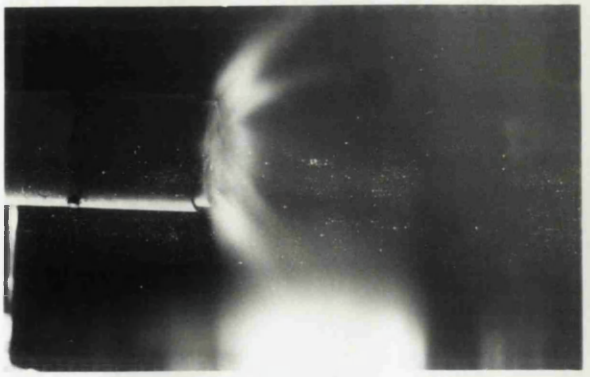

20(f)

FIGURES 20(a) - (f) Photographs of 15, 30, 45, 60, 70, 75° annular swirler flames respectively

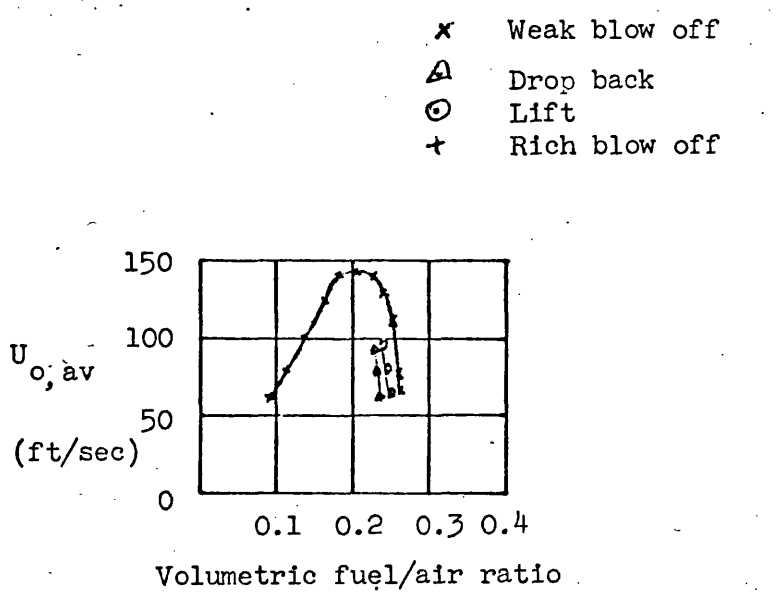

Figure 21 Stability limits of hubless swirling flames from 15° swirler

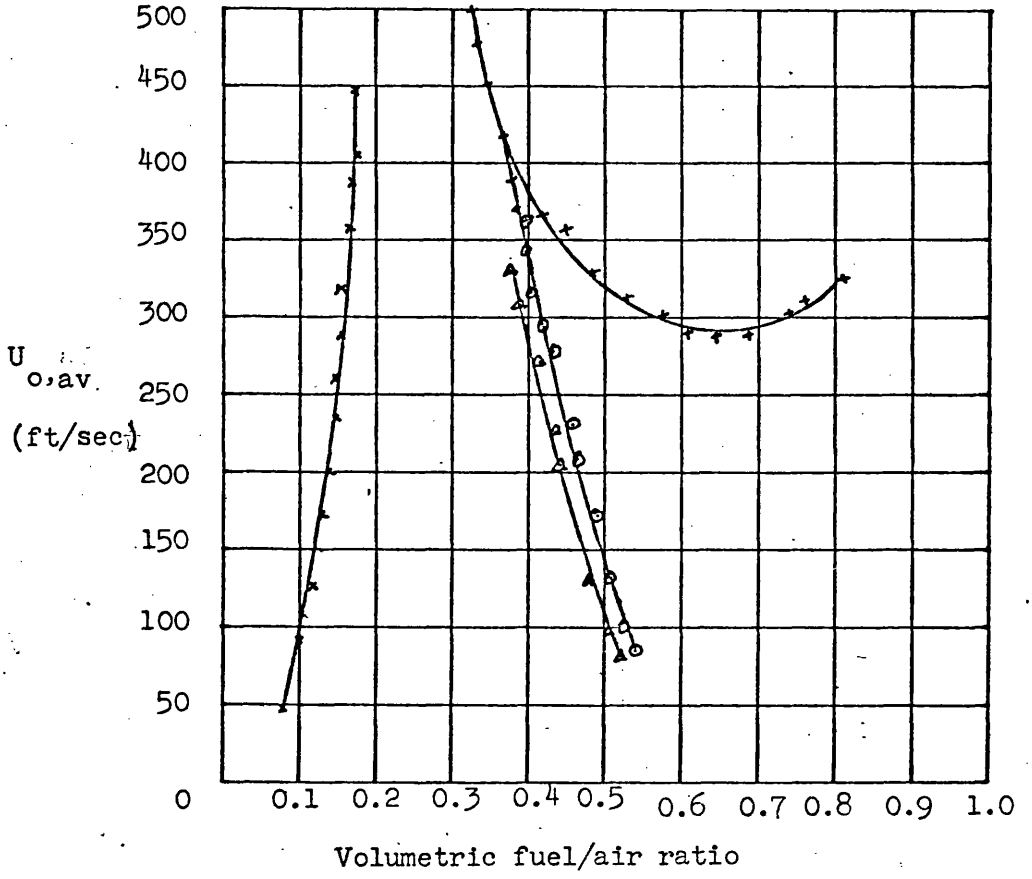

Figure 22. Stability limits of hubless swirling flames from 30° swirler

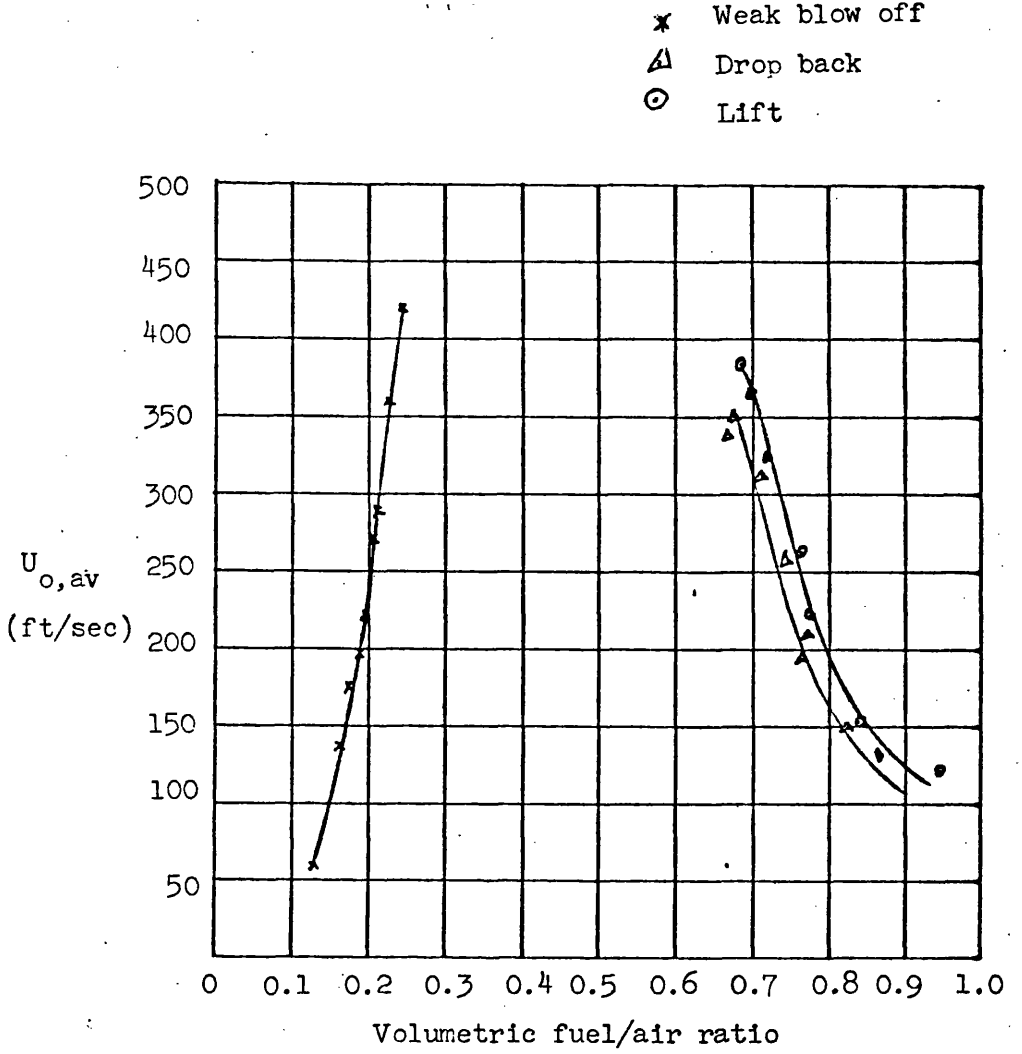

Figure 23. Stability limits of hubless swirling flames from 45° swirler

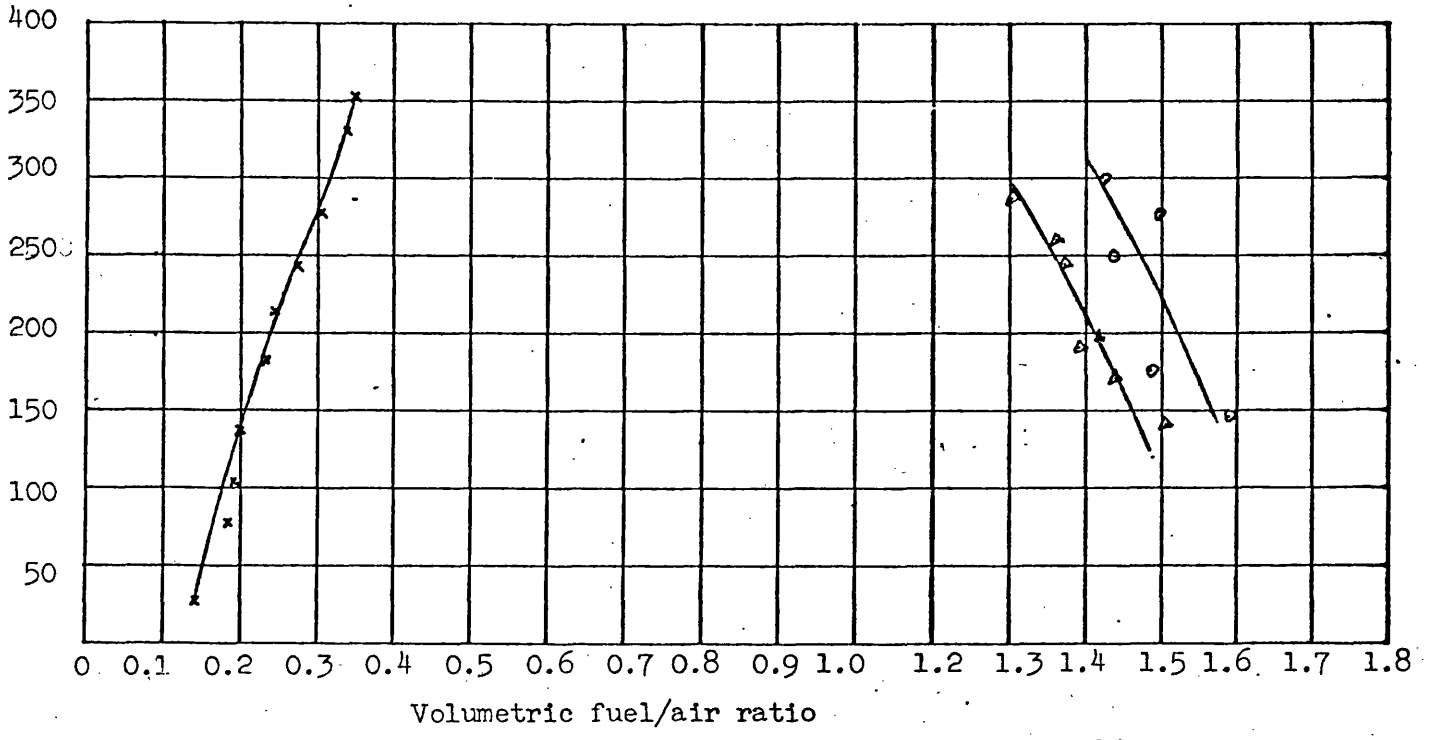

Figure 24. Stability limits of hubless swirling flames from 60° swirler.

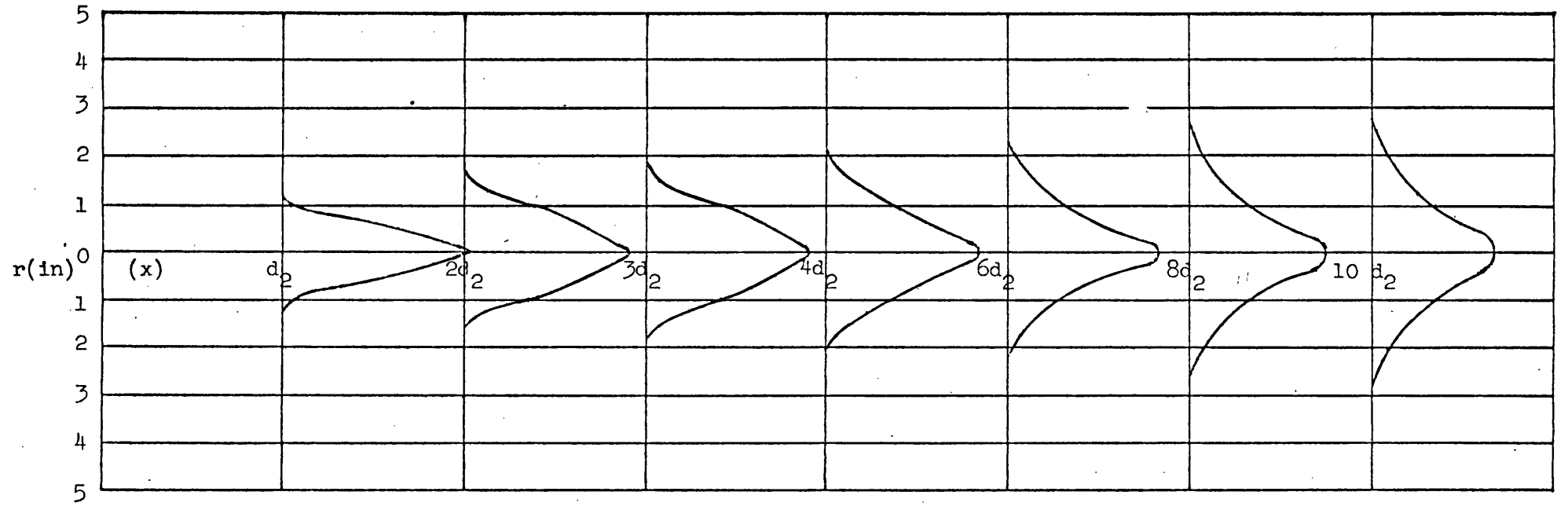

Figure 25. Distributions of axial velocity components for 15° hubless swirler

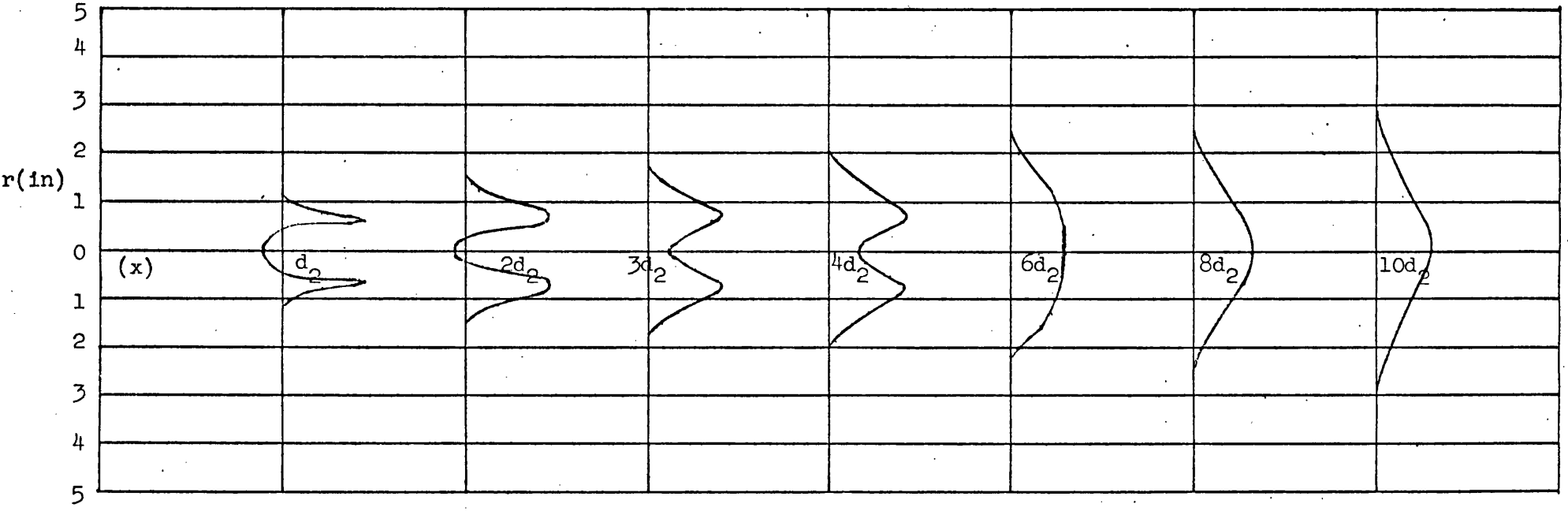

Figure 26 Distributions of axial velocity components for 30° hubless swirler

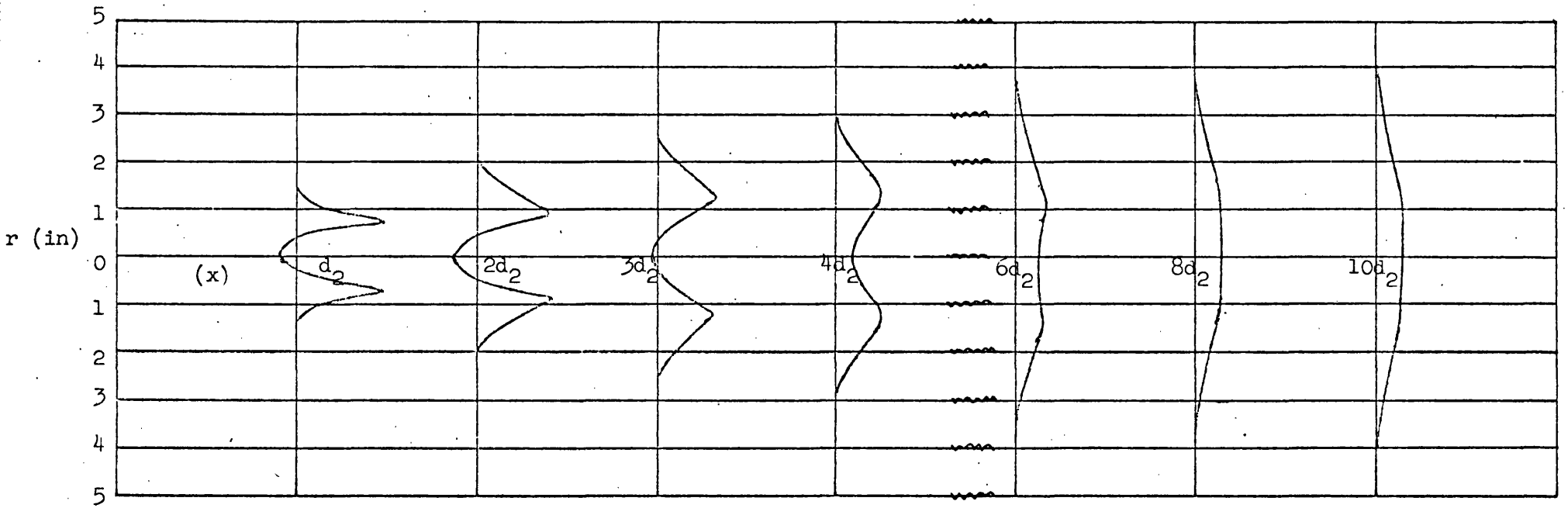

Figure 27. Distributions of axial velocity components for 45° hubless swirler

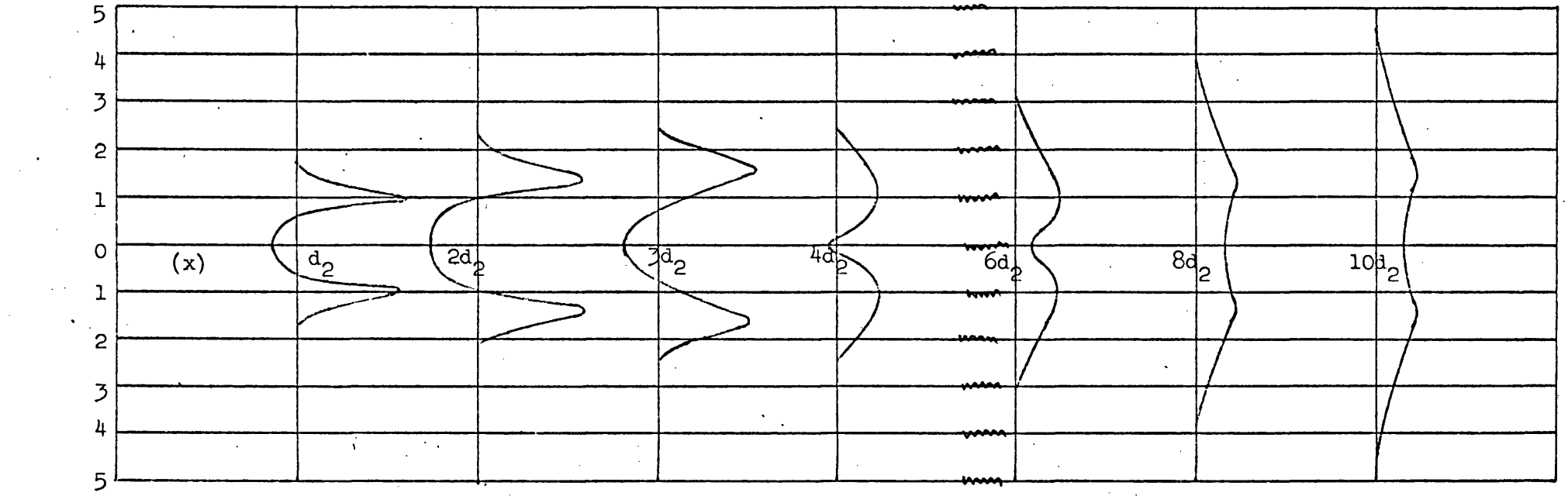

Figure 28. Distributions of axial velocity components for 60° hubless swirler

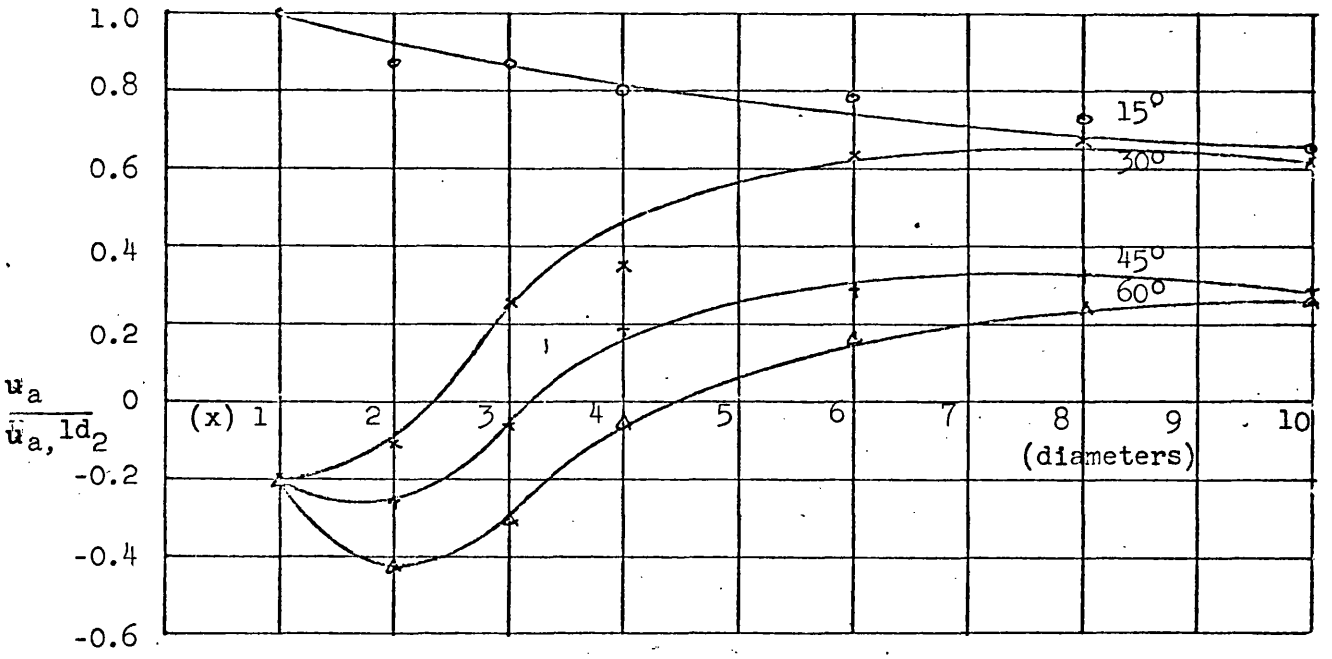

Figure 29 Hubless swirler flames: Decay of axial velocity along the jet axis.

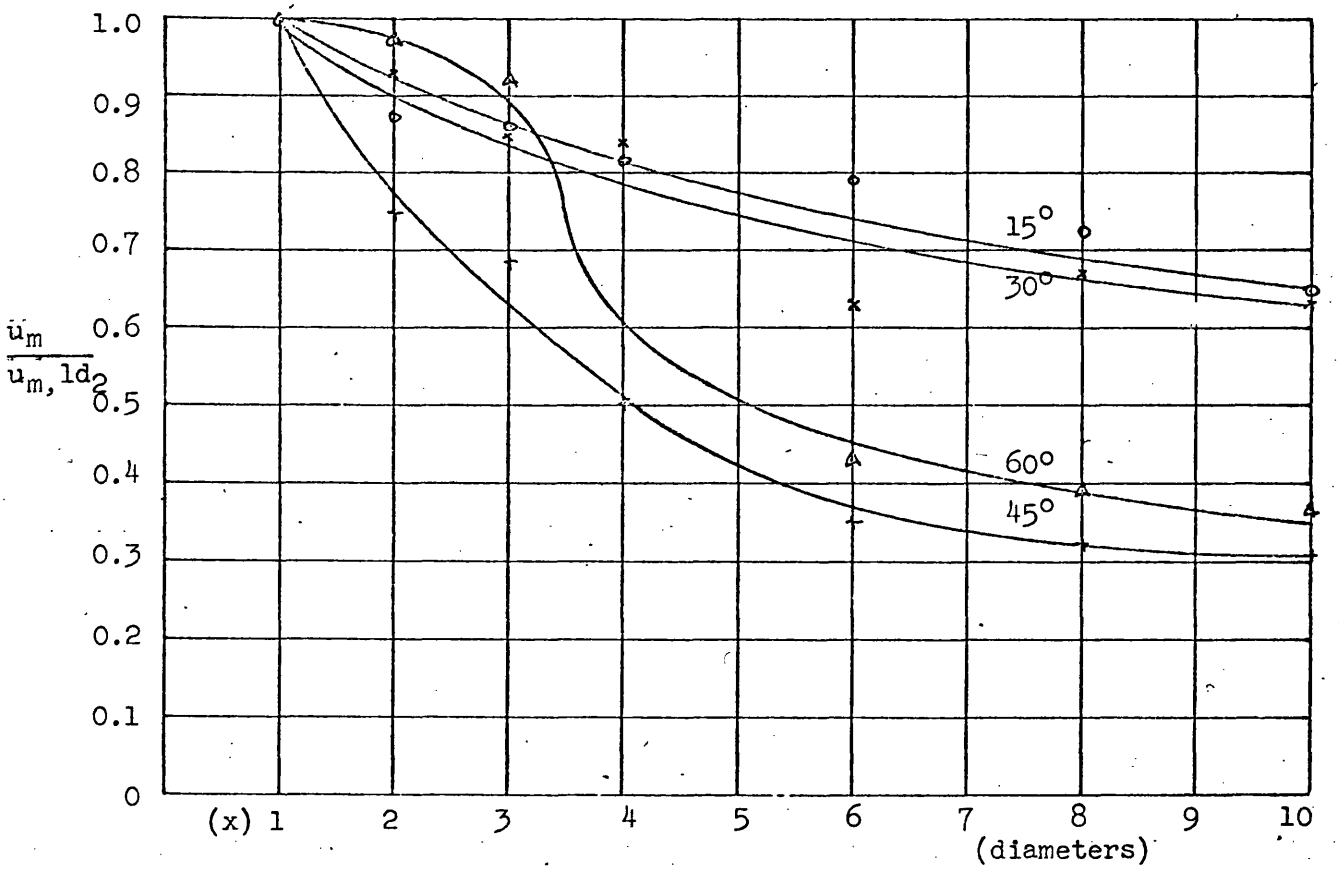

Figure 30. Hubless swirler flames: Decay of maximum axial velocity along the jet

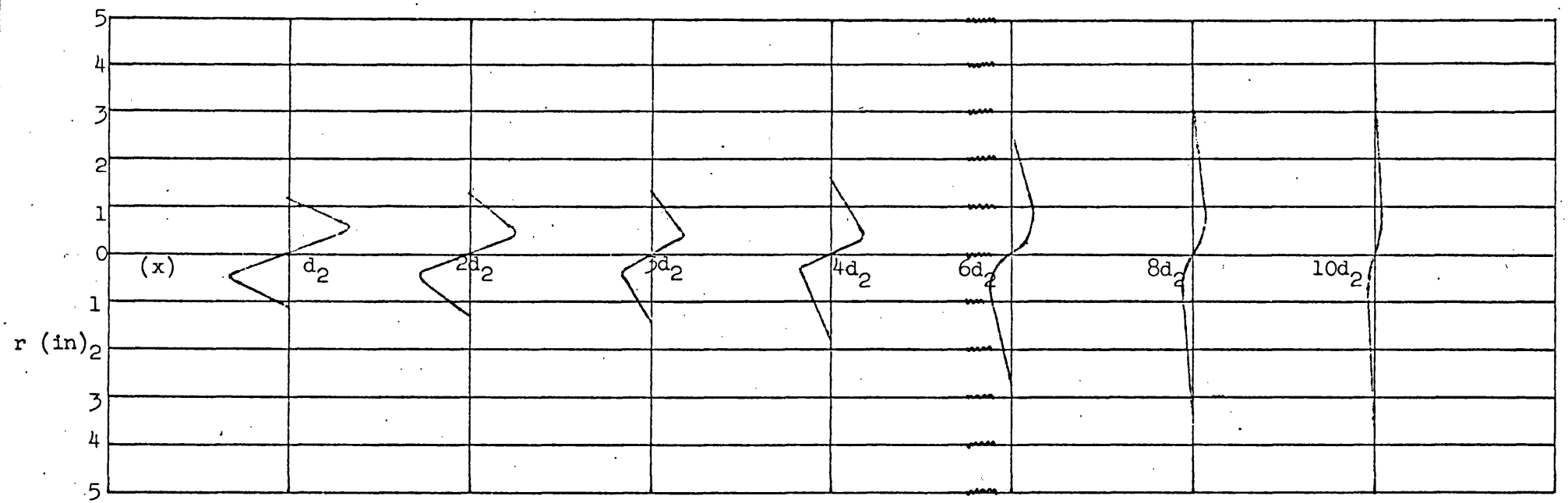

Figure 31. Tangential velocity profiles for the 15° swirler flame

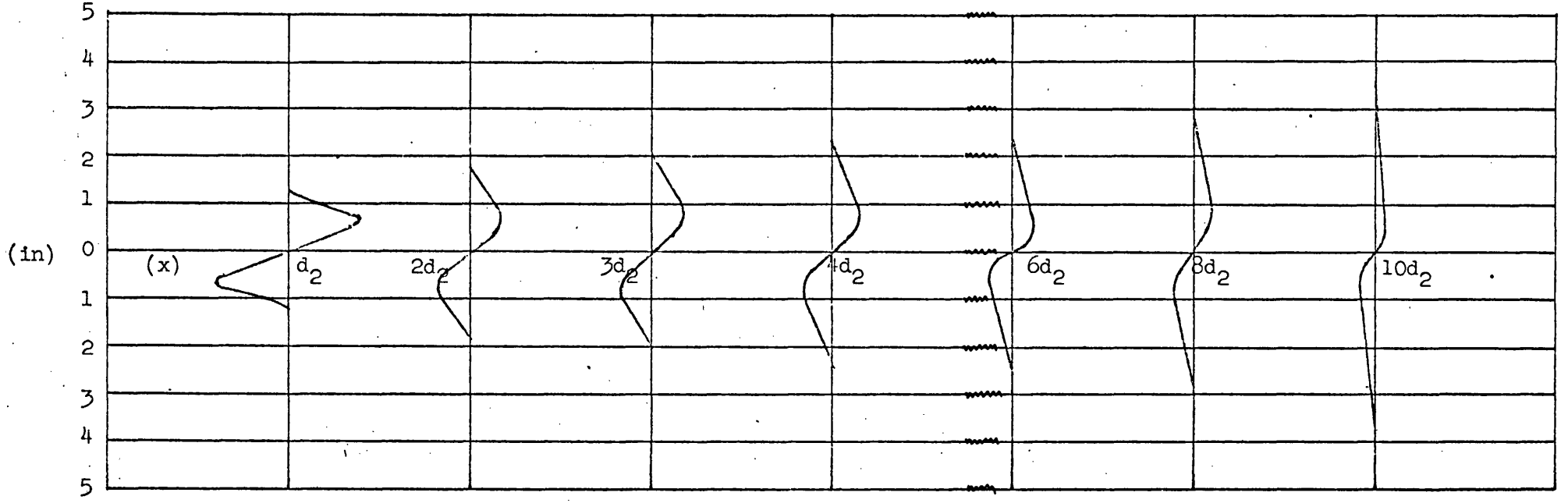

Figure 32. Tangential velocity profiles for the 30° swirler flame

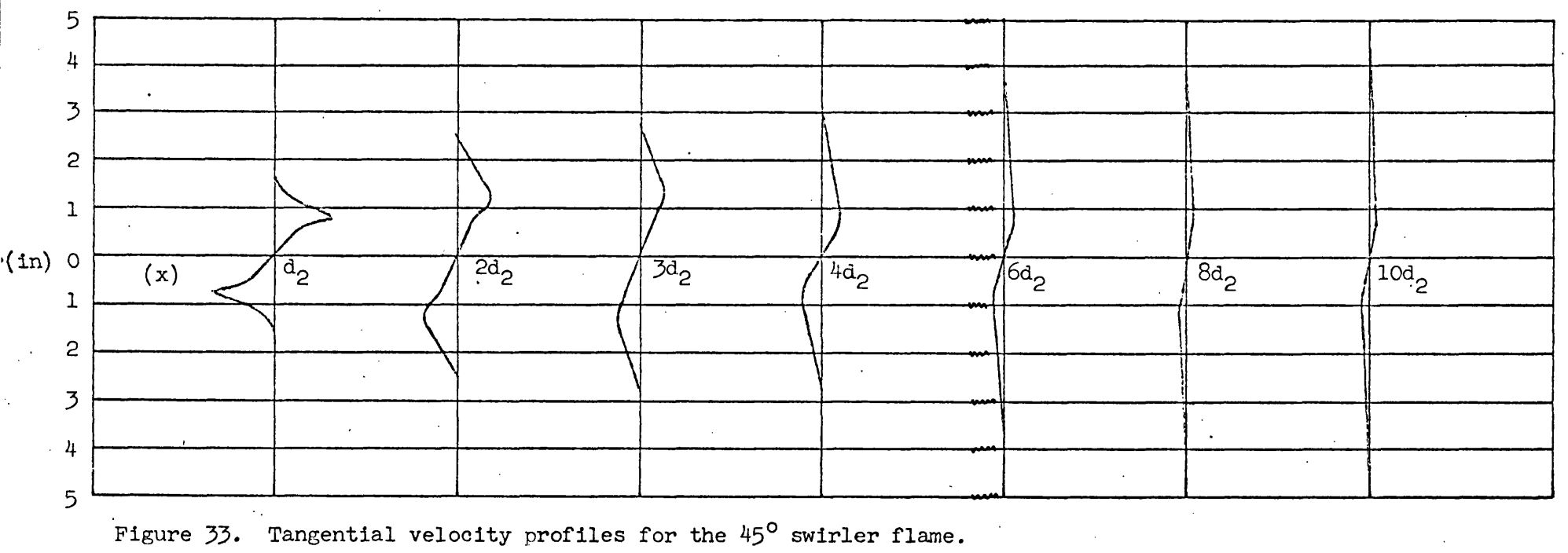

Figure 33. Tangential velocity profiles for the 45° swirler flame.

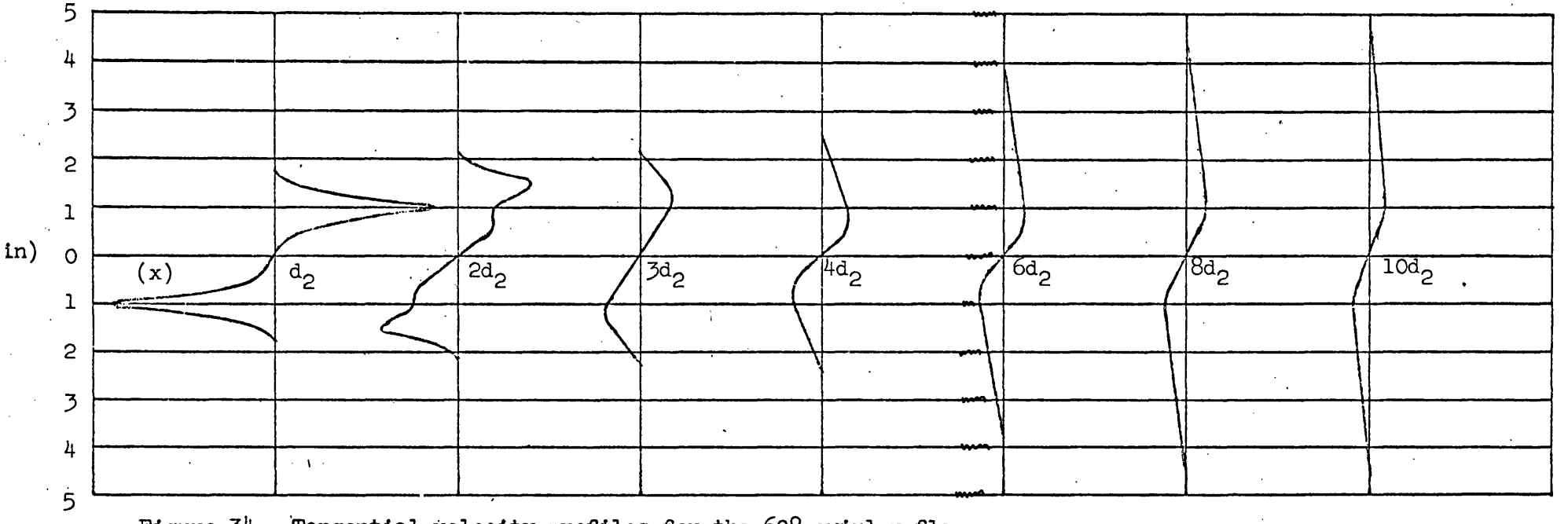

Figure 34. Tangential velocity profiles for the 60° swirler flame.

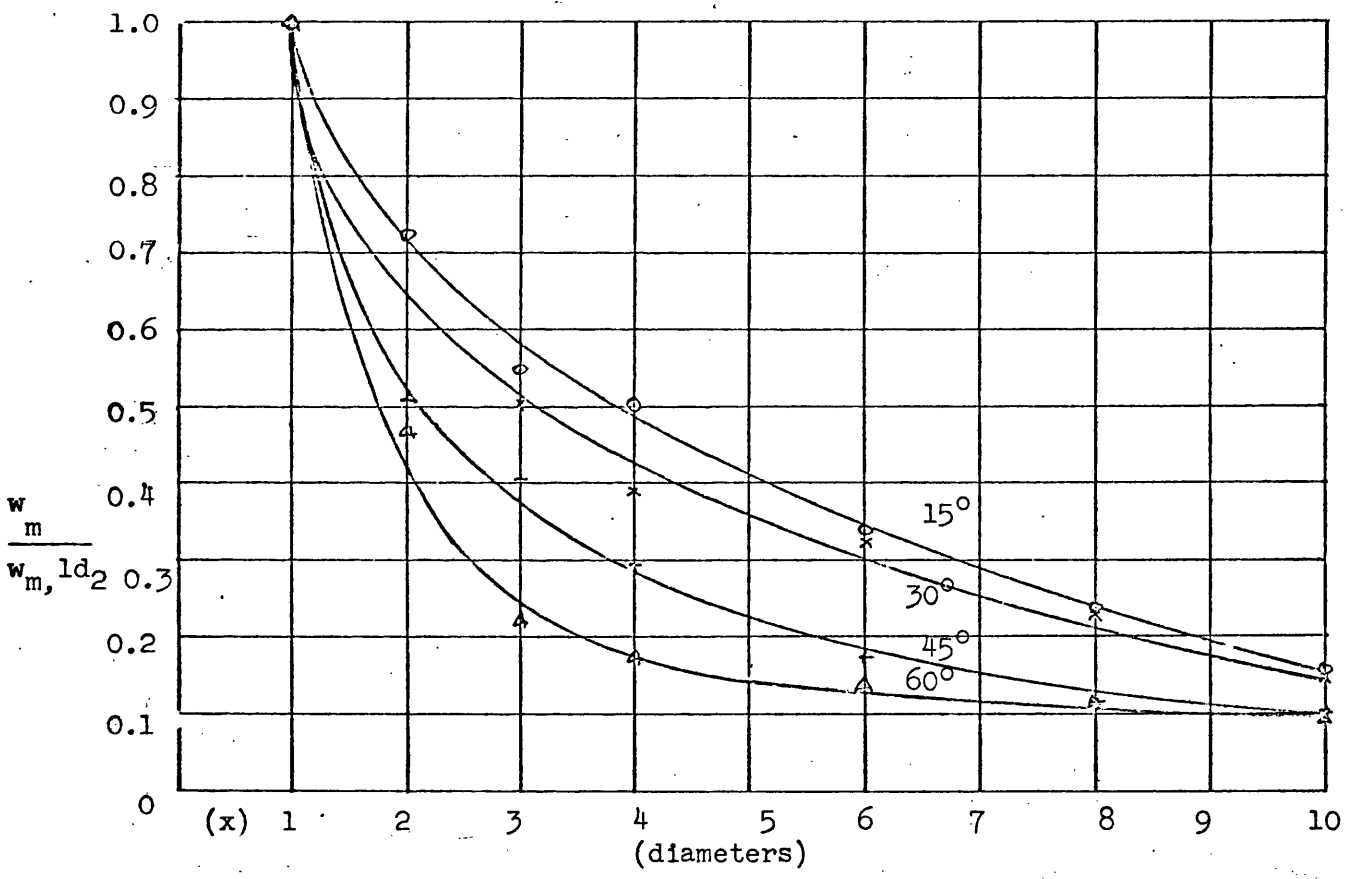

Figure 35 Hubless swirler flames: Decay of maximum tangential velocity along the jet

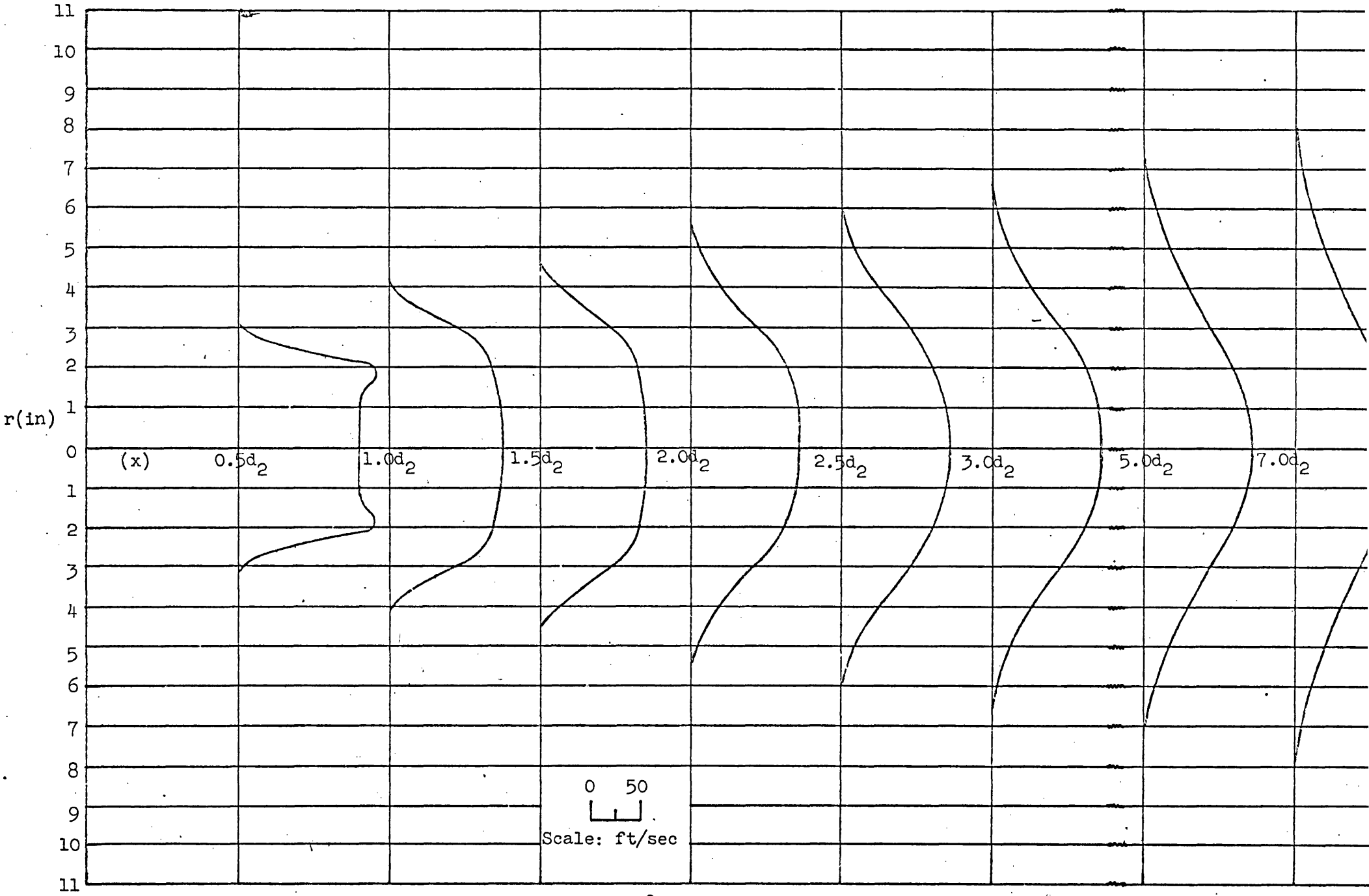

Figure 36. Distribution of axial velocity for 15° annular swirler flame

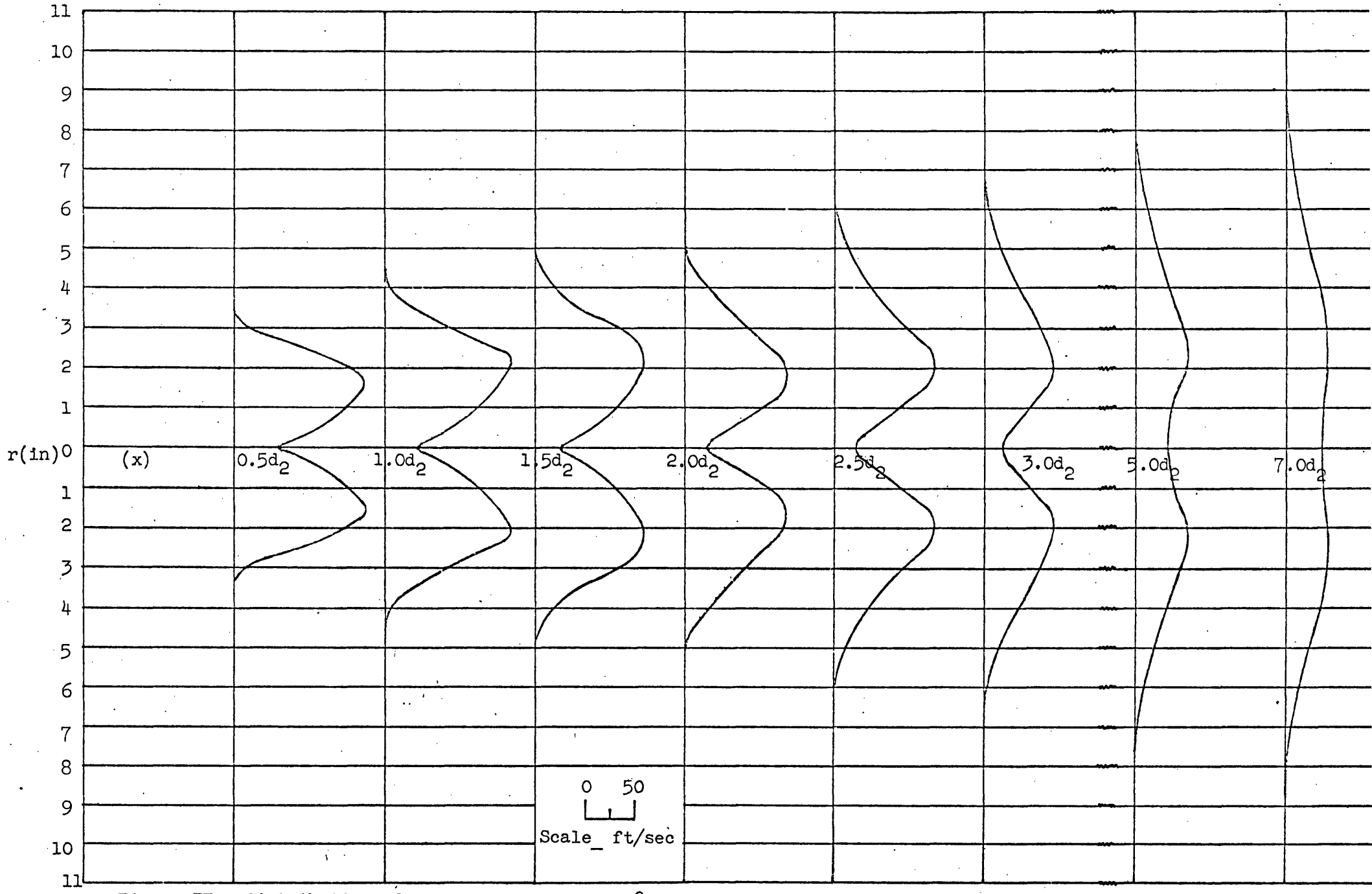

Figure 37. Distribution of axial velocity for 30° annular swirler flame

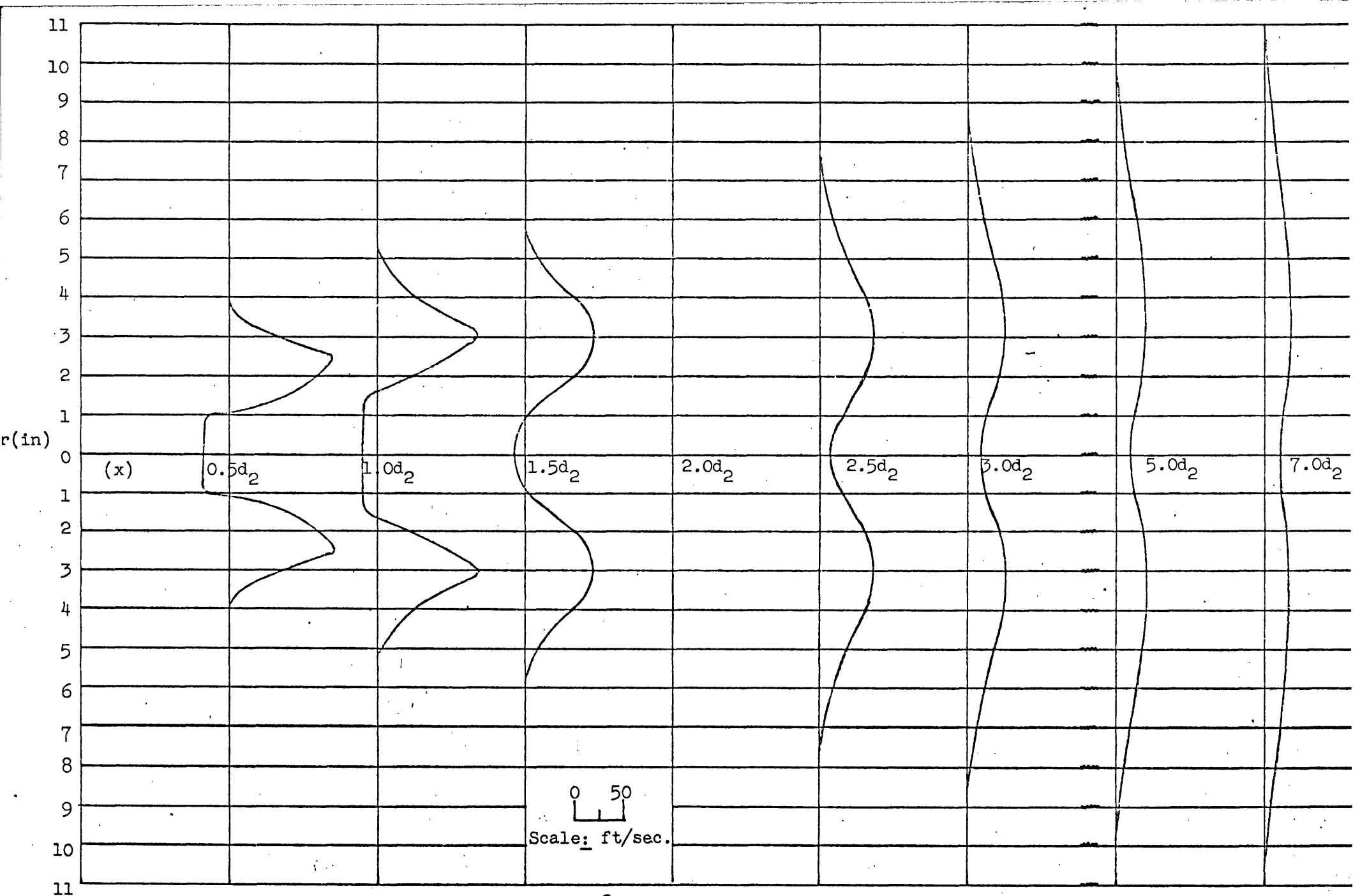

Figure 38. Distribution of axial velocity for 45° annular swirler flame.

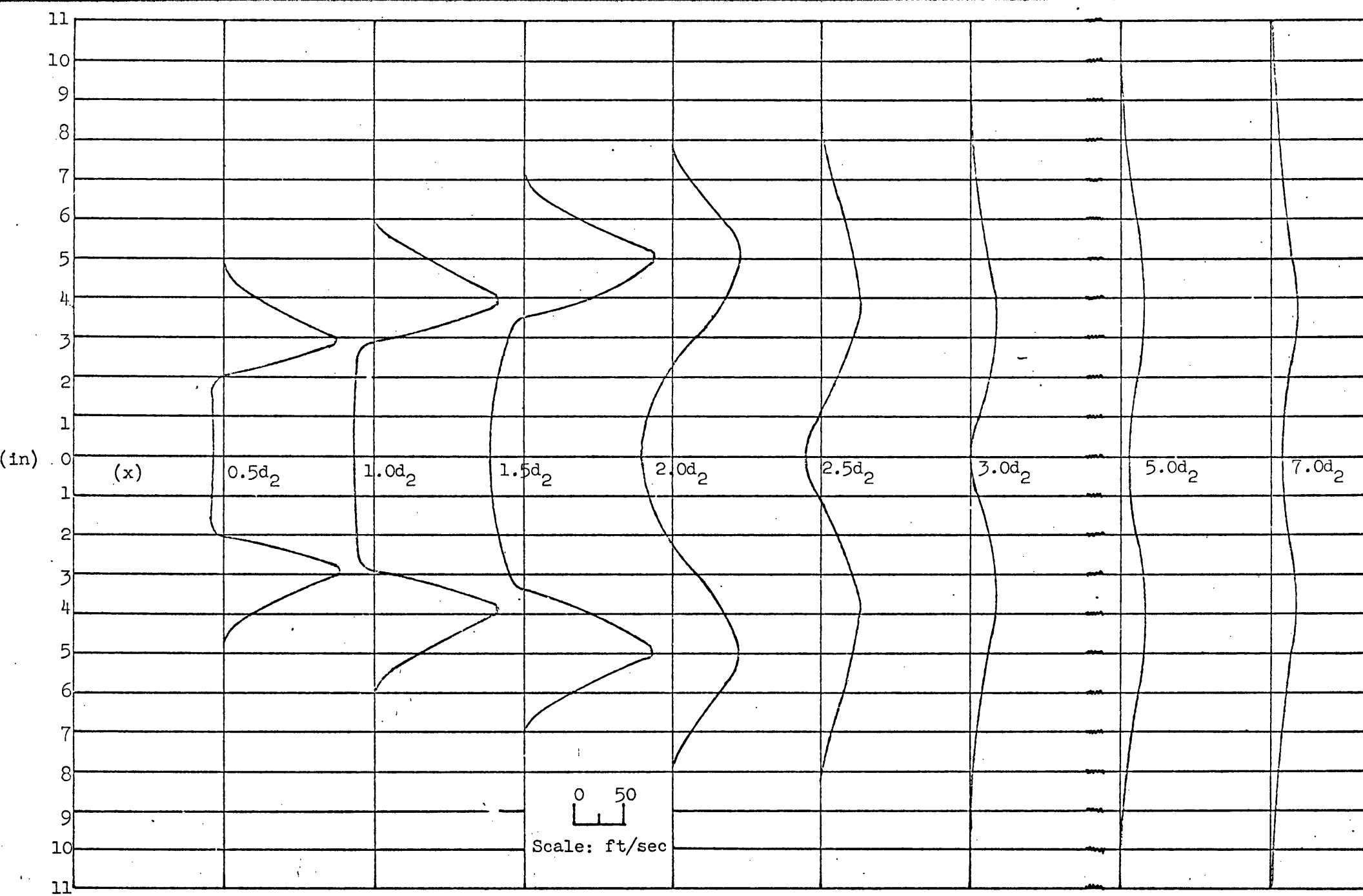

Figure 39 Distribution of axial velocity for 60° annular swirler flame

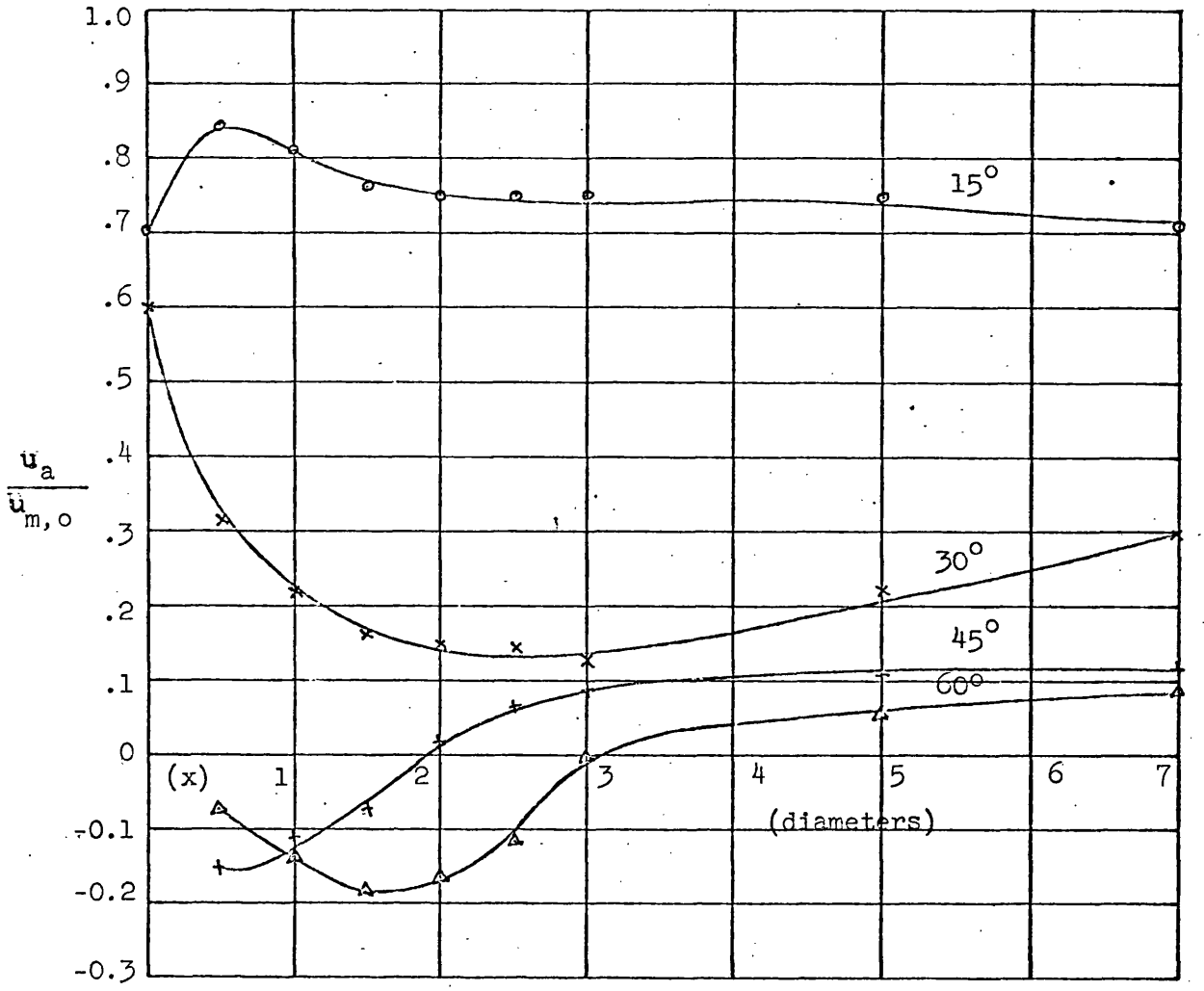

Figure 40. Annular swirler flames: Decay of axial velocity along the jet axis.

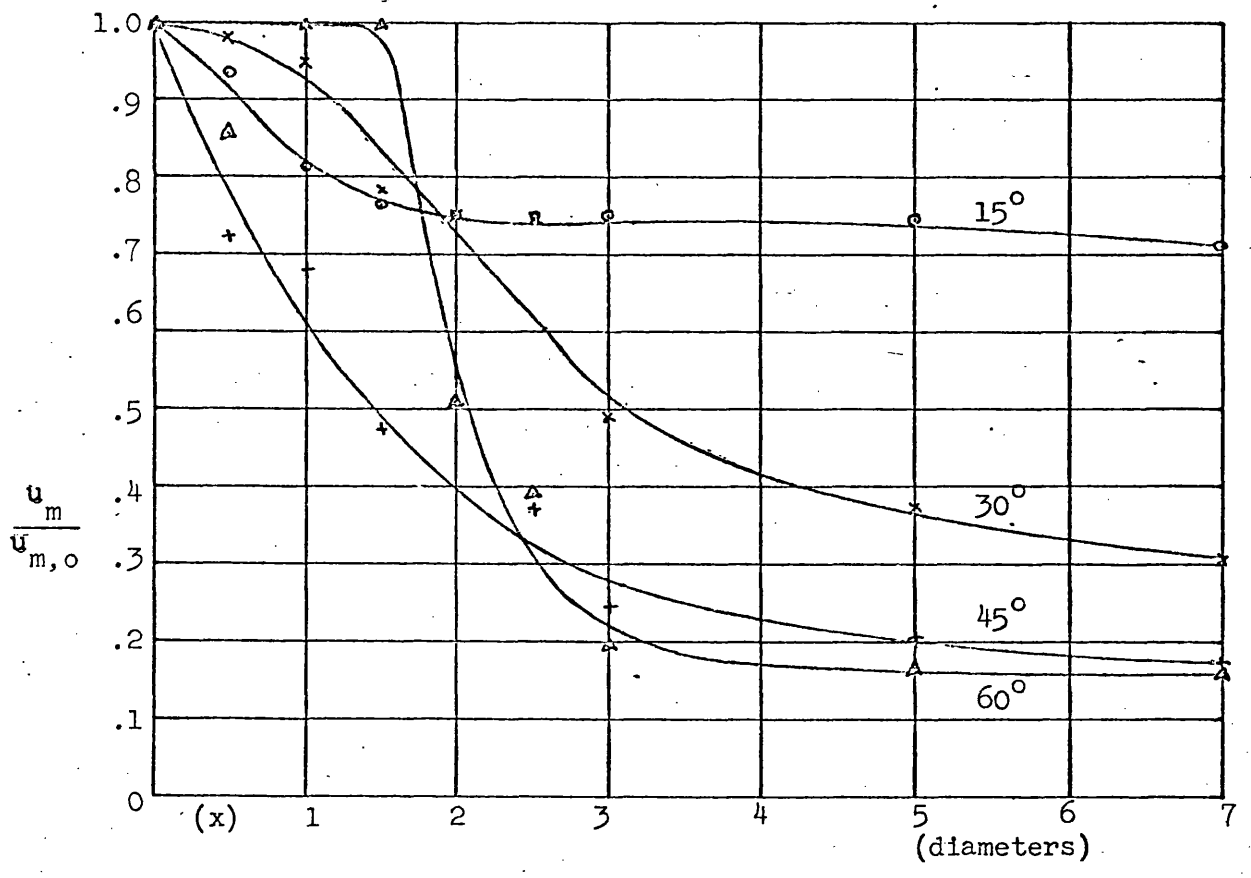

Figure 41 Annular swirler flames: Decay of maximum axial velocity along the jet

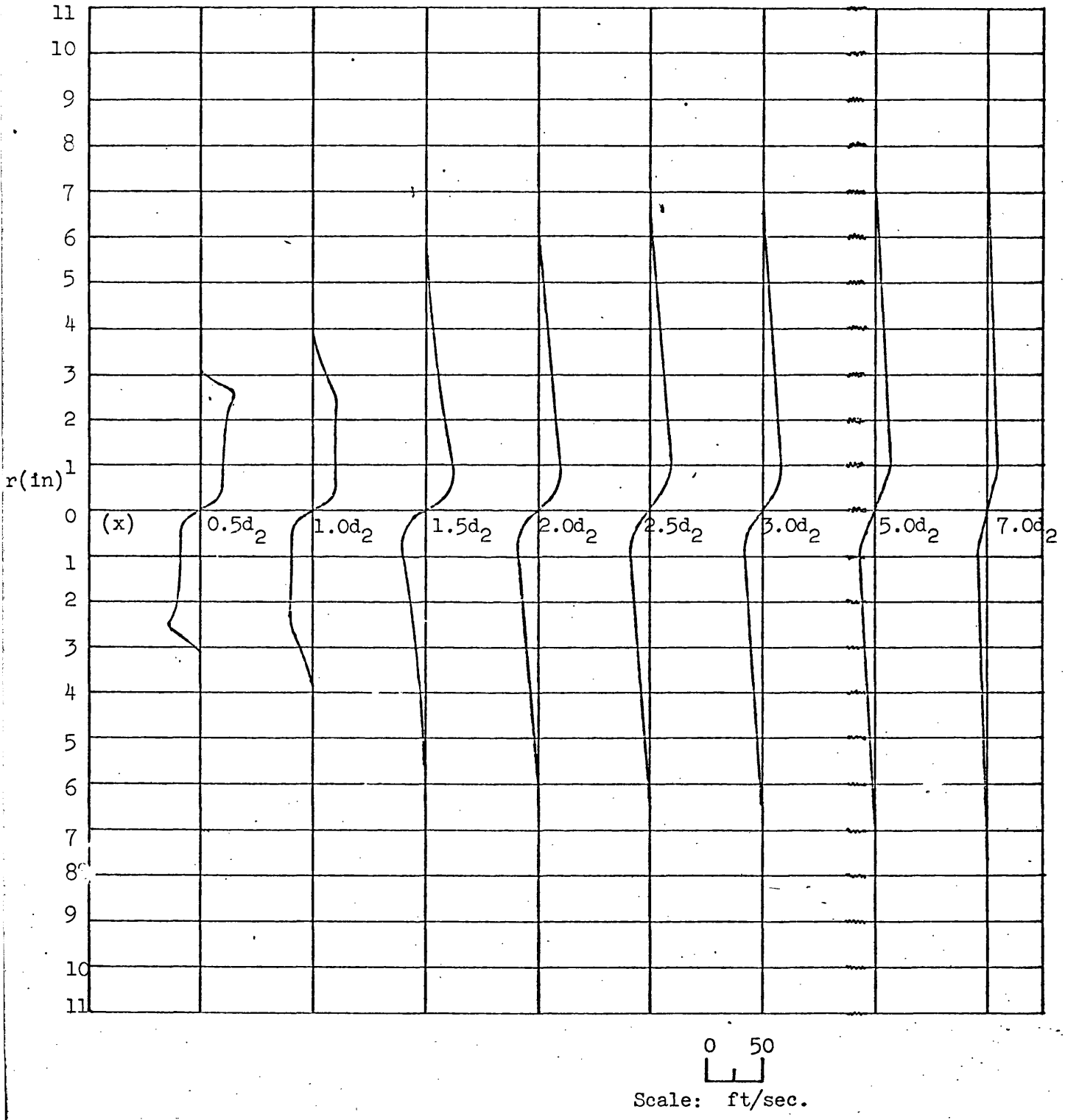

Figure 42. Tangential velocity profiles for 15° annular swirler flame

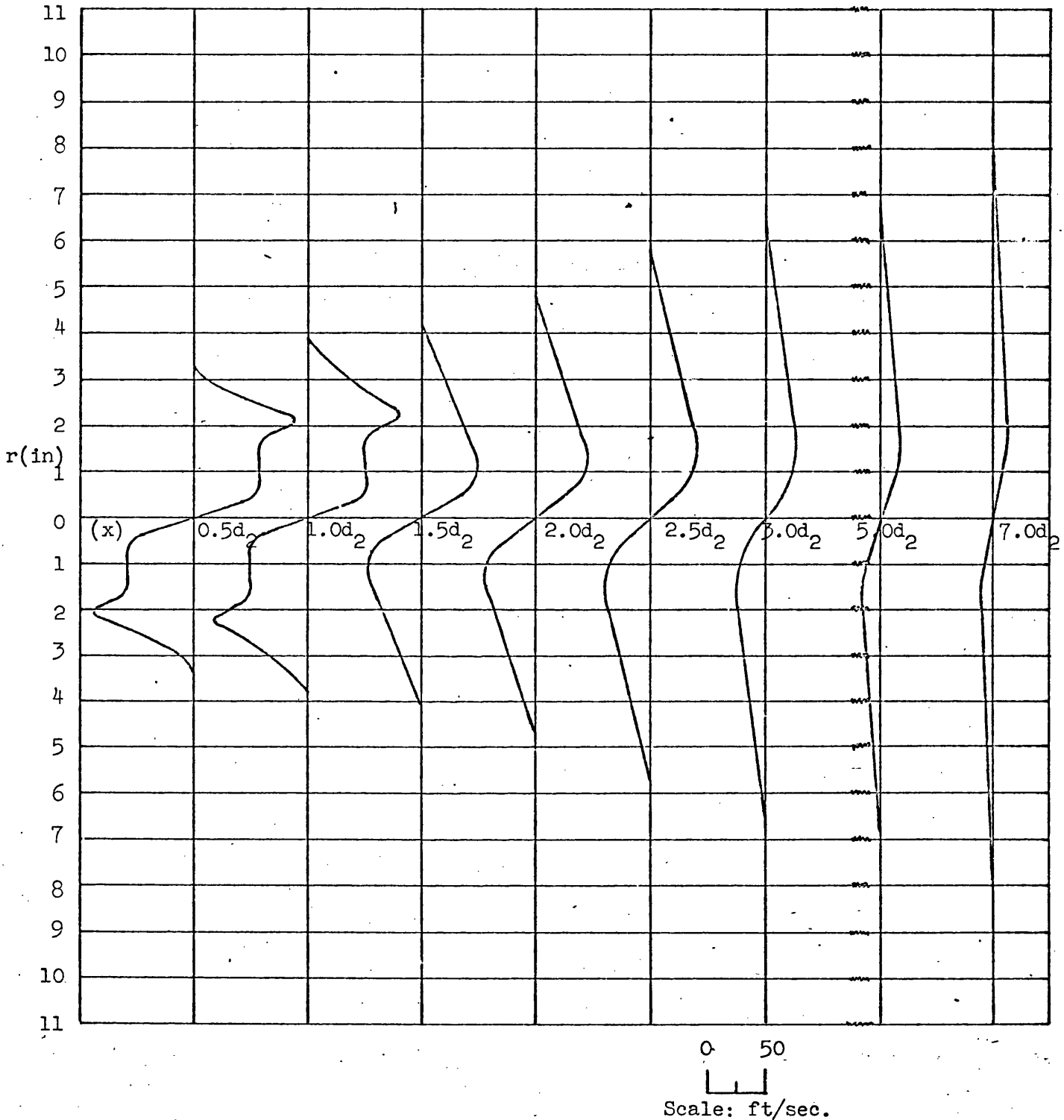

Figure 43. Tangential velocity profiles for the 30° annular swirler flame

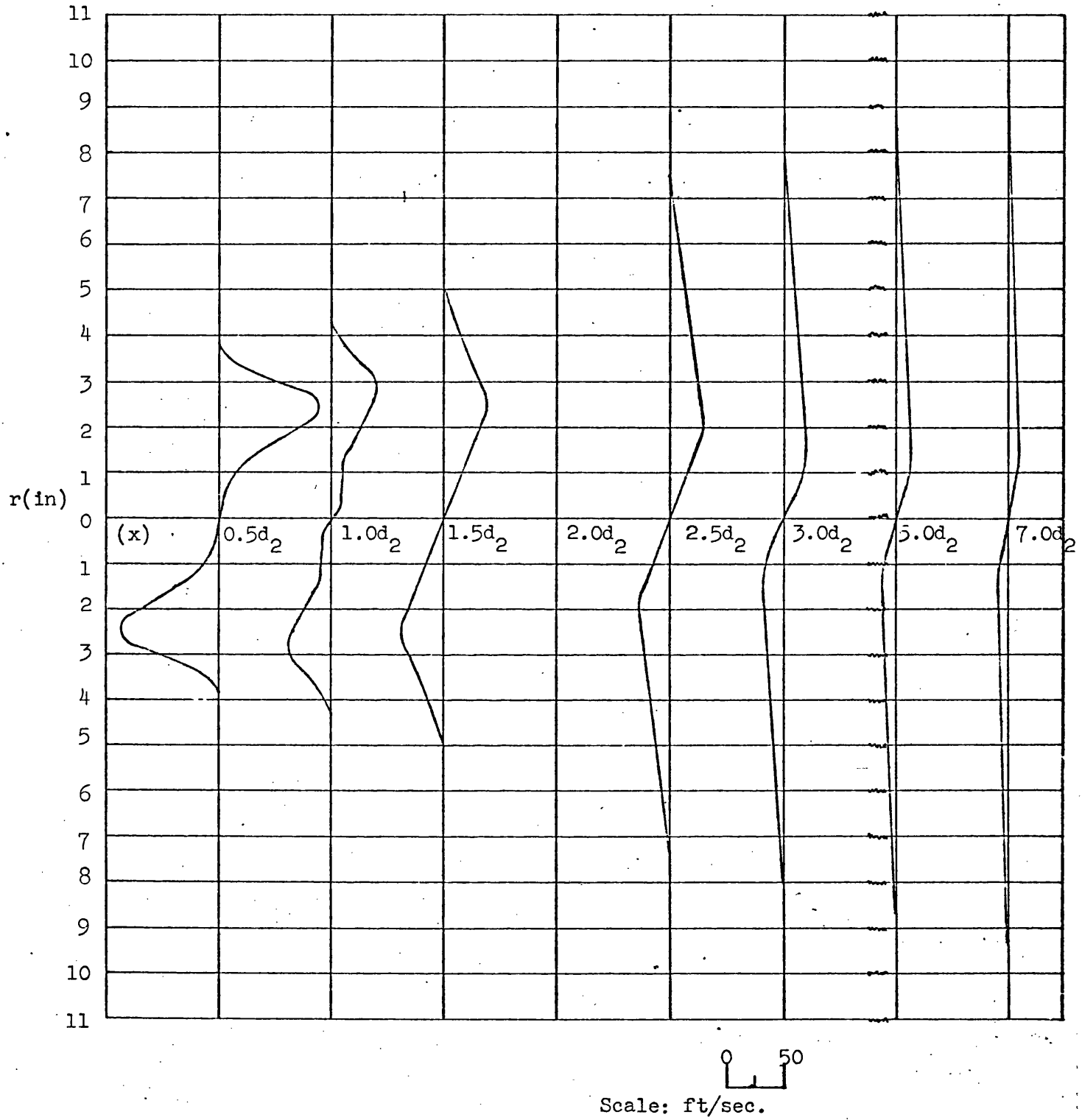

Figure 44. Tangential velocity profiles for the 45° annular swirler flame

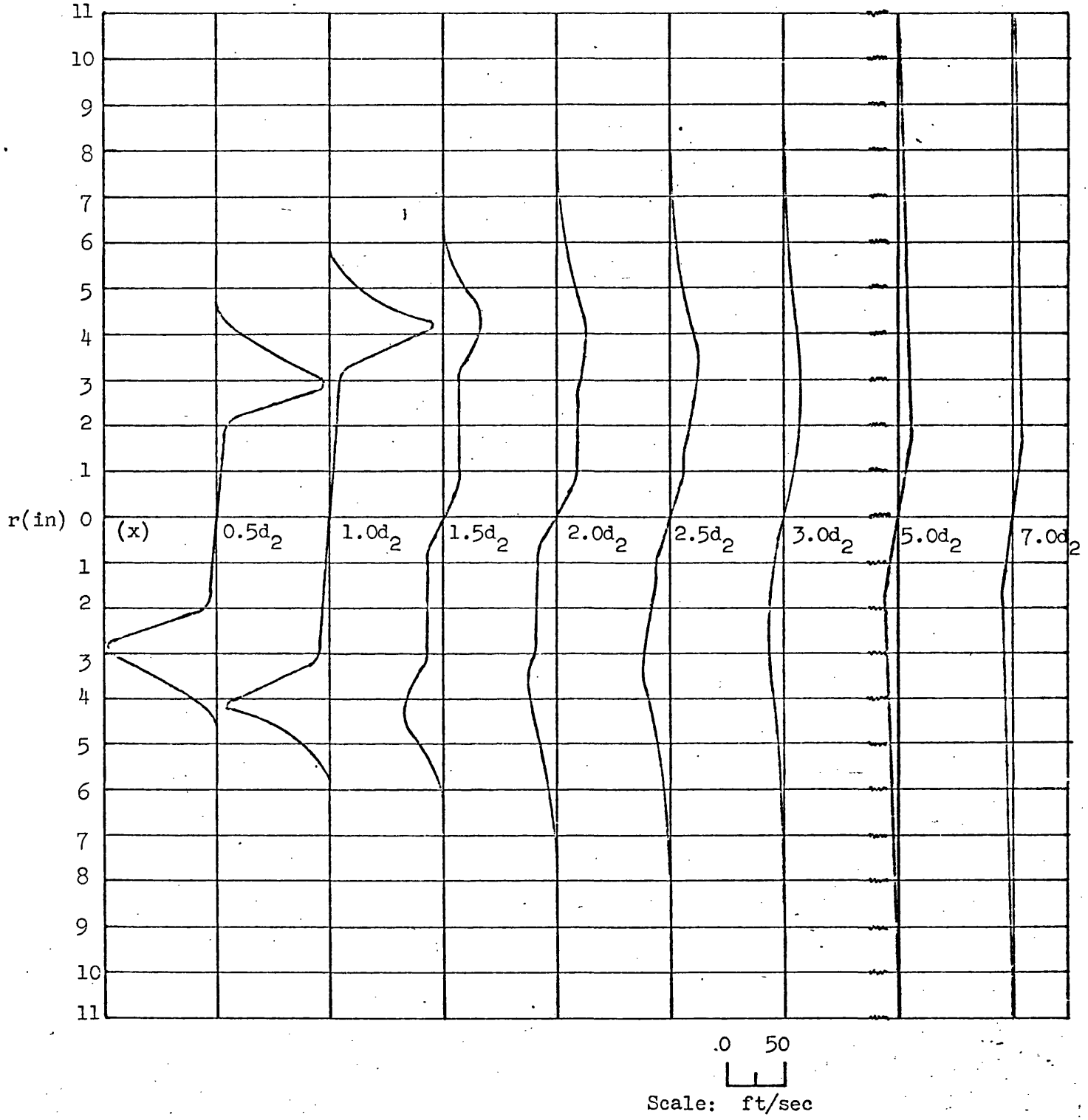

Figure 45. Tangential velocity profiles for the 60° annular swirler flame

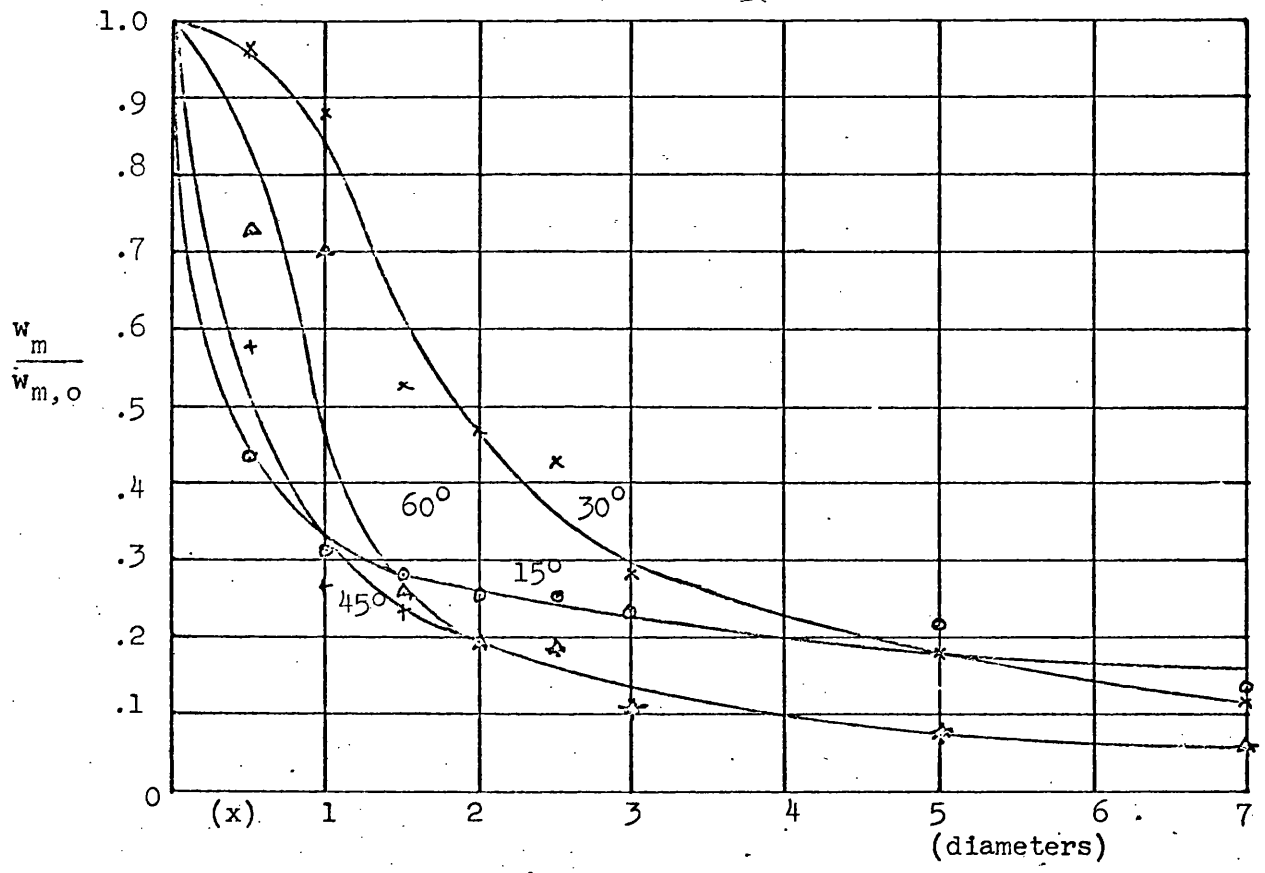

Figure 46. Annular swirler flames: Decay of maximum tangential velocity along the jet

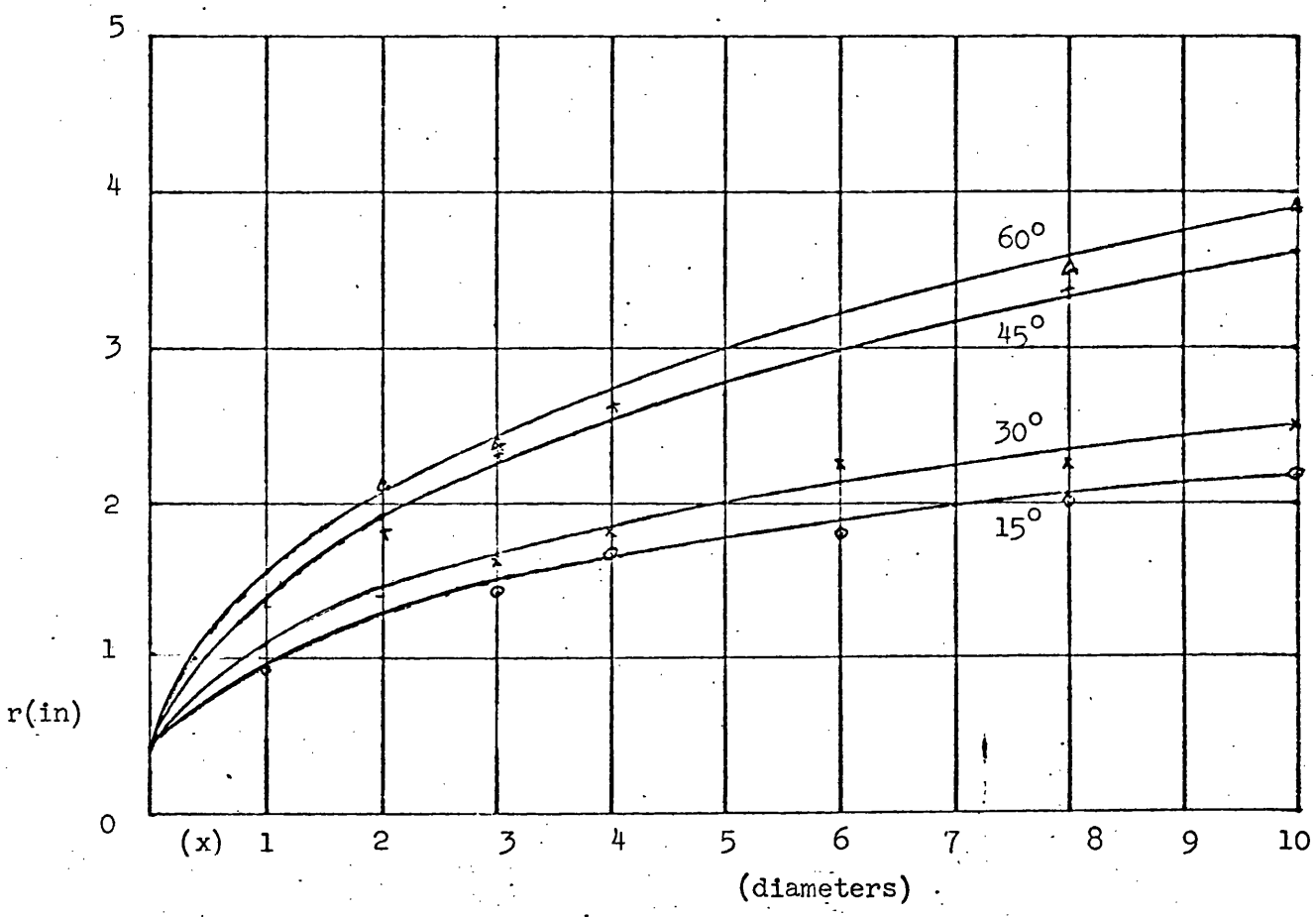

Figure 47. Hubless swirler flames: Variation of jet widths.

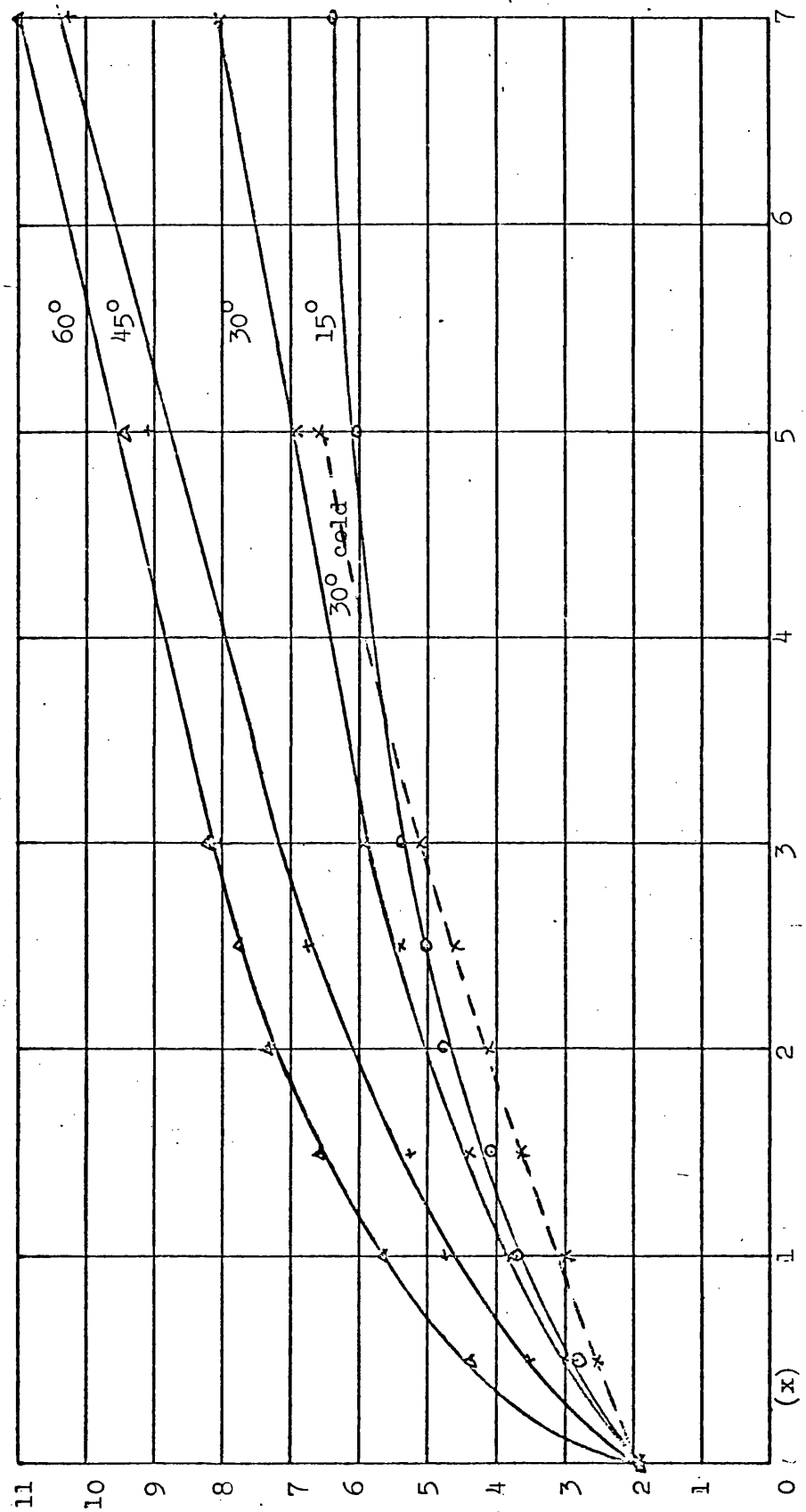

Figure 48 Annular swirler flames: Variation of jet width

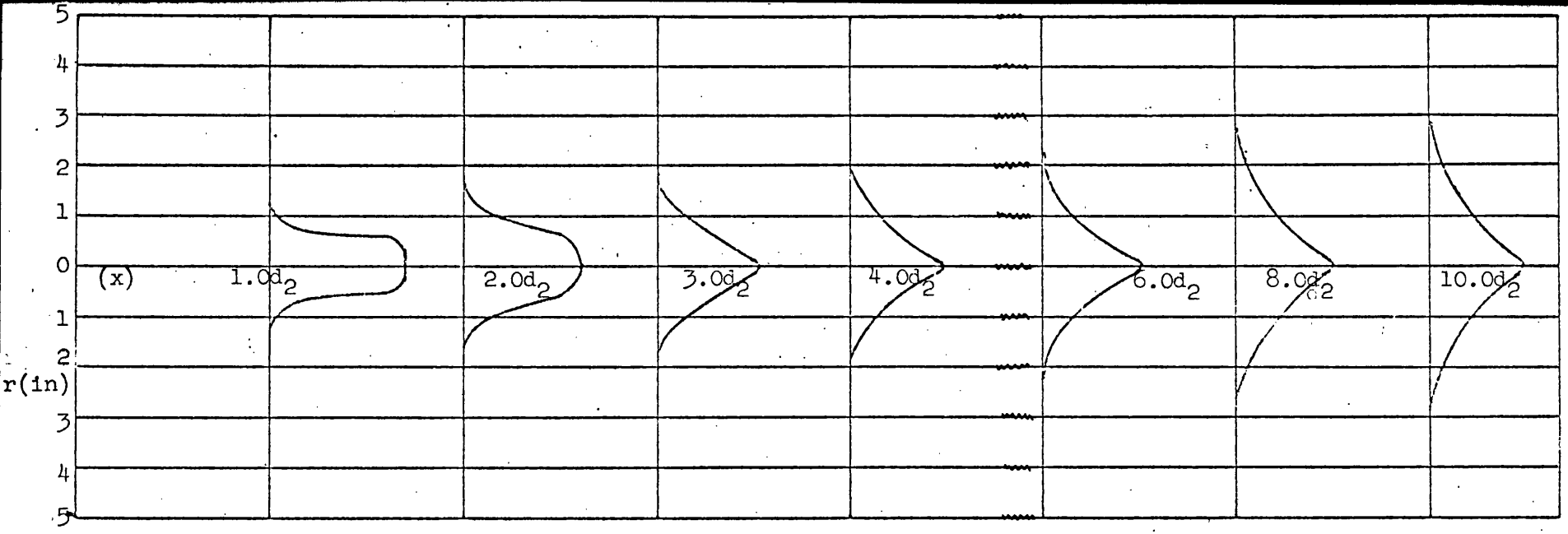

Figure 49. Static pressure (p_{at}-p) profiles for 15° hubless swirler flame

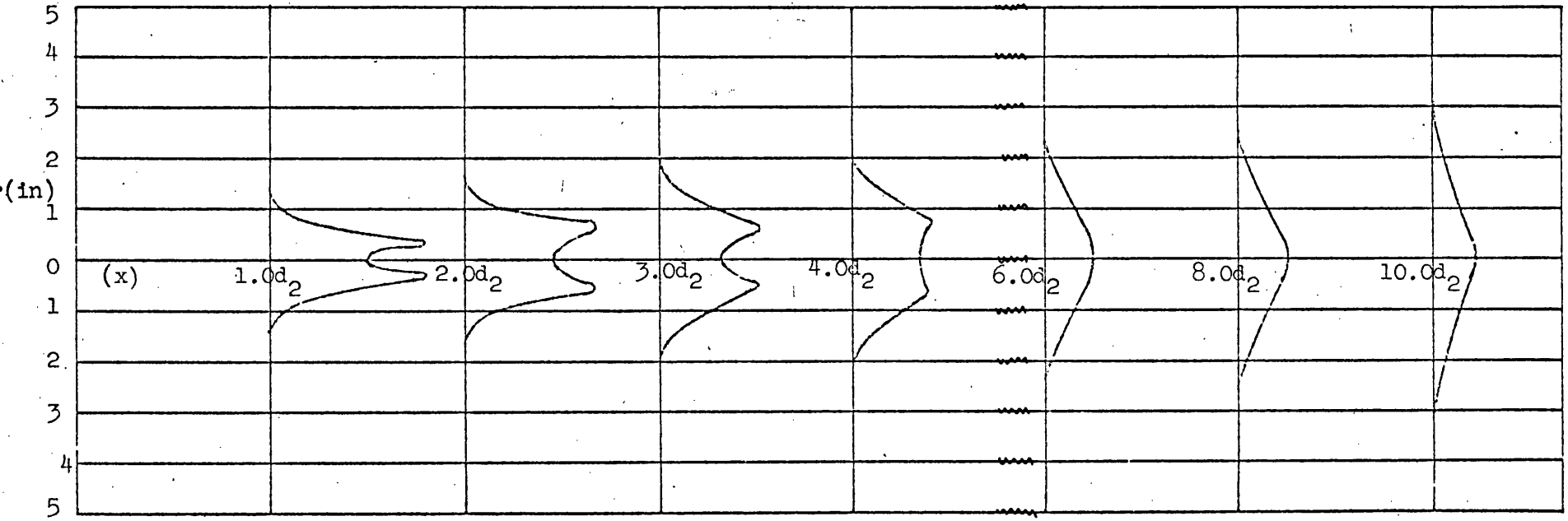

Figure 50. Static pressure (p_{at}-p) profiles for 30° hubless swirler flame

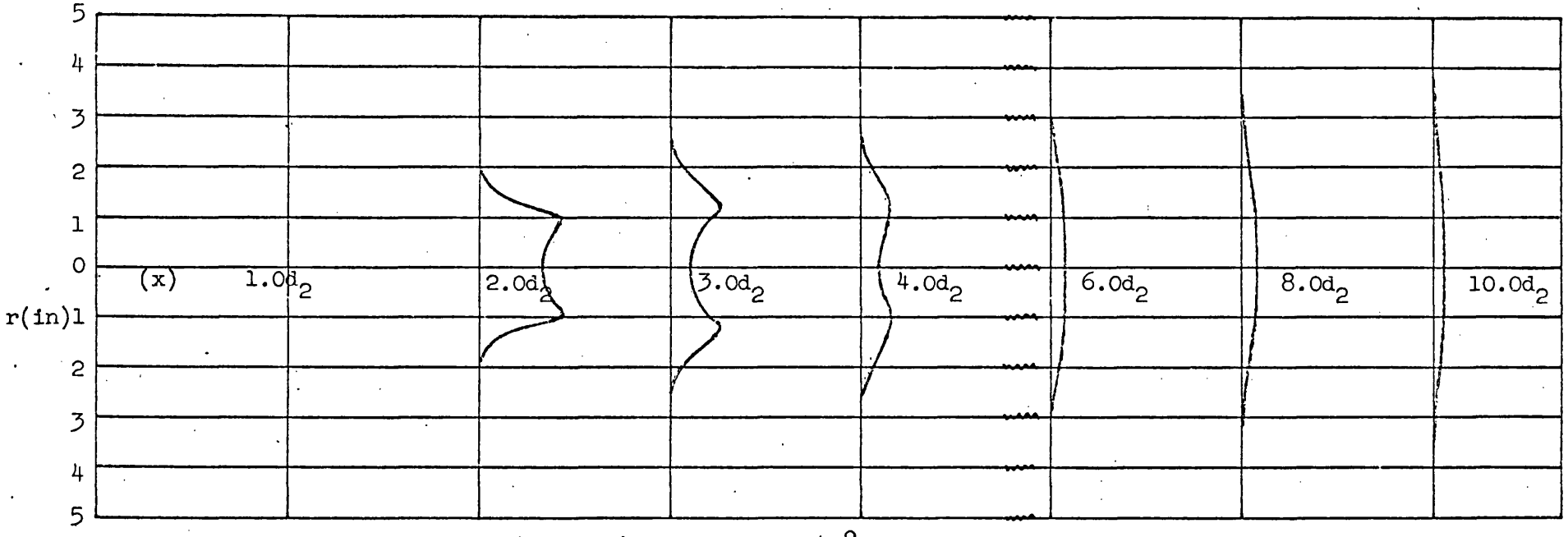

Figure 51. Static pressure (p_{at} - p) profiles for 45° hubless swirler flame

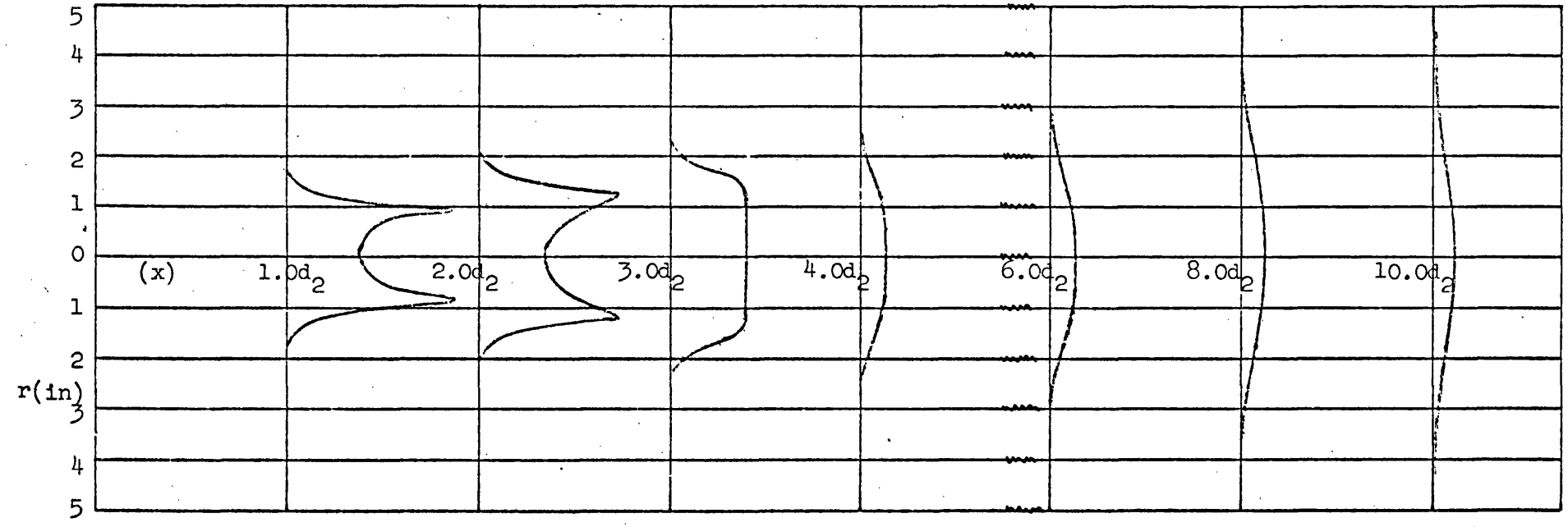

Figure 52. Static pressure (p_{at} - p) profiles for 60° hubless swirler flame

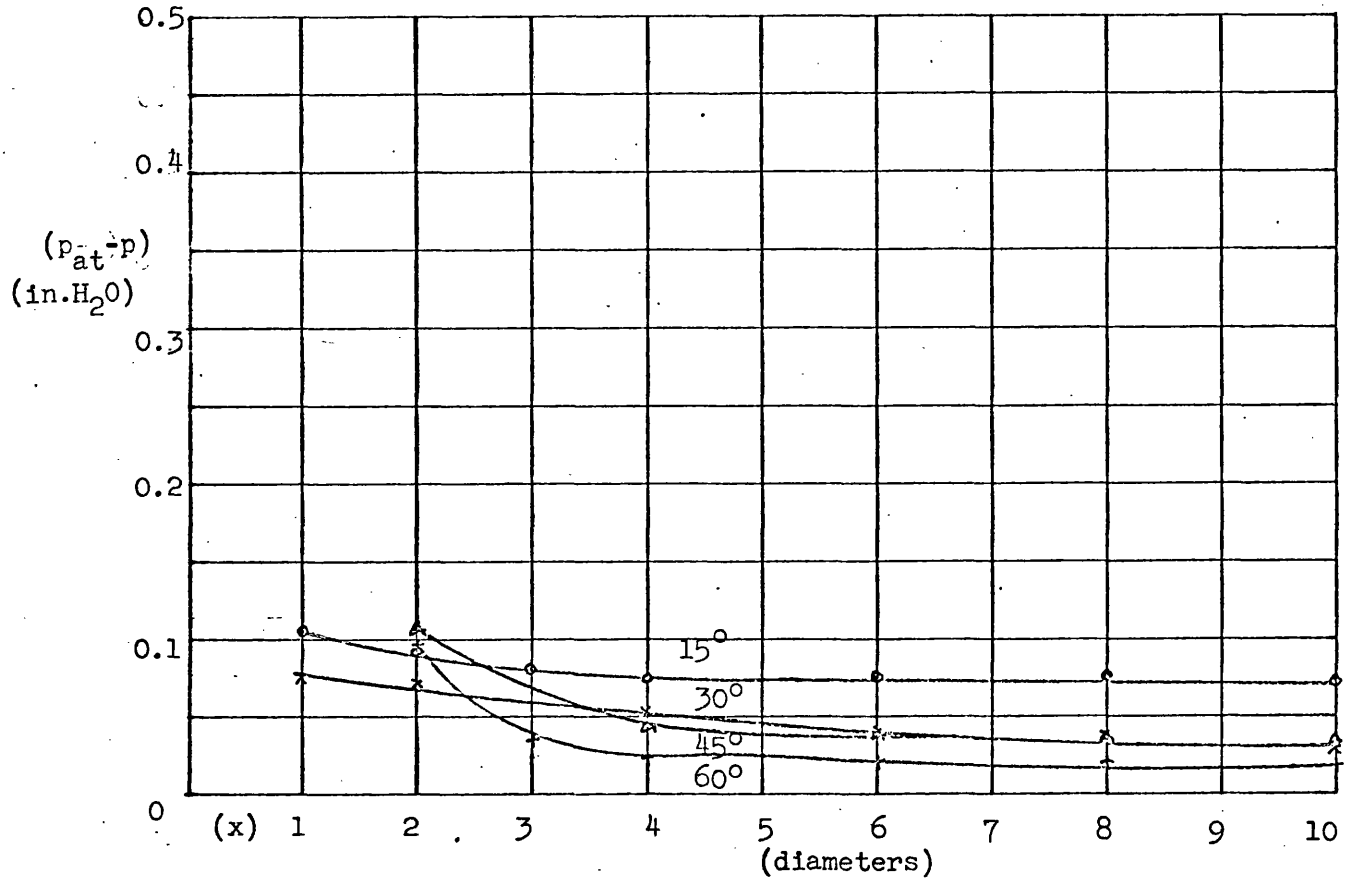

Figure 53. Hubless flames: Variation of static pressure along the jet axis

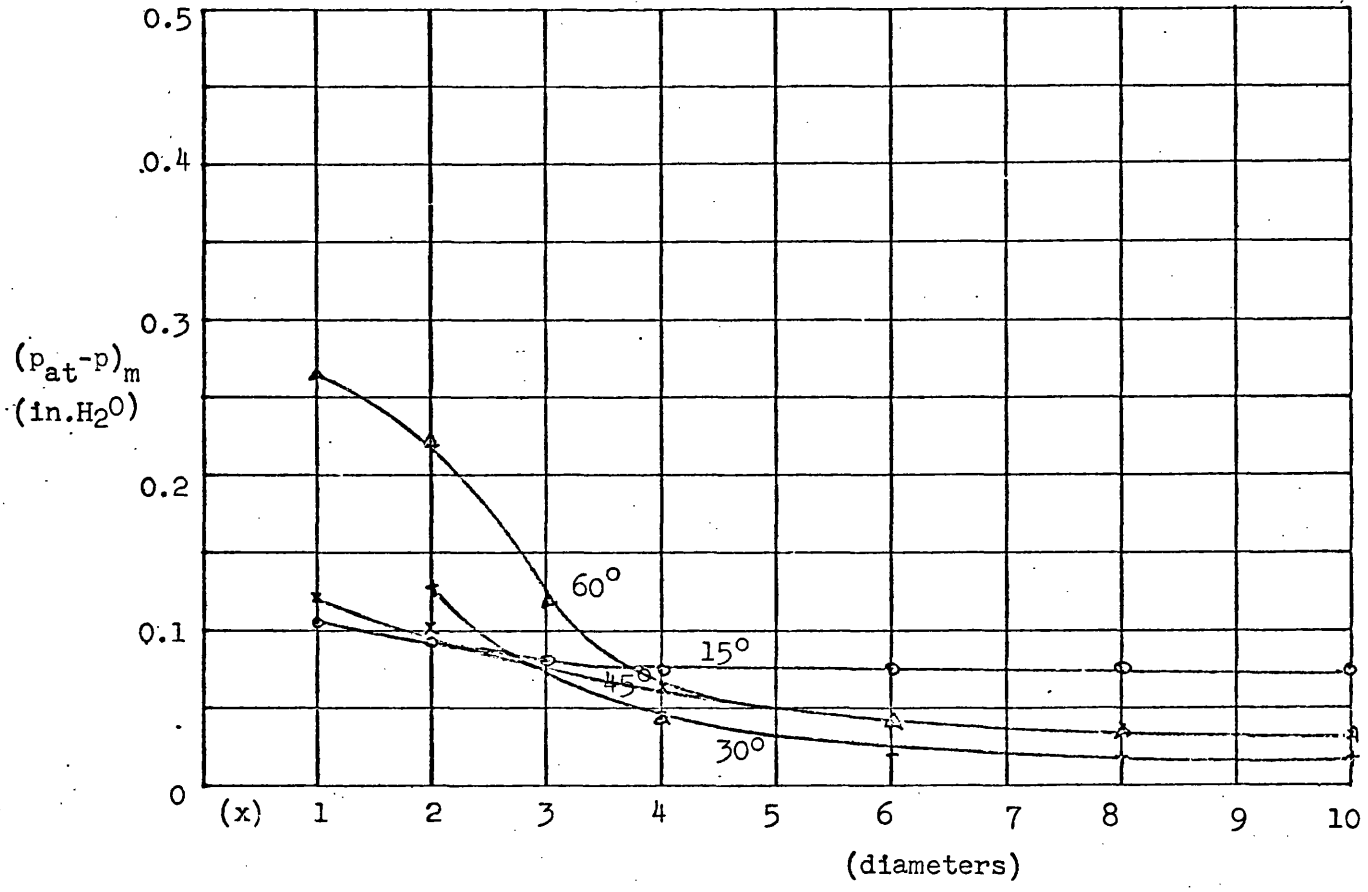

Figure 54. Hubless flames: Variation of minimum static pressure along the jet

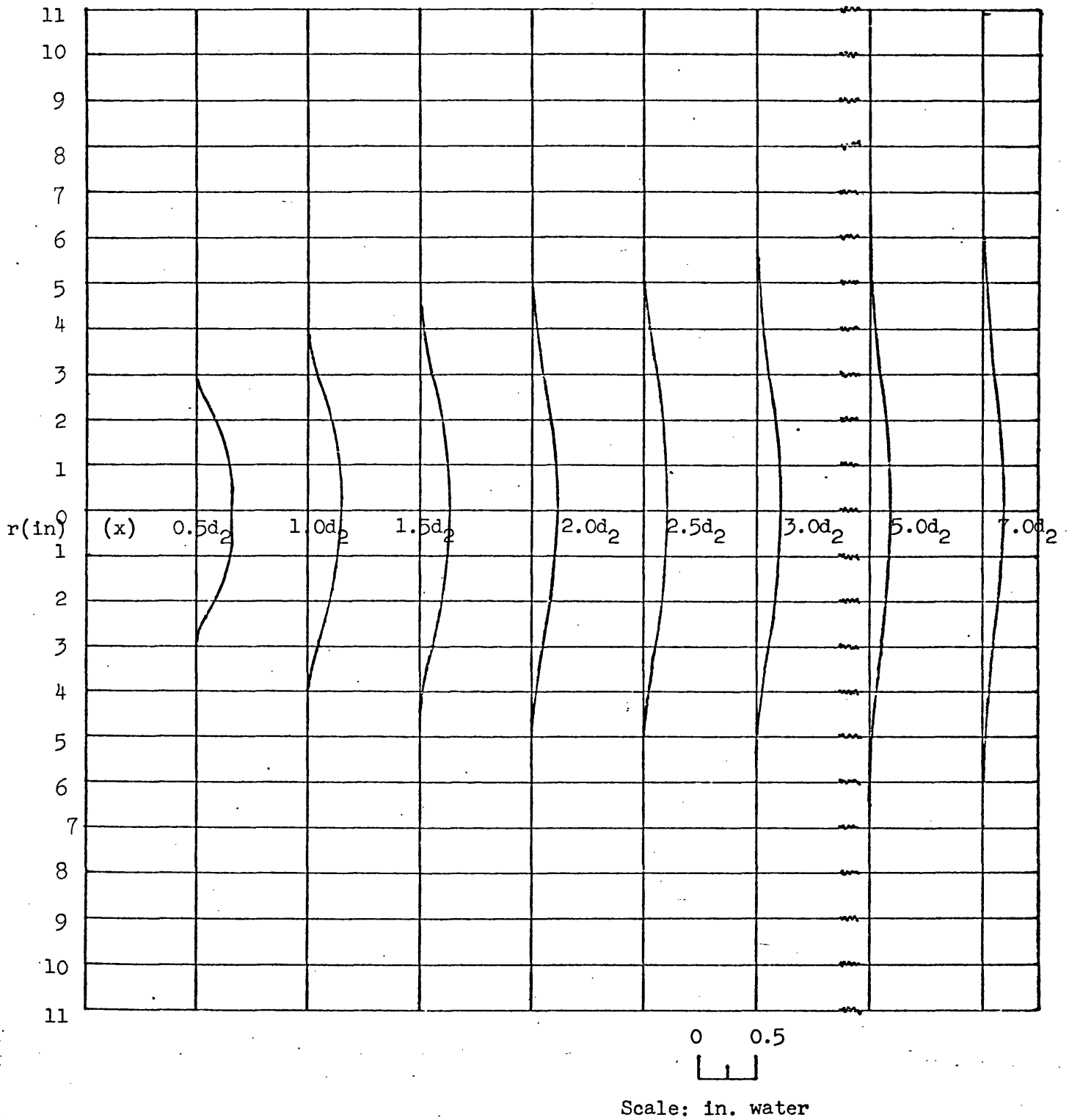

Figure 55. Static pressure (p_{at} - p) profiles for 15° annular swirler flame.

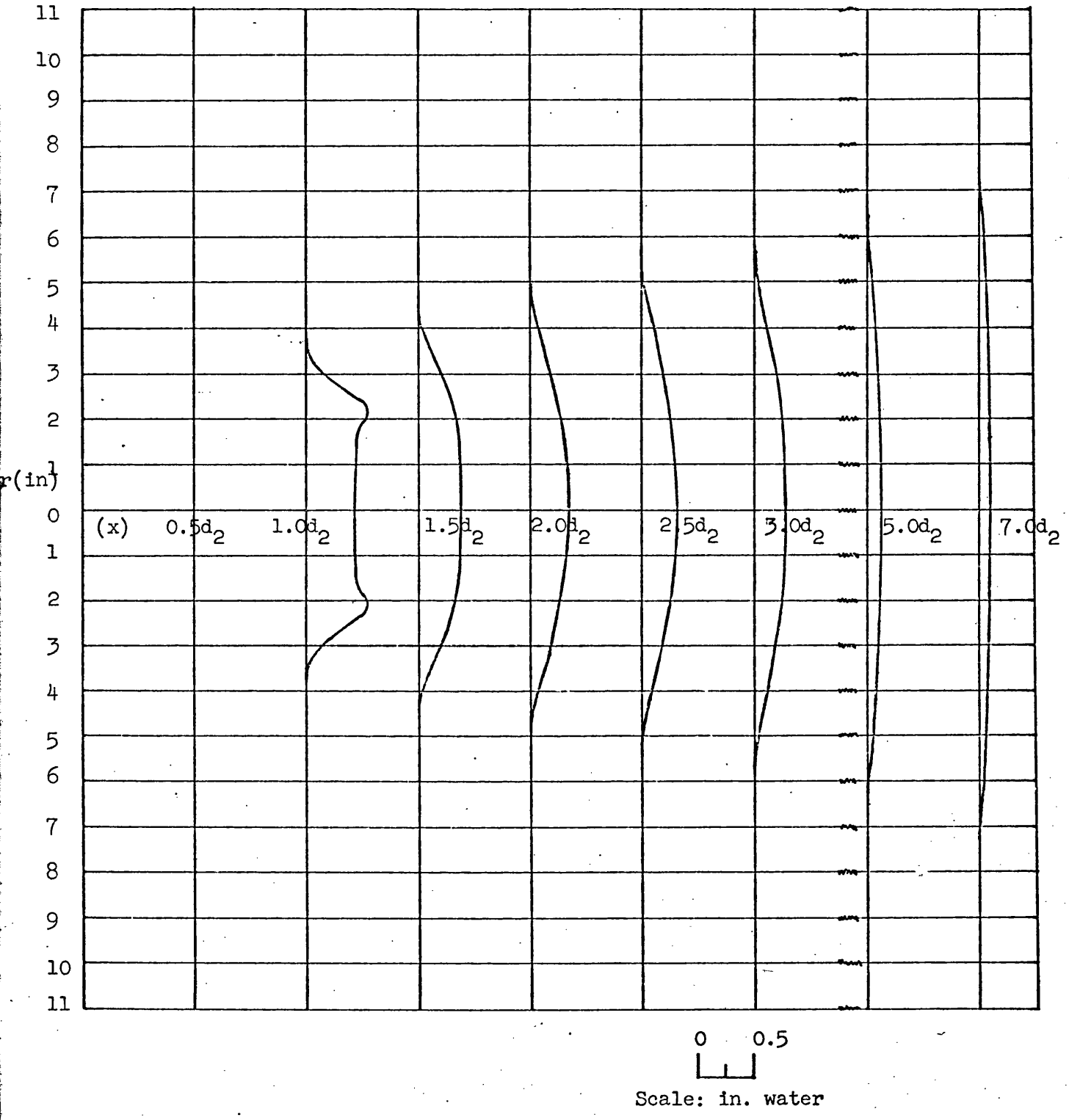

Figure 56 Static pressure (p_{at} - p) profiles for 30° annular swirler flame

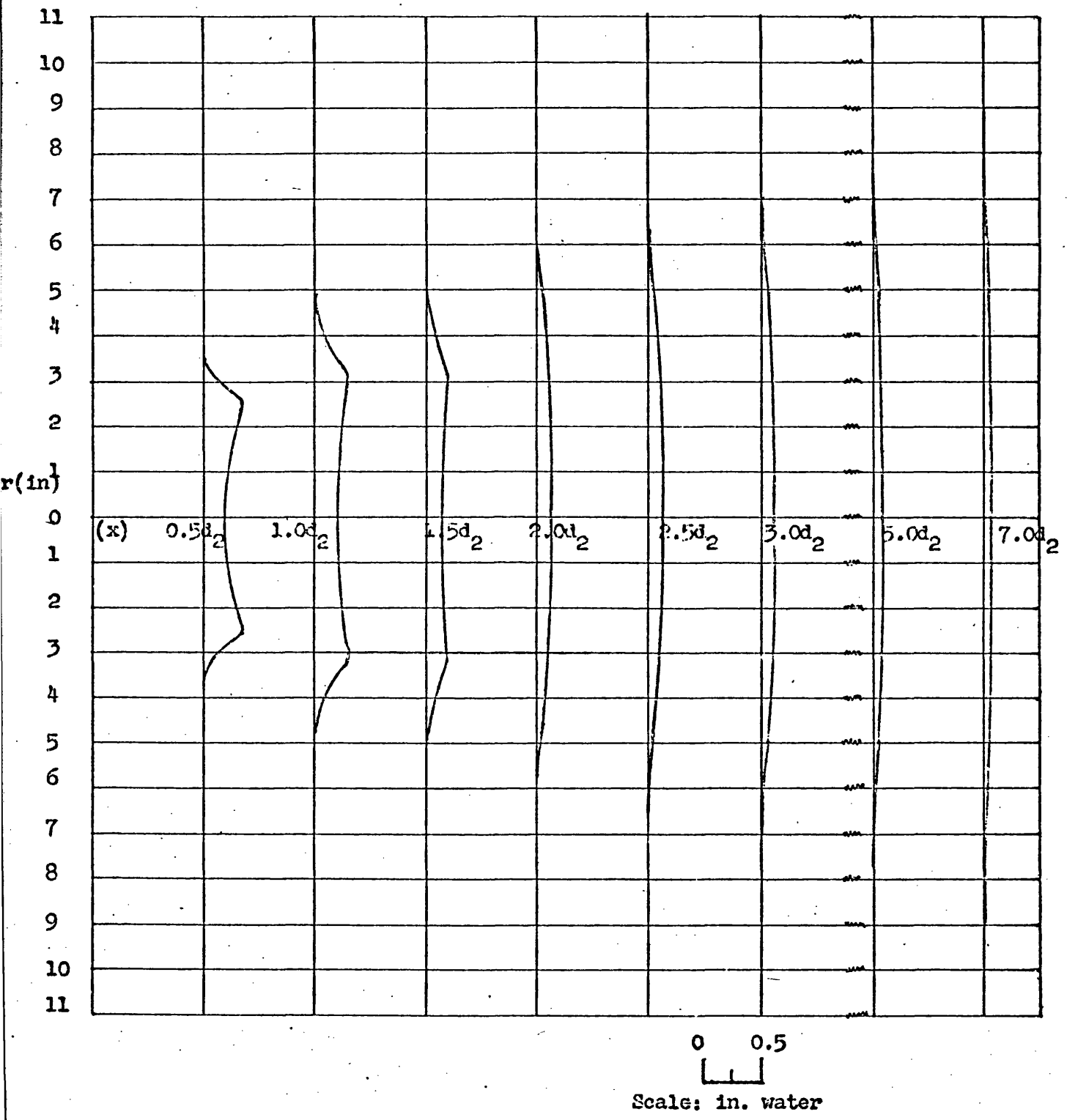

Figure 57. Static pressure (p_{at} - p) profiles for 45° annular swirler flame

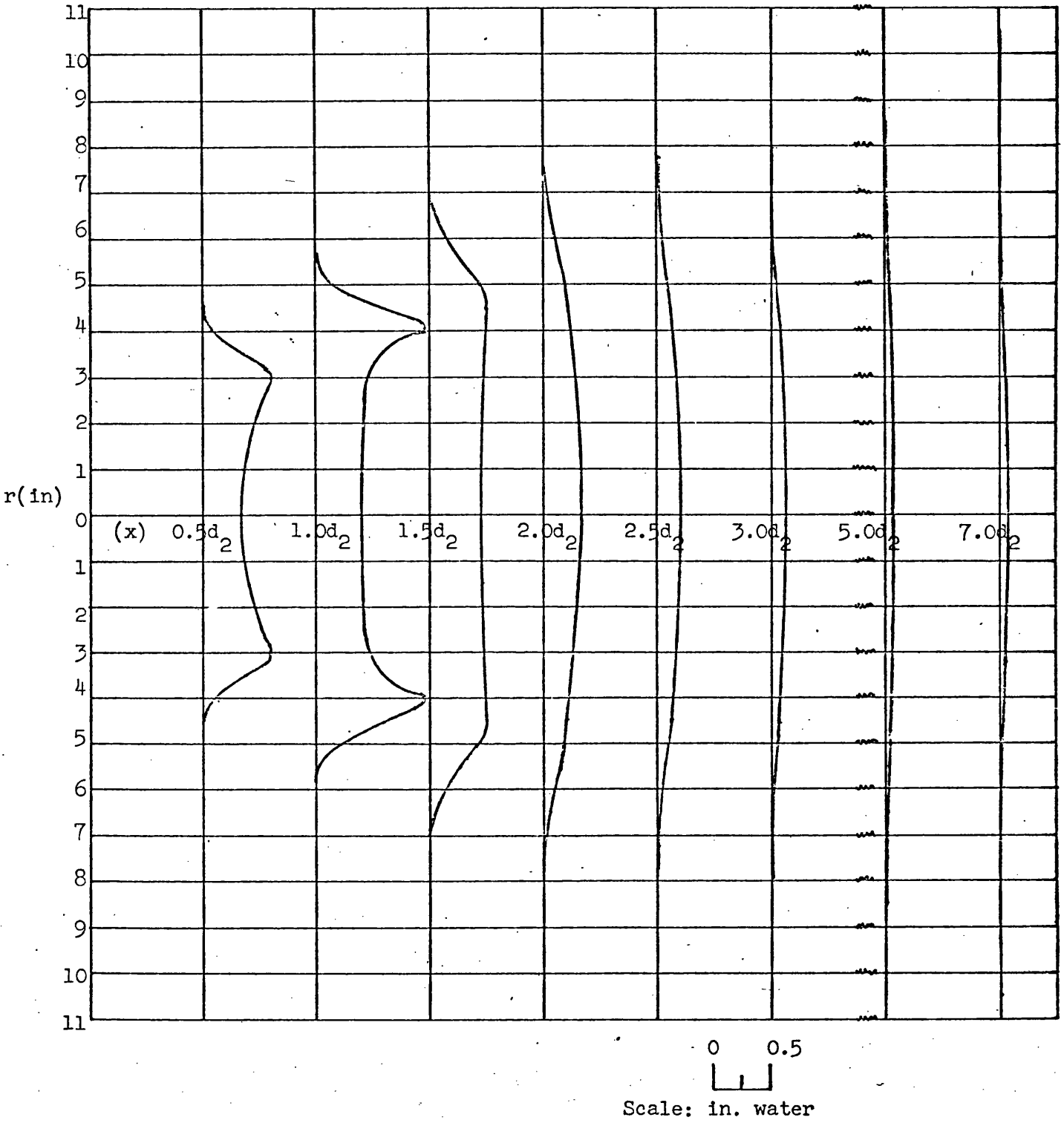

Figure 58 Static pressure (p_{at} - p) profiles for 60° annular swirler flame

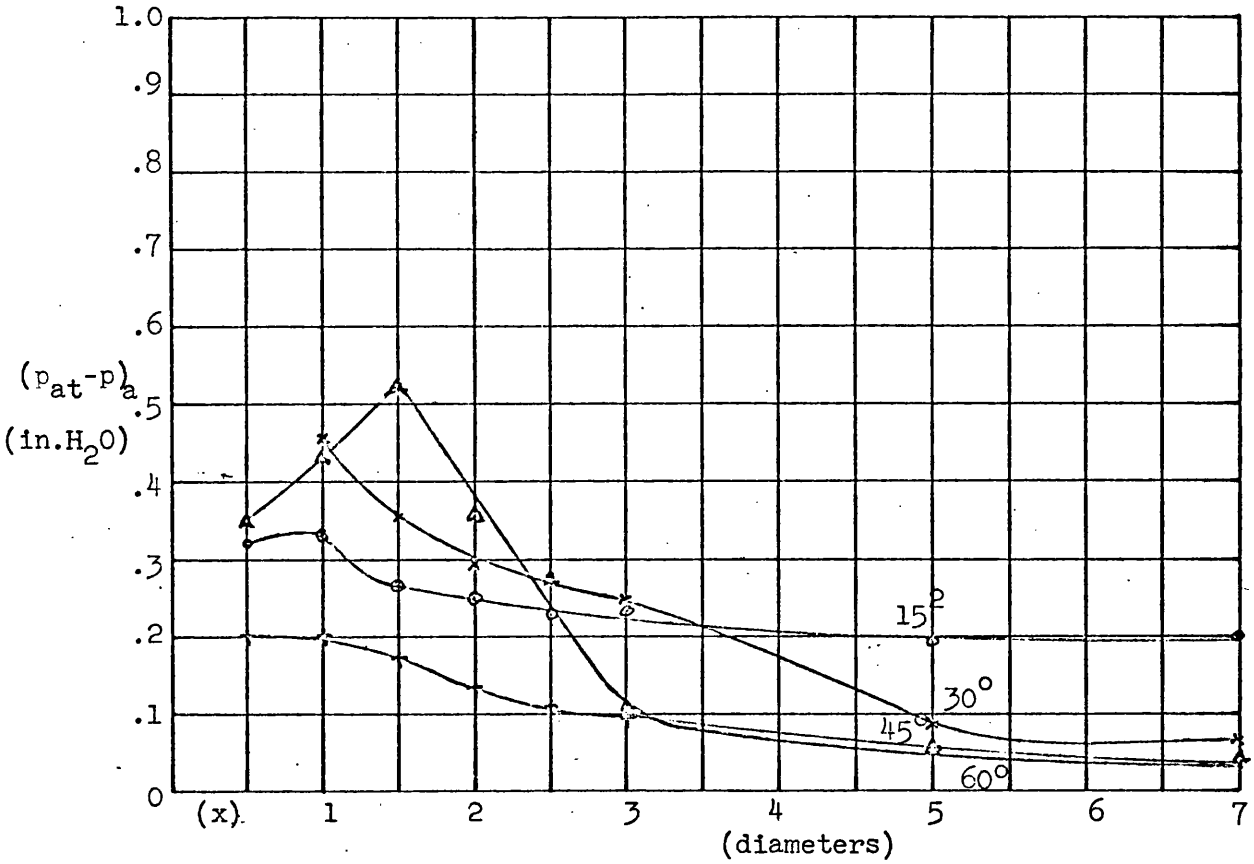

Figure 59 Annular flames: Variation of static pressure along jet axis.

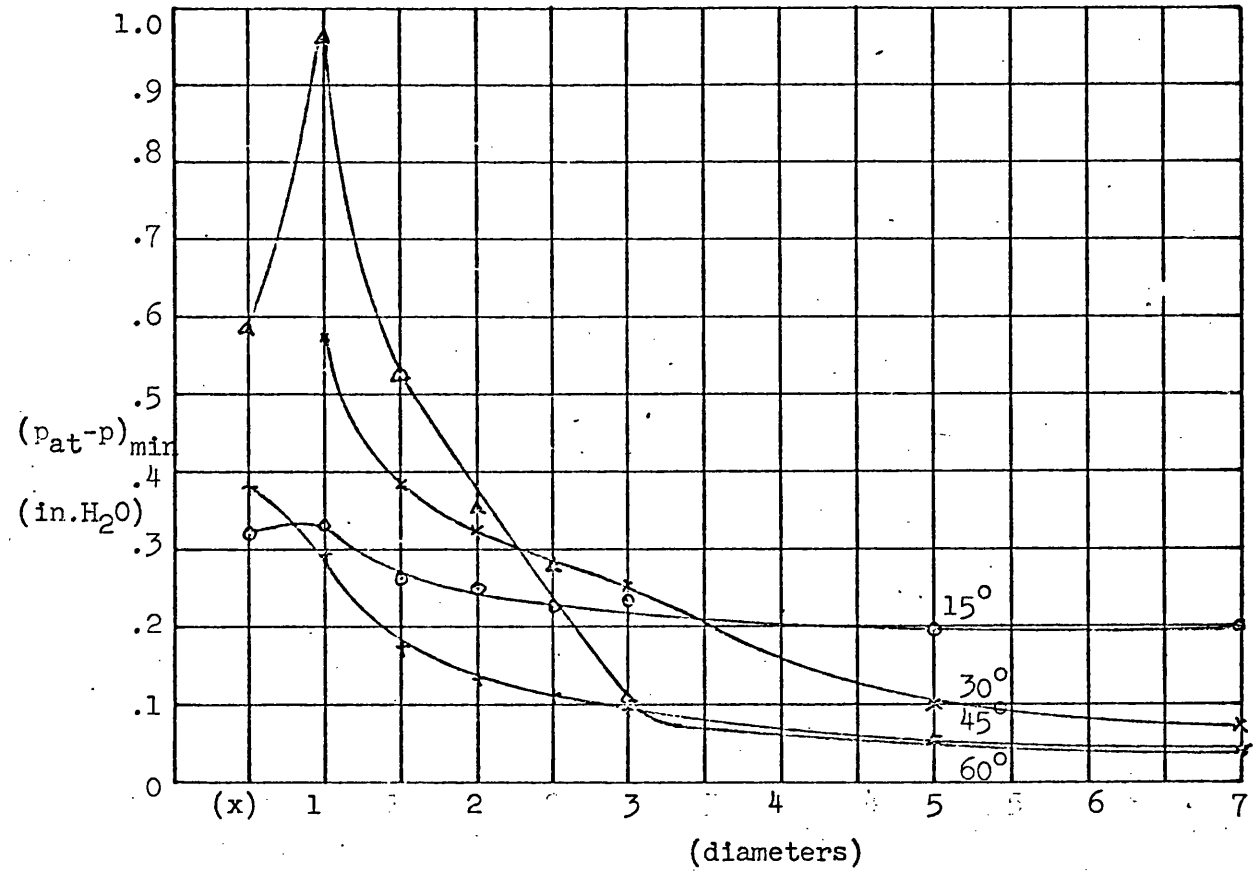

Figure 60: Annular flames: Variation of minimum static pressure along the jet

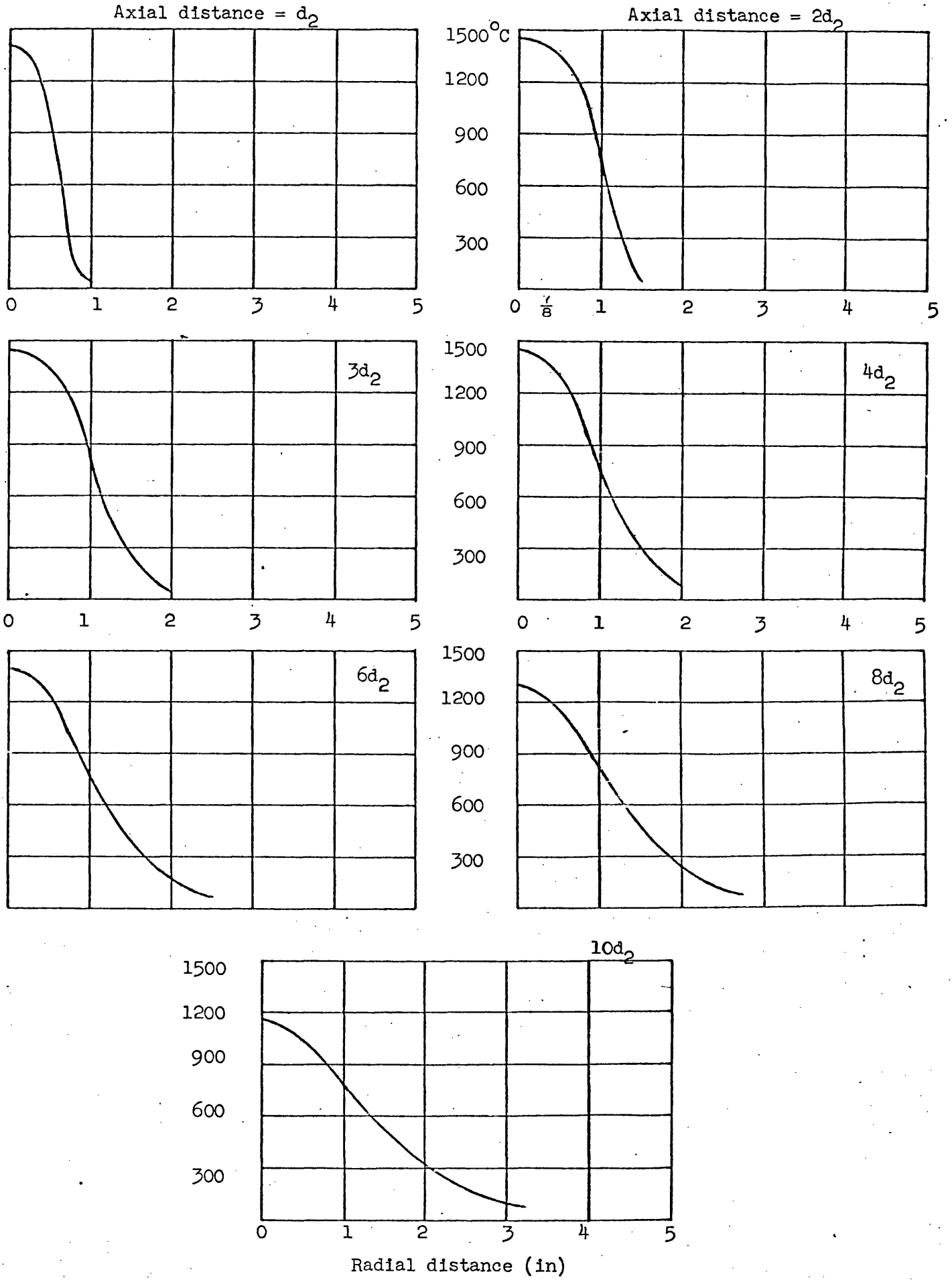

Figure 61. Temperature distribution for 15° hubless swirler flame

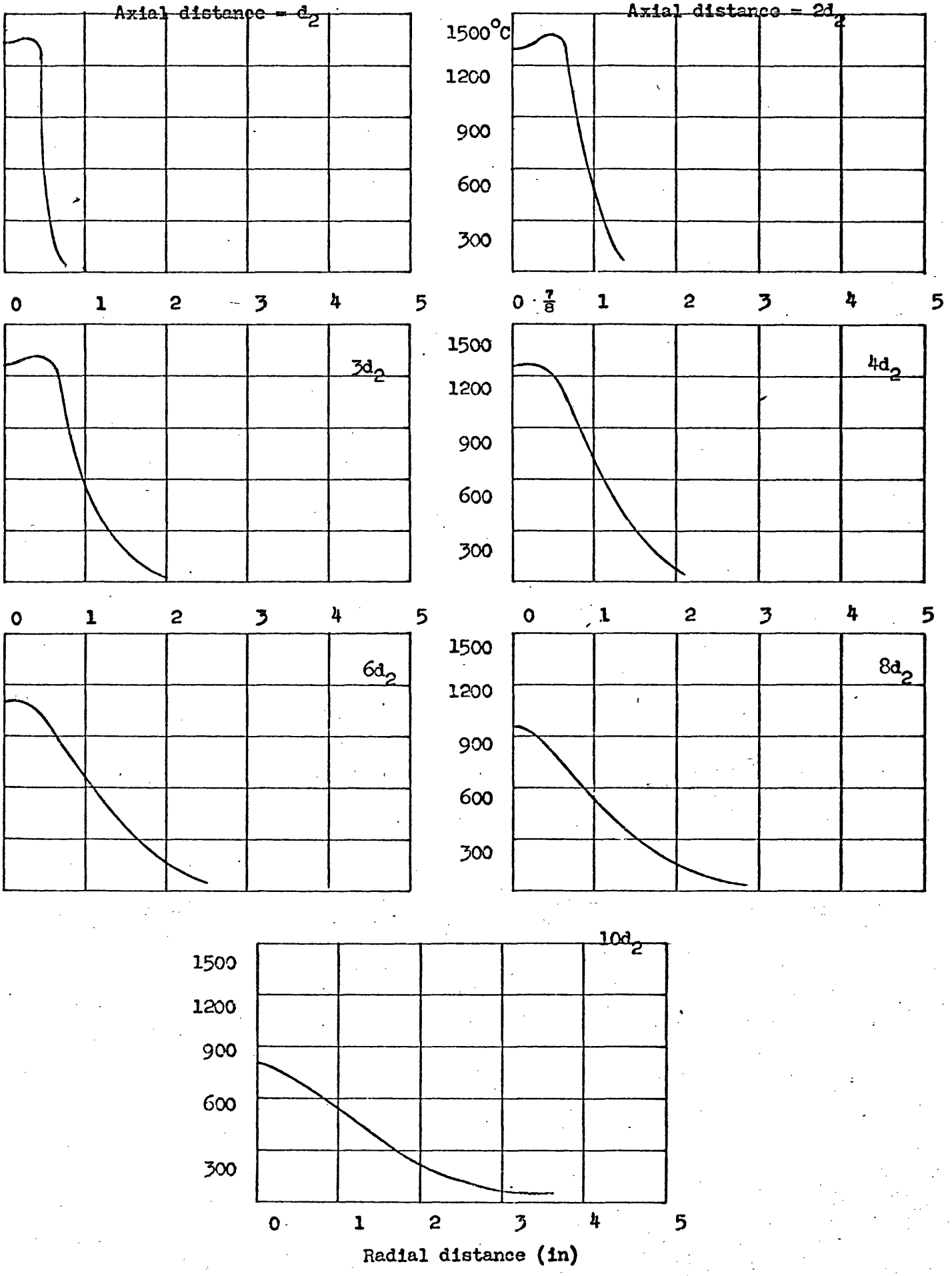

Figure 62. Temperature distribution for 30° hubless swirler flame

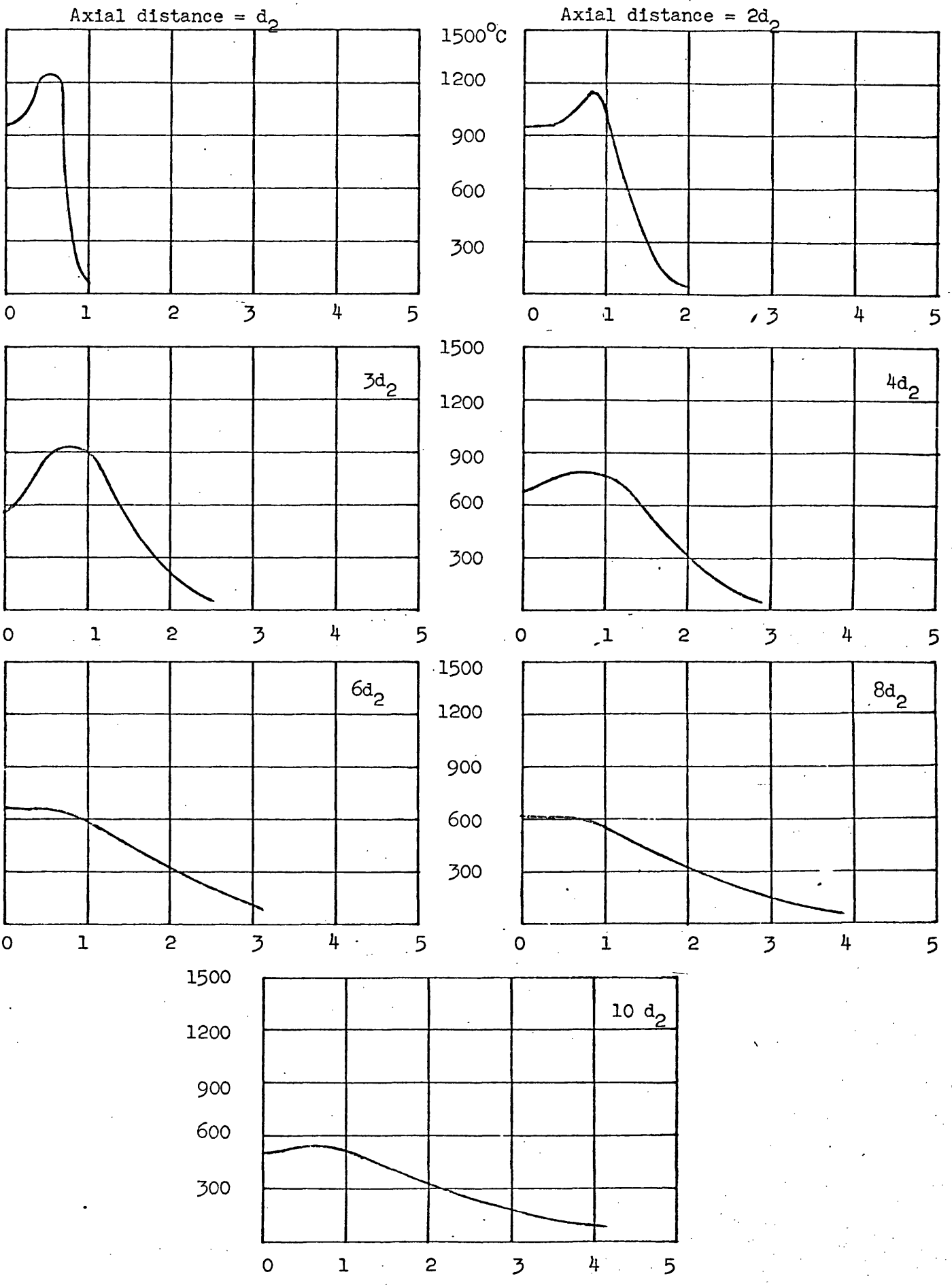

Figure 63 Temperature distribution for 45° hubless swirler flame

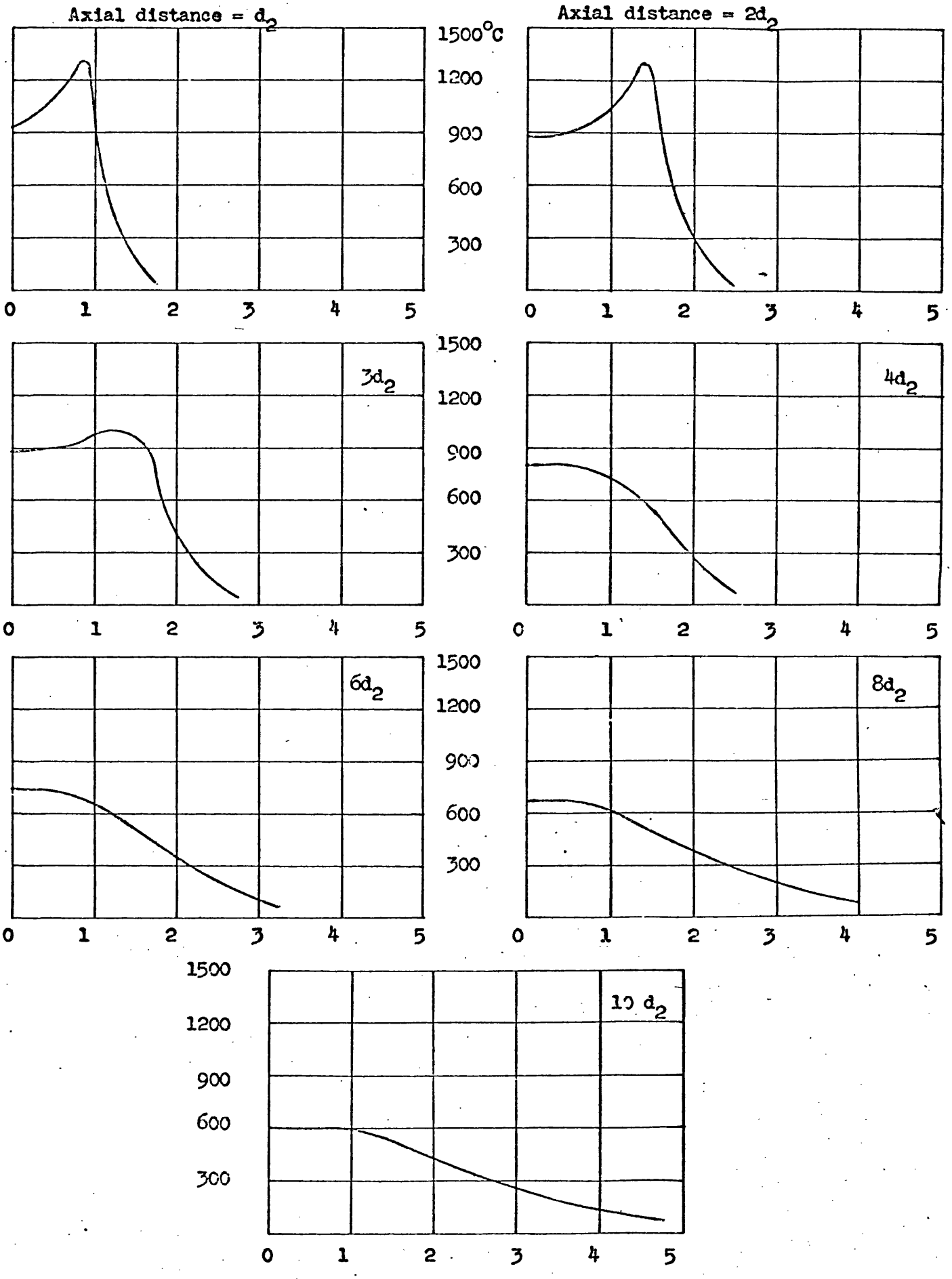

Figure 64 Temperature distribution for 60° hubless swirler flame

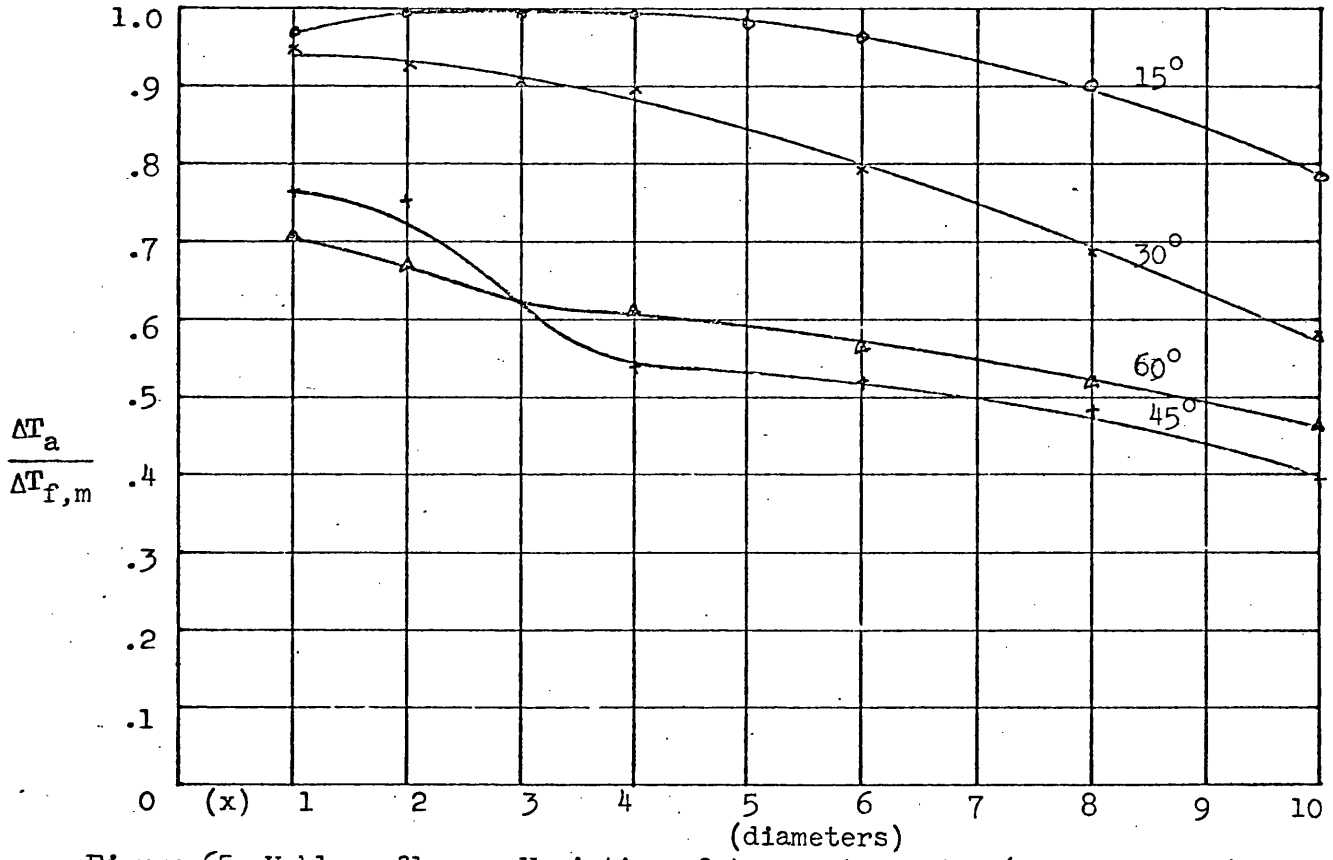

Figure 65. Hubless flames: Variation of temperature rise (above ambient) along the jet axis

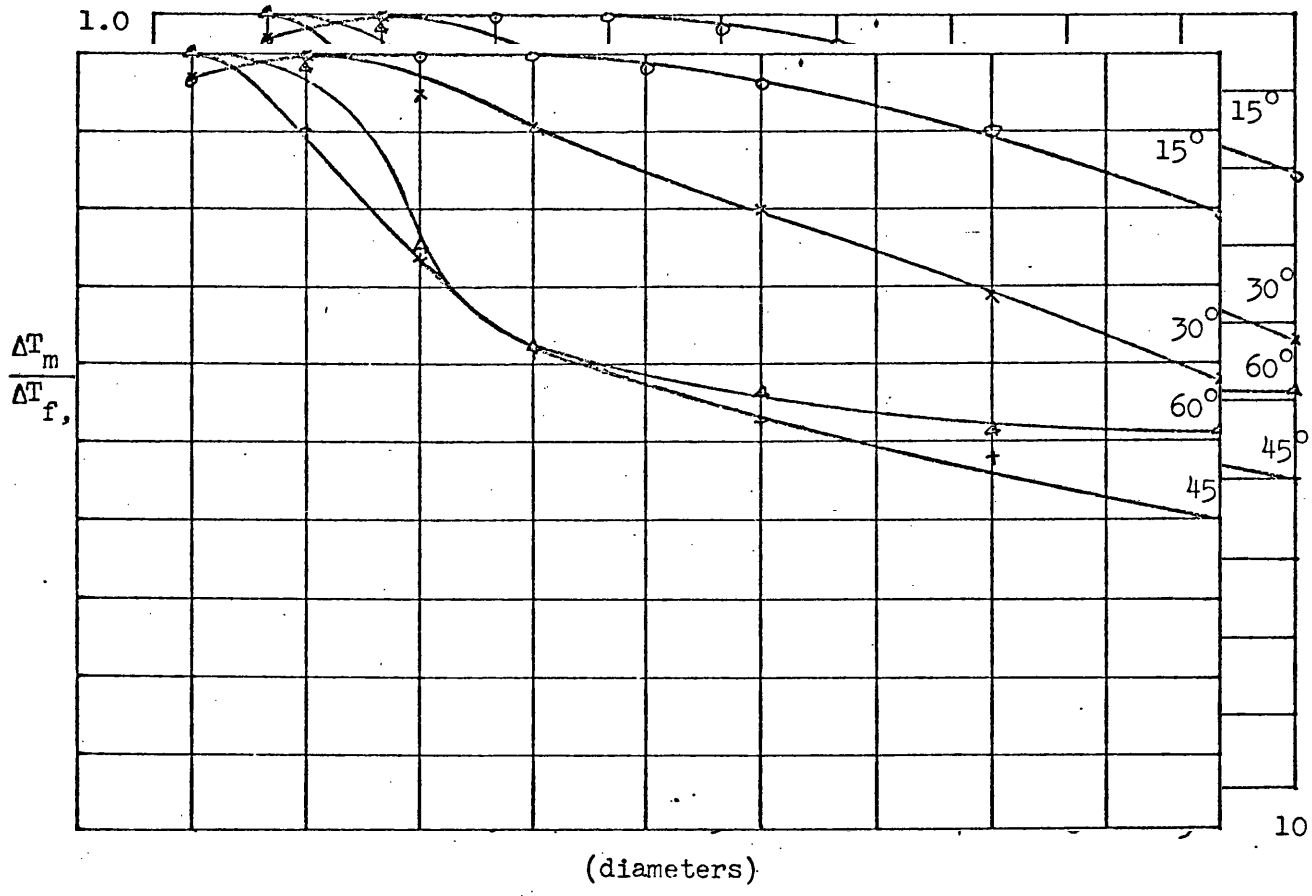

Figure 66. Hubless flame: Variation of maximum temperature rise (above ambient) along the jet

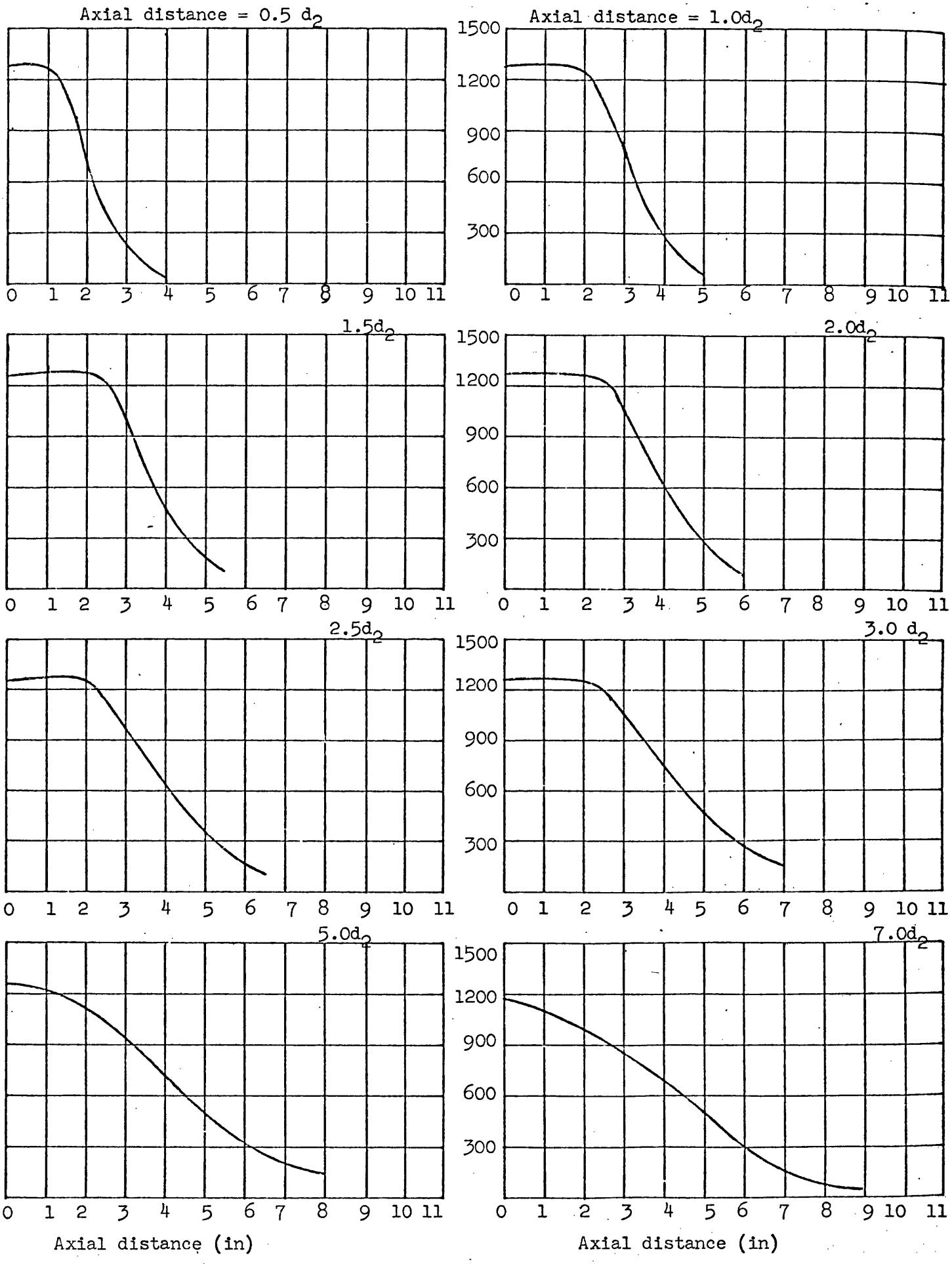

Figure 67 Temperature (°C) distribution for 15° annular swirler flame

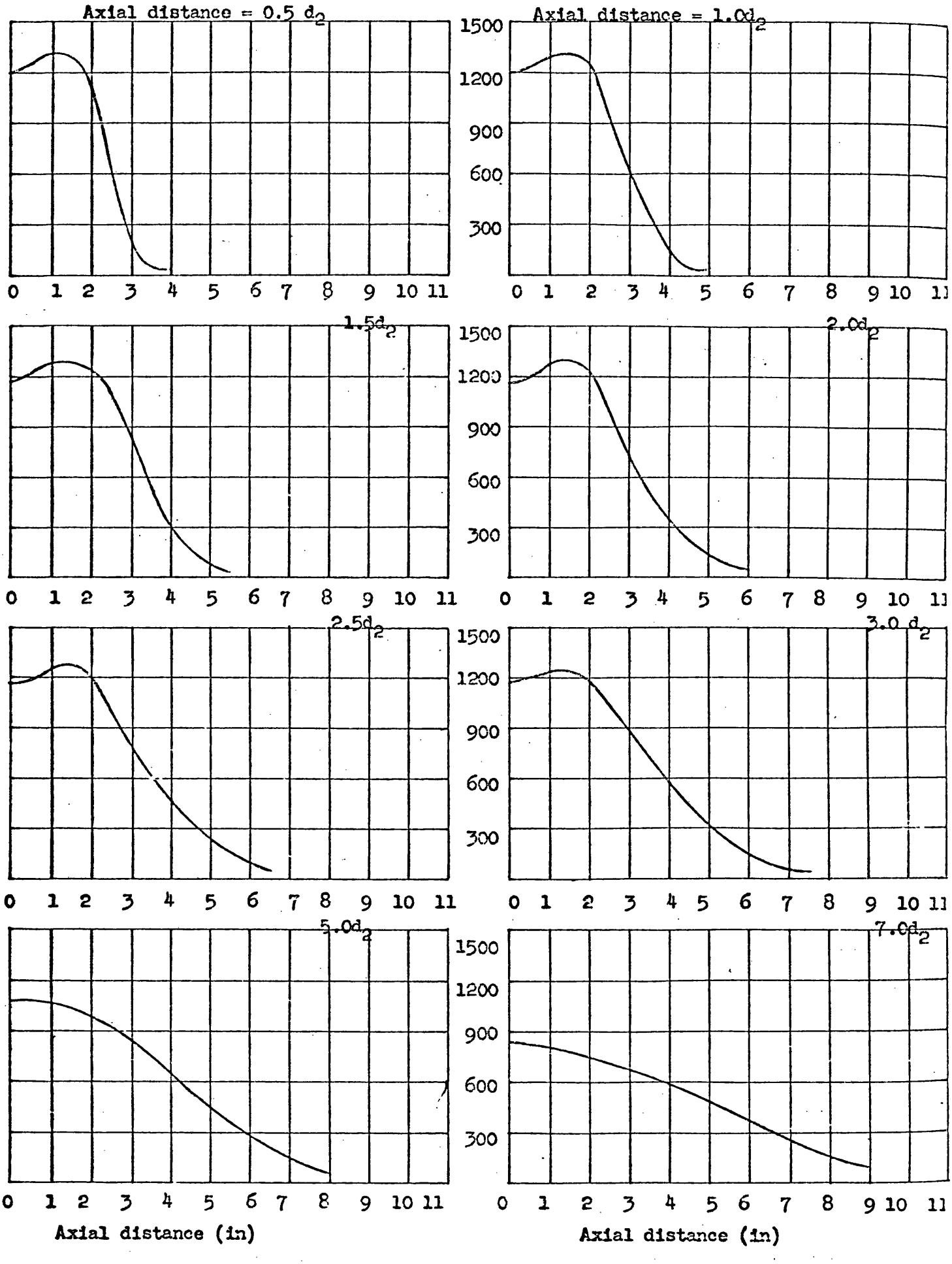
Axial distance = 0.5 d_2
Axial distance = 1.0d_2
1.5d_2
2.0d_2
2.5d_2
3.0 d_2
5.0d_2
7.0d_2
1500
1200
900
600
300
0 1 2 3 4 5 6 7 8 9 10 11
Axial distance (in)

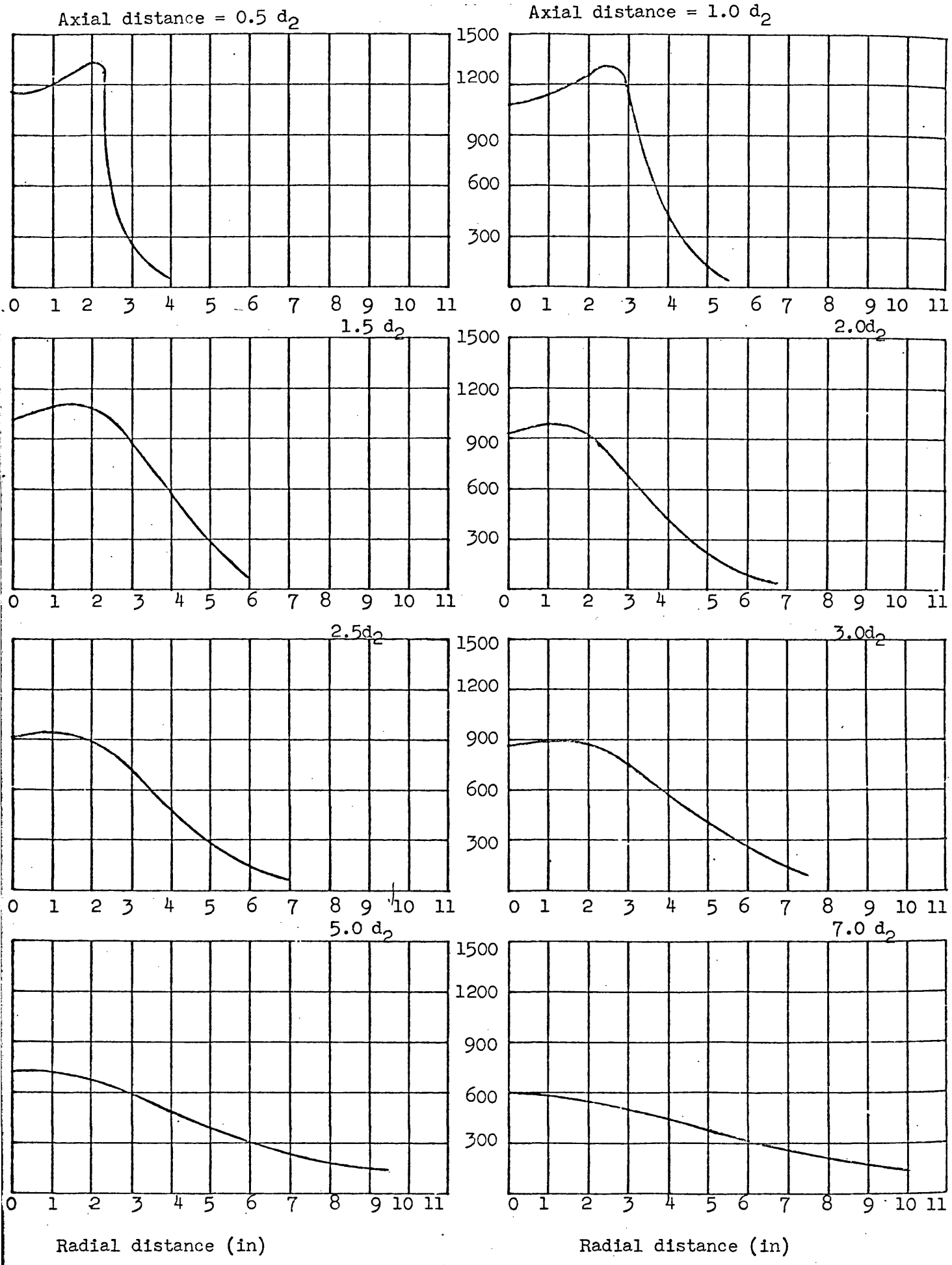

Figure 69 Temperature (^{o}C) distribution for 45^{o} annular swirler flame

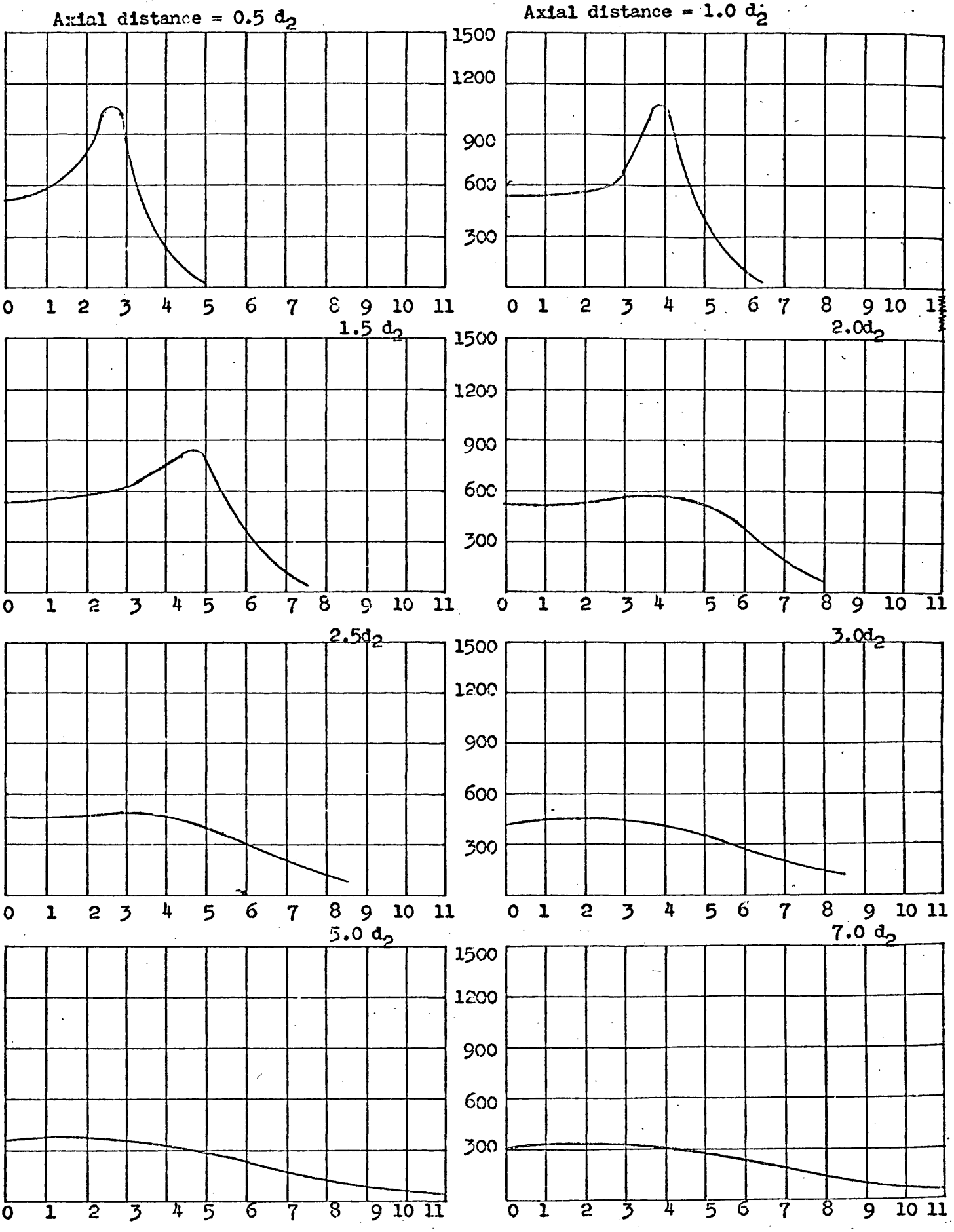

Figure 70 Temperature (^{o}C) distribution for 60^{o} annular swirler flame

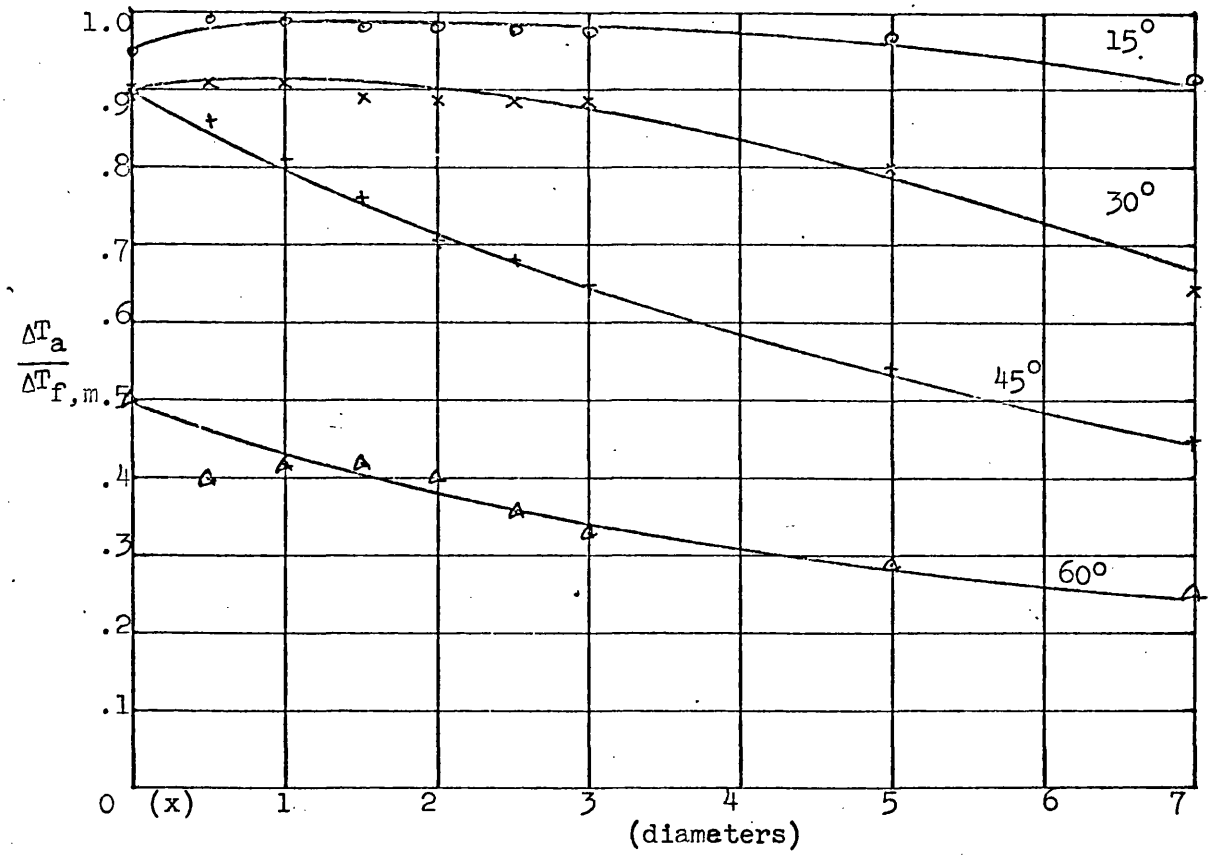

Figure 71. Annular flames: Variation of temperature rise (above ambient) along the jet axis.

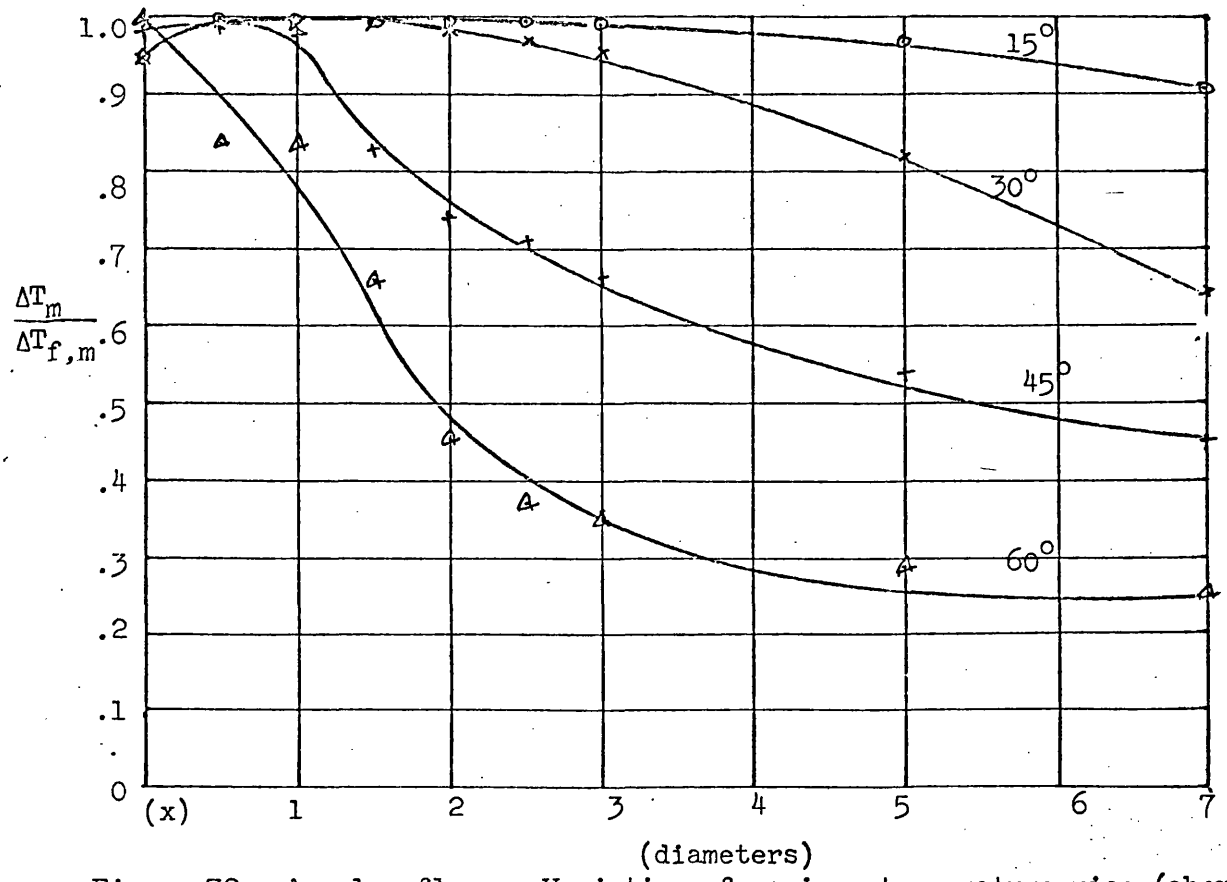

Figure 72. Annular flames: Variation of maximum temperature rise (above ambient) along the jet

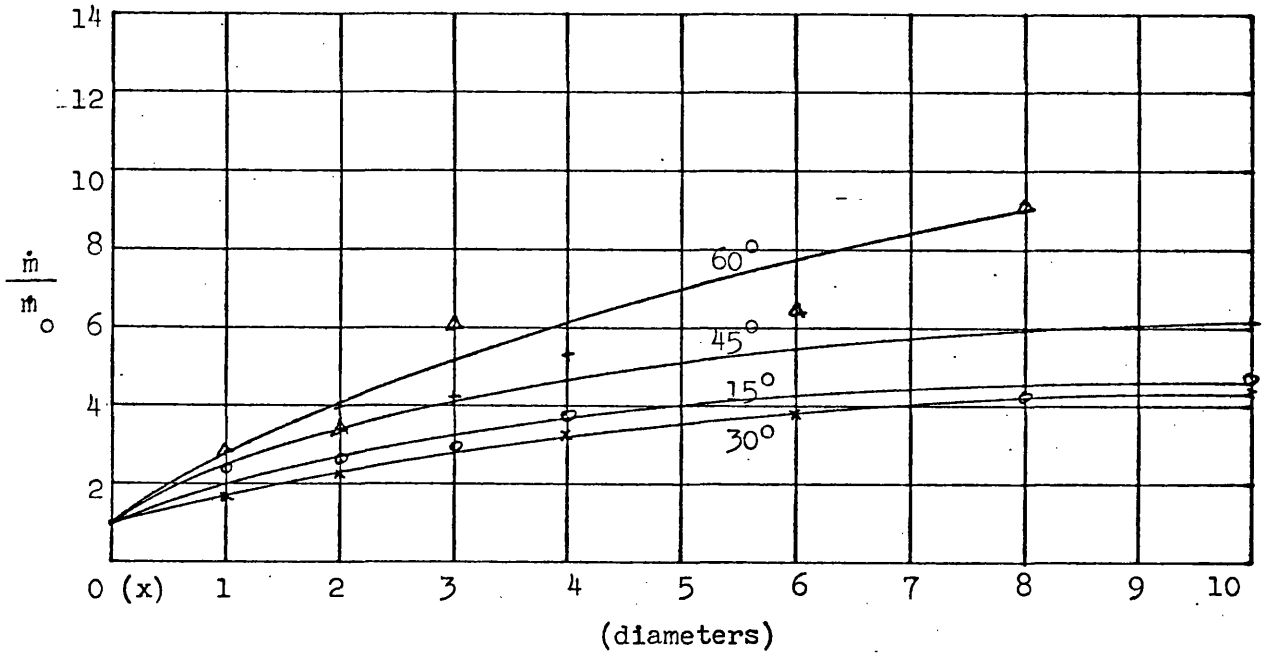

Figure 73 Hubless flames: Variation of mass flow rates along the jet.

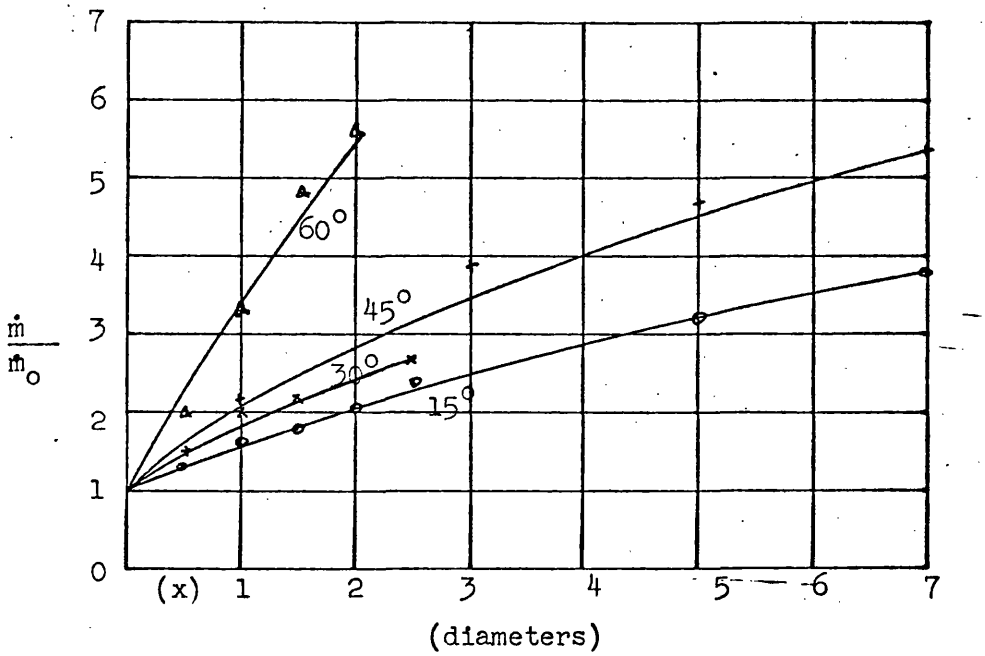

Figure 74 Annular flames: Variation of mass flow rates along the jet

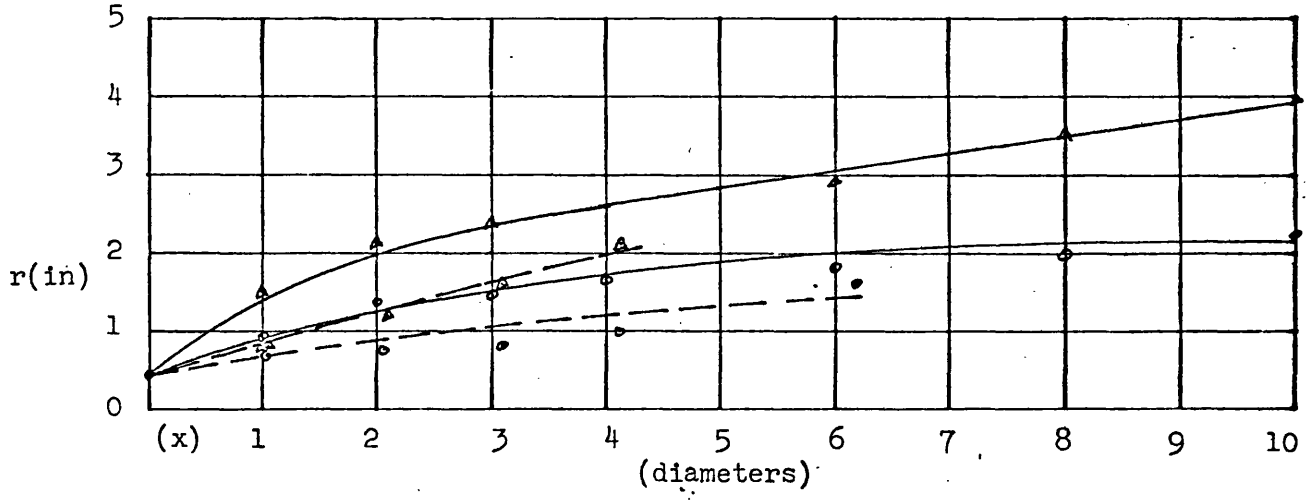

Figure 75(a) Comparison of cold and burning hubless swirling jets widths

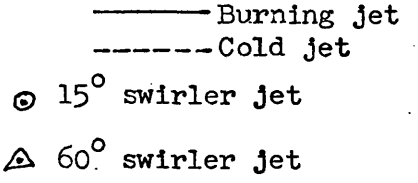

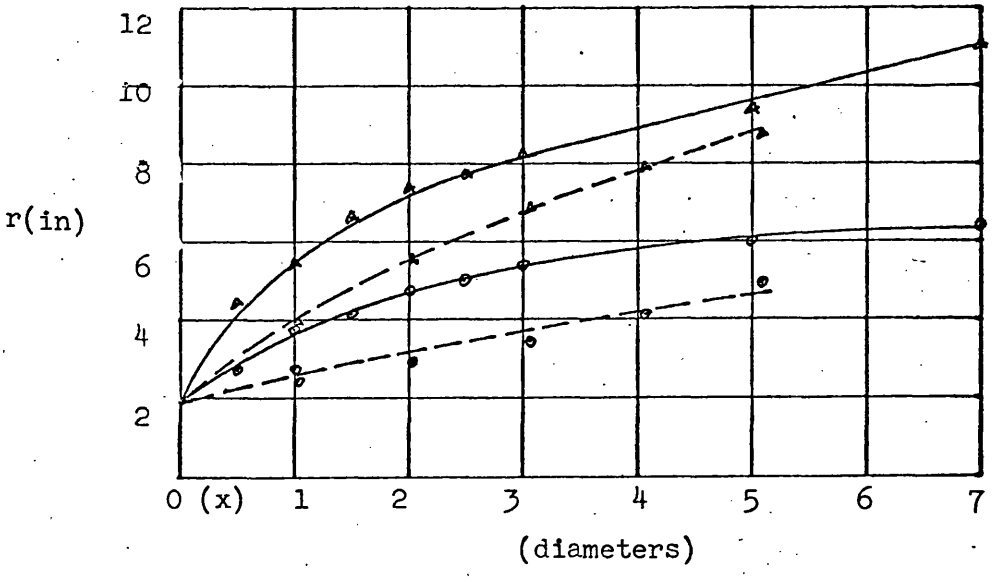

Figure 75(b) Comparison of cold and burning annular swirling jets widths.

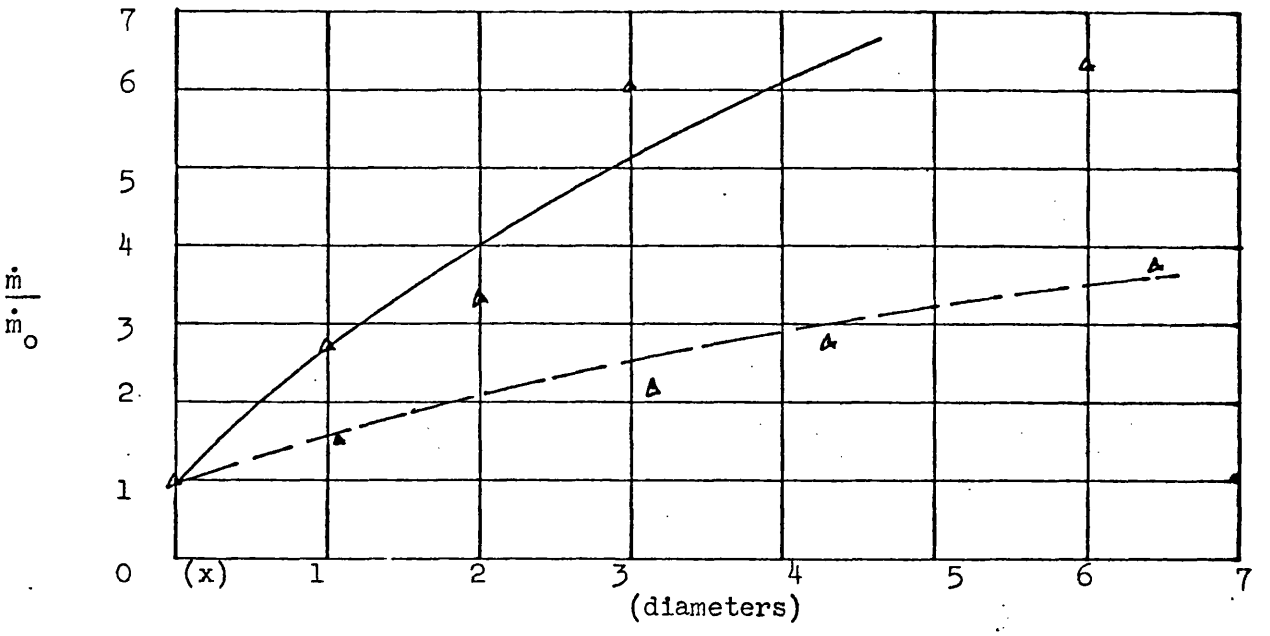

Figure 76(a) 60° hubless swirler: Comparison of the mass flow rates along cold and burning jets

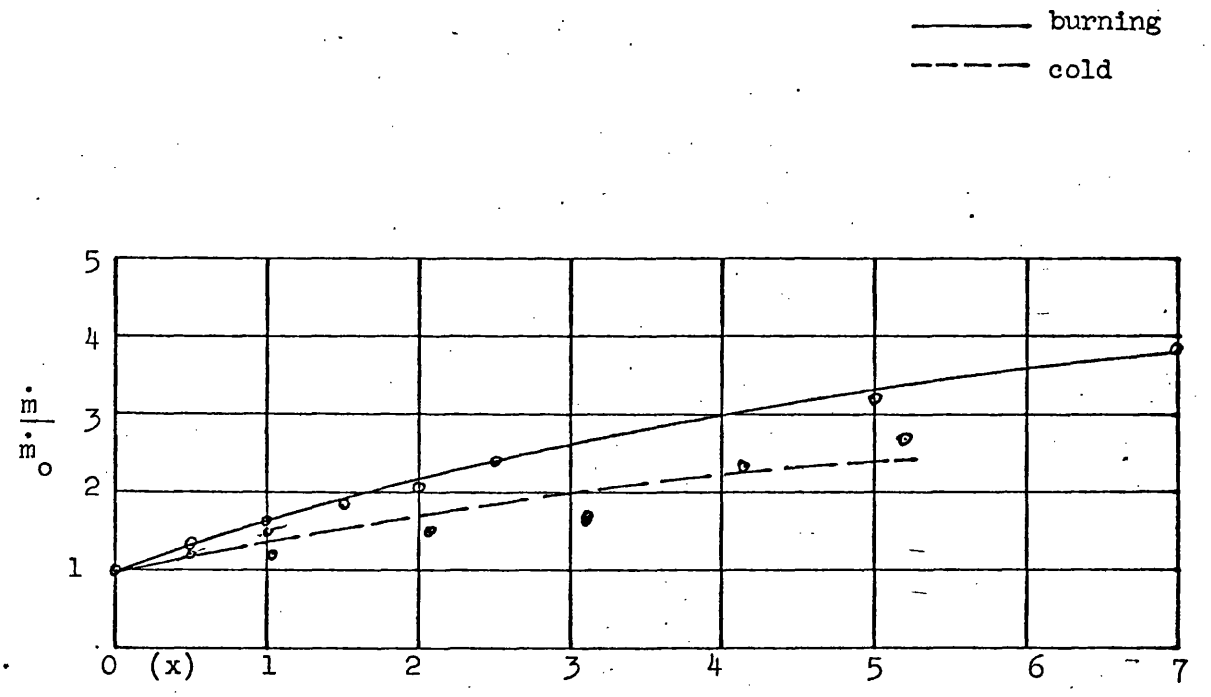

Figure 76(b) 15° annular swirler: Comparison of the mass flow rates along cold and burning jets

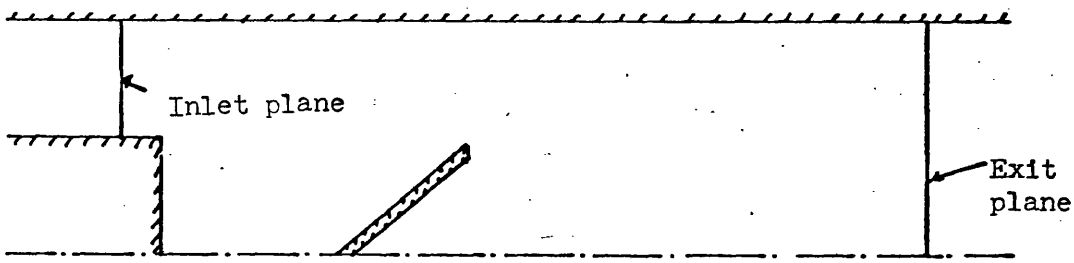

Figure 77. Geometries used in (9)

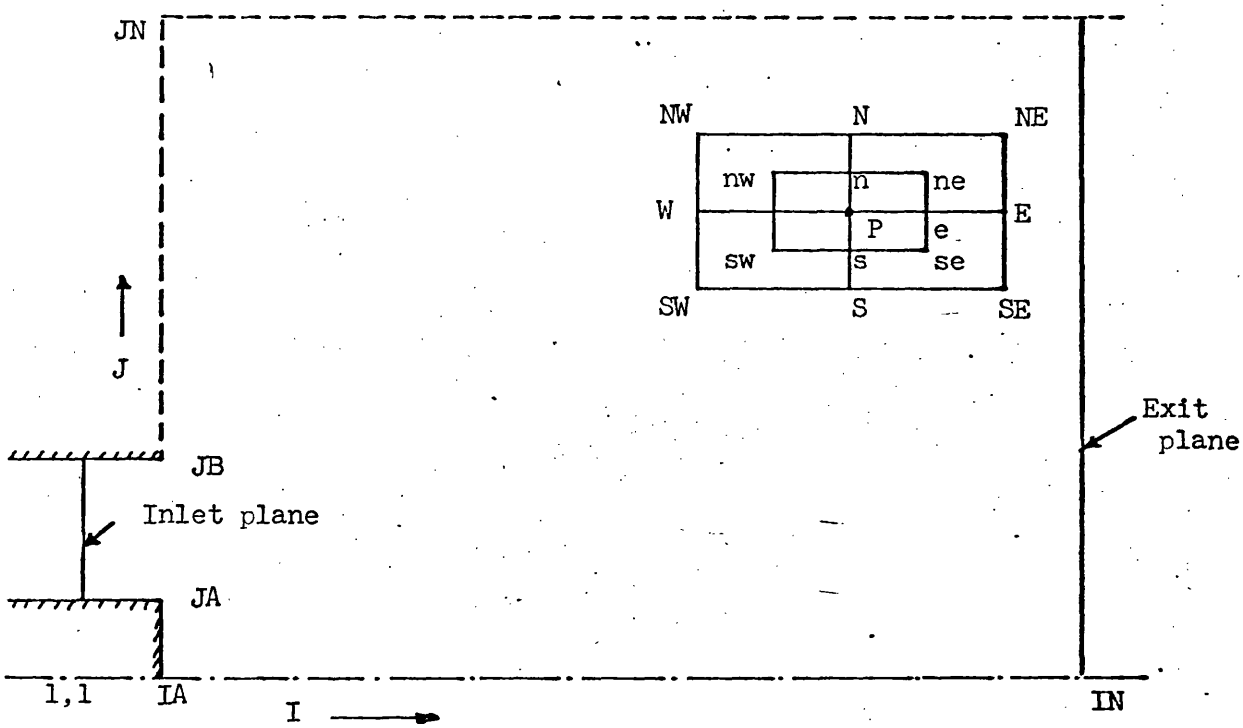

Figure 78. Geometry of the enclosure (for annular flow) with typical control volume of a grid point P.

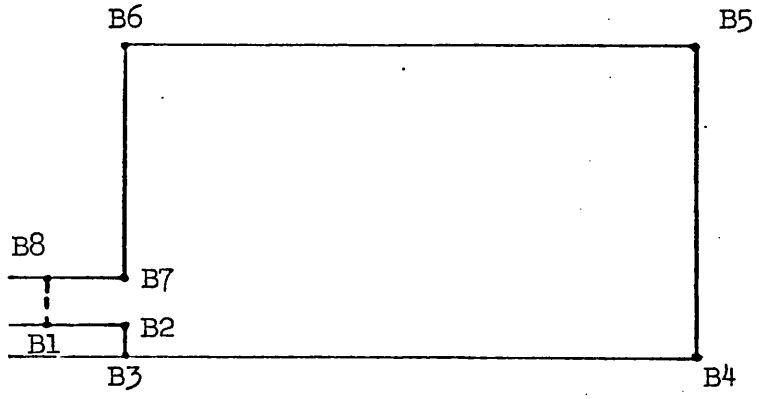

Figure 79. Details of symbols used in Section 7.3

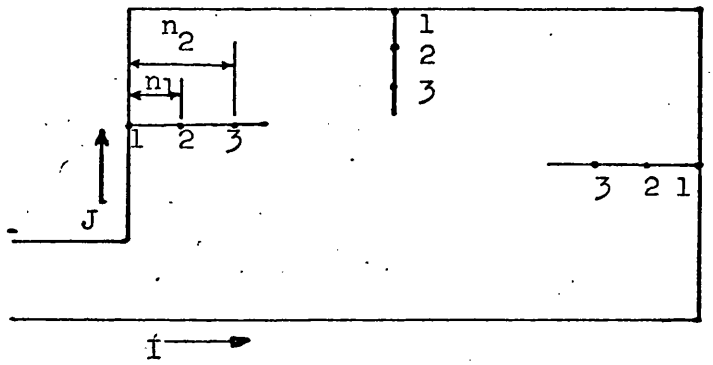

Figure 80. Details of terms in equation (7.10)

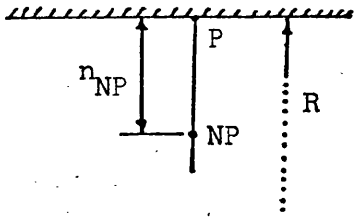

Figure 81. Details of terms in Table 12.

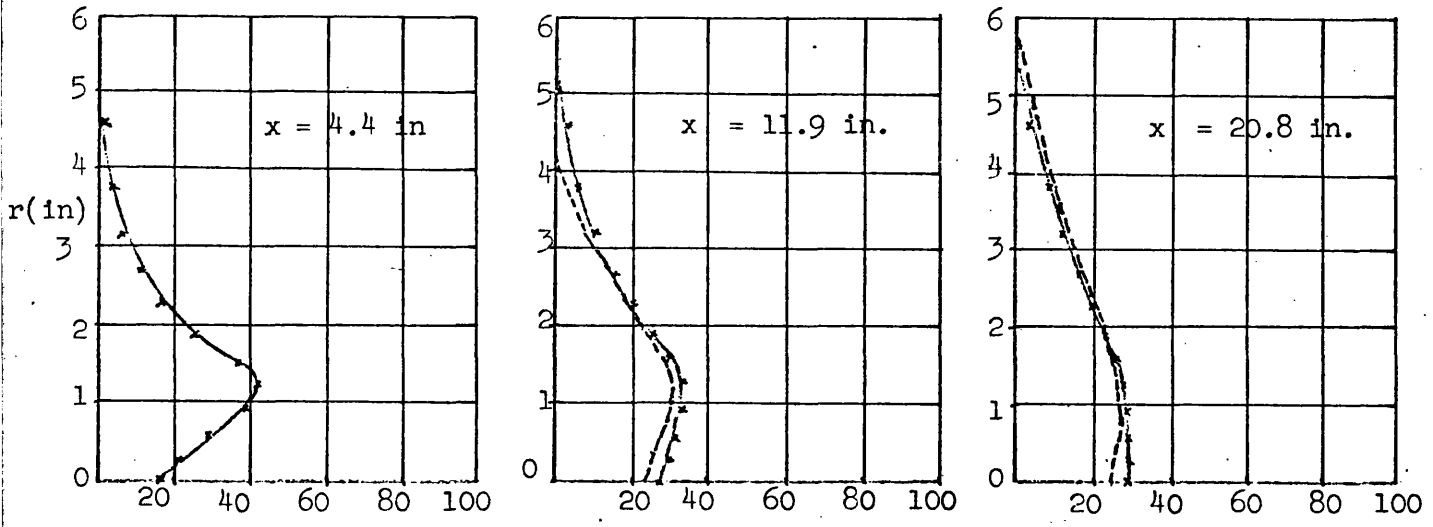

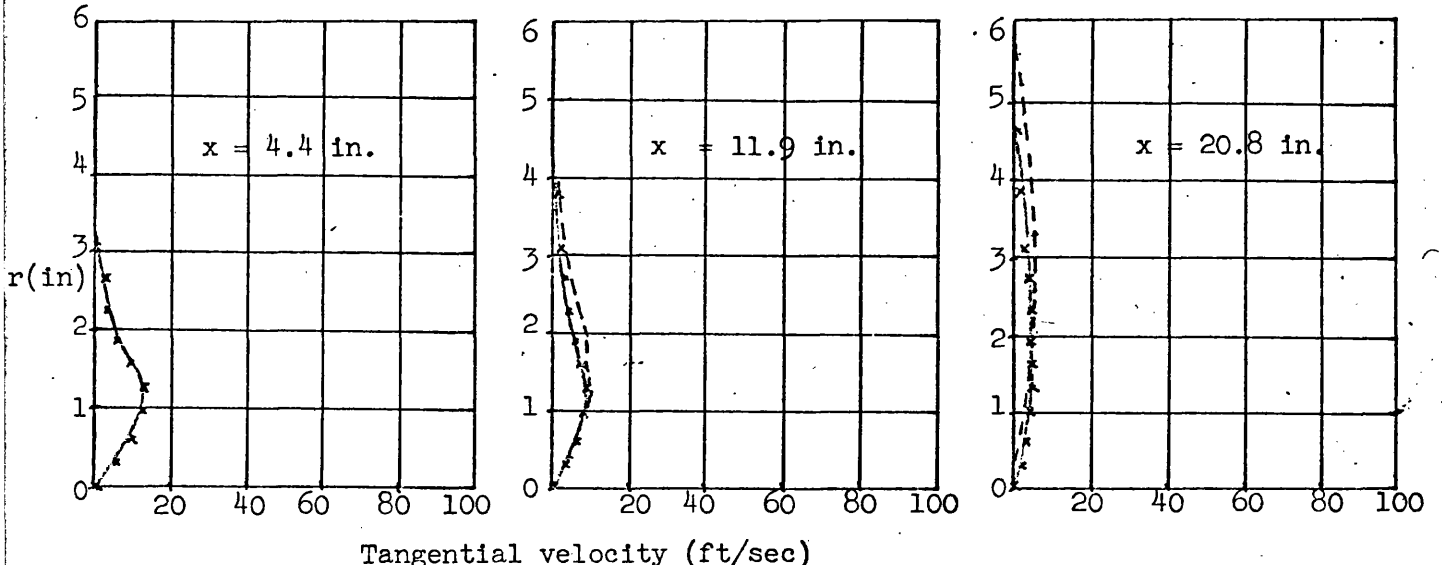

Figure 82 Computed results for annular swirling cold jet with 15° swirler

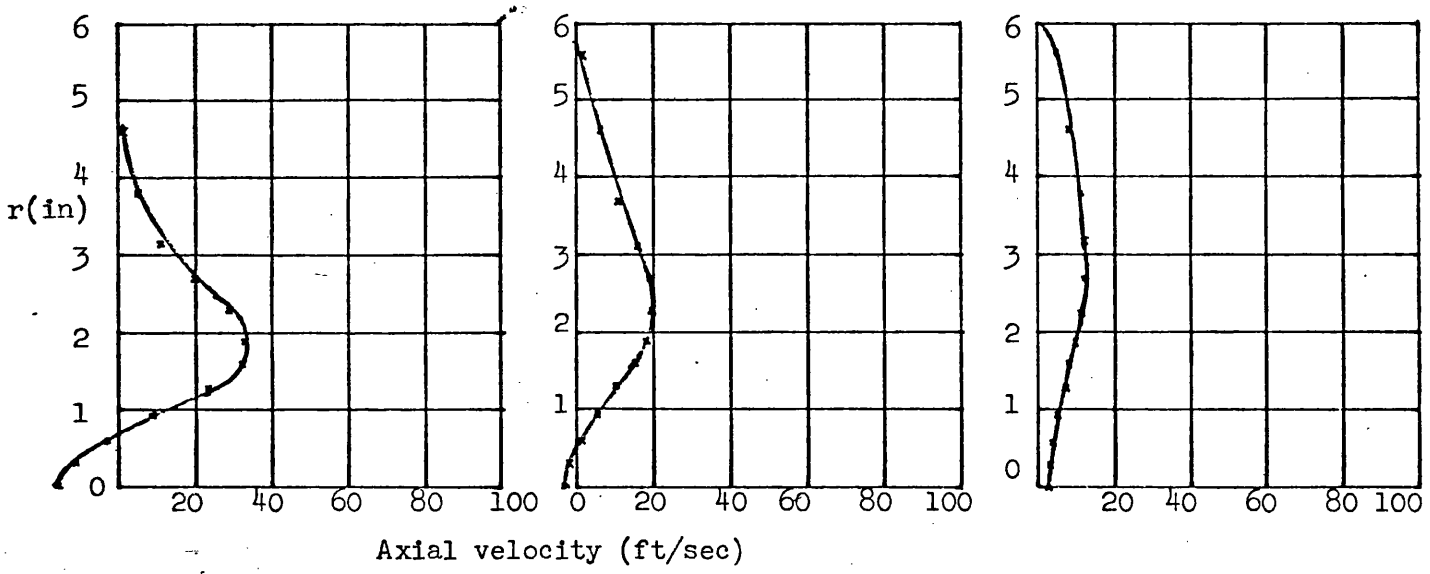

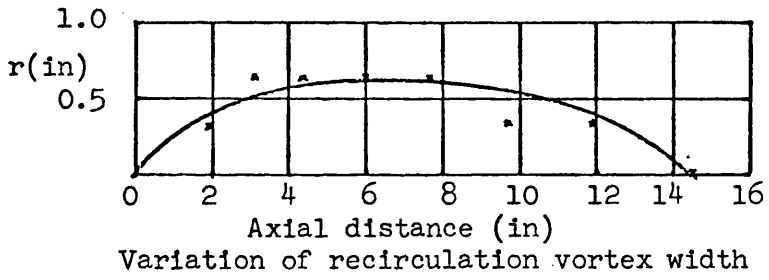

Variation of recirculation vortex width

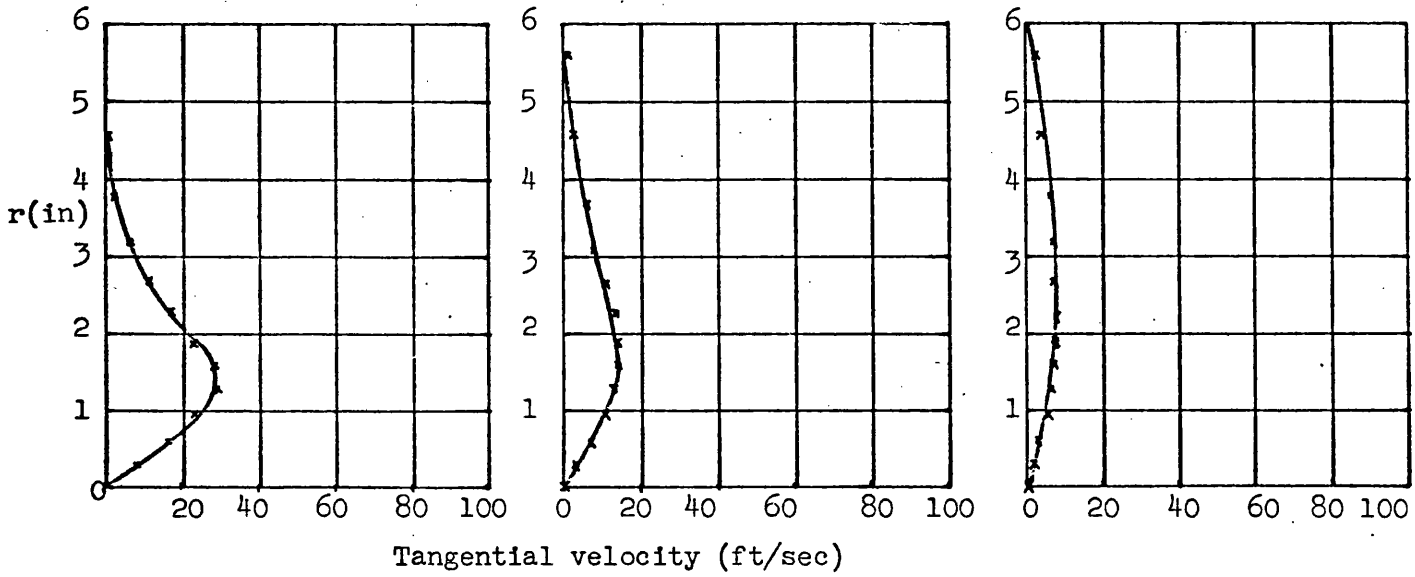

Figure 83 Computed results for annular swirling cold jets with 45° swirler

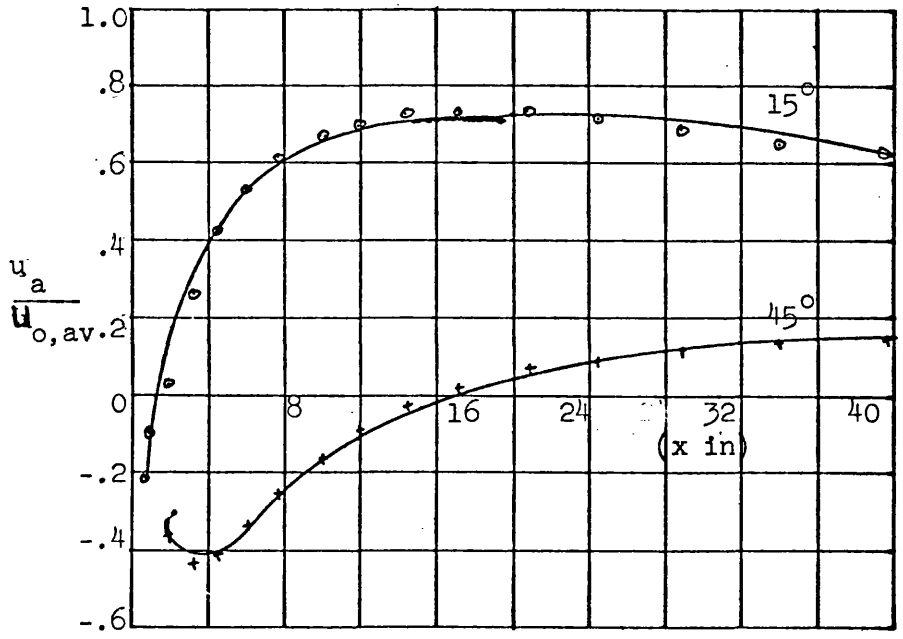

Computed decay of axial velocity along the axis of each of the 15° and 45° annular swirler cold jets

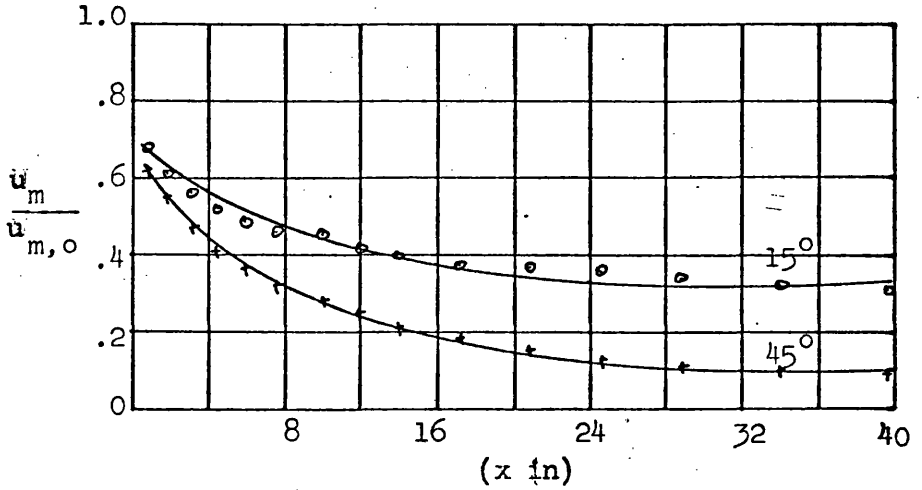

Computed decay of maximum axial velocity along the above jets.

Figure 84

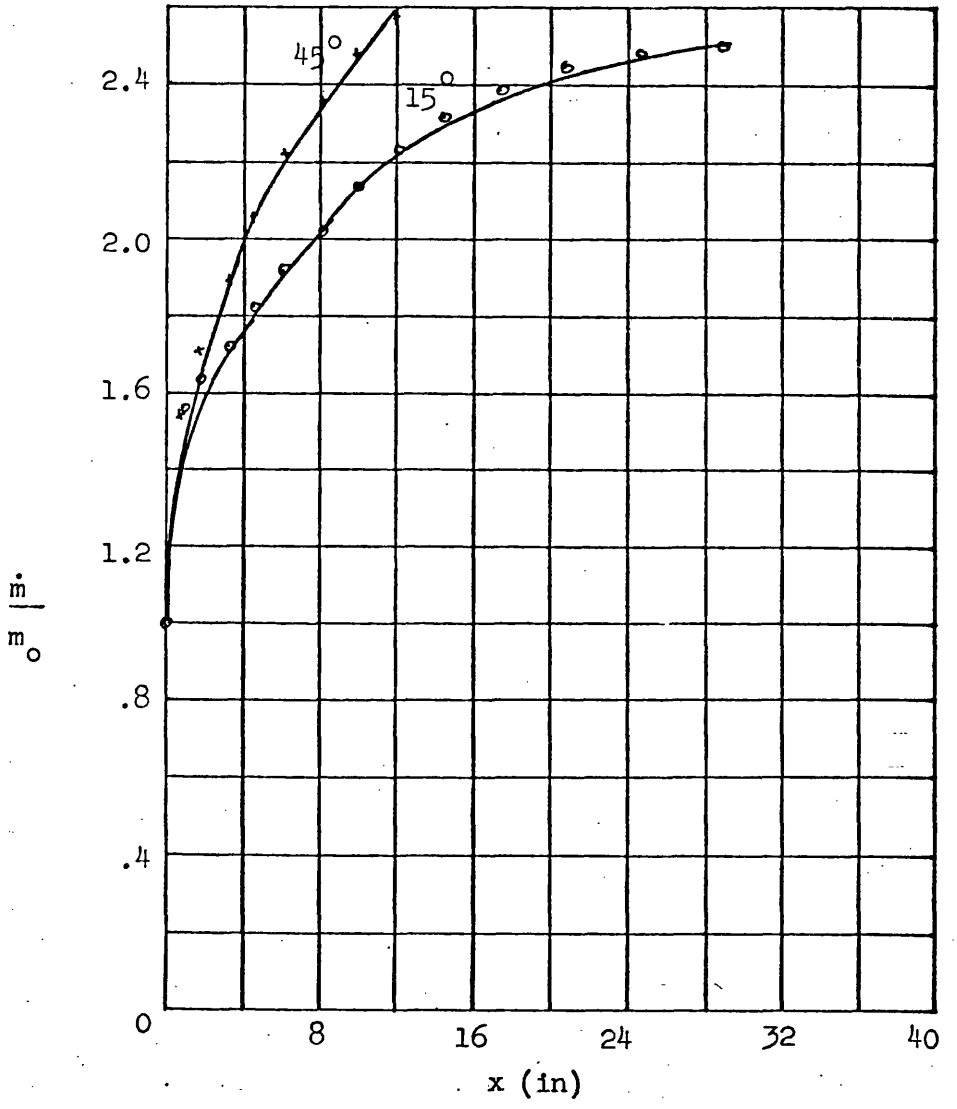

Figure 85 Computed variation of mass flow rates along cold swirling jets with 15° and 45° annular swirlers.

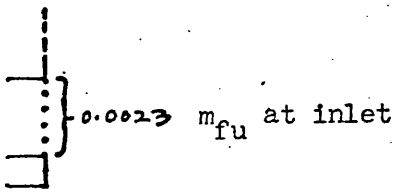

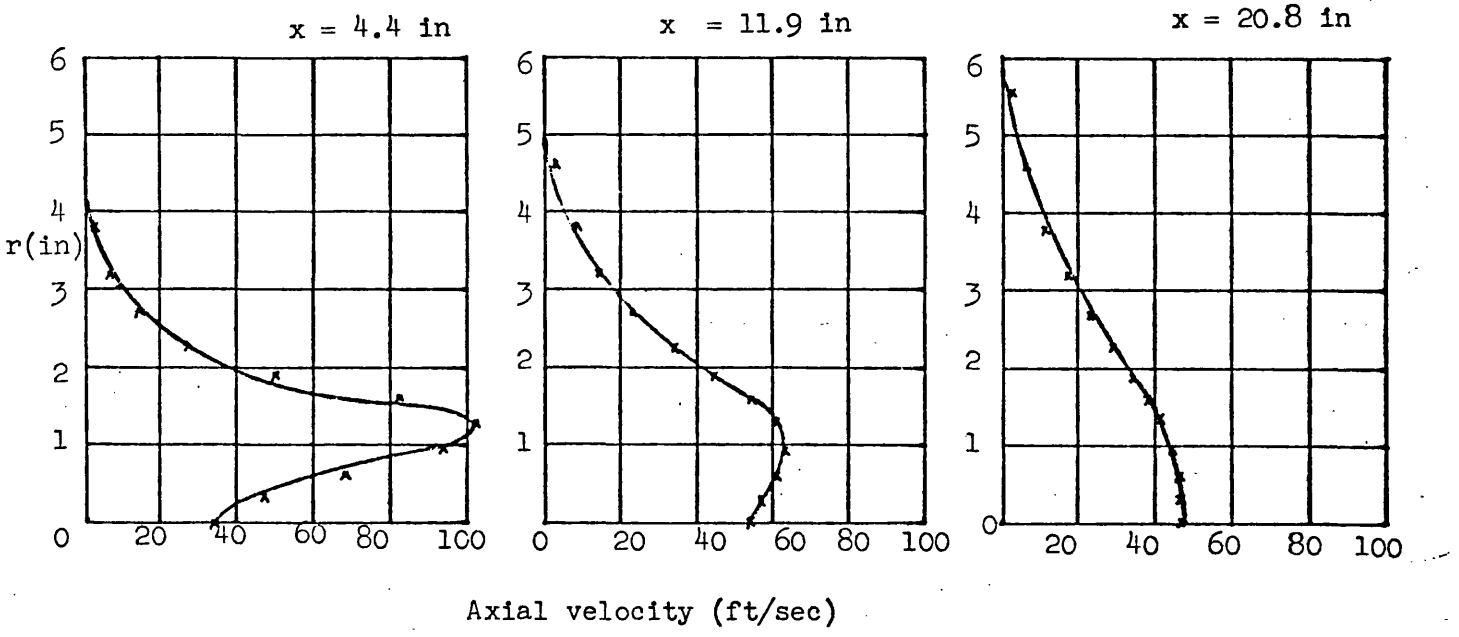

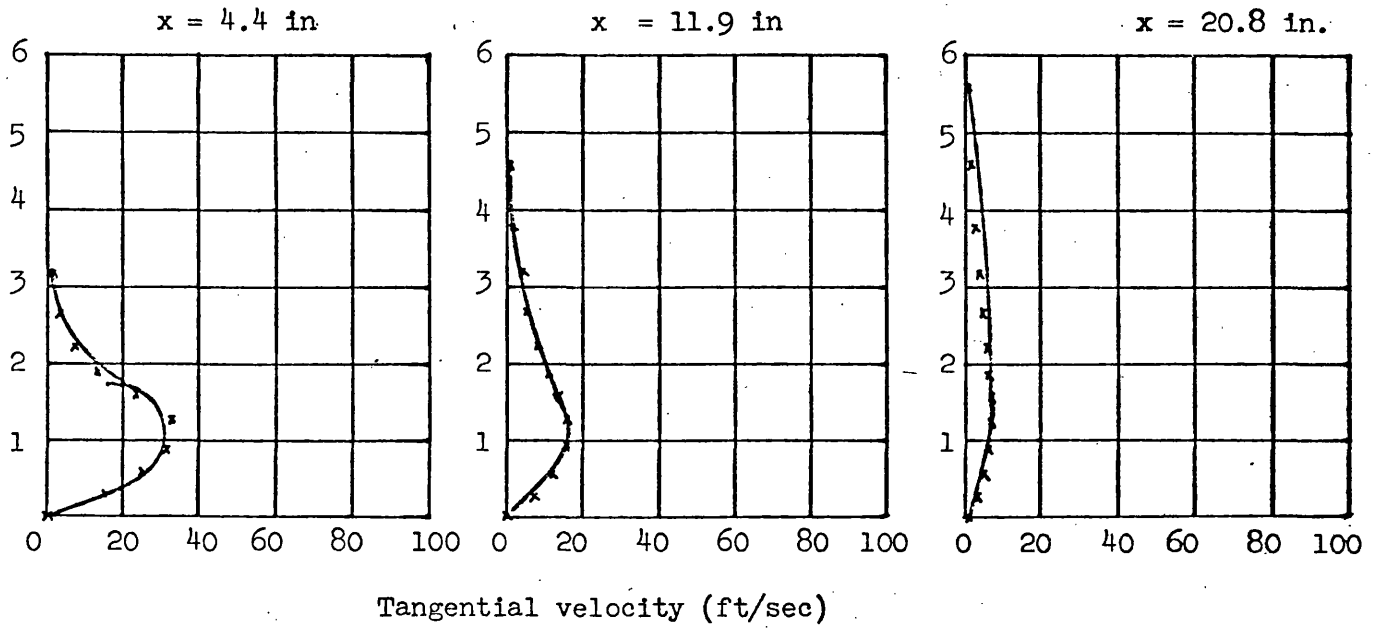

Figure 86 (a) Predicted velocity components for a burning jet with 15° swirler

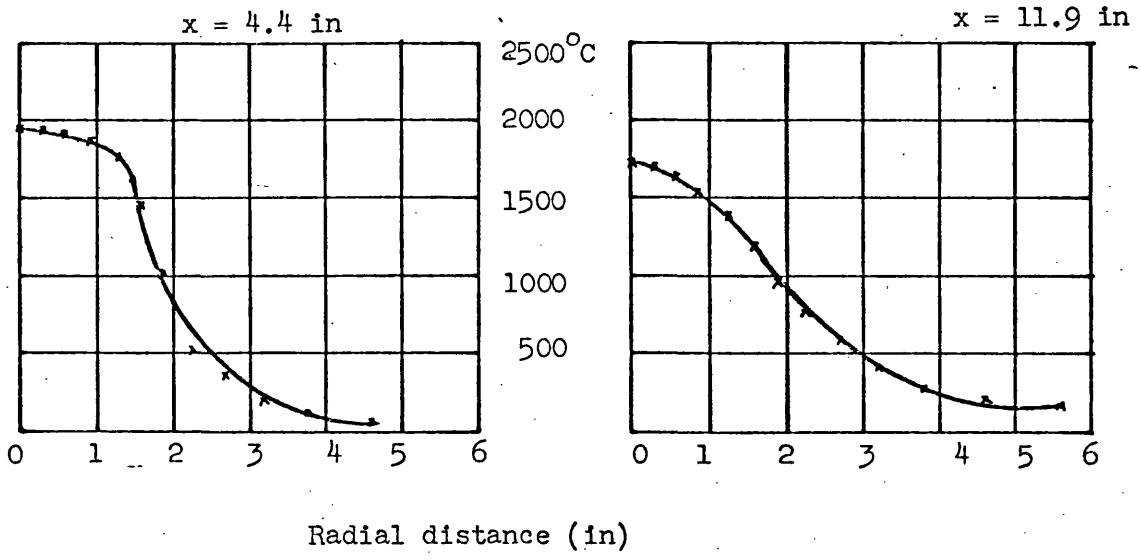

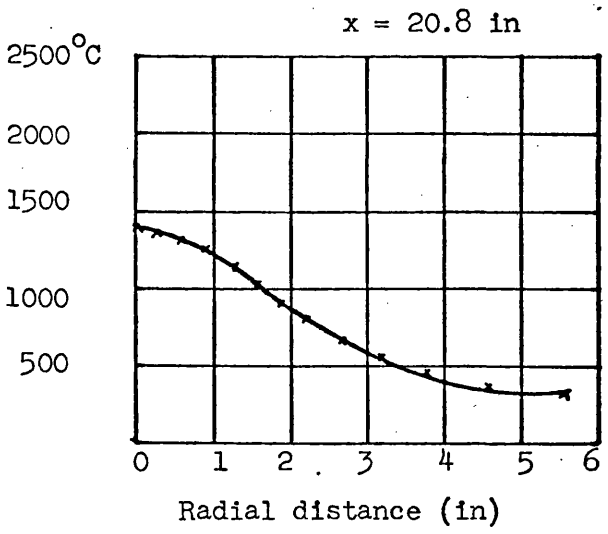

Figure 86 (b) Predicted temperature distribution

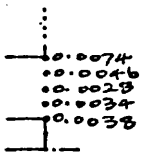

m_{fu} at inlet

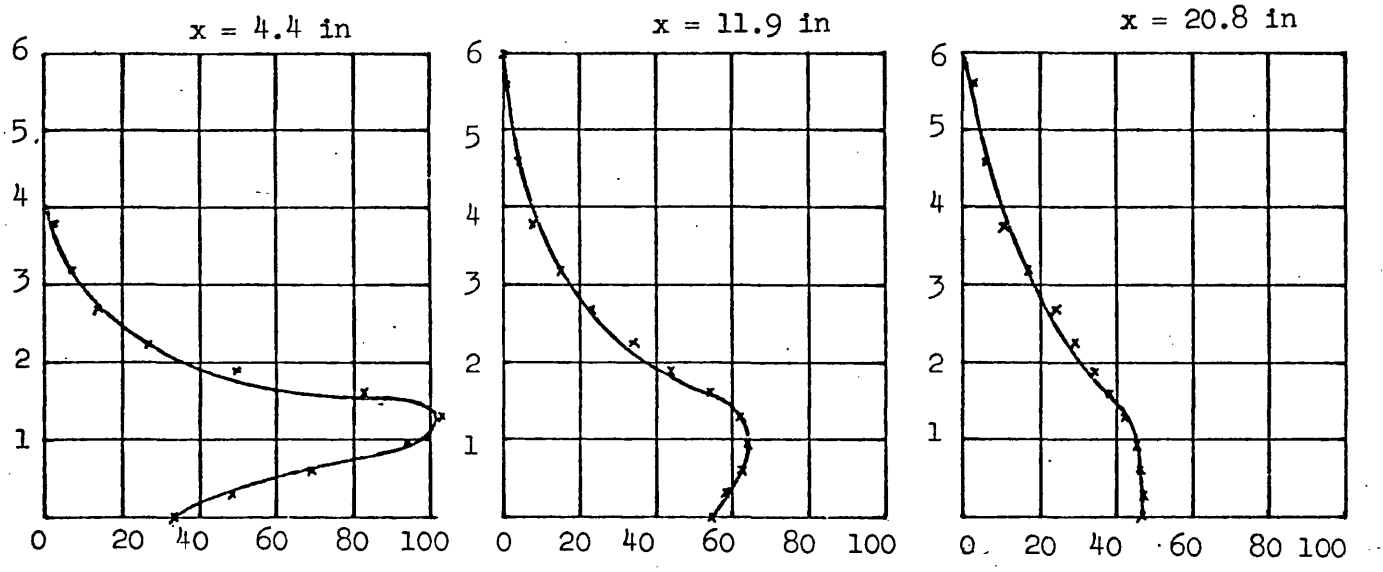

Axial velocity (ft/sec)

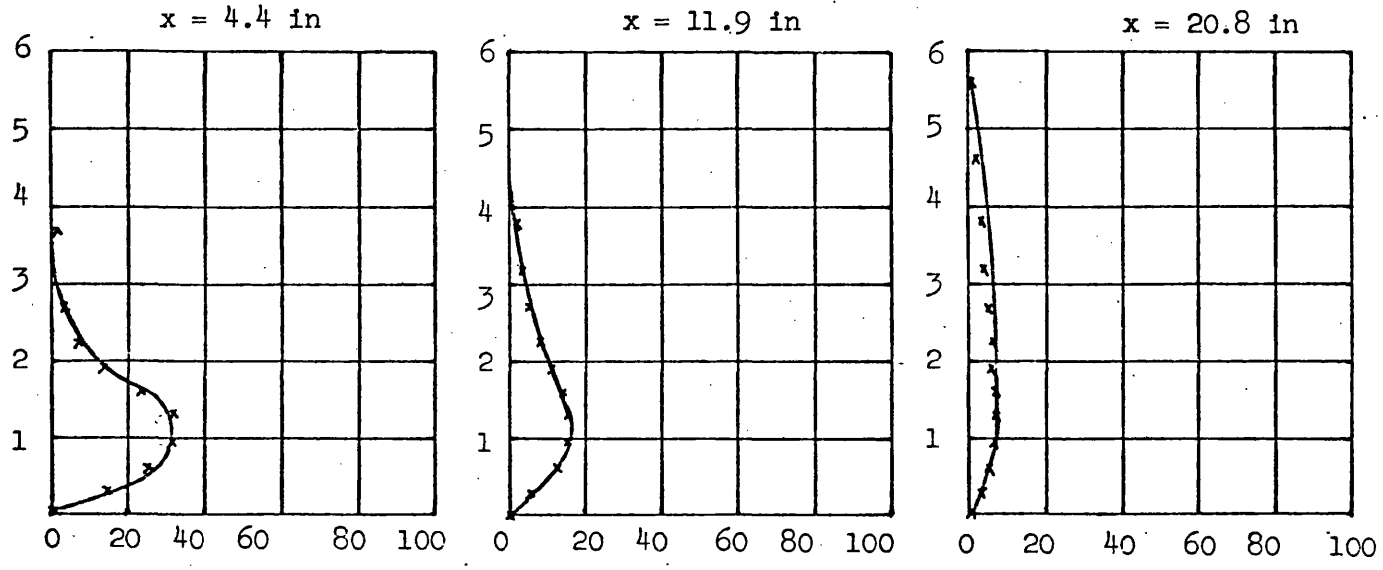

Tangential velocity (ft/sec)

Figure 87 (a) Computed velocity components for a burning jet with 15° swirler

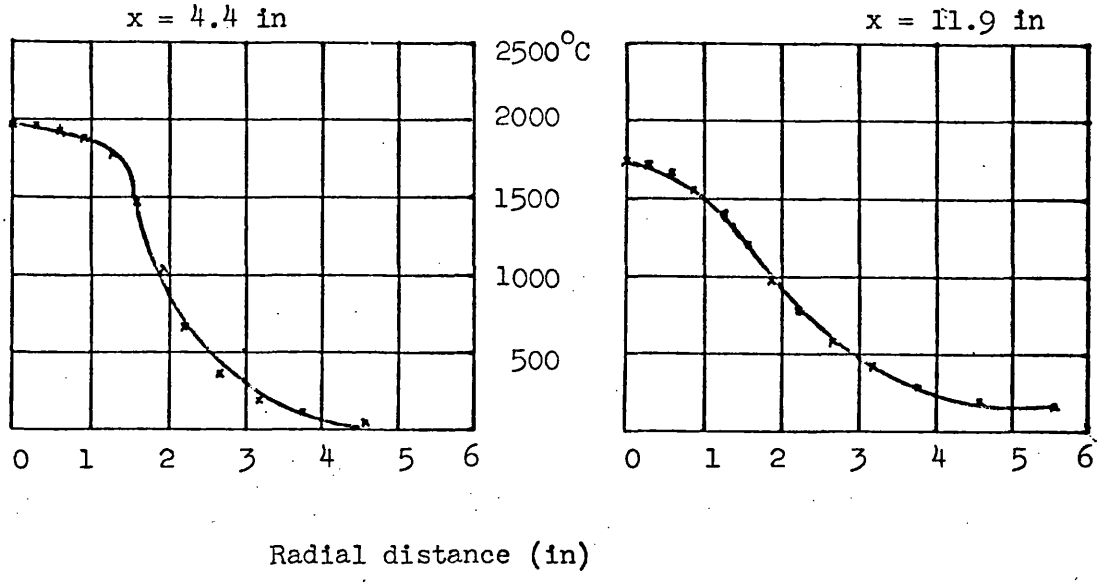

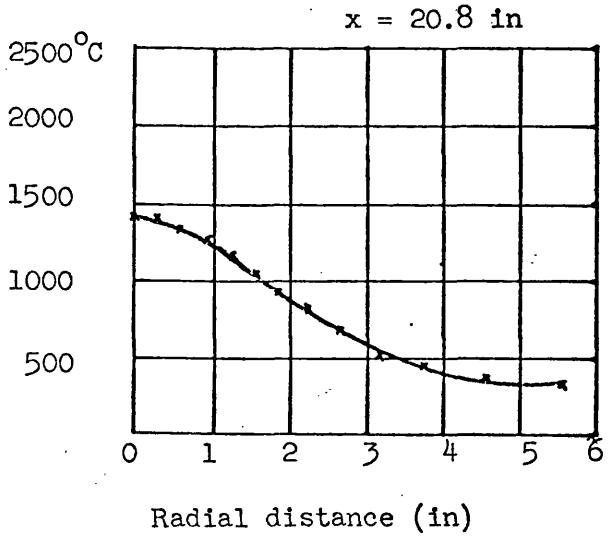

Figure 87 (b) Computed temperature distribution

```
      COMMON  A(16,14,7),G1(16,14),G2(16,14),RO(16,14),ZMU(16,14)
      COMMON  X1(16),X2(14),DELX1(16),DELX2(14),R(14)
      COMMON  ATITLE(12),ASYMBL(12),AGEOM(12),ANAME(6,10)
      COMMON  IMIN(14),IN,JN,INM,JNM,IA,JB,IA,IE
      COMMON  NW,NF,NVT,NZMM,NZML,NZMH,NP
      COMMON  ROREF,PREF,TREF,CPREF,ZMUREF
      COMMON  INDE(7),INDG,INDRO,INDZMU
      COMMON  ROWF
      COMMON  ZMUK,ZAA
      COMMON  STC,HC,HP,FMX
      COMMON  GLOB,ACTE,ZEX
      COMMON  PR(7),ZMW(3),GCPM,GC,ZJC
      COMMON  VINP(9),VING(9),VT(9)
      COMMON  RSDU(7),DIFMAX(7),RP(7),CC,DC,NMAX,NPRTN
      COMMON  NITER,KVORT,IJMP
      COMMON  NVJ,LNJ,LNI
      COMMON  VJ(12)
      COMMON  IIMD(7),JJMD(7),IIMR(7),JJMR(7)
      COMMON  CN,CS,CE,CW,ZW
      COMMON  VANGLE
      DIMENSION  AQ(16,14,12)
      EQUIVALENCE (A(1),AQ(1))
C*****************************************************************
C     SPECIFY ALL PHYSICAL DATA HERE
C*****************************************************************

C*****************************************************************
C    WHEN NO REACTION IS REQD. , PUT HC=0
C     TEMPERATURE VALUES ARE STORED SEPARATELY IN
C                              THE SUBROUTINE TABUCT
C***** WHEN INDZMU=1 ,VISCOSITY IS CALCULATED
C*****************************************************************
      DATA IN,JN,IA,JA,JB/
     1   16,14,1,1,6/
      DATA NW,NF,NVT,NZMM,NZML,NZMH,NP,IE/
     1   1,2,3,4,5,6,7,5/
      DATA STC,HC,HP,FMX/
     1  8.061142,10979.41,863.68,-0.03838/
      DATA PR(1),PR(2),PR(3),PR(4),PR(5),PR(6),PR(7),ZMW(1),ZMW(2),
     1ZMW(3),GCPM,GC,ZJC/
     2  7*1.0,15.39,2*28.96,1545.3,32.2,778./
      DATA ROREF,PREF,TREF,CPREF,ZMUREF/
     1  0.076,2116.8,520.,0.24,0.000013/
      DATA RP(1),RP(2),RP(3),RP(4),RP(5),RP(6),RP(7),CC/
     1   7*1.0,0.005/
      DATA NMAX,NPRTN/
     1  100,10/
      DATA INDG,INDE(1),INDE(2),INDE(3),INDE(4),INDE(5),INDE(6),INDE(7),
     1   INDZMU/6*1,2*2,1/
      DATA LNJ,LNI/
     1     40,120/
      DATA VANGLE/15.0/
      READ 101,(ATITLE(L),L=1,12),(ASYMBL(L),L=1,12),(AGEOM(L),L=1,12),
     1((ANAME(M,N),M=1,6),N=1,10)
      IEND=0
      ITAB=0
```

```
      ROWF=0.10
      GLOB=7.1E09
      ACTE=4.5E04
      ZMUK=.006
      INM=IN-1
      JNM=JN-1
   70 CONTINUE
      ROREF=0.076
C*****************************************************************
C****SPECIFYING X1 AND X2
C*****************************************************************
C                                        IGEOM=1  FOR HUBLESS SWIRLERS
C                                        IGEOM=2 FOR ANNULAR SWIRLERS
      IGEOM=2
      IF (IGEOM.EQ.1) GO TO 995
      JA=3
      JB=7
      GO TO 879
  995 CONTINUE
      AXI=(0.934/72.0)
      RXI=1.175
      X1(1)=0.
      DO 999 I=2,IN
      AANI=I-1
  999 X1(I)=AXI*((RXI**AANI)-1.0)/(RXI-1.0)
      AXJ=(0.0934/12.)
      DO 998 J=1,JB
      AAJ=J-1
  998 X2(J)=AXJ*AAJ
      RXJ=1.500
      JB1=JB+1
      DO 997 J=JB1,JN
      AANJ=J-JB
  997 X2(J)=X2(JB)+AXJ*((RXJ**AANJ)-1.0)/(RXJ-1.0)
      GO TO 996
C                                        FOR ANNULAR  FLOW
  879 AXI=0.07516
      RXI=1.14
      X1(1)=0.
      DO 900 I=2,IN
      AANI=I-1
  900 X1(I)=AXI*((RXI**AANI)-1.)/(RXI-1.)
      AXJ=0.02681
      DO 910 J=1,JB
      AAJ=J-1
  910 X2(J)=AXJ*AAJ
      RXJ=1.255
      JB1=JB+1
      DO 911  J=JB1,JN
      AANJ=J-JB
  911 X2(J)=X2(JB)+AXJ*((RXJ**AANJ)-1.)/(RXJ-1.)
C*****************************************************************
C****SPECIFYING DELX1 AND DELX2
C*****************************************************************
  996 DO 3 I=2,INM
    3 DELX1(I)=0.5*(X1(I+1)-X1(I-1))
      DO 4 J=2,JNM
```

```
    4 DELX2(J)=0.5*(X2(J+1)-X2(J-1))
C*************************************************************************
C*****SPECIFYING IMIN(J)
C*************************************************************************
      DO 5 J=1,JN
      IF (J.LE.JA.OR.J.GE.JB) GO TO 55
      IMIN(J)=1
      GO TO 5
   55 IMIN(J)=IA
    5 CONTINUE
C*************************************************************************
C*****SPECIFYING R(J)
C*************************************************************************
      IF(INDG.EQ.2) GO TO 77
      DO 76 J=1,JN
   76 R(J)=X2(J)
      GO TO 79
   77 DO 78 J=1,JN
   78 R(J)=1.0
   79 CONTINUE
C*************************************************************************
C*****SETTING INITIAL VALUES
C*************************************************************************
      CALL ONINA
      CONTINUE
201   DO 2 J=1,JN
      DO 2 I=1,IN
      G1(I,J)=0.0
      G2(I,J)=0.0
    2 CONTINUE
C   SPECIFYING INITIAL VALUES FOR DEPENDENT VARIABLES
20    CONTINUE
21    IF (INDE(NW).NE.1) GO TO 22
      DO 211 J=1,JN
      DO 211 I=1,IN
      A(I,J,NW)=0.0
211   CONTINUE
22    IF (INDE(NF).NE.1) GO TO 23
      DO 221 J=1,JN
      DO 221 I=1,IN
      A(I,J,NF)=0.0
221   CONTINUE
23    IF (INDE(NVT).NE.1) GO TO 24
      DO 231 J=1,JN
      DO 231 I=1,IN
      A(I,J,NVT)=0.0
231   CONTINUE
24    IF (INDE(NZMM).NE.1) GO TO 25
      DO 241 J=1,JN
      DO 241 I=1,IN
      IF (J.LE.JB.AND.I.EQ.1) GO TO 241
      IF (J.LE.JB.AND.I.GT.1)  A(I,J,NZMM)=0.75*A(I-1,J,NZMM)
      IF (J.GT.JB.AND.I.EQ.1)  A(I,J,NZMM)=0.0
      IF (J.GT.JB.AND.I.GT.1)  A(I,J,NZMM)=0.25*(A(I-1,J,NZMM)+
     1   A(I,J-1,NZMM))
241   CONTINUE
25    IF (INDE(NZML).NE.1) GO TO 26
```

```
      DO 251 J=1,JN
      DO 251 I=1,IN
      IF (J.LE.JB.AND.I.EQ.1) GO TO 251
      IF (J.LE.JB.AND.I.EQ.2) A(I,J,NZML)=A(1,J,NZML)-0.01*J
      IF (J.LE.JB.AND.I.GT.2)  A(I,J,NZML)=0.75*A(I-1,J,NZML)
      IF (J.GT.JB.AND.I.EQ.1)  A(I,J,NZML)=CPREF*(TREF-460.)/HP
      IF (J.GT.JB.AND.I.GT.1)  A(I,J,NZML)=0.25*(A(I-1,J,NZML)+
     1   A(I,J-1,NZML))
251   CONTINUE
26    CONTINUE
      DO 402 J=1,JN
      DO 402 I=1,IN
      RO(I,J)=RGREF
402   CONTINUE
C    INUBR=1 FOR COLD FLOW
C    INUBR=2 FOR COMBUSTION WITH ACTE=45000
C    INUBR=3 FOR COMBUSTION WITH ACTE=30000
C    INUBR=4 FOR COMBUSTION WITH ACTE=60000
      DO 1 INUBR=1,4
      IF (INUBR.EQ.1) HC=0.
      IF (INUBR.EQ.1) GO TO 400
      HC=10979.41
      NMAX=600
      NPRIN=100
      IF (INUBR.EQ.3) ACTE=3.0E04
      IF (INUBR.EQ.4) ACTE=6.0E04
      DO 401 K=1,7
401   RP(K)=0.25
400   CONTINUE
C*****CALCULATING INITIAL DENSITY PROFILE (IF REQD.)
      IF (HC.LE.0.0) GO TO 19
      IF(INDE(NZMM).NE.1) GO TO 19
      CALL DPROF
   19 CONTINUE
C    IF INLET PROFILE IS NOT UNIFORM PUT IENTA=1
      IENTA=1
      IF (IENTA.EQ.1) GO TO 171
      DO 17 J=JA,JB
      VINP(J)=18.29*(SQRT(2.2719/RO(1,J)))
17    CONTINUE
      GO TO 172
171   CONTINUE
      VINP(3)=0.0
      VINP(4)=18.29*(SQRT(0.3635/RO(1,4)))
      VINP(5)=18.29*(SQRT(1.454/RO(1,5)))
      VINP(6)=18.29*(SQRT(0.3635/RO(1,6)))
      VINP(7)=0.0
172   CONTINUE
      ZEX=(1.8*ACTE*ZJC)/(GCPM*28.96)
      CALL HEADCT
      CALL SOLVCT
      IF(INDE(NP).EQ.1) CALL PRESCT
      IEND=222
      CALL PRINCT(IEND,ITAB)
      CALL TABUCT(ITAB)
      ILIN=1
      ILEX=2
```

```
      CALL ENCHK(ILIN,ILEX)
C   SPECIFY SPECIAL PLOTTING VALUES HERE
C***** WHEN IPLT=1 ,VALUES WILL NOT BE PLOTTED.
      IPLT=1
      IF (IPLT.EQ.1) GO TO 1
      IE2=2
      DO 50 K=2,IE2
      VJ(1)=A(4,1,K)
      VJ(2)=A(4,2,K)
      VJ(3)=A(4,3,K)
      VJ(4)=A(4,4,K)
      VJ(5)=A(15,4,K)
      VJ(6)=A(15,6,K)
      VJ(7)=A(15, 8,K)
   49 NVJ=7
   52 CALL PLOTT(K)
   50 CONTINUE
    1 CONTINUE
  111 CONTINUE
  101 FORMAT(12A6)
      CALL EXIT
      END
```

```
      SUBROUTINE  ONINA
      COMMON  A(16,14,7),G1(16,14),G2(16,14),RO(16,14),ZMU(16,14)
      COMMON  X1(16),X2(14),DELX1(16),DELX2(14),R(14)
      COMMON  ATITLE(12),ASYMBL(12),AGEOM(12),ANAME(6,10)
      COMMON  IMIN(14),IN,JN,INM,JNM,JA,JB,IA,IE
      COMMON  NV,NF,NVT,NZMM,NZML,NZMH,NP
      COMMON  RGREF,PREF,TREF,CPREF,ZMUREF
      COMMON  INDE(7),INDG,INDRO,INDZMU
      COMMON  ROWF
      COMMON  ZMUK,ZAA
      COMMON  STC,HC,HP,FMX
      COMMON  GLOB,ACTE,ZEX
      COMMON  PR(7),ZMW(3),GCPM,GC,ZJC
      COMMON  VINP(9),VING(9),VT(9)
      COMMON  RSDU(7),DIFMAX(7),RP(7),CC,DC,NMAX,NPRTN
      COMMON  NITER,KVORT,IJMP
      COMMON  NVJ,LNJ,LNI
      COMMON  VJ(12)
      COMMON  IIMD(7),JJMD(7),IIMR(7),JJMR(7)
      COMMON  CN,CS,CE,CW,ZW
      COMMON  VANGLE
C***SUBROUTINE CALCULATES INLET PROFILES OF FUEL MASS-FRACTION,
C***DIMENSIONLESS ENTHALPY AND DIMENSIONLESS MIXTURE-FRACTION(IF REQD.)
C***  FOR FUEL MASS-FRACTION
      IF (INDL(NZMM).NE.1) GO TO 20
      EPO=0.07622
      A(1,1,NZMM)=0.005*EPO
      A(1,2,NZMM)=0.009*EPO
      A(1,3,NZMM)=0.0500*EPO
      A(1,4,NZMM)=0.0450*EPO
      A(1,5,NZMM)=0.0370*EPO
      A(1,6,NZMM)=0.0600*EPO
      A(1,7,NZMM)=0.0970*EPO
C***FOR DIMENSIONLESS ENTHALPY
20    IF (INDE(NZML).NE.1) GO TO 40
      DO 21 J=JA,JB
21    A(1,J,NZML)=(CPREF*(TREF-460)+A(1,J,NZMM)*HC)/HP
40    CONTINUE
      RETURN
      END
```

```
      SUBROUTINE DPROF
      COMMON  A(16,14,7),G1(16,14),G2(16,14),RO(16,14),ZMU(16,14)
      COMMON  X1(16),X2(14),DELX1(16),DELX2(14),R(14)
      COMMON  ATITLE(12),ASYMBL(12),AGEOM(12),ANAME(6,10)
      COMMON  IMIN(14),IN,JN,INM,JNM,JA,JB,IA,IE
      COMMON  NV,NF,NVT,NZMM,NZML,NZMH,NP
      COMMON  ROREF,PREF,TREF,CPREF,ZMUREF
      COMMON  INDE(7),INDG,INDRO,INDZMU
      COMMON  ROWF
      COMMON  ZMUK,ZAA
      COMMON  STC,HC,HP,FMX
      COMMON  GLOB,ACTE,ZEX
      COMMON  PR(7),ZMW(3),GCPM,GC,ZJC
      COMMON  VINP(9),VING(9),VT(9)
      COMMON  RSDU(7),DIFMAX(7),RP(7),CC,DC,NMAX,NPRTN
      COMMON  NITER,KVORT,IJMP
      COMMON  NVJ,LNJ,LNI
      COMMON  VJ(12)
      COMMON  IIMD(7),JJMD(7),IIMR(7),JJMR(7)
      COMMON  CN,CS,CE,CW,ZW
      COMMON  VANGLE
C*****SUBROUTINE CALCULATES DENSITY AT INLET PLANE
C**********************************************************************
      DO 20 J=JA,JB
      AFU=A(1,J,NZMM)
      AFH=A(1,J,NZML)
      TEMP=(AFH*HP-AFU*HC)/CPREF
      TEMP=TEMP+460.
      IF (INDE(NZMH).EQ.1) GO TO 10
      FOX=STC*(AFU-AFH*FMX)
      GO TO 15
   10 AFF=A(1,J,NZMH)
      FOX=STC*(AFU-AFF*FMX)
   15 CONTINUE
      FIP=1.0-FOX-AFU
      ZMEAN= 1.0/(AFU/ZMW(1) +FOX/ZMW(2) +FIP/ZMW(3))
   20 RO(1,J)=PREF*ZMEAN/(GCPM*TEMP)
      RETURN
      END
```

```
      SUBROUTINE READCT
      COMMON  A(16,14,7),G1(16,14),G2(16,14),RO(16,14),ZMU(16,14)
      COMMON  X1(16),X2(14),DELX1(16),DELX2(14),R(14)
      COMMON  ATITLE(12),ASYMBL(12),AGEOM(12),ANAME(6,10)
      COMMON  IMIN(14),IN,JN,INM,JNM,JA,JB,IA,IE
      COMMON  NW,NF,NVT,NZMM,NZML,NZMH,NP
      COMMON  ROREF,PREF,TREF,CPREF,ZMUREF
      COMMON  INDE(7),INDG,INDRO,INDZMU
      COMMON  ROWF
      COMMON  ZMUK,ZAA
      COMMON  STC,HC,HP,FMX
      COMMON  GLOB,ACTE,ZEX
      COMMON  PR(7),ZMW(3),GCPM,GC,ZJC
      COMMON  VINP(9),VING(9),VT(9)
      COMMON  RSDU(7),DIFMAX(7),RP(7),CC,DC,NMAX,NPRTN
      COMMON  NITER,KVORT,IJMP
      COMMON  NVJ,LNJ,LNI
      COMMON  VJ(12)
      COMMON  IIMD(7),JJMD(7),IIMR(7),JJMR(7)
      COMMON  CN,CS,CE,CW,ZW
      COMMON  VANGLE
      DATA JFL,JFU/0.0,0.0/
C*****************************************************************
C*****SUBROUTINE PRINTS OUT SOME OF THE INFORMATION FED IN.
C*****************************************************************
      PRINT 101 , (ATITLE(L),L=1,12)
      IF(INDG.EQ.2) GO TO 4
      PRINT 104
      GO TO 5
    4 PRINT 105
    5 CONTINUE
      PRINT 106
    8 PRINT 109
      DO 10 K=1,IE
   10 IF (INDE(K).EQ.1) PRINT 110, (ANAME(L,K),L=1,6)
      PRINT 100,(AGEOM(L),L=1,12)
  100 FORMAT(1H ,48HTHE GEOMETRY OF VANE SWIRLER BEING CONSIDERED IS,/,
     1 148H----------,/,40X,12A6)
      PRINT 111,JN,IN
      DO 12 J=1,JN
   12 PRINT 113,J,IMIN(J),R(J)
      AA2=X2(JA)/X2(JB)
      PRINT 201,IA,JA,JB,JFL,JFU,X2(JA),X2(JB),X2(JN),X1(IA),X1(IN),AA2
      PRINT202,(I,I=1,12)
      PRINT203,(X1(I),I=1,12)
      IF (IN.LE.12) GO TO 14
      PRINT 202,(I,I=13,IN)
      PRINT 203,(X1(I),I=13,IN)
   14 PRINT 112,ROREF,PREF,ZMUREF,TREF,CPREF,GC,ZJC
      PRINT 301,STC,HC,HP,FMX,ACTE
      PRINT 115,(ZMW(L),L=1,3),PR(NZML),PR(NZMM),PR(NZMH)
      PRINT 116,CC,DC,NMAX
      PRINT 305
      DO 15 J=JA,JB
   15 PRINT 310,J,VINP(J),RO(I,J)
  101 FORMAT(1H1,35X,43HFINITE-DIFFERENCE  ITERATION SOLUTION  FOR/
```

```
     236X,43H----------//
     320X,12A6//45X,19HIS BEING CONSIDERED/45X,19H----------//)
  104 FORMAT(1H ,50X,18HAXI-SYMMETRIC FLOW)
  105 FORMAT(1H ,50X,16HCARTESIAN COODS.)
  106 FORMAT(1H0,50X,18HFOR TURBULENT FLOW)
109    FORMAT(1H0//46H THE DEPENDENT VARIABLES BEING CONSIDERED ARE,/
     246H --- -------- -------- ----- --------- --- )
110    FORMAT(1H040X,6A6)
111    FORMAT(1H139HTHE GEOMETRICAL INFORMATION SUPPLIED IS/
     240H --- ---------- --------- -------- --//
     341X,44HJN,     THE NUMBER OF ROWS     (DIRECTION-2) =,I3/
     441X,44HIN,     THE NUMBER OF COLUMNS (DIRECTION-1) =,I3//,
     5 40X,1HJ,8X,7HIMIN(J),8X,13HR(J) (=X2(J)),/)
  113 FORMAT(1H 39X,I2,11X,I2,11X,F7.4)
112    FORMAT(37H1THE PHYSICAL INFORMATION SUPPLIED IS/
     237H --- ------- ---------- -------- --//
     310X,50HROREF,  REFERENCE DENSITY FOR THE FLUID.....=,F10.4/
     410X,50HPREF,   REFERENCE PRESSURE FOR THE FLUID.....=,F10.4/
     510X,50HZMUREF, REFERENCE VISCOSITY FOR THE FLUID.....=,F10.8/
     610X,50HTREF,   REFERENCE TEMPRATURE FOR THE FLUID.....=,F10.4/
     710X,50HCPREF,  REFERENCE SPECIFIC-HEAT FOR THE FLUID....=,F10.4/
     810X,50HGC,     GRAVITATIONAL CONSTANT.....=,F10.4/
     710X,50HZJC,    JOULE S MECH.EQUIVALENT FOR HEAT.....=,F10.4/)
  115 FORMAT(1H  9X,60HZMW S  MOLECULAR WTS.OF FUEL,OXIDANT AND PRODUCTS
     1 RESPECT. =,3F10.4,/,
     2 10X,50HPR(NZML) TURBULENT PRANDTL NO.                    =,F6.2,/,
     3 10X,50HPR(NZMM) TURBULENT SCHMIDT NO. FOR FUEL           =,F6.2,/,
     4 10X,51HPR(NZMH) TURBULENT SCHMIDT NO. FOR MIXTURE FRACT. =,F6.2)
116    FORMAT(1H0///36H THE CONTROL INFORMATION SUPPLIED IS/
     236H --- ------- ---------- -------- --//
     310X,50HCC,     THE CONVERGENCY CRITERION.....=,F13.7/
     410X,50HDC,     THE DIVERGENCY  CRITERION.....=,F13.7/
     510X,50HNMAX,   THE MAXIMUM NUMBER OF ITERATIONS.....=,I6)
201    FORMAT(1H0,36X,18HIA,JA,JB,JFL,JFU =,5(I3,1H,),12HRESPECTIVELY,/,1
     1H0,26X,22HRADA,RADB,RADN,DA,DN =,5(F6.3,1H,),17H FT. RESPECTIVELY,
     2/,1H0,32X,25H             (RADA/RADB) =,F6.3,13H RESPECTIVELY,/)
202    FORMAT(1H0,4X,10H  I       ,22(3X,I2,3X))
203    FORMAT(1H ,4X,10H  X1(I)   ,22(F8.4))
301    FORMAT(10X,50HSTC (1 LB OF FUEL REACTS WITH STC LB OF OXIDANT) =,
     1F8.4,/,10X,50HHC         (HEAT OF REACTION, BTU PER LB OF FUEL) =,F
     28.1,/,10X,50HHP         (REFERENCE ENTHALPY FOR INLET BTU/LBM) =,F8
     3.2,/,10X,50HFMX         (REFERENCE (M(FU)-M(OX)/R)) FOR INLET =,F8.
     43,/,10X,50HACTE        (ACTIVATION ENERGY - BTU PER LB MOLE) =,F8.2
     5,/)
  315 FORMAT(//,5X,45HVELOCITY AND DENSITY DISTRIBUTION AT INLET IS,//,
     1  10X,1HJ,4X,16HVELOCITY(FT/SEC),10X,18HDENSITY(LBM/FT**3),/)
  310 FORMAT(1H ,9X,I2,8X,F7.2,19X,F7.4)
      RETURN
      END
```

```
      SUBROUTINE SOLVCT
      COMMON  A(16,14,7),G1(16,14),G2(16,14),RO(16,14),ZMU(16,14)
      COMMON  X1(16),X2(14),DELX1(16),DELX2(14),R(14)
      COMMON  ATITLE(12),ASYMBL(12),AGEOM(12),ANAME(6,10)
      COMMON  IMIN(14),IN,JN,INM,JNM,JA,JB,IA,IE
      COMMON  NW,NF,NVT,NZMM,NZML,NZMH,NP
      COMMON  ROREF,PREF,TREF,CPREF,ZMUREF
      COMMON  INDE(7),INDG,INDRO,INDZMU
      COMMON  ROWF
      COMMON  ZMUK,ZAA
      COMMON  STC,HC,HP,FMX
      COMMON  GLOB,ACTE,ZEX
      COMMON  PR(7),ZMW(3),GCPM,GC,ZJC
      COMMON  VINP(9),VING(9),VT(9)
      COMMON  RSDU(7),DIFMAX(7),RP(7),CC,DC,NMAX,NPRTN
      COMMON  NITER,KVORT,IJMP
      COMMON  NVJ,LNJ,LNI
      COMMON  VJ(12)
      COMMON  IIMD(7),JJMD(7),IIMR(7),JJMR(7)
      COMMON  CN,CS,CE,CW,ZW
      COMMON  VANGLE
C*****************************************************************
C   THIS SUBR. CONTROLS THE ITERATION PROCEDURE
C*****************************************************************
      PRINT 101
      DO 10 K=1,IE
10    IF (INDE(K).EQ.1) PRINT 102,K,(ANAME(L,K),L=1,6)
      PRINT 1031
      IF (IE.EQ.2) PRINT 1032,(ASYMBL(K),K=1,2)
      IF (IE.EQ.3) PRINT 1033,(ASYMBL(K),K=1,3)
      IF (IE.EQ.4) PRINT 1034,(ASYMBL(K),K=1,4)
      IF (IE.EQ.5) PRINT 1035,(ASYMBL(K),K=1,5)
      NITER=1
      NNN=NPRIN
C*********************************** ***************************
C  CALCULATE INLET NF AND NW DISTRIBUTIONS
C*********************************** ***************************
      CALL PROFIL
      IEND=0
      ITAB=0
      ILIN=1
      ILEX=1
      CALL ENCHK(ILIN,ILEX)
      KVORT=0
      CALL  BCONDT(NW)
    1 CALL MVELCT
      IF (HC.LE.0.0) GO TO 20
      IF(INDE(NZMM).NE.1) GO TO 20
      CALL DENSCT
20    CONTINUE
      CALL VISCCT
      CALL MVBCCT
      DO 2 K=1,IE
      DIFMAX(K)=0.
      RSDU(K)=0.
      IIMD(K)=0
```

```
      JJMD(K)=0
      IIMR(K)=0
      JJMR(K)=0
      KVORT=111
    2 IF(INDE(K).EQ.1) CALL FDEQCT(I,J,K)
      III=IIMR(1)
      JJ1=JJMR(1)
      PRINT 104,NITER,(RSDU(K),K=1,IE),(DIFMAX(K),K=1,IE)
      PRINT 107,(IIMR(K),JJMR(K),K=1,IE),(IIMD(K),JJMD(K),K=1,IE)
      RES=RSDU(1)
      DO 3 K=2,IE
3     IF(ABS(RSDU(K)).GT.ABS(RES)) RES=RSDU(K)
      IF(NITER.GT.NMAX) GO TO 5
      IF(NITER-NNN)6,7,7
7     NNN=NNN+NPRIN
      KVORT=111
      CALL  BCONDT(NW)
      CALL PRINCT(IEND,ITAB)
      ILIN=2
      ILEX=2
      CALL ENCHK(ILIN,ILEX)
      PRINT 1031
      IF (IE.EQ.2) PRINT 1032,(ASYMBL(K),K=1,2)
      IF (IE.EQ.3) PRINT 1033,(ASYMBL(K),K=1,3)
      IF (IE.EQ.4) PRINT 1034,(ASYMBL(K),K=1,4)
      IF (IE.EQ.5) PRINT 1035,(ASYMBL(K),K=1,5)
6     CONTINUE
      IF (NITER.EQ.NMAX) GO TO 5
      NITER=NITER+1
      IF(A(4,4,2).GE.1.0E10) GO TO 600
      IF(ABS(RES).GT.CC.OR.NITER.LE.2) GO TO 1
      PRINT 640
      GO TO 610
600   PRINT 650
610   PRINT 660
      KVORT=111
      CALL  BCONDT(NW)
      RETURN
5     PRINT 106,NITER
      PRINT 660
101   FORMAT(1H1///10X,62HFOR EACH ITERATION -NITER- THE MAXIMUM RESIDUE
     2S FOR THE FOLLOWING SHALL BE PRINTED///)
102   FORMAT(1H 40X,I2,3H.  ,6A6)
1031  FORMAT(////1H0,30X,35H..NOTE.. PREFIX  R  DENOTES RESIDUE//)
1032  FORMAT(1X,4HNITR,2(2X,1HR,A6,2X),53X,19HMAXIMUM DIFFERENCES,//)
1033  FORMAT(1X,4HNITR,3(2X,1HR,A6,2X),42X,19HMAXIMUM DIFFERENCES,//)
1034  FORMAT(1X,4HNITR,4(2X,1HR,A6,2X),31X,19HMAXIMUM DIFFERENCES,//)
1035  FORMAT(1X,4HNITR,5(2X,1HR,A6,2X),20X,19HMAXIMUM DIFFERENCES,//)
104   FORMAT(1H I3,5(1PE11.3),2X,5(1PE11.3))
106   FORMAT (32H0THE PROCESS DID NOT CONVERGE IN,I5,13H   ITERATIONS)
107   FORMAT(1H  4X,5(2X,1H(,I2,1H,,I2,1H),2X),2X,
     1              5(2X,1H(,I2,1H,,I2,1H),2X))
640   FORMAT(1H0,10X,21HPROGRAM HAS CONVERGED)
650   FORMAT(1H0,10X,46HPROGRAM HAS NOT CONVERGED BUT RECORDING VALUES)
660   FORMAT(1H0,10X,30HWILL PRINT DEPENDENT VARIABLES)
      RETURN
      END
```

```
      SUBROUTINE PROFIL
      COMMON  A(16,14,7),G1(16,14),G2(16,14),RO(16,14),ZMU(16,14)
      COMMON  X1(16),X2(14),DELX1(16),DELX2(14),R(14)
      COMMON  ATITLE(12),ASYMBL(12),AGEOM(12),ANAME(6,10)
      COMMON  IMIN(14),IN,JN,INM,JNM,JA,JB,IA,IE
      COMMON  NN,NF,NVT,NZMM,NZML,NZMH,NP
      COMMON  ROREF,PREF,TREF,CPREF,ZMUREF
      COMMON  INDE(7),INDG,INDRO,INDZMU
      COMMON  ROWF
      COMMON  ZMUK,ZAA
      COMMON  STC,HC,HP,FMX
      COMMON  GLOB,ACTE,ZEX
      COMMON  PR(7),ZMW(3),GCPM,GC,ZJC
      COMMON  VINP(9),VING(9),VT(9)
      COMMON  RSDU(7),DIFMAX(7),RP(7),CC,DC,NMAX,NPRTN
      COMMON  NITER,KVORT,IJMP
      COMMON  NVJ,LNJ,LNI
      COMMON  VJ(12)
      COMMON  IIMD(7),JJMD(7),IIMR(7),JJMR(7)
      COMMON  CN,CS,CE,CW,ZW
      COMMON  VANGLE
      DIMENSION G(21)
C*************************************** ***************************************
C  CALCULATING INLET STREAM FUNCTION DISTRIBUTION
C     ASSUMING QUADRATIC PROFILE OF G1(I,J)
C*************************************************************************
      DO 10 J=JA,JB
   10 G(J)=RO(1,J)*VINP(J)
C                    IOPEN=1 IF INTEGRATION STARTS FROM THE AXIS
      IOPEN=1
      IF (IOPEN.NE.1) GO TO 11
      A(1,JA,NF)=0.
      JA1=JA+1
      DO 14 J=JA1,JB
      DXH2=0.5*(X2(J)-X2(J-1))
14    A(1,J,NF)=A(1,J-1,NF)+DXH2*(R(J-1)*G(J-1)+R(J)*G(J))
      GO TO 41
11    A(1,JB,NF)=0.0
      JBM=JB-1
      DX2=X2(JB)-X2(JBM)
      AA1=2.*G(JBM)/DX2
      BB1=-G(JBM)/(DX2*DX2)
      DT2=AA1+2.*BB1*X2(JB)
      DT3=AA1*X2(JB)+BB1*X2(JB)*X2(JB)
      R1=X2(JBM)
      R2=X2(JB)
      IF(INDG.EQ.2) GO TO 12
      FCT=(R2**4-R1**4)*BB1/4.0-(R2**3-R1**3)*DT2/3.0+
     1   (R2**2-R1**2)*DT3/2.0
      GO TO 13
   12  FCT=(R2**3-R1**3)*BB1/3.0-(R2**2-R1**2)*DT2/2.0
     1     +(R2-R1)*DT3
   13 CONTINUE
      A(1,JBM,NF)=A(1,JB,NF)-FCT
      JGP=JB-JA
      DO 40 J=2,JGP
```

```
      IJ=JB-J
      IF(IJ.EQ.JA) GO TO 15
      J3=IJ+1
      J2=IJ
      J1=IJ-1
      GO TO 20
   15 J3=IJ+2
      J2=IJ+1
      J1=IJ
   20 CONTINUE
      DT1=G(J1)/((X2(J1)-X2(J2))*(X2(J1)-X2(J3)))
      DT2=G(J2)/((X2(J2)-X2(J1))*(X2(J2)-X2(J3)))
      DT3=G(J3)/((X2(J3)-X2(J1))*(X2(J3)-X2(J2)))
      FC1=DT1+DT2+DT3
      FC2=(DT1*(X2(J2)+X2(J3))+DT2*(X2(J1)+X2(J3))+DT3*(X2(J1)+
     1  X2(J2)))
      FC3=DT1*X2(J2)*X2(J3)+DT2*X2(J3)*X2(J1)+DT3*X2(J1)*X2(J2)
      IF(IJ.EQ.JA) GO TO 30
      IF(INDG.EQ.2) GO TO 24
      FCT=FC1*(X2(J3)**4-X2(J2)**4)/4.0-FC2*(X2(J3)**3-X2(J2)**3)/3.0+
     1  FC3*(X2(J3)**2-X2(J2)**2)/2.0
      GO TO 26
   24 FCT=FC1*(X2(J3)**3-X2(J2)**3)/3.0-FC2*(X2(J3)**2-X2(J2)**2)/2.0+
     1  FC3*(X2(J3)-X2(J2))
   26 GO TO 35
   30 IF(INDG.EQ.2) GO TO 33
      FCT=FC1*(X2(J2)**4-X2(J1)**4)/4.0-FC2*(X2(J2)**3-X2(J1)**3)/3.0+
     1  FC3*(X2(J2)**2-X2(J1)**2)/2.0
      GO TO 35
   33 FCT=FC1*(X2(J2)**3-X2(J1)**3)/3.0-FC2*(X2(J2)**2-X2(J1)**2)/2.0+
     1  FC3*(X2(J2)-X2(J1))
   35 A(1,IJ,NF)=A(1,IJ+1,NF) -FCT
   40 CONTINUE
C*************************************************************************
C  CALCULATING INLET VORTICITY DISTRIBUTION
C*************************************************************************
41    JBM=JB-1
      JA2=JA+1
   49 DO 50 J=JA2,JBM
      J1=J-1
      J2=J
      J3=J+1
      DT1=VINP(J1)/((X2(J1)-X2(J2))*(X2(J1)-X2(J3)))
      DT2= VINP(J2)/((X2(J2)-X2(J1))*(X2(J2)-X2(J3)))
      DT3= VINP(J3)/((X2(J3)-X2(J1))*(X2(J3)-X2(J2)))
      A(1,J,NW)= (X2(J3)-X2(J2))*DT1 +(X2(J1)+X2(J3)-2.*X2(J2))*DT2
     1    +(X2(J1)-X2(J2))*DT3
      A(1,J,NW)=A(1,J,NW)/R(J)
   50 CONTINUE
   51 CONTINUE
      IF(INDE(NVT).NE.1) GO TO 46
      DO 45 J=JA,JB
      VANGLE=(15.0/57.2958)
45    A(1,J,NVT)=VINP(J)*(SIN(VANGLE)/COS(VANGLE))
46    CONTINUE
      RETURN
      END
```

```
      SUBROUTINE MVBCCT
      COMMON  A(16,14,7),G1(16,14),G2(16,14),RO(16,14),ZMU(16,14)
      COMMON  X1(16),X2(14),DELX1(16),DELX2(14),R(14)
      COMMON  ATITLE(12),ASYMBL(12),AGEOM(12),ANAME(6,10)
      COMMON  IMIN(14),IN,JN,INM,JNM,JA,JB,IA,IE
      COMMON  NW,NF,NVT,NZMK,NZML,NZMH,NP
      COMMON  ROREF,PREF,TREF,CPREF,ZMUREF
      COMMON  INDE(7),INDG,INDRO,INDZMU
      COMMON  ROWF
      COMMON  ZMUK,ZAA
      COMMON  STC,HC,HP,FMX
      COMMON  GLOB,ACTE,ZEX
      COMMON  PR(7),ZMW(3),GCPM,GC,ZJC
      COMMON  VINP(9),VING(9),VT(9)
      COMMON  RSDU(7),DIFMAX(7),RP(7),CC,DC,NMAX,NPRTN
      COMMON  NITER,KVORT,IJMP
      COMMON  NVJ,LNJ,LNI
      COMMON  VJ(12)
      COMMON  IIMD(7),JJMD(7),IIMR(7),JJMR(7)
      COMMON  CN,CS,CE,CW,ZW
      COMMON  VANGLE
      DT1(U1,U2,U3)=(U2-U3)/((U1-U2)*(U1-U3))
      DT2(U1,U2,U3)=(2.*U2-U1-U3)/((U2-U1)*(U2-U3))
      DT3(U1,U2,U3)=(U2-U1)/((U3-U1)*(U3-U2))
      YY(YN,YP)=1./(1.-(YP/YN)**2.)
C*****************************************************************
C     THIS SUBROUTINE CALCULATES MASS VELOCITIES G1,G2 ON THE BOUNDARIES
C     ZERO AXIAL GRADIENTS OF STREAM FUNCTION AND VORTICITY AT EXIT.
C*****************************************************************
      DO 1 J=JA,JB
      G1(1,J)=RO(1,J)*VINP(J)
    1 G2(1,J)=0.
      G1(IA,JN)=0.0
      G2(IA,JN)=0.0
      BB=YY(2.0*DELX1(IA+1),X1(IA+1)-X1(IA))
      JB2=JB+1
      DO 2 J=JB2,JNM
      G1(IA,J)=BB*G1(IA+1,J)-(BB-1.0)*G1(IA+2,J)
    2 G2(IA,J)=0.0
      DO 31 J=2,JNM
      FY1=DT1(X2(J-1),X2(J),X2(J+1))
      FY2=DT2(X2(J-1),X2(J),X2(J+1))
      FY3=DT3(X2(J-1),X2(J),X2(J+1))
      G1(IN,J)=(FY1*A(IN,J-1,NF)+FY2*A(IN,J,NF)+FY3*A(IN,J+1,NF))/R(J)
      G2(IN,J)=0.0
31    CONTINUE
      DX2=X2(2)-X2(1)
      FC1=2.0
      FC2=DX2
      IF(INDG.EQ.2) FC1=1.0
      IF(INDG.EQ.2) FC2=1.0
      IA2=IA+1
      DO 10 I=IA2,IN
      G1(I,1)=FC1*(A(1,2,NF)-A(I,1,NF))/(FC2*DX2)
   10 G2(I,1)=0.
      BB=YY((X2(JN)-X2(JNM-1)),(X2(JN)-X2(JNM)))
```

```
      IA1=IA+1
      DO 20 I=IA1,INM
      G1(I,JN)=0.0
      G2(I,JN)=0.0
20    CONTINUE
      IF (IA.EQ.1) GO TO 26
      DO 21 I=1,IA
      G1(I,JB)=0.
21    G2(I,JB)=0.
      DO 25 I=1,IA
      G1(I,JA)=0.0
   25 G2(I,JA)=0.0
   26 IF (JA.EQ.1)  GO TO 24
      DO 27 J=1,JA
      G1(IA,J)=0.0
   27 G2(IA,J)=0.0
   24 CONTINUE
      RETURN
      END
```

```
      SUBROUTINE MVELCT
      COMMON  A(16,14,7),G1(16,14),G2(16,14),RO(16,14),ZMU(16,14)
      COMMON  X1(16),X2(14),DELX1(16),DELX2(14),R(14)
      COMMON  ATITLE(12),ASYMBL(12),AGEOM(12),ANAME(6,10)
      COMMON  IMIN(14),IN,JN,INM,JNM,JA,JB,IA,IE
      COMMON  NW,NF,NVT,NZMM,NZML,NZMH,NP
      COMMON  ROREF,PREF,TREF,CPREF,ZMUREF
      COMMON  INDE(7),INDG,INDRO,INDZMU
      COMMON  ROWF
      COMMON  ZMUK,ZAA
      COMMON  STC,HC,HP,FMX
      COMMON  GLOB,ACTE,ZEX
      COMMON  PR(7),ZMW(3),GCPR,GC,ZJC
      COMMON  VINP(9),VING(9),VT(9)
      COMMON  RSDU(7),DIFMAX(7),RP(7),CC,DC,NMAX,NPRTN
      COMMON  NITER,KVORT,IJMP
      COMMON  NVJ,LNJ,LNI
      COMMON  VJ(12)
      COMMON  IIMD(7),JJMD(7),IIMR(7),JJMR(7)
      COMMON  CN,CS,CE,CW,ZW
      COMMON  VANGLE
      DT1(U1,U2,U3)=(U2-U3)/((U1-U2)*(U1-U3))
      DT2(U1,U2,U3)=(2.*U2-U1-U3)/((U2-U1)*(U2-U3))
      DT3(U1,U2,U3)=(U2-U1)/((U3-U1)*(U3-U2))
C*************************************************************************
C   THIS SUBR. CALCULATES G1 AND G2 AT ALL POINTS  NOT ON THE BOUND.
C*************************************************************************
      DO 30 J=2,JNM
      IL=IMIN(J)+1
      DO 30 I=IL,INM
      FY1=DT1(X2(J-1),X2(J),X2(J+1))
      FY2=DT2(X2(J-1),X2(J),X2(J+1))
      FY3=DT3(X2(J-1),X2(J),X2(J+1))
      FX1=DT1(X1(I-1),X1(I),X1(I+1))
      FX2=DT2(X1(I-1),X1(I),X1(I+1))
      FX3=DT3(X1(I-1),X1(I),X1(I+1))
      G1(I,J)=(FY1*A(I,J-1,NF)+FY2*A(I,J,NF)+FY3*A(I,J+1,NF))/R(J)
      G2(I,J)=(FX1*A(I-1,J,NF)+FX2*A(I,J,NF)+FX3*A(I+1,J,NF))/(-R(J))
   30 CONTINUE
      RETURN
      END
```

```
      SUBROUTINE FDEQCT(I,J,K)
      COMMON  A(16,14,7),G1(16,14),G2(16,14),RO(16,14),ZMU(16,14)
      COMMON  X1(16),X2(14),DELX1(16),DELX2(14),R(14)
      COMMON  ATITLE(12),ASYMBL(12),AGEOM(12),ANAME(6,10)
      COMMON  IMIN(14),IN,JN,INM,JNM,JA,JB,IA,IE
      COMMON  NW,NF,NVT,NZMM,NZML,NZMH,NP
      COMMON  RGREF,PREF,TREF,CPREF,ZMUREF
      COMMON  INDE(7),INDG,INDRO,INDZMU
      COMMON  ROWF
      COMMON  ZMUK,ZAA
      COMMON  STC,HC,HP,FMX
      COMMON  GLOB,ACTE,ZEX
      COMMON  PR(7),ZMW(3),GCPM,GC,ZJC
      COMMON  VINP(9),VING(9),VT(9)
      COMMON  RSDU(7),DIFMAX(7),RP(7),CC,DC,NMAX,NPRTN
      COMMON  NITER,KVORT,IJMP
      COMMON  NVJ,LNJ,LNI
      COMMON  VJ(12)
      COMMON  IIMD(7),JJMD(7),IIMR(7),JJMR(7)
      COMMON  CN,CS,CE,CW,ZW
      COMMON  VANGLE
      WC1H(WK,DELF,ROP,DELRO,RAD)=-(DELF/(DX2*DX2))
     4                           /(RAD*(ROP*(RAD/3.+5.*WK*DX2/24.)
     5                           +DELRO*(5.*RAD/24.+3.*WK*DX2/20.)))
      WC2H(WK,ROP,DELRO,RAD)=-(RAD+WK*DX2)*
     2                                 (ROP*(RAD/6.+WK*DX2/8.)
     3                                 +DELRO*(RAD/8.+WK*DX2/10.))
     4                           /(RAD*(ROP*(RAD/3.+5.*WK*DX2/24.)
     5                           +DELRO*(5.*RAD/24.+3.*WK*DX2/20.)))
      WC1V(DELF,ROP,DELRO,ETA2)=-DELF/(((ETA2*DX1)**2)*
     1                                (ROP/3.+5.*DELRO/24.))
      WC2V(ROP,DELRO)=-(ROP/6.+DELRO/8.)/(ROP/3.+5.*DELRO/24.)
      YY(YN,YP)=1./(1.-(YP/YN)**2.)
      DT1(U1,U2,U3)=(U2-U3)/((U1-U2)*(U1-U3))
      DT2(U1,U2,U3)=(2.*U2-U1-U3)/((U2-U1)*(U2-U3))
      DT3(U1,U2,U3)=(U2-U1)/((U3-U1)*(U3-U2))
C*************************************** ***************************************
C   FINITE DIFFERENCE EQUATION SUBROUTINE
C*************************************** ***************************************
      DO 10 J=2,JNM
      IL=IMIN(J)+1
      DO 10 I=IL,INM
      IF(K.EQ.NW.AND.(J.EQ.JA.AND.I.EQ.(IA+1))) GO TO 100
      IF (K.EQ.NW.AND.(J.EQ.JB.AND.I.EQ.(IA+1))) GO TO 100
      GO TO 110
C*****************************************************************************
C     CALCULATING VORTICITIES AT PTS. ONE MESH AWAY FROM PROTRUDING EDGES
C*****************************************************************************
100   CALL    SORCCT(1,J,NF,SOURCE,ZQ)
      CALL COEFCT(I,J,NF)
      ZZ=A(I,J,NW)
      XX=A(I,J,NF)*(CE+CW+CN+CS)
      XX=XX-(CE*A(I+1,J,NF)+CW*A(I-1,J,NF)+CN*A(I,J+1,NF)
     1    +CS*A(I,J-1,NF))
      A(I,J,NW)=(XX-SOURCE)/RO(I,J)+ZZ
      ISKP=2
```

```
      GO TO 222
110   CONTINUE
      CALL SORCCT(I,J,K,SOURCE,ZO)
      CALL COEFCT(I,J,K)
      IF(K.NE.NW) GO TO 2
C*************************************************************************
C***  INCORPORATING B.C. FOR VORTICITY IN THE FINITE DIFF. FORMULATION
C*************************************************************************
      ZW=0.
      ZWMU=0.0
      WKN=-1.
      WKP=1.0
      IF(INDG.EQ.2) WKN=0.0
      IF(INDG.EQ.2) WKP=0.0
      ISKP=2
      IF (I.EQ.IL.AND.J.LT.JA) GO TO 500
      IF (J.EQ.JNM.AND.I.GT.IA) GO TO 503
      IF (J.EQ.(JB-1).AND.I.LE.IA) GO TO 501
      IF(J.EQ.(JA+1).AND.I.LE.IA) GO TO 502
      IF (I.EQ.IL.AND.J.GT.JB) GO TO 504
      ISKP=1
      GO TO 999
  500 LIEW=I-1
      CQEW=CW
      DX1=ABS(X1(LIEW)-X1(I))
      A(LIEW,J,NW)=WC1V(A(I,J,NF)-A(LIEW,J,NF),RO(LIEW,J),
     1                  RO(I,J)-RO(LIEW,J), R(J))
      ZW=CQEW*WC2V(RO(LIEW,J),RO(I,J)-RO(LIEW,J))
      ZWMU=ZWMU+ZW*ZMU(LIEW,J)
      GO TO 999
501   LJNS=J+1
      WKNS=WKN
      IF (J.EQ.JB) RADNS=R(JB)
      IF (J.EQ.JNM) RADNS=R(JN)
      CQNS=CN
      GO TO 666
502   LJNS=J-1
      IF (JA.EQ.1) GO TO 999
      WKNS=WKP
      RADNS=R(JA)
      CQNS=CS
666   DX2=ABS(X2(LJNS)-X2(J))
      A(I,LJNS,NW)=WC1H(WKNS,A(I,J,NF)-A(I,LJNS,NF),RO(I,LJNS),
     1                  RO(I,J)-RO(I,LJNS),RADNS)
      ZW=CQNS*WC2H(WKNS,RO(I,LJNS),RO(I,J)-RO(I,LJNS),RADNS)
      ZWMU=ZWMU+ZW*ZMU(I,LJNS)
      GO TO 999
503   LJ=J+1
      BB=YY((X2(LJ)-X2(LJ-2)),(X2(LJ)-X2(LJ-1)))
      A(I,LJ,NW)=0.0
      ZW=0.
      ZWMU=0.
      GO TO 999
504   LI=I-1
      BB=YY((X1(LI+2)-X1(LI)),(X1(LI+1)-X1(LI)))
      A(LI,J,NW)=BB*A(LI+1,J,NW)-(BB-1.0)*A(LI+2,J,NW)
      ZW=0.
```

```
      ZWMU=0.
999   CONTINUE
C***********************************************************************
C***  END VORTICITY B.C. SPECIAL FORMULATION
C***********************************************************************
1     CONTINUE
      CALL  CONVEC(I,J,K,AU,ZU)
      ANUM=CE*ZMU(I+1,J)*A(I+1,J,K) +CW*ZMU(I-1,J)*A(I-1,J,K)
     2      +CN*ZMU(I,J+1)*A(I,J+1,K) +CS*ZMU(I,J-1)*A(I,J-1,K)
     3       +AU+SOURCE
      ADNM=(CE+CW+CN+CS)*ZMU(I,J)-ZWMU+ZU+ZQ
      GO TO 4
    2 IF(K.NE.NF) GO TO 3
      IF(K.EQ.NF.AND.(J.EQ.JA.AND.I.EQ.(IA+1))) GO TO 223
      IF (K.EQ.NF.AND.(J.EQ.JB.AND.I.EQ.(IA+1))) GO TO 223
      GO TO 224
  223 A(I,J,NF)=A(I-1,J,NF)
      GO TO 10
  224 CONTINUE
      ANUM=CE*A(I+1,J,K) +CW*A(I-1,J,K) +CN*A(I,J+1,K) +CS*A(I,J-1,K)
     2              +SOURCE
      ADNM=CE+CW+CN+CS     +ZQ
      GO TO 4
    3 CALL  CONVEC(I,J,K,AU,ZU)
      ANUM=CE*A(I+1,J,K) +CW*A(I-1,J,K) +CN*A(I,J+1,K) +CS*A(I,J-1,K)
     2       +AU+SOURCE
      ADNM=CE+CW+CN+CS+ZU+ZQ
    4 ZZ=A(I,J,K)
      A(I,J,K)=ANUM/ADNM
      COMP=0.0
      IF (K.EQ.NZMM.AND.A(I,J,K).LE.COMP) A(I,J,K)=0.0
  222 CONTINUE
      DIF=A(I,J,K)-ZZ
      IF(K.NE.NW) GO TO 750
      IF(ISKP.EQ.1) GO TO 750
      ANORM=A(I,J,K)
      GO TO 760
  750 ANORM=.25*(A(I,J+1,K)+A(I,J-1,K)+A(I+1,J,K)+A(I-1,J,K))
      IF(ABS(ANORM).LT.ABS(A(I,J,K))) ANORM=A(I,J,K)
      IF(K.EQ.NZMM.AND.ANORM.LT.3.0E-05) ANORM=3.0E-05
  760 IF(ABS(ANORM).LT.1.0E-10) GO TO 300
      RS=DIF/ANORM
      GO TO 310
  300 RS=0.0
  310 CONTINUE
      A(I,J,K)=ZZ+RP(K)*DIF
      IF(ABS(RS).LE.ABS(RSDU(K))) GO TO 60
      RSDU(K)=RS
      IIMR(K)=I
      JJMR(K)=J
   60 CONTINUE
      IF(ABS(DIF).LE.ABS(DIFMAX(K))) GO TO 65
      DIFMAX(K)=DIF
      IIMD(K)=I
      JJMD(K)=J
   65 CONTINUE
10    CONTINUE
      CALL BOUNCT(K)
      RETURN
      END
```

```
      SUBROUTINE SORCCT(I,J,K,SOURCE,ZQ)
      COMMON  A(16,14,7),G1(16,14),G2(16,14),RO(16,14),ZMU(16,14)
      COMMON  X1(16),X2(14),DELX1(16),DELX2(14),R(14)
      COMMON  ATITLE(12),ASYMBL(12),AGEOM(12),ANAME(6,10)
      COMMON  IMIN(14),IN,JN,INM,JNM,JA,JB,IA,IE
      COMMON  NW,NF,NVT,NZMM,NZML,NZMH,NP
      COMMON  ROREF,PREF,TREF,CPREF,ZMUREF
      COMMON  INDE(7),INDG,INDRO,INDZMU
      COMMON  ROWF
      COMMON  ZMUK,ZAA
      COMMON  STC,HC,HP,FMX
      COMMON  GLOB,ACTE,ZEX
      COMMON  PR(7),ZMW(3),GCPM,GC,ZJC
      COMMON  VINF(9),VING(9),VT(9)
      COMMON  RSDU(7),DIFMAX(7),RP(7),CC,DC,NMAX,NPRTN
      COMMON  NITER,KVORT,IJMP
      COMMON  NVJ,LNJ,LNI
      COMMON  VJ(12)
      COMMON  IIMD(7),JJMD(7),IIMR(7),JJMR(7)
      COMMON  CN,CS,CE,CW,ZW
      COMMON  VANGLE
C     SOURCE TERMS IN FINITE DIFFERENCE FORM
C*****************************************************************
      GO TO (1,2,4,31,3,3,3),K
   31 IF(INDE(NZMM).NE.1) GO TO 3
      IF(INDE(NZMM).EQ.1) GO TO 5
C*****************************************************************
C     FOR VORTICITY
C*****************************************************************
1     SOURCE=0.
      DEN=6.*DELX1(I)*DELX2(J)*R(J)
      S1=(RO(I,J+1)-RO(I,J-1))*(VS2(I+1,J)-VS2(I-1,J))
      S2=-(RO(I+1,J)-RO(I-1,J))*(VS2(I,J+1)-VS2(I,J-1))
      SOURCE=SOURCE+(S1+S2)/DEN
      IF(INDG.EQ.2) GO TO 25
      SOURCE=SOURCE+2.*ZMU(I,J)*(A(I,J+1,NW)-A(I,J-1,NW))/
     1                    ((X2(J+1)-X2(J-1))*R(J))
      IF(INDE(NVT).EQ.1) SOURCE=SOURCE+(RO(I+1,J)*(A(I+1,J,NVT)**2)
     1     -RO(I-1,J)*(A(I-1,J,NVT)**2))/((X1(I+1)-X1(I-1))*R(J)*R(J))
   25 CONTINUE
      ZQ=0.
      RETURN
C*****************************************************************
C     FOR STREAM FUNCTION
C*****************************************************************
2     SOURCE=RO(I,J)*A(I,J,NW)
      S1=(RO(I+1,J)-RO(I-1,J))*(A(I+1,J,NF)-A(I-1,J,NF))
      S1=S1/((X1(I+1)-X1(I-1))**2)
      S2=(RO(I,J+1)-RO(I,J-1))*(A(I,J+1,NF)-A(I,J-1,NF))
      S2=S2/((X2(J+1)-X2(J-1))**2)
      SOURCE=SOURCE-(S1+S2)/(R(J)*R(J)*RO(I,J))
      ZQ=0.
      RETURN
C*****************************************************************
C     FOR OTHER DEPENDENT VARIABLES
3     SOURCE=0.
```

```
      ZG=0.
      RETURN
C*****************************************************************
C     FOR SWIRL VELOCITY
C*****************************************************************
4     ZG=0.
      SOURCE=-(ZMU(I,J)/R(J)+(ZMU(I,J+1)-ZMU(I,J-1))/(X2(J+1)-X2(J-1))
     1        +G2(I,J))*A(I,J,NVT)/R(J)
      RETURN
C*****************************************************************
C     FOR FUEL MASS FRACTION
C*****************************************************************
    5 CONTINUE
      AFU=A(I,J,NZMM)
      AFH=A(I,J,NZML)
      IF (HC.LE.0.0) GO TO 350
      IF(AFU.LE.0.0) GO TO 350
      IF (INDE(NZMH).EQ.1) GO TO 100
      FOX=STC*(AFU-AFH*FMX)
      GO TO 150
  100 AFF=A(I,J,NZMH)
      FOX=STC*(AFU-AFF*FMX)
  150 IF(FOX.LE.0.0) GO TO 350
      TEMP=(AFH*HP-AFU*HC)/CPREF
      IF (TEMP.GE.300) GO TO 250
      TEMP=TREF
  250 CONTINUE
      FIP=1.0-FOX-AFU
      ZMEAN=1.0/(AFU/ZMW(1)+FOX/ZMW(2)+FIP/ZMW(3))
      TEMP=TEMP+460.
      SORC=(PREF*ZMEAN)/(TEMP*GCPM)
      SORC=SORC*SORC
      SORC=SORC*GLOB*AFU*FOX*(TEMP**.5)
      SORC=SORC/(EXP(ZEX/TEMP))
      RPSO=1.0
      SOURCE=-RPSO*SORC
      ZG=0.0
      RETURN
  350 ZG=0.0
  450 SOURCE=0.0
      RETURN
      END
```

```
      SUBROUTINE COEFCT(I,J,K)
      COMMON  A(16,14,7),G1(16,14),G2(16,14),RO(16,14),ZMU(16,14)
      COMMON  X1(16),X2(14),DELX1(16),DELX2(14),R(14)
      COMMON  ATITLE(12),ASYMBL(12),AGEOM(12),ANAME(6,10)
      COMMON  IMIN(14),IN,JN,INM,JNM,JA,JB,IA,IE
      COMMON  NV,NF,NVT,NZMM,NZML,NZMH,NP
      COMMON  ROREF,PREF,TREF,CPREF,ZMUREF
      COMMON  INDE(7),INDG,INDRO,INDZMU
      COMMON  ROWF
      COMMON  ZMUK,ZAA
      COMMON  STC,HC,HP,FMX
C*************************************************************
C     FOR FUEL MASS FRACTION
C*************************************************************
      COMMON  GLOB,ACTE,ZEX
      COMMON  PR(7),ZMW(3),GCPM,GC,ZJC
      COMMON  VINP(9),VING(9),VT(9)
      COMMON  RSDU(7),DIFMAX(7),RP(7),CC,DC,NMAX,NPRIN
      COMMON  NITER,KVORT,IJMP
      COMMON  NVJ,LNJ,LNI
      COMMON  VJ(12)
      COMMON  IIMD(7),JJMD(7),IIMR(7),JJMR(7)
      COMMON  CN,CS,CE,CW,ZW
      COMMON  VANGLE
      DIMENSION D(6)
C*************************************************************
C     CALCULATE C'S FOR CYLINDRICAL COORDS AND UNIFORM RECTANGULAR MESH
C*************************************************************
C*************************************************************
C     FOR VORTICITY
C*************************************************************
      IF(K.NE.NV) GO TO 2
      DO 10 L=1,5
10    D(L)=1.
      GO TO 20
C*************************************************************
C     FOR STREAM FUNCTION
C*************************************************************
2     IF(K.NE.NF) GO TO 3
      D(1)=1./(R(J)*R(J))
      D(2)=D(1)
      D(4)=D(1)
      GO TO 60
C*************************************************************
C     FOR SWIRL VELOCITY
C*************************************************************
3     IF(K.NE.NVT) GO TO 15
      D(1)=ZMU(I  ,J  )
      D(2)=ZMU(I+1,J  )
      D(3)=ZMU(I  ,J+1)
      D(4)=ZMU(I-1,J  )
      D(5)=ZMU(I  ,J-1)
      GO TO 20
C*************************************************************
C     FOR OTHER DEPENDENT VARIABLES
C*************************************************************
```

```
15      D(1)=ZMU(I  ,J  )/PR(K)
        D(2)=ZMU(I+1,J  )/PR(K)
        D(3)=ZMU(I  ,J+1)/PR(K)
        D(4)=ZMU(I-1,J  )/PR(K)
        D(5)=ZMU(I  ,J-1)/PR(K)
20      CONTINUE
        CE=(D(2)+D(1))/((X1(I+1)-X1(I))*2.*DELX1(I))
        CW=(D(1)+D(4))/((X1(I)-X1(I-1))*2.*DELX1(I))
        CN=(D(3)*R(J+1)/R(J)+D(1))/((X2(J+1)-X2(J))*2.*DELX2(J))
        CS=(D(1)+D(5)*R(J-1)/R(J))/((X2(J)-X2(J-1))*2.*DELX2(J))
        GO TO 50
   40   CONTINUE
        CE=(D(2)+D(1))/((X1(I+1)-X1(I))*2.*DELX1(I))
        CW=(D(1)+D(4))/((X1(I)-X1(I-1))*2.*DELX1(I))
        CN=2.0/((R(J+1)+R(J)+R(J)+R(J))*(X2(J+1)-X2(J))*DELX2(J))
        CS=2.0/((R(J-1)+R(J)+R(J)+R(J))*(X2(J)-X2(J-1))*DELX2(J))
50      CONTINUE
        RETURN
        END
```

```
      SUBROUTINE CONVEC(I,J,K,AU,ZU)
      COMMON  A(16,14,7),G1(16,14),G2(16,14),RO(16,14),ZMU(16,14)
      COMMON  X1(16),X2(14),DELX1(16),DELX2(14),R(14)
      COMMON  ATITLE(12),ASYMBL(12),AGEOM(12),ANAME(6,10)
      COMMON  IMIN(14),IN,JN,INM,JNM,JA,JB,IA,IE
      COMMON  NW,NF,NVT,NZMM,NZML,NZMH,NP
      COMMON  ROREF,PREF,TREF,CPREF,ZMUREF
      COMMON  INDE(7),INDG,INDRO,INDZMU
      COMMON  ROWF
      COMMON  ZMUK,ZAA
      COMMON  STC,HC,HP,FMX
      COMMON  GLOB,ACTE,ZEX
      COMMON  PR(7),ZMW(3),GCPM,GC,ZJC
      COMMON  VINP(9),VING(9),VT(9)
      COMMON  RSDU(7),DIFMAX(7),RP(7),CC,DC,NMAX,NPRTN
      COMMON  NITER,KVORT,IJMP
      COMMON  NVJ,LNJ,LNI
      COMMON  VJ(12)
      COMMON  IIMD(7),JJMD(7),IIMR(7),JJMR(7)
      COMMON  CN,CS,CE,CW,ZW
      COMMON  VANGLE
C     TANK-AND-TUBE FORMULATUON OF THE CONVECTUON TERM
      DX1=DELX1(I)
      DX2=DELX2(J)
      GM1E=0.25*(A(I,J+1,NF)-A(I,J-1,NF)+A(I+1,J+1,NF)-A(I+1,J-1,NF))
     1   /(R(J)*DX2)
      GM1W=0.25*(A(I,J+1,NF)-A(I,J-1,NF)+A(I-1,J+1,NF)-A(I-1,J-1,NF))
     1   /(R(J)*DX2)
      GM2S=-0.25*(A(I+1,J,NF)-A(I-1,J,NF)+A(I+1,J-1,NF)-A(I-1,J-1,NF))
     1     /(R(J)*DX1)
      GM2N=-0.25*(A(I+1,J,NF)-A(I-1,J,NF)+A(I+1,J+1,NF)-A(I-1,J+1,NF))
     1     /(R(J)*DX1)
      AU=0.
      ZU=0.
      IL=IMIN(J)+1
      IF(GM1W)1,3,2
1     ZU=-GM1W/DX1
      GO TO 3
2     AU=GM1W*A(I-1,J,K)/DX1
      IF(K.EQ.NW.AND.(I.EQ.IL.AND.J.LE.JA)) GO TO 500
3     IF(GM2S)4,6,5
4     ZU=ZU-GM2S/DX2
      GO TO 6
5     AU=AU+GM2S*A(I,J-1,K)/DX2
      IF(K.EQ.NW.AND.(I.LE.IA.AND.J.EQ.(JA+1))) GO TO 501
6     IF(GM1E)7,9,8
7     AU=AU-GM1E*A(I+1,J,K)/DX1
      GO TO 9
8     ZU=ZU+GM1E/DX1
9     IF(GM2N)10,11,11
10    AU=AU-GM2N*A(I,J+1,K)/DX2
      IF (K.EQ.NW.AND.J.EQ.JNM.OR.J.EQ.(JB-1)) GO TO 503
      RETURN
11    ZU=ZU+GM2N/DX2
      RETURN
500   ZU=ZU-GM1W*ZW/(CW*DX1)
      GO TO 3
501   ZU=ZU-GM2S*ZW/(CS*DX2)
      GO TO 6
503   ZU=ZU+GM2N*ZW/(CN*DX2)
      RETURN
      END
```

```
      SUBROUTINE   BCONDT(K)
      COMMON  A(16,14,7),G1(16,14),G2(16,14),RO(16,14),ZMU(16,14)
      COMMON  X1(16),X2(14),DELX1(16),DELX2(14),R(14)
      COMMON  ATITLE(12),ASYMBL(12),AGEOM(12),ANAME(6,10)
      COMMON  IMIN(14),IN,JN,INM,JNM,JA,JB,IA,IE
      COMMON  NW,NF,NVT,NZMM,NZML,NZMH,NP
      COMMON  ROREF,PREF,TREF,CPPEF,ZMUREF
      COMMON  INDE(7),INDG,INDRO,INDZMU
      COMMON  ROWF
      COMMON  ZMUK,ZAA
      COMMON  STC,HC,HP,FMX
      COMMON  GLOB,ACTE,ZEX
      COMMON  PR(7),ZMW(3),GCPM,GC,ZJC
      COMMON  VINP(9),VING(9),VT(9)
      COMMON  RSDU(7),DIFMAX(7),RP(7),CC,DC,NMAX,NPR,N
      COMMON  NITER,KVORT,IJMP
      COMMON  NVJ,LNJ,LNI
      COMMON  VJ(12)
      COMMON  IIMD(7),JJMD(7),IIMR(7),JJMR(7)
      COMMON  CN,CS,CE,CW,ZW
      COMMON  VANGLE
      WVW(    DELF,WQ,ROP,DELRO,ETA2)= -(    DELF/((ETA2*DX1)**2)
     1                                  +WQ*(ROP/6.+DELRO/8.))
     2                                 /(ROP/3.+5.*DELRO/24.)
      WHW(WK,DELF,WQ,ROP,DELRO,RAD)=  -(    DELF/(DX2*DX2)
     1                                 +WQ*(RAD+WK*DX2)*
     1                                 (ROP*(RAD/6.+WK*DX2/8.)
     3                                  +DELRO*(RAD/8.+WK*DX2/10.)))
     4                          /(RAD*(ROP*(RAD/3.+5.*WK*DX2/24.)
     5                          +DELRO*(5.*RAD/24.+3.*WK*DX2/20.)))
      DT1(U1,U2,U3)=(U2-U3)/((U1-U2)*(U1-U3))
      DT2(U1,U2,U3)=(2.*U2-U1-U3)/((U2-U1)*(U2-U3))
      DT3(U1,U2,U3)=(U2-U1)/((U3-U1)*(U3-U2))
      YY(YN,YP)=1./(1.-(YP/YN)**2)
C*************************************************************************
C     BOUNDARY CONDITION SUBROUTINE FOR ALL DEPENDENT VARIABLES.
C*************************************************************************


      GO TO (1,2,3,4,5,6,6),K
C*************************************************************************
C     FOR VORTICITY.....A(I,J,NW)
C*************************************************************************
1     CONTINUE
      WKN=-1.
      WKP=1.
      IF(INDG.EQ.2) WKN=0.0
      IF(INDG.EQ.2) WKP=0.0
      IF(KVORT.NE.111) GO TO 111
      DX2=X2(JB)-X2(JB-1)
      DO  11 I=1,IA
11    A(I,JB,NW)=WHW(WKN,A(I,JB-1,NF)-A(I,JB,NF),A(I,JB-1,NW),RO(I,JB),
     1               RO(I,JB-1)-RO(I,JB),R(JB))
      IA1=IA+1
      DO 12 I=IA1,INM
12    A(I,JN,NW)=0.0
```

```
      IF (JA.EQ.1) GO TO 169
      JA1=JA-1
      DX1=X1(IA+1)-X1(IA)
      IF (JA.EQ.2) JA1=JA
      BB=YY(2.*DELX1(IA+1),X1(IA+1)-X1(IA))
      DO 102 J=2,JA1
  102 A(IA,J,NW)=WVW(A(IA+1,J,NF)-A(IA,J,NF),A(IA+1,J,NW),
     1       RO(IA,J),RO(IA+1,J)-RO(IA,J), R(J))
  169 JB2=JB+1
      BB=YY(2.*DELX1(IA+1),X1(IA+1)-X1(IA))
      DO 171 J=JB2,JNM
171   A(IA,J,NW)=BB*A(IA+1,J,NW)-(BB-1.)*A(IA+2,J,NW)
      A(IA,JN,NW)=0.0
      A(IA,1,NW)=0.0
      IF (JA.EQ.1) GO TO 111
      DX2=X2(JA+1)-X2(JA)
      DO 101 I=1,IA
  101 A(I,JA,NW)=WHW(WKP,A(I,JA+1,NF)-A(I,JA,NF),A(I,JA+1,NW),
     1       RO(I,JA),RO(I,JA+1)-RO(I,JA),R(JA))
111   IA2=IA+1
      IF(INDG.EQ.2) GO TO 155
      DO 10 I=IA2,IN
      A(I,1,NW)=0.0
   10 CONTINUE
      GO TO 157
  155 DO 156 I=IA2,IN
  156 A(I,1,NW)=0.0
  157 CONTINUE
      I=IN
      BB=YY(2.*DELX1(I-1),X1(I)-X1(I-1))
      DO 170 J=2,JN
170   A(I,J,NW)=BB*A(I-1,J,NW)-(BB-1.)*A(I-2,J,NW)
100   CONTINUE
      RETURN
C*****************************************************************
C   FOR STREAM FUNCTION..... A(I,J,NF)
C*****************************************************************
2     CONTINUE
      DO 200 I=1,IA
200   A(I,JB,NF)=A(1,JB,NF)
      JB2=JB+1
      DO 205 J=JB2,JN
      DXH2=0.5*(X2(J)-X2(J-1))
      DTH2=DXH2*(R(J-1)*G1(IA,J-1)+R(J)*G1(IA,J))
      A(IA,J,NF)=A(IA,J-1,NF)
      COMP=0.0
205   IF (DTH2.GT.COMP)  A(IA,J,NF)=A(IA,J,NF)+DTH2
      DO 202 I=1,IA
  202 A(I,JA,NF)=A( 1,JA,NF)
      DO 204 J=1,JA
  204 A(IA,J,NF)=A(IA,JA,NF)
      IA1=IA+1
      BB=YY(2.*DELX2(JN-1),X2(JN)-X2(JN-1))
      DO 201 I=IA1,IN
      A(I,JN,NF)=BB*A(I,JN-1,NF)-(BB-1.0)*A(I,JN-2,NF)
      IF (A(I,JN,NF).LE.A(I-1,JN,NF))  A(I,JN,NF)=A(I-1,JN,NF)
201   CONTINUE
```

```
      DO 212 I=IA,IN
  212 A(I,1,NF)=A(IA,1,NF)
  216 CONTINUE
      BB=YY(2.*DELX1(IN-1),X1(IN)-X1(IN-1))
      DO 220 J=2,JNM
  220 A(IN,J,NF)=BB*A(IN-1,J,NF)-(BB-1.)*A(IN-2,J,NF)
299   RETURN
C*****************************************************************
C   FOR SWIRL VELOCITY
C*****************************************************************
3     CONTINUE
      BB=YY(2.*DELX1(IN-1),X1(IN)-X1(IN-1))
      DO 301 J=1,JN
      A(IN,J,NVT)=BB*A(IN-1,J,NVT)-(BB-1.)*A(IN-2,J,NVT)
301   CONTINUE
      RETURN
C*****************************************************************
C    FOR FUEL MASS FRACTION AND DIMENSIONLESS ENTHALPY
C    FOR MIXTURE FRACTION
C*****************************************************************
4     CONTINUE
      IF  (JA.EQ.1)  GO  TO  401
      BB=YY(2.*DELX1(IA+1),X1(IA+1)-X1(IA))
      JA1=JA-1
      DO 402 J=1,JA1
      A(IA,J,NZMM)=BB*A(IA+1,J,NZMM)-(BB-1.)*A(IA+2,J,NZMM)
      IF (A(IA,J,NZMM).LT.0.0)  A(IA,J,NZMM)=0.0
402   CONTINUE
401   CONTINUE
      BB=YY(2.*DELX2(JN-1),X2(JN)-X2(JN-1))
      IA1=IA+1
      DO 403 I=IA1,IN
      A(I,JN,NZMM)=BB*A(I,JN-1,NZMM)-(BB-1.)*A(I,JN-2,NZMM)
      IF (A(I,JN,NZMM).LE.0.0)  A(I,JN,NZMM)=0.0
      IA3=6
      IF (I.LE.IA3)  A(I,JN,NZMM)=A(I-1,JN,NZMM)
403   CONTINUE
      BB=YY((X2(JA+2)-X2(JA)),(X2(JA+1)-X2(JA)))
      IF (IA.EQ.1) GO TO 410
      DO 405 I=2,IA
405   A(I,JA,NZMM)=BB*A(I,JA+1,NZMM)-(BB-1.)*A(I,JA+2,NZMM)
410   CONTINUE
      BB=YY(2.*DELX2(JB-1),X2(JB)-X2(JB-1))
      IF (IA.EQ.1) GO TO 404
      DO 406 I=2,IA
406   A(I,JB,NZMM)=BB*A(I,JB-1,NZMM)-(BB-1.)*A(I,JB-2,NZMM)
404   CONTINUE
      JB2=JB+1
      DO 407 J=JB2,JN
      A(IA,J,NZMM)=0.0
407   CONTINUE
      BB=YY(2.*DELX2(2),X2(2)-X2(1))
      IA2=IA+1
      DO 408 I=IA2,IN
      A(I,1,NZMM)=BB*A(I,2,NZMM)-(BB-1.)*A(I,3,NZMM)
      IF (A(I,1,NZMM).LT.0.0) A(I,1,NZMM)=0.5*(A(I,1,NZMM)+A(I,2,NZMM))
      IF (A(I,1,NZMM).LT.0.0) A(I,1,NZMM)=0.5*(A(I,1,NZMM)+A(I,2,NZMM))
```

```
      IF (A(I,1,NZMM).LT.0.0) A(I,1,NZMM)=A(I,2,NZMM)
408   CONTINUE
      BB=YY(2.*DELX1(IN-1),X1(IN)-X1(IN-1))
      DO 409 J=2,JNM
      A(IN,J,NZMM)=BB*A(IN-1,J,NZMM)-(BB-1.)*A(IN-2,J,NZMM)
      IF (A(IN,J,NZMM).LE.0.0) A(IN,J,NZMM)=A(IN-1,J,NZMM)
409   CONTINUE
      RETURN
5     CONTINUE
      REFVL=CPREF*(TREF-460.)/HP
      IF (JA.EQ.1) GO TO 501
      BB=YY(2.*DELX1(IA+1),X1(IA+1)-X1(IA))
      JA1=JA-1
      DO 502 J=1,JA1
      A(IA,J,NZML)=BB*A(IA+1,J,NZML)-(BB-1.)*A(IA+2,J,NZML)
502   CONTINUE
501   CONTINUE
      BB=YY(2.*DELX2(JN-1),X2(JN)-X2(JN-1))
      IA1=IA+1
      DO 503 I=IA1,IN
      A(I,JN,NZML)=BB*A(I,JN-1,NZML)-(BB-1.)*A(I,JN-2,NZML)
      IF (A(I,JN,NZML).LE.REFVL) A(I,JN,NZML)=REFVL
      IA3=6
      IF (I.LE.IA3) A(I,JN,NZML)=A(I-1,JN,NZML)
503   CONTINUE
      BB=YY((X2(JA+2)-X2(JA)),(X2(JA+1)-X2(JA)))
      IF (IA.EQ.1) GO TO 510
      DO 505 I=2,IA
505   A(I,JA,NZML)=BB*A(I,JA+1,NZML)-(BB-1.)*A(I,JA+2,NZML)
510   CONTINUE
      BB=YY(2.*DELX2(JB-1),X2(JB)-X2(JB-1))
      IF (IA.EQ.1) GO TO 504
      DO 506 I=2,IA
506   A(I,JB,NZML)=BB*A(I,JB-1,NZML)-(BB-1.)*A(I,JB-2,NZML)
504   CONTINUE
      JB2=JB+1
      DO 507 J=JB2,JN
      A(IA,J,NZML)=CPREF*(TREF-460.)/HP
507   CONTINUE
      BB=YY(2.*DELX2(2),X2(2)-X2(1))
      IA2=IA+1
      DO 508 I=IA2,IN
      A(I,1,NZML)=BB*A(I,2,NZML)-(BB-1.)*A(I,3,NZML)
      IF (A(I,1,NZML).LT.0.0) A(I,1,NZML)=0.5*(A(I,1,NZML)+A(I,2,NZML))
      IF (A(I,1,NZML).LT.0.0) A(I,1,NZML)=0.5*(A(I,1,NZML)+A(I,2,NZML))
      IF (A(I,1,NZML).LT.0.0) A(I,1,NZML)=A(I,2,NZML)
508   CONTINUE
      BB=YY(2.*DELX1(IN-1),X1(IN)-X1(IN-1))
      DO 509 J=2,JNM
      A(IN,J,NZML)=BB*A(IN-1,J,NZML)-(BB-1.)*A(IN-2,J,NZML)
      IF (A(IN,J,NZML).LE.0.0) A(IN,J,NZML)=A(IN-1,J,NZML)
509   CONTINUE
      RETURN
    6 CONTINUE
      RETURN
      END
```

```
      SUBROUTINE PRINCT(IEND,ITAB)
      COMMON  A(16,14,7),G1(16,14),G2(16,14),RO(16,14),ZMU(16,14)
      COMMON  X1(16),X2(14),DELX1(16),DELX2(14),R(14)
      COMMON  ATITLE(12),ASYMBL(12),AGEOM(12),ANAME(6,10)
      COMMON  IMIN(14),II,JN,IIN,JN1,JA,JB,IA,IE
      COMMON  NP,NF,NT,NZMM,NZML,NZMH,NP
      COMMON  RUREF,RKEF,TREF,CPREF,ZMUREF
      COMMON  INDE(7),INDG,INDRO,INDZMU
      COMMON  RUF
      COMMON  ZMUK,ZMA
      COMMON  STC,RC,RP,FMA
      COMMON  GLOB,ACTE,ZEA
      COMMON  PR(7),ZM(3),GCPR,GC,ZJC
      COMMON  VINP(9),VING(9),VT(9)
      COMMON  RSDU(7),DIFMAX(7),RP(7),CC,DC,NMAX,NPRIN
      COMMON  NITER,NVORT,IJMP
      COMMON  NVO,LNO,LN1
      COMMON  VO(12)
      COMMON  IIMO(7),JJMO(7),IIMR(7),JJMR(7)
      COMMON  CN,CS,CE,CW,ZW
      COMMON  VANGLE
C*****************************************************************
C     THIS SUBROUTINE PRINTS OUT PART OF THE RESULTS FOR EASY EXAMINATIO
C*****************************************************************
      IT=IE+1
      IDM=INDE(NZMM)
      IDL=INDE(NZML)
      IDH=INDE(NZMH)
      IF(IDM.EQ.1.AND.(IDL.NE.1.AND.IDH.NE.1)) IT=IE+2
      IF(IDM.EQ.1.AND.(IDL.EQ.1.AND.IDH.NE.1)) IT=IE+2
      IF(IDM.EQ.1.AND.(IDL.NE.1.AND.IDH.EQ.1)) IT=IE+2
      IF(IDM.EQ.1.AND.(IDL.EQ.1.AND.IDH.EQ.1)) IT=IE+1
      IT=IE
70    CONTINUE
80    CONTINUE
      IF(INDE(NP).EQ.1) IT=IT+1
      ITAB=IT
      JX=1
      IX=1
      DO 10 K=1,IT
      IF(IEND.EQ.222) GO TO 82
   81 IF(K.GT.IE) GO TO 10
   82 CONTINUE
      PRINT 100,(ANAME(L,K),L=1,6),NITER
      DO 5 JJ=1,JN,JX
      J=JN+1-JJ
      II1=IMIN(J)
      II2=IN
    4 CONTINUE
      IEMPTY=(II1-1)/IX
      IF(IEMPTY.GE.1) GO TO 3
      PRINT 101,J,(A(I,J,K),I=II1,II2,IX)
      GO TO 2
3     GO TO (31,32,33,34,35),IEMPTY
31    PRINT 201 ,J,(A(I,J,K),I=II1,II2,IX)
      GO TO 2
```

```
      PRINT 202 ,J,(A(I,J,K),I=II1,II2,IX)
      GO TO 2
33    PRINT 203 ,J,(A(I,J,K),I=II1,II2,IX)
      GO TO 2
34    PRINT 204 ,J,(A(I,J,K),I=II1,II2,IX)
      GO TO 2
35    PRINT 205 ,J,(A(I,J,K),I=II1,II2,IX)
2     CONTINUE
    5 CONTINUE
      PRINT 102,(I,I=1,IN,IX)
      IF (K.EQ.NW) PRINT 105 , INDG
10    CONTINUE
100   FORMAT(1H1,35X,21HTHE  DISTRIBUTION  OF.6A6//
     1   ,2X,23HNUMBER  OF  ITERATION =,I5//)
  102 FORMAT(1H0,//,11(I11),/,11(I11),/,11(I11))
  101 FORMAT(1H0,I2,2X,11(1PE11.3),/,4X,11(1PE11.3),/,4X,11(1PE11.3))
  201 FORMAT(1H0,I2,13X,10(1PE11.3),/,4X,11(1PE11.3),/,4X,11(1PE11.3))
  202 FORMAT(1H0,I2,24X, 9(1PE11.3),/,4X,11(1PE11.3),/,4X,11(1PE11.3))
  203 FORMAT(1H0,I2,35X, 8(1PE11.3),/,4X,11(1PE11.3),/,4X,11(1PE11.3))
  204 FORMAT(1H0,I2,46X, 7(1PE11.3),/,4X,11(1PE11.3),/,4X,11(1PE11.3))
  205 FORMAT(1H0,I2,57X, 6(1PE11.3),/,4X,11(1PE11.3),/,4X,11(1PE11.3))
  105 FORMAT(1H 10X,7HINDG = ,I2)
      RETURN
      END
```

```
      SUBROUTINE TABUCT(ITAB)
      COMMON  A(16,14,7),G1(16,14),G2(16,14),RO(16,14),ZMU(16,14)
      COMMON  X1(16),X2(14),DELX1(16),DELX2(14),R(14)
      COMMON  ATITLE(12),ASYMBL(12),AGEOM(12),ANAME(6,10)
      COMMON  IMIN(14),IN,JN,INM,JNM,JA,JB,IA,IE
      COMMON  NW,NF,NVT,NZMM,NZML,NZMH,NP
      COMMON  ROREF,PREF,TREF,CPREF,ZMUREF
      COMMON  INDE(7),INDG,INDRO,INDZMU
      COMMON  ROWF
      COMMON  ZMUK,ZAA
      COMMON  STC,HC,HP,FMX
      COMMON  GLOB,ACTE,ZEX
      COMMON  PR(7),ZMW(3),GCPM,GC,ZJC
      COMMON  VINP(9),VING(9),VT(9)
      COMMON  RSDU(7),DIFMAX(7),RP(7),CC,DC,NMAX,NPRTN
      COMMON  NITER,KVORT,IJMP
      COMMON  NVJ,LNJ,LNI
      COMMON  VJ(12)
      COMMON  IIMD(7),JJMD(7),IIMR(7),JJMR(7)
      COMMON  CN,CS,CE,CW,ZW
      COMMON  VANGLE
      DIMENSION   TMPR(16,14)
C*****************************************************************
C   THIS SUBR. TABULATES THE COMPLETE SET OF RESULTS
C   TEMPERATURE STORED SEPARATELY
C*****************************************************************
      IQ=ITAB
      IF(ITAB.EQ.7) IQ=6
      IF (HC.LE.0.0) GO TO 71
      DO 70 J=1,JN
      IL=IMIN(J)
      DO 70 I=IL,IN
      TMPR(I,J)=T(I,J)
      TMPR(I,J)=(5*(TMPR(I,J)-32))/9
70    CONTINUE
71    CONTINUE
      IF (HC.LE.0.0) GO TO 9
      PRINT105,(ASYMBL(K),K=1,IQ)
      GO TO 8
9     PRINT 101 ,(ASYMBL(K),K=1,IQ)
8     CONTINUE
      ILINE=0
      DO 1 J=1,JN
      IL=IMIN(J)
      DO 1 I=1,IN
      ILINE=ILINE+1
      IF (I.LT.IL) PRINT 104,I,J
      IF(I.LT.IL) GO TO 10
      W=A(1,J,1)*R(J)
      V1=G1(I,J)/RO(I,J)
      V2=G2(I,J)/RO(I,J)
      IF (HC.LE.0.0) GO TO 7
      PRINT 102,I,J,V1,V2,RO(I,J),ZMU(I,J),TMPR(I,J),W,(A(I,J,K),K=2,IQ)
      GO TO 10
7     PRINT   102, I,J,V1,V2,RO(I,J),ZMU(I,J),W,(A(I,J,K),K=2,IQ)
   10 CONTINUE
      IF(ILINE/IN*IN.EQ.ILINE) PRINT  103
      IF (HC.LE.0.0) GO TO 6
      IF(IN.LT.19.AND.ILINE/(3*IN)*(3*IN).EQ.ILINE) PRINT  105,
     2(ASYMBL(K),K=1,IQ)
      GO TO 5
6     IF(IN.LT.19.AND.ILINE/(3*IN)*(3*IN).EQ.ILINE) PRINT  101,
     2(ASYMBL(K),K=1,IQ)
5     CONTINUE
```

```
      IF(IN.LT.22) GO TO 1
      IF (NC.LE.0.0) GO TO 4
      IF(IN.LE.22.AND.ILINE/(2*IN)*(2*IN).EQ.ILINE) PRINT 105,
     2(ASYMBL(K),K=1,IQ)
      GO TO 3
4     IF(IN.LE.22.AND.ILINE/(2*IN)*(2*IN).EQ.ILINE) PRINT 101,
     2(ASYMBL(K),K=1,IQ)
3     CONTINUE
      IF (NC.LE.0.0) GO TO 11
      IF(IN.LE.22) GO TO 1
      IF(ILINE/55*55.EQ.ILINE) PRINT 105,
     2(ASYMBL(K),K=1,IQ)
      GO TO 1
11    IF(ILINE/55*55.EQ.ILINE) PRINT 101,
     2(ASYMBL(K),K=1,IQ)
1     CONTINUE
105   FORMAT(7H1  I  J,44H        V1          V2       DENSITY     VISC  ,
     1  11H  TEMP(OC) ,8(5X,A6))
 101  FORMAT(7H1  I  J,44H        V1          V2       DENSITY     VISC  ,
     1 8(5X,A6))
 102  FORMAT(1H ,2I3,11(1PE11.3))
103   FORMAT(1H )
 104  FORMAT(1H ,2(I5))
      RETURN
      END
```

```
      SUBROUTINE DENSCT
      COMMON  A(16,14,7),G1(16,14),G2(16,14),RO(16,14),ZMU(16,14)
      COMMON  X1(16),X2(14),DELX1(16),DELX2(14),R(14)
      COMMON  ATITLE(12),ASYMBL(12),AGEOM(12),ANAME(6,10)
      COMMON  IMIN(14),IN,JN,INM,JNM,JA,JB,IA,IE
      COMMON  NW,NF,NVT,NZMM,NZML,NZMH,NP
      COMMON  ROREF,PREF,TREF,CPREF,ZMUREF
      COMMON  INDE(7),INDG,INDRO,INDZMU
      COMMON  ROWF
      COMMON  ZMUK,ZAA
      COMMON  STC,HC,HP,FMX
      COMMON  GLOB,ACTE,ZEX
      COMMON  PR(7),ZMW(3),GCPM,GC,ZJC
      COMMON  VINP(9),VING(9),VT(9)
      COMMON  RSDU(7),DIFMAX(7),PP(7),CC,DC,NMAX,NPRTN
      COMMON  NITER,KVORT,IJMP
      COMMON  NVJ,LNJ,LNI
      COMMON  VJ(12)
      COMMON  IIMD(7),JJMD(7),IIMR(7),JJMR(7)
      COMMON  CN,CS,CE,CW,ZW
      COMMON  VANGLE
C*****************************************************************
C   MIXTURE DENSITY CALCULATION
C*****************************************************************
      DO 40 J=1,JN
      IL=IMIN(J)
      DO 40 I=IL,IN
      AFU=A(I,J,NZMM)
      IF(AFU.GT.1.) AFU=1.0
      IF(AFU.GT.-1.0E-5) GO TO 15
      AFU=0.0
15    CONTINUE
      IF (AFU.LE.1.0E-20) AFU=0.0
      AFH=A(I,J,NZML)
      TEMP=(AFH*HP-AFU*HC)/CPREF
   50 CONTINUE
      IF (INDE(NZMH).EQ.1) GO TO 25
      FOX=STC*(AFU-AFH*FMX)
      GO TO 35
   25 AFF=A(I,J,NZMH)
   30 FOX=STC*(AFU-AFF*FMX)
   35 CONTINUE
      IF(FOX.GT.-1.E-05) GO TO 20
      FOX=0.0
   20 CONTINUE
      FIP=1.0-FOX-AFU
      ZMEAN=1.0/(AFU/ZMW(1)+FOX/ZMW(2)+FIP/ZMW(3))
      TEMP=TEMP+460.
      IF (TEMP.LE.TREF) TEMP=TREF
      DENSTY=(ZMEAN*PREF)/(GCPM*TEMP)
      RO(I,J)=ROWF*DENSTY+(1.0-ROWF)*RO(I,J)
   40 CONTINUE
      RETURN
      END
```

```
      SUBROUTINE VISCCT
      COMMON  A(16,14,7),G1(16,14),G2(16,14),RO(16,14),ZMU(16,14)
      COMMON  X1(16),X2(14),DELX1(16),DELX2(14),R(14)
      COMMON  AFILE(12),ASYMBL(12),AGEOM(12),ANAME(6,10)
      COMMON  IMIN(14),IMAX(14),JMIN(14),JMAX(14),JA,JB,IA,IE
      COMMON  NA,NF,NT,IZMU,NZMIL,NZMIH,NP
      COMMON  RUREF,PREF,TREF,CPREF,ZMUREF
      COMMON  INDE(7),INDG,INDRO,INDZMU
      COMMON  RUNF
      COMMON  ZMUR,ZAA
      COMMON  STC,HC,HF,PMX
      COMMON  GLOB,ACTE,ZEX
      COMMON  PR(7),ZM(8),GCFM,GC,ZJC
      COMMON  VINP(9),VING(9),VT(9)
      COMMON  RSOO(7),DIFMAX(7),RP(7),CC,DC,NMAX,NPRIN
      COMMON  NITER,KVORT,IJMP
      COMMON  NVJ,LNJ,LNI
      COMMON  VJ(12)
      COMMON  IMD(7),JMD(7),IMR(7),JMR(7)
      COMMON  CN,CS,CE,CW,ZM
      COMMON  VANGLE
C       VISCOSITY CALCULATION
C         MASS FLOW FOR PLANE FLOW
C         BASED ON SQUARE CROSS SECTION OF DUCT
C*************************************************************
C  TOTAL MASS FLOW
C*************************************************************
      IF (NITER.GE.3) GO TO 9
      IF (INDZMU.NE.2) GO TO 9
      IF(INDG.EQ.2) GO TO 5
      ZMU1=2.0*3.141*2*(A(1,JB,NF)-A(1,JA,NF))
      GO TO 6
    5 ZMU1=4.0*(X2(JB)-X2(1))*(A(1,JB,NF)-A(1,JA,NF))
    6 CONTINUE
C*************************************************************
C FINDING EFFECTIVE V**2 WITH LINEAR INTERPOLATION
C*************************************************************
      V2EFF=0.0
      JA2=JA+1
      DO 30 J=JA2,JB
      J1=J-1
      J2=J
      FT1=VINP(J1)*VINP(J1)
      FT2=(VINP(J2)-VINP(J1))/(X2(J2)-X2(J1))
      FT3=VINP(J1)*FT2*2.
      FT4=FT2*FT2
      IF(INDG.EQ.2) GO TO 15
      SUM=FT4*(X2(J2)**4-X2(J1)**4)/4.+(FT3-2.*FT4*X2(J1))*(X2(J2)**3-
     1 X2(J1)**3)/3.+(FT1+FT4*X2(J1)*X2(J1)-FT3*X2(J1))*(X2(J2)**2-
     2X2(J1)**2)/2.0
      GO TO 25
   15 SUM=FT4*(X2(J2)**3-X2(J1)**3)/3. +(FT3-2.*FT4*X2(J1))*(X2(J2)**2-
     1 X2(J1)**2)/2. +(FT1+FT4*X2(J1)*X2(J1)-FT3*X2(J1))*(X2(J2)-
     2 X2(J1))
   25 CONTINUE
      V2EFF=V2EFF+SUM
```

```
30 CONTINUE
   FC1=.5*(X2(JB)*X2(JB)-X2(JA)*X2(JA))
   IF(INDG.EQ.2) FC1=X2(JB)-X2(JA)
   V2EFF=V2EFF/FC1
   ZMVV=ZMU1*V2EFF
   IF (INDE(NVT).EQ.1) ZMVV=ZMVV+ZMU1*(A(1,JB-1,NVT)**2)
   ZMVV=ZMVV**0.3333
   AA=ZMUK*((2.*X2(JN))**0.66667)*ZMVV/(X1(IN)**.33333)
   ZAA=AA
 9 CONTINUE
   DO 10 J=1,JN
   IL=IMIN(J)
   DO 10 I=IL,IN
   IF (INDZMU.NE.1) GO TO 8
   ZMU(I,J)=ZAA*(RO(I,J)**0.66667)
   GO TO 10
 8 ZMU(I,J)=ZMUREF
10 CONTINUE
   RETURN
   END
```

```
      FUNCTION T(I,J)
      COMMON  A(16,14,7),G1(16,14),G2(16,14),RO(16,14),ZMU(16,14)
      COMMON  X1(16),X2(14),DELX1(16),DELX2(14),R(14)
      COMMON  ATITLE(12),ASYMBL(12),AGEOM(12),ANAME(6,10)
      COMMON  IMIN(14),IN,JN,INM,JNM,JA,JB,IA,IE
      COMMON  NW,NF,NVT,NZMM,NZML,NZMH,NP
      COMMON  ROREF,PREF,TREF,CPREF,ZMUREF
      COMMON  INDE(7),INDG,INDRO,INDZMU
      COMMON  ROWF
      COMMON  ZMUK,ZAA
      COMMON  STC,HC,HP,FMX
      COMMON  GLOB,ACTE,ZEX
      COMMON  PR(7),ZMW(3),GCPM,GC,ZJC
      COMMON  VINP(9),VING(9),VT(9)
      COMMON  RSDU(7),DIFMAX(7),RP(7),CC,DC,NMAX,NPRTN
      COMMON  NITER,KVORT,IJMP
      COMMON  NVJ,LNJ,LNI
      COMMON  VJ(12)
      COMMON  IIMD(7),JJMD(7),IIMR(7),JJMR(7)
      COMMON  CN,CS,CE,CW,ZW
      COMMON  VANGLE
C*****************************************************************
C    TEMPERATURE CALCULATION
C*****************************************************************
      AFU=A(I,J,NZMM)
      AFH=A(I,J,NZML)
      TEMP=(AFH*HP-AFU*HC)/CPREF
      TEOF=TREF-460.
      IF (TEMP.LE.TEOF) TEMP=TEOF
      T=TEMP
      RETURN
      END
```

```
FUNCTION VS2(I,J)
COMMON  A(16,14,7),G1(16,14),G2(16,14),RO(16,14),ZMU(16,14)
COMMON  X1(16),X2(14),DELX1(16),DELX2(14),R(14)
COMMON  ATITLE(12),ASYMBL(12),AGEOM(12),ANAME(6,10)
COMMON  IMIN(14),IN,JN,INM,JNM,JA,JB,IA,IE
COMMON  NW,NF,NVT,NZMM,NZML,NZMI,NP
COMMON  ROREF,PREF,TREF,CPREF,ZMUREF
COMMON  INDE(7),INDG,INDRO,INDZMU
COMMON  ROWF
COMMON  ZMUK,ZAA
COMMON  STC,HC,HP,FMX
COMMON  GLOB,ACTE,ZEX
COMMON  PR(7),ZMW(3),GCPM,GC,ZJC
COMMON  VINP(9),VING(9),VT(9)
COMMON  RSDU(7),DIFMAX(7),RP(7),CC,DC,NMAX,NPR,N
COMMON  NITER,KVORT,IJMP
COMMON  NVJ,LNJ,LNI
COMMON  VJ(12)
COMMON  IIMD(7),JJMD(7),IIMR(7),JJMR(7)
COMMON  CN,CS,CE,CW,ZW
COMMON  VANGLE
VS2     =(G1(I,J)*G1(I,J)+G2(I,J)*G2(I,J))/(RO(I,J)*RO(I,J))
RETURN
END
```

```
      SUBROUTINE PLOT(K)
      COMMON  A(16,14,7),G1(16,14),G2(16,14),R0(16,14),ZMU(16,14)
      COMMON  X1(16),X2(14),DELX1(15),DELX2(14),R(14)
      COMMON  ATITLE(12),ASYMBL(12),AGEOM(12),ANAME(6,10)
      COMMON  IMAX(14),IL,JL,IM,JM,J1,J4,JB,IA,IE
      COMMON  NS,NP,NVT,NZMU,NZRL,NZRH,NP
      COMMON  RUREF,RREF,TREF,CPREF,ZMUREF
      COMMON  INDE(7),INDG,INDR0,INDZMU
      COMMON  RUNF
      COMMON  ZMUK,ZAA
      COMMON  STC,HC,HP,FMA
      COMMON  GLOB,ACTE,ZEX
      COMMON  PR(7),ZM(3),GCPM,GC,ZJC
      COMMON  VINP(9),VING(9),VT(9)
      COMMON  RSOO(7),DIFMAX(7),RP(7),CC,DC,NMAX,MPRIN
      COMMON  NITER,NVORT,IJMP
      COMMON  NVO,LNV,LNI
      COMMON  VO(12)
      COMMON  IIMR(7),JJMR(7),IIMR(7),JJMR(7)
      COMMON  CN,CS,CL,CM,CW
      COMMON  VANGLE
      DIMENSION X(120),XL(120),YL(50),        IGB(50),XA(33),XSYM(12)
      DATA XEMTY,XBOUN,XSYM(1),XSYM(2),XSYM(3),XSYM(4),XSYM(5),XSYM(6)
     1XSYM(7),XSYM(8),XSYM(9),XSYM(10),XSYM(11),XSYM(12)/
     2  1H ,1H.,1H1,1H2,1H3,1H4,1H5,1H6,1H7,1H8,1H9,1HA,1HB,1HC/
      LNI1=LNI-1
      LNJ1=LNJ-1
      XSP=X1(IM)/FLOAT(LNI1)
      YSP=X2(JM)/FLOAT(LNJ1)
      XSP2=.5*XSP
      XL(1)=0.0
      DO 10 I=2,LNI
   10 XL(I)=XL(I-1)+XSP
      YL(1)=0.0
      DO 20 J=2,LNJ
   20 YL(J)=YL(J-1)+YSP
      ISTB=X1(IA)/XSP+1.5
      JSTB=X2(JA)/YSP+1.5
      DO 25 J=1,LNJ
      IF(J.GT.JSTB) GO TO 23
      IGB(J)=ISTB
      GO TO 25
   23 IGB(J)=2.0
   25 CONTINUE
      IG=IE
      PRINT 300
      PRINT 305 ,ASYMBL(K)
      PRINT 310,(VO(L),L=1,NVO)
      PRINT 320
      DO 900 JJ=1,LNJ
      J=(LNJ+1)-JJ
      DO 40 I=1,LNI
   40 X(I)=XEMTY
      IF(J.LE.1.AND.J.NE.LNJ) GO TO 50
      DO 45 I=1,LNI
   45 X(I)=XBOUN
```

```
      GO TO 880
   50 DO 55 J1=2,JN
      IF(X2(J1).GE.YL(J)) GO TO 60
   55 CONTINUE
      LOOP=1
      PRINT 350,LOOP
      GO TO 910
   60 DY=YL(J)-X2(J1-1)
      DO 65 I=1,IN
   65 XA(I)=A(I,J1-1,K)+DY*(A(I,J1,K)-A(I,J1-1,K))/(X2(J1)-X2(J1-1))
      XVF=XA(1)+XSP2*(XA(2)-XA(1))/(X1(2)-X1(1))
      IST=IGB(J)+1
      DO 870 I=IST,LNI1
      DO 70 I1=2,IN
      IF(X1(I1).GE.XL(I)) GO TO 75
   70 CONTINUE
      LOOP=2
      PRINT 350,LOOP
      GO TO 910
   75 DX=XL(I)-X1(I1-1)
      GRD=(XA(I1)-XA(I1-1))/(X1(I1)-X1(I1-1))
      XV=XA(I1-1)+DX*GRD
      XVB=XVF
      XVF=XA(I1-1)+(DX+XSP2)*GRD
      DO 80 KL=1,NVJ
      NN=0
      IF(VJ(KL).GE.XV.AND.VJ(KL).LE.XVF) NN=I
      IF(VJ(KL).LE.XV.AND.VJ(KL).GE.XVF) NN=I
      IF(VJ(KL).GE.XV.AND.VJ(KL).LE.XVB) NN=I
      IF(VJ(KL).LE.XV.AND.VJ(KL).GE.XVB) NN=I
      IF(NN.EQ.0) GO TO 80
      X(I)=XSYM(KL)
   80 CONTINUE
  870 CONTINUE
      IF(J.GT.JGH) GO TO 880
      IF(J.LT.JGH) GO TO 83
      DO 82 KGI=1,ISTB
   82 X(KGI)=XBOUN
      GO TO 880
   83 X(ISTB)=XBOUN
  880 CONTINUE
      PRINT 340,YL(J),(X(IP),IP=1,LNI)
  900 CONTINUE
  910 CONTINUE
  300 FORMAT(1H1)
  305 FORMAT(25H1CONSTANT-VALUE PLOT OF  ,A6//23H NUMBERS REFER TO THE
     139HCONSTANT-VALUES PLOTTED,VALUES BEING...//)
  310 FORMAT(1H ,3H1= ,1PE11.3,3X,3H2= ,1PE11.3,3X,3H3= ,1PE11.3,3X,
     1      3H4= ,1PE11.3,3X,3H5= ,1PE11.3,/, 4H 6= ,1PE11.3,3X,
     2     3H7= ,1PE11.3,3X,3H8= ,1PE11.3,3X,3H9= ,1PE11.3,3X,
     3     3HA= ,1PE11.3,/,4H B= ,1PE11.3,3X,3HC= ,1PE11.3)
  101 FORMAT(12A6)
  320 FORMAT(1H ,//)
  340 FORMAT(1H ,F4.2,1X,120A1)
  350 FORMAT(1H ,10X,27HINTERPOLATING FAILED LOOP =,I2)
      RETURN
      END
```

```
      FUNCTION ADF(I,J,LX,KQ)
      COMMON  A(16,14,7),G1(16,14),G2(16,14),RO(16,14),ZMU(16,14)
      COMMON  X1(16),X2(14),DELX1(16),DELX2(14),R(14)
      COMMON  ATITLE(12),ASYMBL(12),AGEOM(12),ANAME(6,10)
      COMMON  IMIN(14),IN,JN,INM,JNM,JA,JB,IA,IE
      COMMON  NW,NF,NVT,NZMM,NZML,NZMH,NP
      COMMON  ROREF,PREF,TREF,CPREF,ZMUREF
      COMMON  INDE(7),INDG,INDRO,INDZMU
      COMMON  ROWF
      COMMON  ZMUK,ZAA
      COMMON  STC,HC,HP,FMX
      COMMON  GLOB,ACTE,ZEX
      COMMON  PR(7),ZMW(3),GCPM,GC,ZJC
      COMMON  VINP(9),VING(9),VT(9)
      COMMON  RSDU(7),DIFMAX(7),RP(7),CC,DC,NMAX,NPRIN
      COMMON  NITER,KVORT,IJMP
      COMMON  NVJ,LNJ,LNI
      COMMON  VJ(12)
      COMMON  IIMD(7),JJMD(7),IIMR(7),JJMR(7)
      COMMON  CN,CS,CE,CW,ZW
      COMMON  VANGLE
      DIMENSION  AQ(16,14,12)
      DIMENSION BENQ(20),BWSR(20),BP(20)
      EQUIVALENCE (A(1),AQ(1))
      DF(AA,BB,CC,DD,EE,FF)=((EE*EE-FF*FF)*DD+
     1   FF*FF*BB-EE*EE*CC)/(EE*FF*(AA*EE+FF))
C*****************************************************************
C     THIS FUNCTION EVALUATES FIRST DERIVATIVES ACCORDING TO THE
C     THREE-POINT QUADRATIC APPROXIMATION.
C     DEPENDING ON THE POSITION OF THE POINT (I,J) , THERE ARE FIVE
C     DIFFERENT EXPRESSIONS FOR THE DERIVATIVE.
C*****************************************************************
      M=1
      IF (I.LE.IA.AND.I.GE.1)  GO TO 300
300   IF (J.EQ.JB) GO TO 94
      IF (I.EQ.IA.AND.J.GT.JB) GO TO 93
      IF (J.EQ.JA.AND.I.LT.IA) GO TO 92
      IF(J.EQ.1) GO TO 92
      IF(J.LE.JA.AND.I.EQ.IA) GO TO 93
      IF (J.GT.JA.AND.J.LT.JB.AND.I.EQ.1) GO TO 93
      IF(J.EQ.JN) GO TO 94
      IF(I.EQ.IN) M=5
      GO TO 99
92    M=2
      GO TO 99
93    M=3
      GO TO 99
94    M=4
99    CONTINUE
      GO TO (1,2,3,4,5),M
C*****************************************************************
C      M=1...FOR POINTS NOT ON ANY OF THE BOUNDARIES
C*****************************************************************
1     PN=1.
      IF(LX.EQ.1) GO TO 12
13    IF (J.EQ.1.OR.(J.EQ.JA.AND.I.LT.IA)) GO TO 21
```

```
      IF (J.EQ.JN.OR.(J.EQ.JB.AND.I.LT.IA)) GO TO 4,
      DO 10 L=1,12
      BENQ(L)=AQ(I,J+1,L)
      BWSR(L)=AQ(I,J-1,L)
10    BP(L)=AQ(I,J,L)
      XENQ=X2(J+1)-X2(J)
      XWSR=X2(J)-X2(J-1)
      GO TO 100
12    IF (J.GT.JA.AND.J.LT.JB.AND.I.EQ.1) GO TO 31
      IF(J.LE.JA.AND.I.EQ.IA) GO TO 31
      IF (I.EQ.IA.AND.J.GT.JB) GO TO 31
      IF(I.EQ.IN) GO TO 51
      DO 11 L=1,12
      BENQ(L)=AQ(I+1,J,L)
      BWSR(L)=AQ(I-1,J,L)
11    BP(L)=AQ(I,J,L)
      XENQ=X1(I+1)-X1(I)
      XWSR=X1(I)-X1(I-1)
      GO TO 100
C*****************************************************************
C       M=2...FOR POINTS ON THE AXIS , E.T.C.
C*****************************************************************
2     IF(LX.EQ.1) GO TO 1
21    PN=-1.
      DO 20 L=1,12
      BENQ(L)=AQ(I,J+1,L)
      BWSR(L)=AQ(I,J+2,L)
20    BP(L)=AQ(I,J,L)
      XENQ=X2(J+1)-X2(J)
      XWSR=X2(J+2)-X2(J)
      GO TO 100
C*****************************************************************
C       M=3...FOR POINTS ON THE INLET PLANE, E.T.C.
C*****************************************************************
3     IF(LX.NE.1) GO TO 1
31    PN=-1.
      DO 30 L=1,12
      BENQ(L)=AQ(I+1,J,L)
      BWSR(L)=AQ(I+2,J,L)
30    BP(L)=AQ(I,J,L)
      XENQ=X1(I+1)-X1(I)
      XWSR=X1(I+2)-X1(I)
      GO TO 100
C*****************************************************************
C       M=4...FOR POINTS ON THE OUTER BOUNDARY (JN) , E.T.C.
C*****************************************************************
4     IF(LX.EQ.1) GO TO 1
41    PN=-1.
      DO 40 L=1,12
      BENQ(L)=AQ(I,J-1,L)
      BWSR(L)=AQ(I,J-2,L)
40    BP(L)=AQ(I,J,L)
      XENQ=X2(J-1)-X2(J)
      XWSR=X2(J-2)-X2(J)
      GO TO 100
C*****************************************************************
C       M=5...FOR POINTS ON THE EXIT PLANE
```

```
C*************************************************************************
5       IF(LX.NE.1) GO TO 1
51      PN=-1.
        DO 50 L=1,12
        BENQ(L)=AG(I-1,J,L)
        BWSR(L)=AG(I-2,J,L)
50      BP(L)=AG(I,J,L)
        XENQ=X1(I-1)-X1(I)
        XWSR=X1(I-2)-X1(I)
        GO TO 100
100     CONTINUE
        BENQ(15)=BENQ(8)/BENQ(10)
        BENQ(16)=BENQ(9)/BENQ(10)
        BWSR(15)=BWSR(8)/BWSR(10)
        BWSR(16)=BWSR(9)/BWSR(10)
        BP(15)=BP(8)/BP(10)
        BP(16)=BP(9)/BP(10)
        ADF=DF(PN,BENQ(KQ),BWSR(KQ),BP(KQ),XENQ,XWSR)
        RETURN
        END
```

```
      SUBROUTINE PRESCT
      COMMON  A(16,14,7),G1(16,14),G2(16,14),R0(16,14),ZMU(16,14)
      COMMON  X1(16),X2(14),DELX1(15),DELX2(14),R(14)
      COMMON  ATITLE(12),AGYRDL(12),AGEOM(12),ANAME(6,10)
      COMMON  IMIN(14),IJCON,IN,JM,JA,JB,IA,IE
      COMMON  IM,RF,W1,ZMIN,NEWL,NZMH,NP
      COMMON  RO2EF,PREF,TREF,CPREF,ZMUREF
      COMMON  IMAE(7),IJCG,INDR0,INDZMU
      COMMON  RGAS
      COMMON  ZMAX,ZMA
      COMMON  STO,RC,NP,FMX
      COMMON  CLOS,ACTE,ZEX
      COMMON  PR(7),ZM(9),GCPR,GC,ZJC
      COMMON  VINP(9),VING(9),VT(9)
      COMMON  RSDU(7),DIFMAX(7),NP(7),CC,DC,NMAX,NPRIN
      COMMON  NITER,NVORT,IJMP
      COMMON  NVO,LNO,LN1
      COMMON  VJ(12)
      COMMON  IIMD(7),JJMD(7),IIMR(7),JJMR(7)
      COMMON  CN,CS,CE,CW,ZW
      COMMON  VANGLE
      DIMENSION PI(16),PJ(14)
      DIMENSION  AG(16,14,12)
      EQUIVALENCE (A(1),AG(1))
C*****************************************************************
C*** EVALUATE P ALONG REFERENCE LINE
C*****************************************************************
      JRF=JA+2
      JRF1=JRF-1
      JRF2=JRF+1
      IN=PREF/144.
      RIN=IN
      DO 1 J=JRF1,JRF2
      DO 1 I=1,IN
      AG(I,J,12)=ZMU(I,J)*(1.333*ADF(I,J,1,15)-.6667*ADF(I,J,2,16))
      IF(INDG.EQ.1) AG(I,J,12)=AG(I,J,12)-.6667*ZMU(I,J)*G2(I,J)/
     1 (RO(I,J)*R(J))
    1 CONTINUE
      DO 2 I=1,IN
    2 A(I,JRF,NP)=ADF(I,JRF,1,12)-G1(I,JRF)*ADF(I,JRF,1,15)
      DO 3 J=JRF1,JRF2
      DO 3 I=1,IN
    3 AG(I,J,12)=ZMU(I,J)*(ADF(I,J,2,15)+ADF(I,J,1,16))
      DO 4 I=1,IN
      A(I,JRF,NP)=(A(I,JRF,NP)+ADF(I,JRF,2,12)-G2(I,JRF)*ADF(I,JRF,2,15)
     1 )/GC
      IF(INDG.EQ.1) A(I,JRF,NP)=A(I,JRF,NP)+(ZMU(I,JRF)*(ADF(I,JRF,2,15)
     1  +ADF(I,JRF,1,16)))/GC
    4 CONTINUE
      PI(1)=PREF
      DO 5 I=2,IN
    5 PI(I)=PI(I-1)+0.5*(A(I-1,JRF,NP)+A(I,JRF,NP))*(X1(I)-X1(I-1))
C*****************************************************************
C   EVALUATING DP/DR IN THE REST OF THE FIELD
C*****************************************************************
      DO 100 J=1,JM
```

```
      IL=IMIN(J)
      DO 100 I=IL,IN
      A(I,J,12)=-.5067*ADF(I,J,1,15)
      IF(IN.EQ.1.AND.J.EQ.1) GO TO 95
      A(I,J,12)=A(I,J,12)+1.333*ADF(I,J,2,16)
      IF(IN.EQ.2) A(I,J,12)=A(I,J,12)-.5067*G2(I,J)/(R(J)*RO(I,J))
   95 A(I,J,12)=A(I,J,12)*ZMU(I,J)
  100 CONTINUE
      DO 101 J=1,JN
      IL=IMIN(J)
      DO 101 I=IL,IN
  101 A(I,J,NP)=ADF(I,J,2,12)
      DO 102 J=1,JN
      IL=IMIN(J)
      DO 102 I=IL,IN
  102 A(I,J,12)=ZMU(I,J)*(ADF(I,J,2,15)+ADF(I,J,1,16))
      DO 103 J=2,JN
      IL=IMIN(J)
      DO 103 I=IL,IN
      A(I,J,NP)=A(I,J,NP)+ADF(I,J,1,12)-G1(I,J)*ADF(I,J,1,16)
     1 -G2(I,J)*ADF(I,J,2,16)
      IF(IN.EQ.2) GO TO 103
      A(I,J,NP)=A(I,J,NP)+2.*ZMU(I,J)*(ADF(I,J,2,16)
     1  -G2(I,J)/(RO(I,J)*R(J)))/R(J)
      IF(IN.EQ.NVT).EQ.1) A(I,J,NP)=A(I,J,NP)+RO(I,J)*(A(I,J,NVT)**2)
     1  /R(J)
  103 A(I,J,NP)=A(I,J,NP)/GC
C*************************************************************
C  DP/DR ZERO ALONG AXIS
C*************************************************************
      IL=IMIN(1)
      DO 107 I=IL,IN
  107 A(I,1,NP)=0.0
C*************************************************************
C    EVALUATING  P  AT POINTS OTHER THAN REFERENCE LINE
C*************************************************************
      IL=IMIN(J)
      DO 202 I=IL,IN
      PJ(JRF)=P1(I)
      DO 202 J=JRF2,JN
  202 PJ(J)=PJ(J-1)+0.5*(A(I,J-1,NP)+A(I,J,NP))*(X2(J)-X2(J-1))
      JBT=1
      IF(I.LT.IA) JBT=JA
      JGP=JRF-JBT
      DO 204 JG=1,JGP
      J=JRF-JG
  204 PJ(J)=PJ(J+1)-0.5*(A(I,J+1,NP)+A(I,J,NP))*(X2(J+1)-X2(J))
      DO 205 J=JBT,JN
      A(I,J,NP)=PJ(J)/144.
      A(I,J,NP)=A(I,J,NP)-RNT
  205 CONTINUE
  206 CONTINUE
      PRINT 300,JRF,RNT
  300 FORMAT(1H0,10X,17HREFERENCE ROW J =,I4,//,10X,
     1  32HSTATIC PRESSURE VALUES SHOWN ARE,F8.3,2X,
     2   31H(LBF/IN**2) MINUS ACTUAL VALUES)
      RETURN
      END
```

```
      SUBROUTINE ENCHK(ILIN,ILEX)
      COMMON  A(16,14,7),G1(16,14),G2(16,14),RO(16,14),ZMU(16,14)
      COMMON  X1(16),X2(14),DELX1(16),DELX2(14),R(14)
      COMMON  ATITLE(12),ASYMBL(12),AGEOM(12),ANAME(6,10)
      COMMON  IMIN(14),IN,JN,INM,JNM,JA,JB,IA,IE
      COMMON  NM,NF,NVT,NZMM,NZML,NZMH,NP
      COMMON  ROREF,PREF,TREF,CPREF,ZMUREF
      COMMON  INDE(7),INDG,INDRO,INDZMU
      COMMON  ROWF
      COMMON  ZMUK,ZAA
      COMMON  STC,HC,HP,FMX
      COMMON  GLOB,ACTE,ZEX
      COMMON  PR(7),ZMW(3),GCPM,GC,ZJC
      COMMON  VINP(9),VING(9),VT(9)
      COMMON  RSDU(7),DIFMAX(7),RP(7),CC,DC,NMAX,NPRTN
      COMMON  NITER,KVORT,IJMP
      COMMON  NVJ,LNJ,LNI
      COMMON  VJ(12)
      COMMON  IIMD(7),JJMD(7),IIMR(7),JJMR(7)
      COMMON  CI,CS,CE,CW,ZW
      COMMON  VANGLE
      DIMENSION STR(14)
C*************************************************************************
C       NOTE.  FLOW RATES INDICATED ARE BASED
C       ON UNIT WIDTH OF DUCT FOR PLANE FLOW
C*************************************************************************
      IF(IE.EQ.2) GO TO 60
      IF(INDE(NZML).EQ.1.AND.INDE(NZMM).NE.1) GO TO 2
      GO TO 4
    2 IVRB=1
      MSFRC=NZML
      GO TO 8
    4 IF(INDE(NZMM).EQ.1) GO TO 6
      IF(IE.EQ.2) GO TO 60
      GO TO 60
    6 IVRB=3
      MSFRC=NZMM
    8 CONTINUE
      DO 50 KK=1,IVRB
      DO 50 INOUT=ILIN,ILEX
      I=1
      JBT=JA
      JNT=JB
      IF(INOUT.EQ.2) I=INM
      IF(INOUT.EQ.2) JBT=1
      IF (INOUT.EQ.2) JNT=JN
      GO TO (10,14,18),KK
   10 DO 12 J=JBT,JNT
   12 STR(J)=A(I,J,MSFRC)
      GO TO 22
   14 DO 16 J=JBT,JNT
   16 STR(J)=A(I,J,NZML)*HP
      GO TO 22
   18 DO 20 J=JBT,JNT
   20 STR(J)=T(I,J)*CPREF
   22 CONTINUE
```

```
      JNMT=JNT-1
      SUM=0.5*(A(I,JNT,MF)-A(I,JNMT,MF))*(STR(JNT)+STR(JNMT))
      IF(INDO.EQ.1) SUM=SUM*3.14162*2.
      IF(I.EQ.INM) GO TO 26
      DO 24 J=JA,JNT
   24 STR(J)=STR(J)*X1P(J)*RO(I,J)
      GO TO 30
   26 DO 28 J=1,JNT
   28 STR(J)=STR(J)*G1(I,M,J)
   30 CONTINUE
      JST2=JST+1
      DO 40 J=JST2,JNMT
      IF (J.EQ.JNMT) GO TO 34
      J3=J+1
      J2=J
      J1=J-1
      GO TO 36
   34 J3=J
      J2=J-1
      J1=J-2
   36 CONTINUE
      DT1=STR(J1)/((X2(J1)-X2(J2))*(X2(J1)-X2(J3)))
      DT2=STR(J2)/((X2(J2)-X2(J1))*(X2(J2)-X2(J3)))
      DT3=STR(J3)/((X2(J3)-X2(J1))*(X2(J3)-X2(J2)))
      FC1=DT1+DT2+DT3
      FC2=DT1*(X2(J2)+X2(J3))+DT2*(X2(J1)+X2(J3))+DT3*(X2(J1)+X2(J2))
      FC3=DT1*X2(J2)*X2(J3)+DT2*X2(J1)*X2(J3)+DT3*X2(J1)*X2(J2)
      IF (J.EQ.JNMT) GO TO 42
      IF(INDO.EQ.2) GO TO 38
      FCT=FC1*(X2(J2)**4-X2(J1)**4)/4.0-FC2*(X2(J2)**3-X2(J1)**3)/3.0+
     1  FC3*(X2(J2)**2-X2(J1)**2)/2.0
      GO TO 40
   38 FCT=FC1*(X2(J2)**3-X2(J1)**3)/3.0-FC2*(X2(J2)**2-X2(J1)**2)/2.0+
     1  FC3*(X2(J2)-X2(J1))
   40 GO TO 46
   42 IF(INDO.EQ.2) GO TO 44
      FCT=FC1*(X2(J3)**4-X2(J2)**4)/4.0-FC2*(X2(J3)**3-X2(J2)**3)/3.0+
     1   FC3*(X2(J3)**2-X2(J2)**2)/2.0
      GO TO 46
   44 FCT=FC1*(X2(J3)**3-X2(J2)**3)/3.0-FC2*(X2(J3)**2-X2(J2)**2)/2.0+
     1  FC3*(X2(J3)-X2(J2))
   46 SUM=SUM+FCT
      IF(KK.EQ.1.AND.I.EQ. 1) FLG1=SUM
      IF(KK.EQ.1.AND.I.EQ.INM) FLG2=SUM
      IF(KK.EQ.2.AND.I.EQ. 1) ENT1=SUM
      IF(KK.EQ.2.AND.I.EQ.INM) ENT2=SUM
      IF(KK.EQ.3.AND.I.EQ. 1) TMP1=SUM
      IF(KK.EQ.3.AND.I.EQ.INM) TMP2=SUM
   50 CONTINUE
      FLM1=FLG1*HC
      FLM2=FLG2*HC
      SMEN1=FLM1+TMP1
      SMEN2=FLM2+TMP2
      FRACT=(FLG1-FLG2)*100./FLG1
      PRINT 210
      IF(ILIN.EQ.2) GO TO 56
      PRINT 220, FLG1
```

```
      IF (IVRB.EQ.3) PRINT 240,FLH1,TMP1,SMEN1,ENT1
      IF(ILEX.EQ.1) GO TO 60
   50 PRINT 230 , FLO2
      IF (IVRB.EQ.3) PRINT 240,FLH2 ,TMP2,SMEN2,ENT2
      IF(ILIN.EQ.2) GO TO 60
      IF (IVRB.EQ.3) PRINT 250 , FRACT
   60 CONTINUE
  210 FORMAT(1H1,///,53X,14HENTHALPY CHECK,//,30X,46H(FOR CARTESIAN COOD
     1S. UNIT WIDTH OF DUCT USED))
  220 FORMAT(1H0,//,20X,6H INLET, /,38X,16HFUEL FLOW RATE =,
     1  1PE11.3,3H LBM/SEC)
  230 FORMAT(1H0,//,20X,6HOUTLET,/,38X,16HFUEL FLOW RATE =,
     1  1PE11.3,3H LBM/SEC)
  240 FORMAT(1H0,/,41X,18HENTHALPY IN FUEL =,1PE11.3,6H BTU/SEC,/,32X,
     1 27HENTHALPY IN TERMS OF HEAT =,1PE11.3,3H BTU/SEC,/,58X,
     2  13H------------,/,59X,1PE11.3,//,31X,28HTOTAL ENTHALPY(INTEGRAT
     3ED) =,1PE11.3,6H BTU/SEC)
  250 FORMAT(1H0,//,20X,35HPER CENT FUEL CONVERTED INTO HEAT =,1PE11.3)
      RETURN
       END
```

Data cards

```
ISOTHERMAL SWIRLING JET ISSUEING FROM VANE SWIRLERS
VORT  STRMF SWVEL MFRAC DENTL
15 DEGREES VANE ANGLE , HUBLESS SWIRLER
VORTICITY    A(I,J,1)                STREAM  FUNCTION  A(I,J,2)
SWIRL  VELOCITY    A(I,J,3)          FUEL MASS FRACTION  A(I,J,4)
DIMENSIONLESS  ENTHALPY  A(I,J,5)
```

and two blank cards.

ABSTRACT

The research work described in this thesis is a continuation of the previous studies carried out in the University of Glasgow on swirling jets issuing from vane swirlers.

A test-rig suitable for investigations of combustion systems was designed. The vane swirlers used for the investigations were to the same design as those used by Mathur (5) for investigating cold swirling jets. The measuring instruments were calibrated and the analysis for the temperature correction due to radiation from the thermocouple bead was carried out. For all the experiments, premixed stream of town gas and air was used.

Flame stabilisation tests were conducted mainly with hubless swirlers. With the hubless swirlers, stable flames are held at the junction of the swirler vane tips. With each of the annular swirlers, the chemical reaction started from inside the swirler tube. The results of the tests show that highly stable flames are obtainable with vane swirlers. The width of the stable flame region of the stability limits loop increases with swirl although for any given flow velocity, the fuel/air ratios at weak and rich blow-off limits increase with swirl. For flames issuing from swirlers with vane angles of 70 and 75 degrees with both geometries, wall flame jets were formed.

The aerodynamic measurements were made with hubless and annular swirlers. The analysis of the results show a strong dependence of the flow distributions in the flow field on the swirler exit conditions. As the rotational energy increases, a greater proportion of the nozzle fluid is forced into the outer part of the jet by the centrifugal forces. This concentration of stream lines causes increases in the flow velocities at those radial points in the swirler flow section as a result of which the static pressures at these points drop. The effect of this is that the maximum axial velocity components, temperatures and minimum static pressures are displaced from the jet axis near the swirler exit. The radial displacements of these aerodynamic variables increase with swirl. All the variables generally decay as the axial distance from the swirler exit increases and the rates of decay depend on the swirl number. The maximum values of the above parameters on cross-sectional planes (minimum for pressure) ultimately tend to the jet axis and the positions at which the values reach the axis depend on swirl. Throughout the lengths of the jets investigated, the static pressures remain subatmospheric.

The minimum swirler vane angle with which a recirculation vortex will be established in hubless swirler flames in 30 degrees. The corresponding angle with annular swirlers is 45 degrees. For the same swirler geometry, the characteristics and dimensions of the recirculation vortex increases with swirl.

The analyses made of the jet widths show that swirling jets expand rapidly immediately downstream of the exit and the rate of expansion increases with swirl. At sufficiently far axial distances from the swirler exit, the expansion rates become linear.

Computations of the axial fluxes of linear and angular momenta, and

and the mass flow rates at the cross-sectional planes of measurements show that the fluxes of momenta along the jet are conserved. The entrainment rates increase with swirl in both swirler geometries.

The comparison of the above results with cold swirling jets show differences in the jet developments. The minimum vane angle for the establishment of recirculation vortex in cold swirling jets increase to 45 degrees. For both swirler geometries and swirlers with corresponding vane angles, the maximum widths of the recirculation vortices increase in burning jets. The burning jets also have higher expansion and entrainment rates than the cold equivalents.

The prediction method formulated at Imperial College, London, (8),(9) was further developed for the computation of flow distributions in cold and burning swirling jets. The program was also modified for processing in a KDF9 or UNIVAC 1108 computer. The results predicted by the method are generally similar to those experimentally obtained. With specification of correct inlet profiles, the program will predict accurate results for cold jets. For burning jets, further improvements are still required in the inlet specification of the combustion parameters and also in the turbulence representation.